71-0225-02-00

CR 114401

STUDY OF AUTOMATIC AND MANUAL TERMINAL GUIDANCE AND CONTROL SYSTEMS FOR SPACE SHUTTLE VEHICLES

VOLUME II - SECTION IV THROUGH APPENDIX B

FINAL REPORT
(MARCH 1970 THROUGH MARCH 1971)

AUGUST 1971

BY

STEPHEN OSDER
ROGER KELLER

SPERRY FLIGHT SYSTEMS DIVISION
SPERRY RAND CORPORATION
PHOENIX, ARIZONA

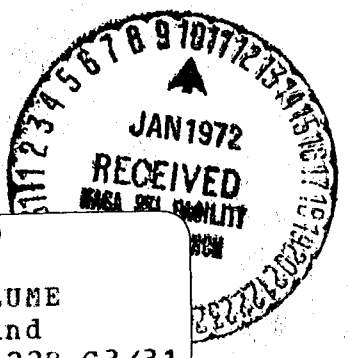

STUDY OF AUTOMATIC AND MANUAL TERMINAL GUIDANCE AND CONTROL SYSTEMS FOR SPACE SHUTTLE VEHICLES

VOLUME II - SECTION IV THROUGH APPENDIX B

FINAL REPORT
(MARCH 1970 THROUGH MARCH 1971)

AUGUST 1971

BY

STEPHEN OSDER
ROGER KELLER

SPERRY FLIGHT SYSTEMS DIVISION
SPERRY RAND CORPORATION
PHOENIX, ARIZONA

PREPARED FOR

NATIONAL AERONAUTICS AND SPACE ADMINISTRATION
AMES RESEARCH CENTER
MOFFETT FIELD, CALIFORNIA
PER CONTRACT NAS 2-5804

PREPARED BY

SPERRY FLIGHT SYSTEMS DIVISION
SPERRY RAND CORPORATION
PHOENIX, ARIZONA

FOREWORD

This report was prepared by the Advanced Systems and Avionics Department, Sperry Flight Systems Division of the Sperry Rand Corporation under NASA Contract NAS2-5804, "Study of Automatic and Manual Terminal Guidance and Control Systems for Horizontal Landing of Space Shuttle Vehicles". The work was administered under the direction of the Guidance and Navigation Branch of the NASA Ames Research Center's Full Scale and Systems Research Division, with Mr. Donald W. Smith as Technical Monitor. Contributions of the following individuals at the Sperry Flight Systems Division are acknowledged:

Dr. John Dunfield	High Altitude Energy Management and Flareout Simulator Studies
Mr. Randall Gaylor	Manual/Flight Director Modes, Energy Management Techniques and Direction of the NASA ARC Simulator Evaluations
Mr. George Yeh	Design of the EADI/NASA Simulation Interface
Mr. Robert Eslinger	Study of Candidate Flight Test Aircraft for Simulating SSV Landings
Mr. Robert Jacobson	Study of Candidate Navigation Sensors for SSV Landing

Also acknowledged are the contributions of NASA's Guidance and Navigation Branch and the Simulator Computer Systems Branch in operating the NASA visual scene simulator for the final performance verifications and evaluations.

TABLE OF CONTENTS

VOLUME I

TABLE OF CONTENTS (cont)

TABLE OF CONTENTS (cont)

LIST OF ILLUSTRATIONS

LIST OF ILLUSTRATIONS (cont)

LIST OF ILLUSTRATIONS (cont)

LIST OF ILLUSTRATIONS (cont)

LIST OF ILLUSTRATIONS (cont)

LIST OF ILLUSTRATIONS (cont)

SECTION IV

SYSTEM DESIGN STUDIES

SECTION IV

SYSTEM DESIGN STUDIES

INTRODUCTION

This section summarizes various guidance and control design studies that were performed for three specific space shuttle candidate vehicles: The McDonnell Douglas Low Cross-Range Orbiter, designated MDAC-1 and MDAC-2 (two versions which evolved from April 1970 through November 1970), the Lockheed Missile and Space Company Delta Wing Orbiter (LSC-8MX) and the North American Rockwell Twin-Fin, Delta Wing Orbiter, designated SSV-134C. Additional design studies with the McDonnell Douglas High Cross-Range Delta Wing vehicle will be covered in a separate supplementary report. Descriptions of the various vehicles are given in Section IIIA on "Vehicle Mission and Performance Requirements".

The study results reported here were obtained with three types of simulations. They were:

- Small perturbation 3 degree of freedom (lateral-directional and longitudinal separated) for fixed point autopilot and stability augmentation system design.

- Quasi 5-degree-of-freedom simulations for trajectory segments - 100,000 to 20,000 feet; 20,000 feet to first flare; 20,000 feet to touchdown. These simulations used velocity axis equations and approximated lateral-directional dynamics with closed loop transfer functions. Winds were approximated with gusts only.

- 6-degree-of-freedom simulations using body axis equations for vehicle dynamics. All aerodynamics were stored in look-up tables. Complete wind models (high altitude, low altitude, and turbulence) were included. This simulation was used for final system refinement and performance verification with trajectories run from 100,000 feet to touchdown.

Additional studies and performance verification in the NASA ARC visual scene simulator are summarized in Section V of this report.

A. MDAC LOW CROSS-RANGE, STRAIGHT WING VEHICLE SYSTEM DESIGN STUDIES

1. Vehicle Aero Summary

Characteristics	MDAC-2	MSC "245"
	Circa 7/70	Circa 1/70
Weight (landing) - pounds	210,000	155,000
Wing Span (b) - feet	114.94	113.5
MAC ($\bar{c}$) - feet	17.86	17.53
I_{xx} - (slug-foot^2 x 10^6)	1.85	0.778
I_{yy} - (slug-foot^2 x 10^6)	16.4	5.85
I_{zz} - (slug-foot^2 x 10^6)	16.6	5.95
I_{xz} - (slug-foot^2 x 10^6)	-0.028	-
Ref Area (S) feet^2	1,900	1,850
Wing Loading (W/S) - pounds/foot^2	110	83.7
Peak L/D at Landing Condition	6.15	6.83
α for L/D_P - degrees	6.0	7.5
*Pitch Control Power - M_{δ_e} (1/sec)	-1.24	-3.20
*Roll Control Power - L_{δ_A} (1/sec^2)	2.44	3.04
*Yaw Control Power - N_{δ_R} (1/sec^2)	-0.430	-0.289
*For Land Condition - Q = 150 pounds/foot^2		

The above table compares salient characteristics of the latest MDAC LCR configuration with the early MSC straight wing reference design (MSC-245). Pertinent information regarding landing characteristics is the relatively low α for peak L/D (compared to delta wing vehicles), the high wing loading, and the excellent control power obtainable from the aerodynamic surfaces. The control power parameter is torque to inertia ratio or degrees per second^2 of vehicle angular acceleration per degree of surface deflection (at a reference Q). Table 3-1 in

Section IIIA compares these aerodynamic characteristics for all candidate space shuttle vehicles that were studied.

The interesting aerodynamic characteristics of this class of vehicle are in the erratic and severely unstable variations in lateral-directional moment and force coefficients in the region of 40 degrees $> \alpha >$ 10 degrees at transonic and subsonic speeds. As discussed in the previous section on Transition Maneuver Concepts, this region was only penetrated for 2.5 seconds when dynamic pressures had still not risen to above 50 pounds per foot^2. A complete description of the aero model and the tabulated data for the digital simulation table look-up routines are given in Reference 29.

The important aerodynamic properties that establish the approach flight path equilibrium angles and speeds for the MDAC LCR vehicle are the L/D characteristics. These are converted to the glide angle versus airspeed curves as shown in Figures 4-1 and 4-2. The minimum and maximum weight bounds for the preliminary vehicle design (MDAC-1) corresponded to a wing loading range of 84.5 pounds per foot^2 to 124.5 pounds per foot^2. An equilibrium speed of 300 knots is considered a reasonable speed that would allow surplus energy for coping with headwind conditions. From the MDAC-1 data of Figure 4-1, a -12 degree glide angle could handle minimum to maximum weight vehicles with an equilibrium speed range of 275 to 350 knots. When the updated LCR vehicle design data was obtained, the -12 degree approach glide path should have given a 280-knot equilibrium speed for the (MDAC-2) (as shown in Figure 4-2). Since an equilibrium velocity is never attained (because the drag equation is never in equilibrium as explained in Section IIIB), and the calculation procedure that defines the curves on Figures 4-1 and 4-2 involves some approximations, the actual speed obtained in the simulation flights by the MDAC-2 vehicle on the -12 degree approach path was about 300 knots.

Control surface characteristics are:

δ_A - Aileron Deflection Limits = ±20 degrees

δ_R - Rudder Deflection Limits = ±30 degrees

δ_E - Elevator Deflection Limits = +30, -40 degrees

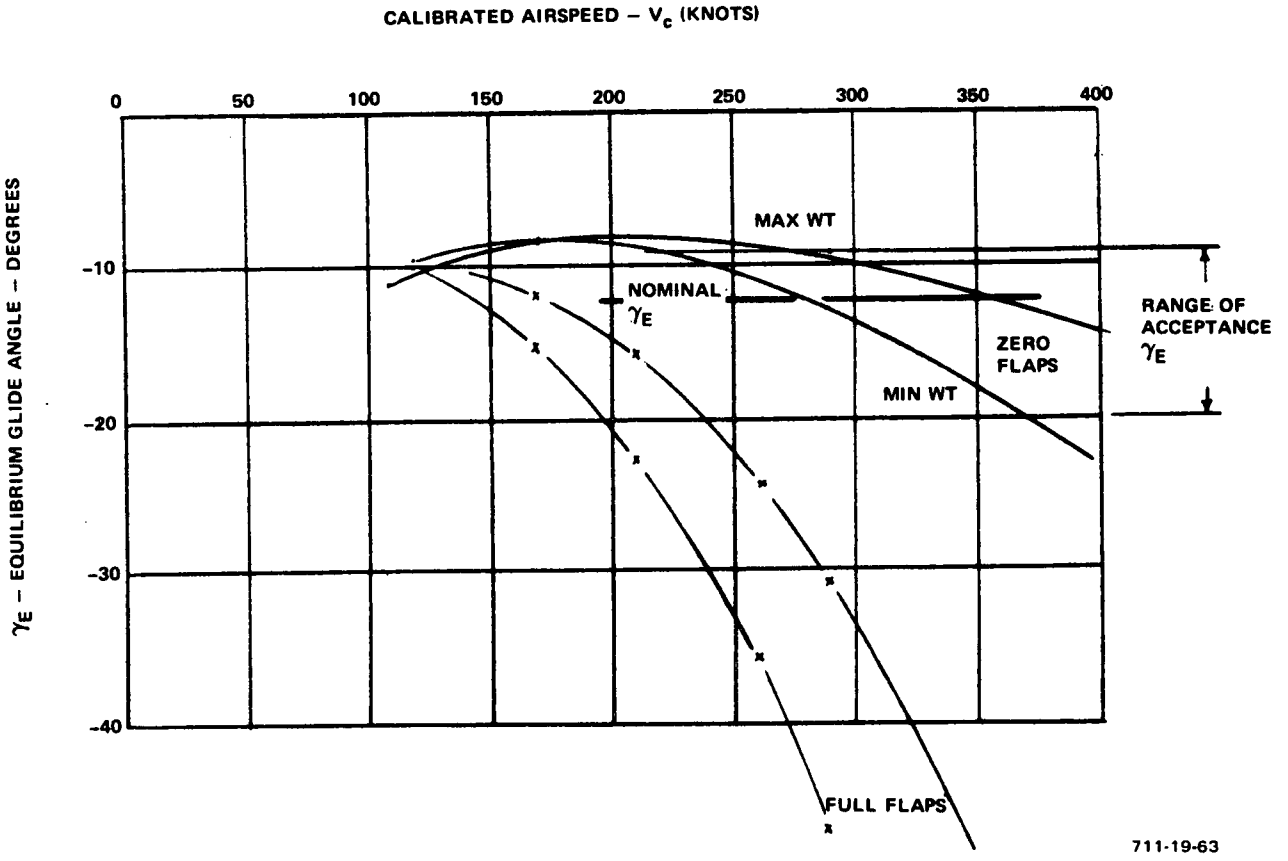

Figure 4-1
LCR (Straight Wing) MDAC-1 Glide Angle
versus Airspeed Characteristics

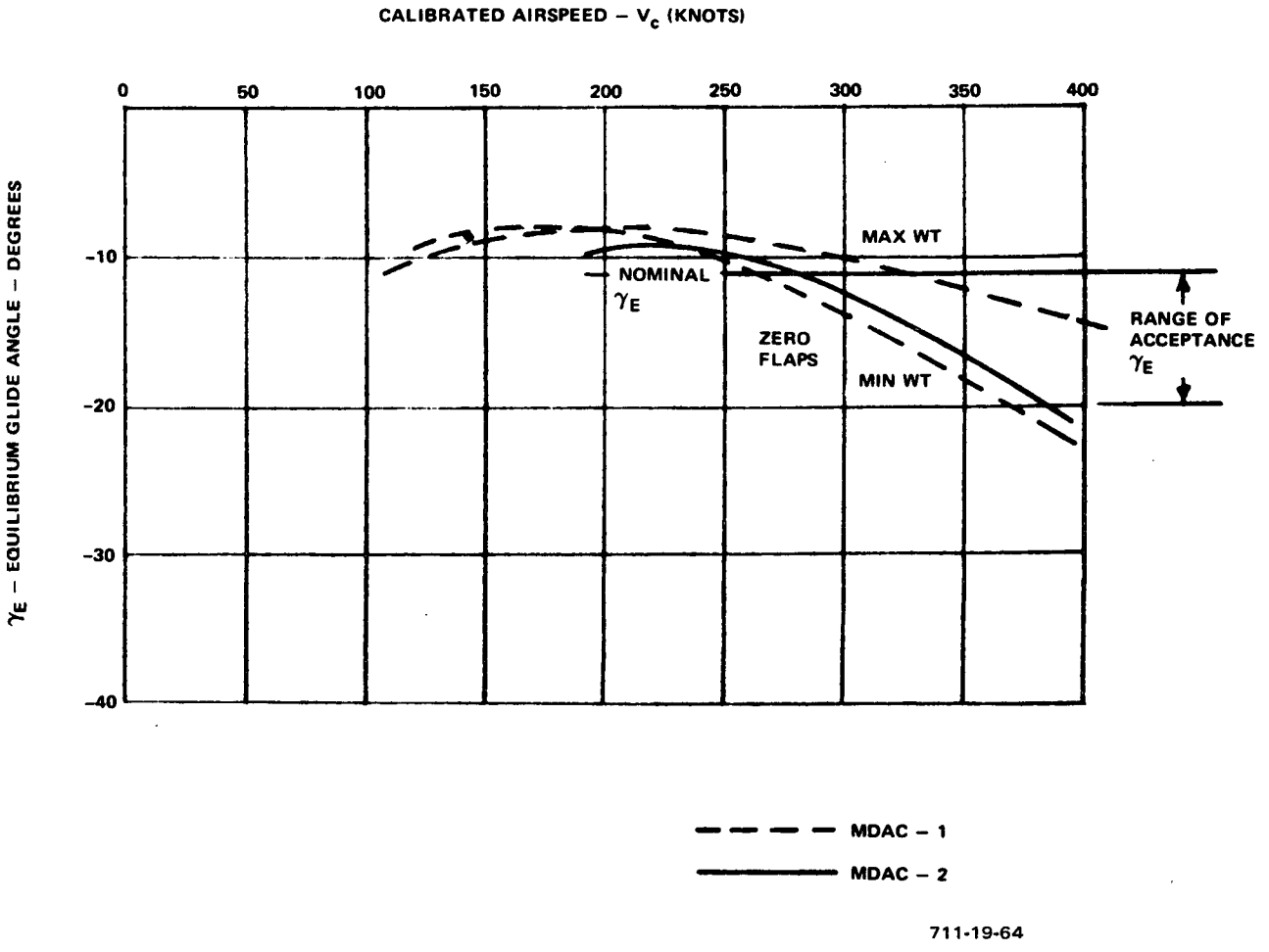

Figure 4-2
LCR (Straight Wing) MDAC-2 Glide Angle
versus Airspeed Characteristics

δ_F - Flap Deflection Limits = $\leqslant$ 50 degrees

δ_{SB} - Speed Brake Deflection Limits = $\leqslant$ 25 degrees

2. Attitude Stabilization and Autopilot Parameters

a. Pitch Stabilization and Vertical Flight Path Control

The closed loop control equations and gains used for the MDAC-2 vehicle are:

$$\delta_{E_{COMMAND}} = k_\theta \left[\left(\theta_E + \frac{k_q}{k_\theta} \frac{\tau S}{\tau S + 1} q \right) \left(1 + \frac{k_{INT}}{S} \right) \right] \qquad (4\text{-}1)$$

where:

$k_\theta = 2 \frac{300}{Q}$ ... max = 4.0

$\frac{k_q}{k_\theta} = 0.75$

$\tau = 2.0$ seconds

$k_{INT} = 0.05$ to 0.1

On the various glide paths the closed loop control equation is:

$$\theta_C = k_\gamma (\gamma_{REF} - \gamma) + k_h h_e \left(1 + \frac{a_2}{S} \right) \qquad (4\text{-}2)$$

where:

$k_h = 0.067 \frac{500}{V}$ degree per foot (V in feet per second)

$a_2 = 0.05$ to 0.08

$k_\gamma = 1.0$ to 1.5 degrees per degree

b. Lateral Directional Stabilization

The roll control equation is:

$$-\delta_{AC} = \left[\left(p - p_{com} \right) \frac{k_p}{k_\phi} + \left(\phi - \phi_C \right) \right] k_\phi \qquad (4\text{-}3)$$

where:

$$\frac{k_p}{k_\phi} = 0.5$$

$$k_\phi = 2.5 \ \frac{300}{Q}$$

The rudder or yaw control equation is:

$$\delta_{R_C} = k_r \left(r - \frac{g}{V} \sin \phi_C \right) \frac{\tau_4 S}{\tau_4 S + 1} + \frac{k_{A_y}}{\tau_5 S + 1} A_y + \delta_{A_6} \, k_{RA} \left[\frac{\tau_6 S}{(\tau_6 S + 1)(\tau_7 S + 1)} \right] \qquad (4\text{-}4)$$

where:

$$k_r = 2.0 \left(\frac{300}{Q} \right)$$

$$\tau_4 = 2.5$$

$$k_{A_y} = 0.2 \left(\frac{300}{Q} \right)$$

$$\tau_5 = 0.1$$

$$k_{RA} = 0$$

$$\tau_6 = 5.0$$

$$\tau_7 = 0.2$$

The reaction control system gain and the transition maneuver gains were given in Section IIIC. Manual control system gains were defined in Section IIID.

The high altitude nominal trajectory that defines the nominal potential and kinetic energy errors for the pitch guidance [see Section IVC, equations (3-102), (3-103) and (3-104)] involves a stored table. That table is given as Table 4-1 below.

TABLE 4-1

NOMINAL TRAJECTORY

D_K (ft)	$C_1(D_K)$ (ft)	$C_2(D_K)$ (ft/sec)
0	25,000	568
5,000	27,200	580
10,000	31,000	575
15,000	37,500	525
20,000	45,000	370
25,000	53,000	440
30,000	60,000	490
35,000	66,000	600
40,000	72,000	680
45,000	77,000	770
50,000	82,000	880
55,000	86,000	960
60,000	91,000	1,080
65,000	95,000	1,200
70,000	100,000	1,385
75,000	106,000	1,600
80,000	109,000	1,740
85,000	113,000	1,920
90,000	118,000	2,120
95,000	122,000	2,240
100,000	126,000	2,360

The nominal elevator program that establishes a reference elevator trim position for each α and Mach number [δ_{E_α} (α, M) of equation (3-109), Section IIIC.8] is given in Table 4-2.

TABLE 4-2

PROGRAMMED ELEVATOR COMMAND (δ_{E_α}), PRETRANSITION MANEUVERING

α	δ_E (degrees)					
	M = 0.3	M = 0.6	M = 0.9	M = 1.1	M = 1.5	M = 2.0
40	-18.0	-4.4	21.3	-8.3	-8.0	-13.3
50	-20.4	-3.6	26.0	-4.7	-14.2	-21.1
60	-23.1	-10.8	-0.2	-7.1	-21.3	-28.9
70	-25.0	-26.0	-29.0	-31.5	-33.8	-36.7

3. Terminal Glide Acquisition

In studies with the MDAC LCR vehicle, speed brakes were used on the approach glide path only to reduce airspeed when speed exceeded the desired nominal value.

Acquisition trajectories for the -12 degree glide path with the MDAC-2 vehicle are shown in Figure 4-3. Initial conditions are a -12 degree glide angle, dynamic pressure of 295 pounds per foot^2, and angle of attack of 2-1/2 degrees at 20,000 feet of altitude. Various glide slope acquisition runs that result in nominal and off-nominal velocities (in 5-percent increments) at flare to shallow glide slope initiation are shown on this figure. The guidance law imposes maximum angle of attack, maximum speed, maximum and minimum flight path angle constraints, and maximum acceleration constraints. The down-range or overshoot window for a -10 percent off-nominal velocity is 4.8 nautical miles. Run 1 shows the imposition of an angle-of-attack constraint that limited the intercept angle to the α corresponding to the maximum L/D (α = 6 degrees).

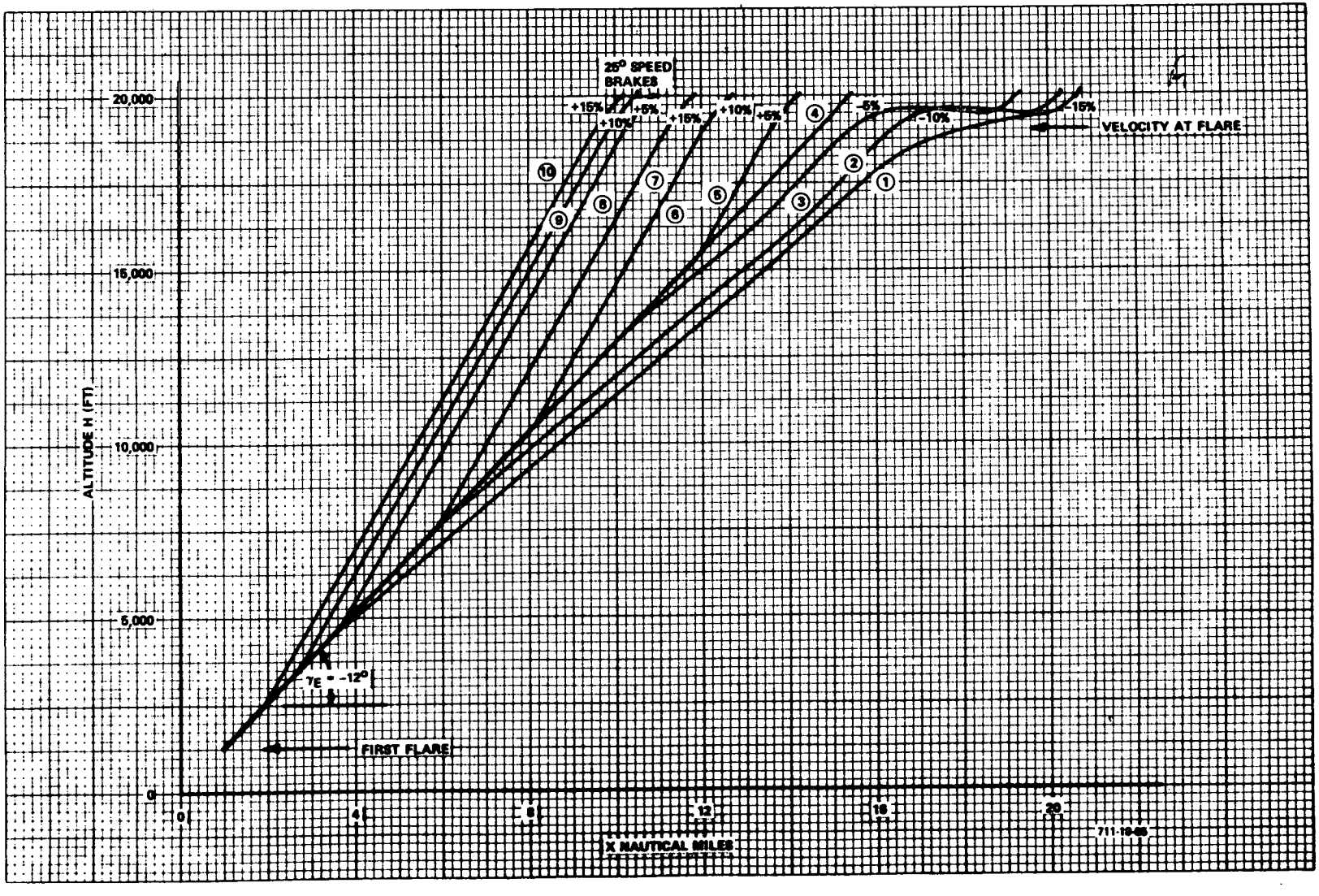

Figure 4-3
MDAC-2 LCR Orbiter Equilibrium Glide Path Acquisition Trajectories

A large overshoot capture of the glide slope would actually be achieved by turning 360 degrees and approaching the glide slope from below. Runs 7 and 10 demonstrate the apparent limit for which a dive into the glide slope from an overshooting initial condition can be employed (for operation without and with speed brakes respectively). The range errors for an approach in which the vehicle has +10 percent velocity error at flare is 2.8 nautical miles. This window can be extended by deploying full speed brakes (cases 8, 9, 10 of Figure 4-3). Note that the total window at 20,000 feet is about 10 nautical miles if the flareout system can cope with ±15 percent velocity errors.

Figure 4-4 shows velocity versus altitude histories for these acquisition trajectories. The nominal velocity decreases since equivalent airspeed tends to remain constant as air density increases. All trajectories converge toward the nominal after the glide path is intercepted. Figure 4-5 shows the dynamic pressure transients associated with the acquisition trajectories. The dynamic pressure histories diverge from the nominal until the glide path is acquired. All pressure trajectories converge once the terminal path is reached. The consequence of flying at the peak L/D is shown to effectively establish a minimum dynamic pressure in runs (1), (2), and (3) of Figure 4-5. Speed brake deployment for attenuation of excess velocity is shown in run (8). Speed brakes not only extend the maximum permissible range, but they reduce the peak dynamic pressure transient.

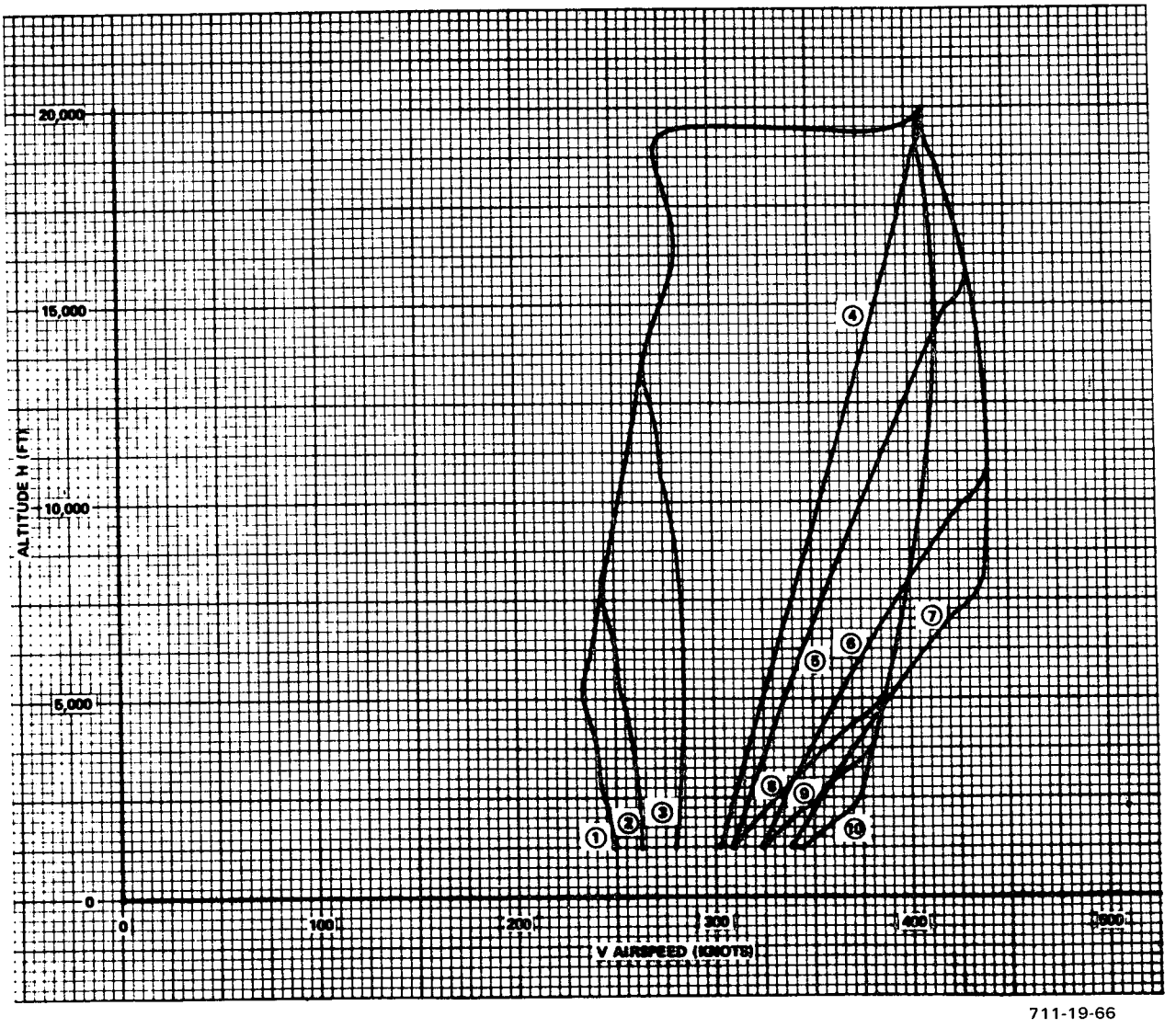

Figure 4-4
MDAC-2 LCR Orbiter Velocity for
Glide Path Acquisition Trajectories

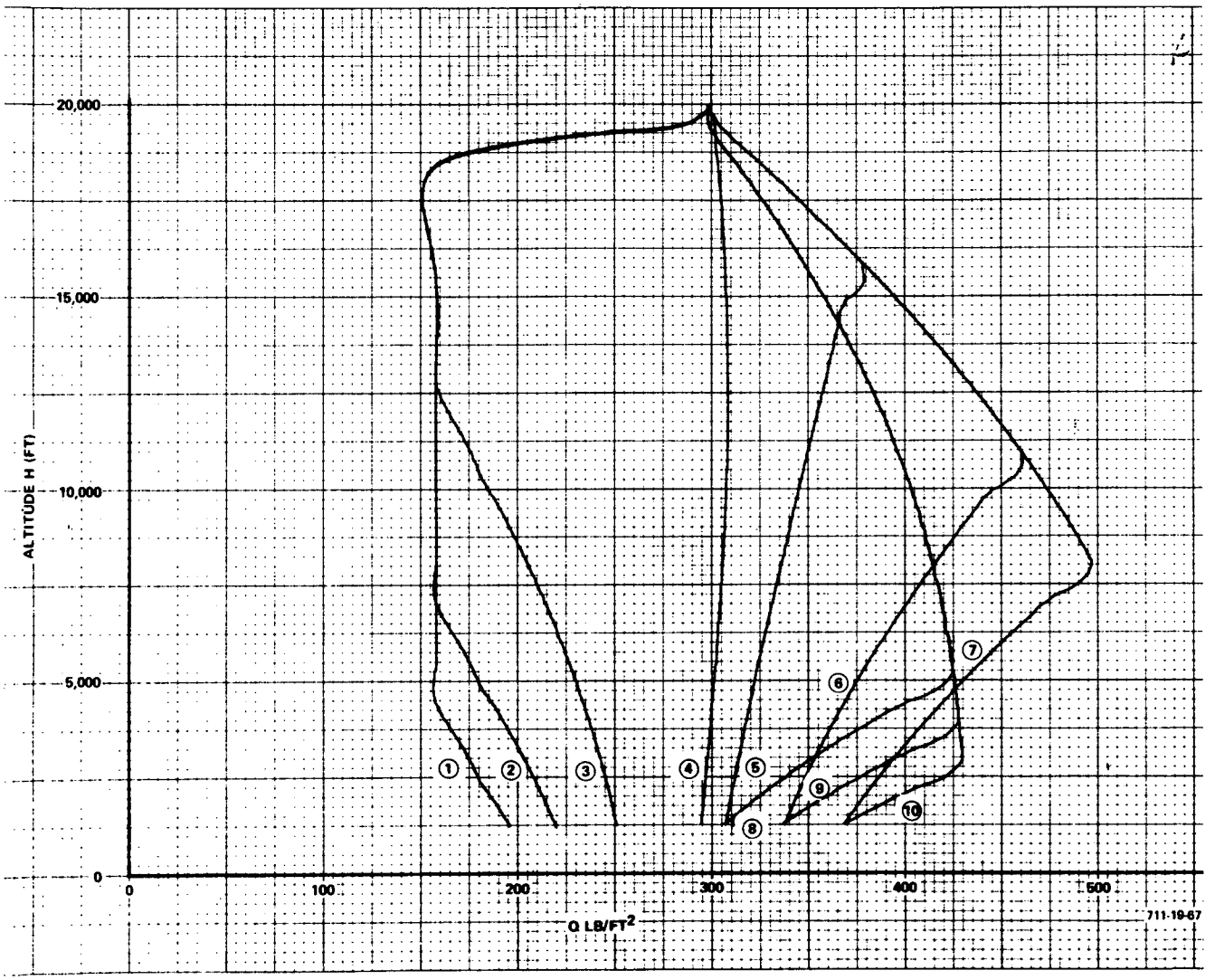

Figure 4-5
MDAC-2 LCR Dynamic Pressure for
Glide Path Acquisition Trajectories

4. Flareout and Glide Path Geometry Trade-Offs

a. First Flare and Shallow Glide Path Tracking

The geometric relationship between the steep angle approach glide path and the shallow glide path is dependent upon the equilibrium approach speed, the desired normal acceleration in the first flare maneuver and the speed brake and flap deployment techniques. These trade-offs were done with the MDAC-1 vehicle.

Flareout trajectories for several modes of flap and speed brake deployment are shown in Figure 4-6 for landing touchdowns at a nominal angle of attack of 4 degrees and vertical velocity of -2 feet per second.

Noting that the trajectories on Figure 4-6 represent the lightest weight version of the MDAC-1 vehicle, it is seen that a landing speed as low as 135 knots is attained at the nominal landing α of about 4 degrees. (Final designs gave landing speeds of 165 to 180 knots.) Figure 4-6 shows four different glide path geometries that start and complete the landing phase with the same speeds. Case 1 starts the first flare at about 1100 feet and acquires the shallow (2-1/2°) glide path at 800 feet. It is capable of this extended run on the shallow glide path because it delays flap deployment until an altitude of 200 feet. Flaps are deployed at 5 degrees per second and full flaps = 50 degrees. It is probably an operationally unacceptable procedure to delay deployment until 200 feet. This is especially true because, to minimize the number of variables, landing gear was deployed concurrently with flaps.

Case (2) shows a landing with only 20 degrees of flaps (40 percent), deployed at 300 feet. This gives a 600 foot shallow glide path run. Case (3) uses only 400 feet of shallow glide path but uses full flaps. Case (4) delays acquisition of the shallow glide path until an altitude of 300 feet but it requires 50 percent speedbrakes in addition to full flaps to achieve the landing speed. (Note that final flare starts at an altitude of 60 feet, c.g. height.)

In theory, more or less speed brake could be employed during the flare to attenuate off-nominal velocity errors. In practice the MDAC-1 vehicle required an unobtainable speed brake deflection to eliminate modest off-nominal velocities. For example, a plus five percent off-nominal velocity required 136 percent speed brake deployment to establish a nominal touchdown. It appears that

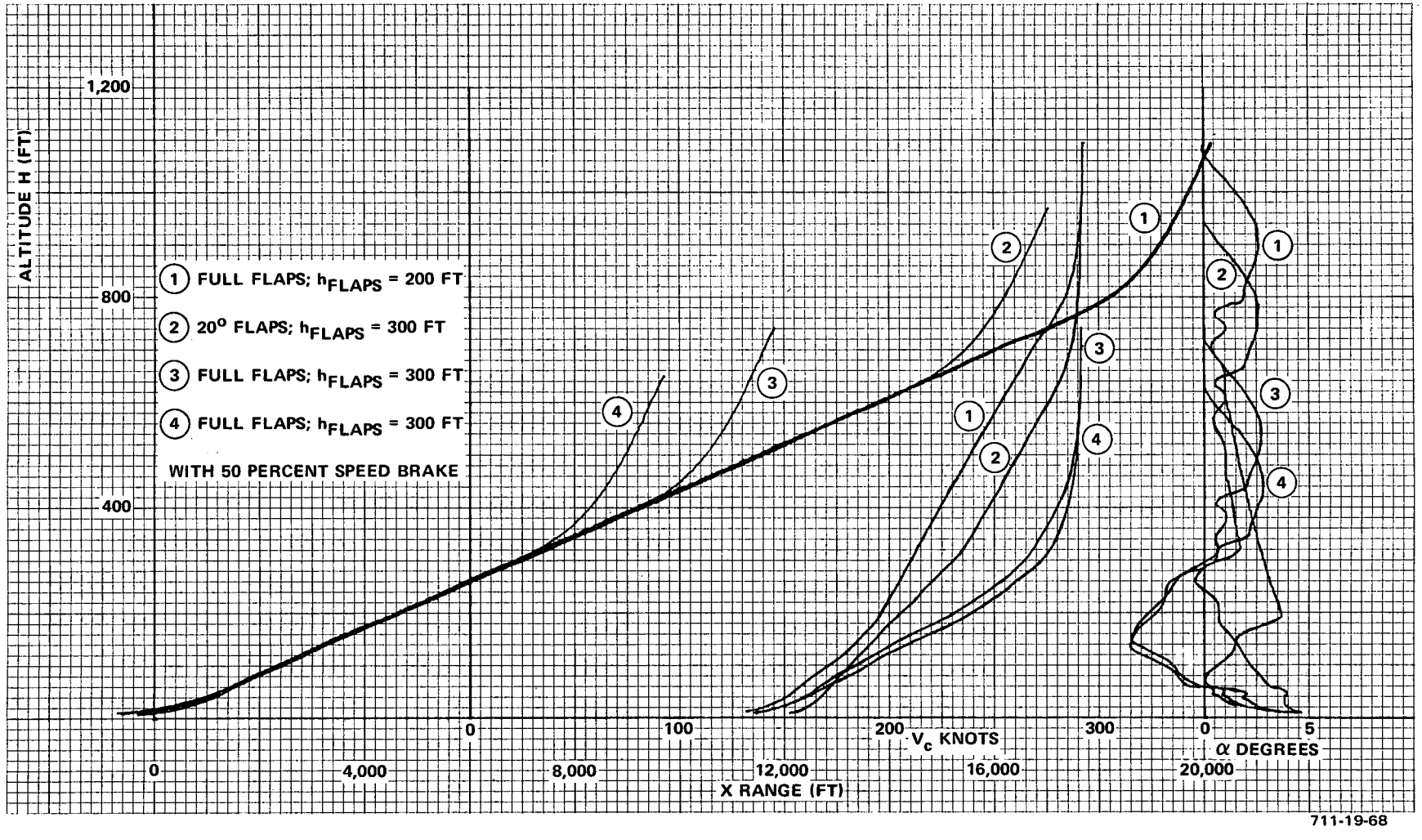

Figure 4-6
LCR (Straight Wing) MDAC: W/S = 84.5 Flareout Trajectory
Trade-Offs for Various Speed Brake and Flap
Deployment Histories for $\alpha_{T_{Nominal}}$ = 4 degrees

speed brakes can be used more effectively during the equilibrium glide descent but they should be retracted for the nominal flareout. Removal of the nominal speed brake deployment adds an additional 100 feet of altitude to the shallow glide slope traverse.

If we select the glide path geometry of case (1) of Figure 4-6, how well would that system cope with the maximum weight (W/S = 124.5) configuration which must arrive at first flare with a significantly greater speed. There are several techniques available to cope with this problem including speed modulation with speed brakes. Figure 4-7 shows that a variable altitude flap deployment strategy can provide good speed convergence and a successful flareout. The speed difference at touchdown is about 24 knots whereas the speed difference at first flare was about 63 knots. The higher speed vehicle deployed flaps at 340 feet while the lower speed vehicle deployed flaps at 200 feet.

b. Final Flare

The nominal landing procedure used was:

- -12 degrees glide slope to first flare at 870 feet
- Shallow glide path acquired at 520 feet
- Landing gear and full flaps deployed at 5 degrees per second at an altitude of 200 feet
- Final flare starts at 60 feet (c.g. height)*
- Touchdown at -2 foot per second, $\dot{h}$, 167 knots, V at an angle of attack of approximately 6 degrees

Figure 4-8 show landings for nominal and ±50 foot errors in the first flare initiating altitudes which result in negligible range and speed errors and vertical velocity error. Figures 4-9 and 4-10 show terminal trajectories and h and $\dot{h}$ phase plane results for sustained step vertical wind gusts of 10 fps applied at altitudes of 100, 300, 500, and 700 feet. Touchdown dispersions are small with the exception of a wind gust applied at 100 feet of altitude which resulted in a touchdown $\dot{h}$ error of about -2 feet per second.

---

*Height of c.g. at touchdown = $1.5 + 10.9 \sin\theta + 13.4 \cos\theta$ or about 15.9 feet for a nominal touchdown.

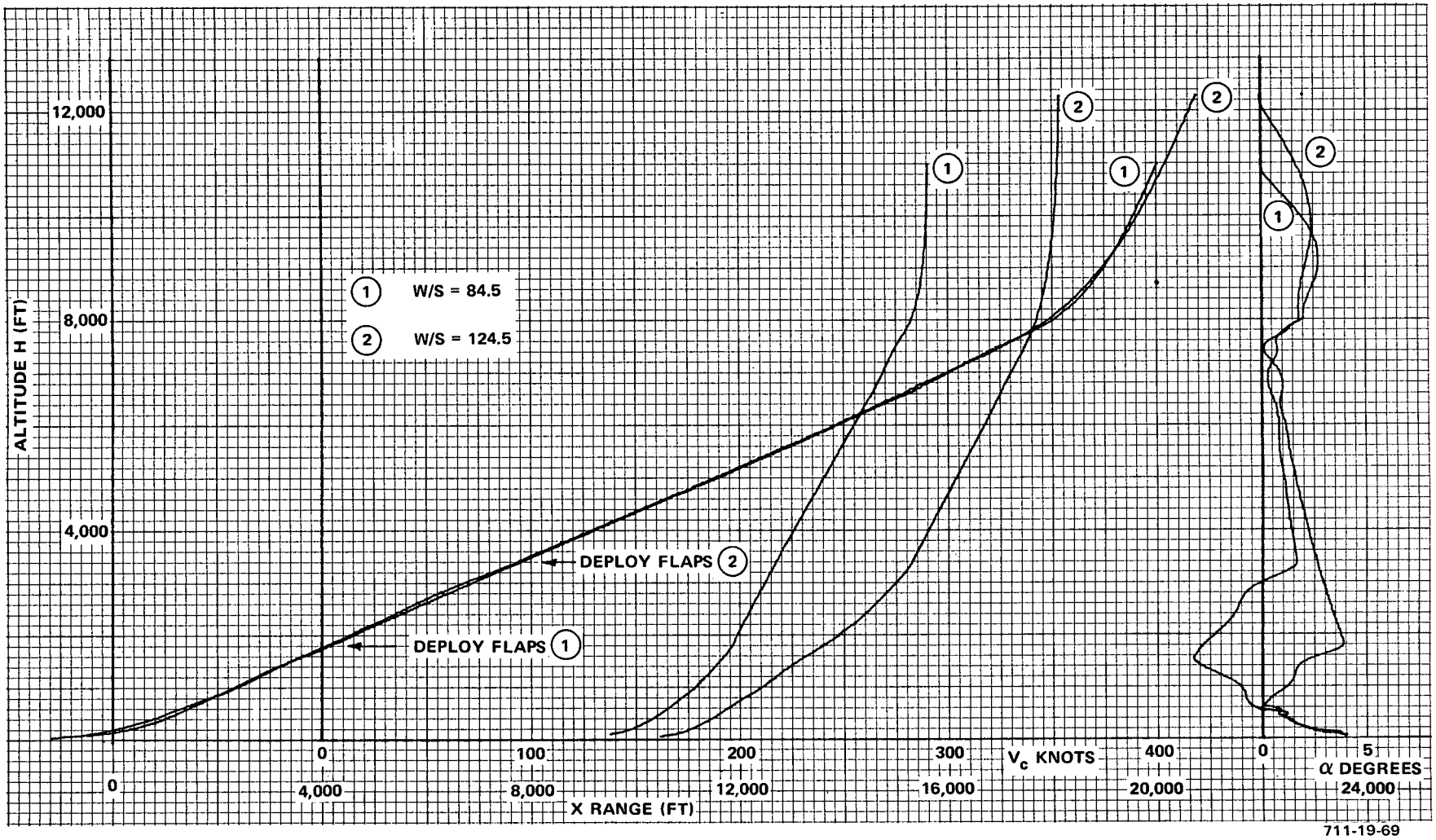

Figure 4-7
LCR (Straight Wing) MDAC Flareout Trajectories,
W/S = 84.5 and 124.5, Control Laws Updated for
Maximum Weight Orbiter from Minimum Weight Baseline

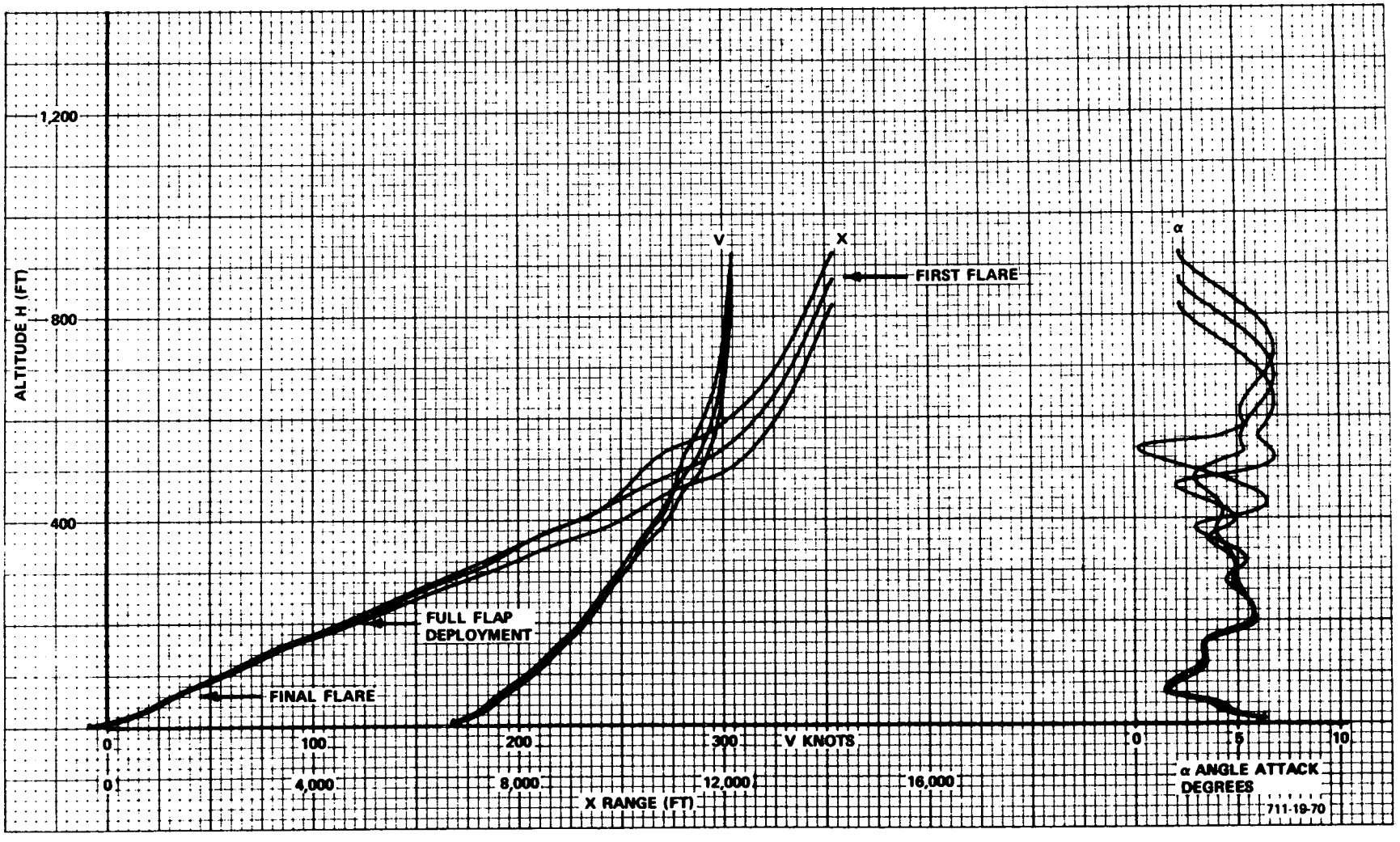

Figure 4-8
MDAC-2 LCR Orbiter Flareout Trajectories
for ±50 feet Initial Flare Errors

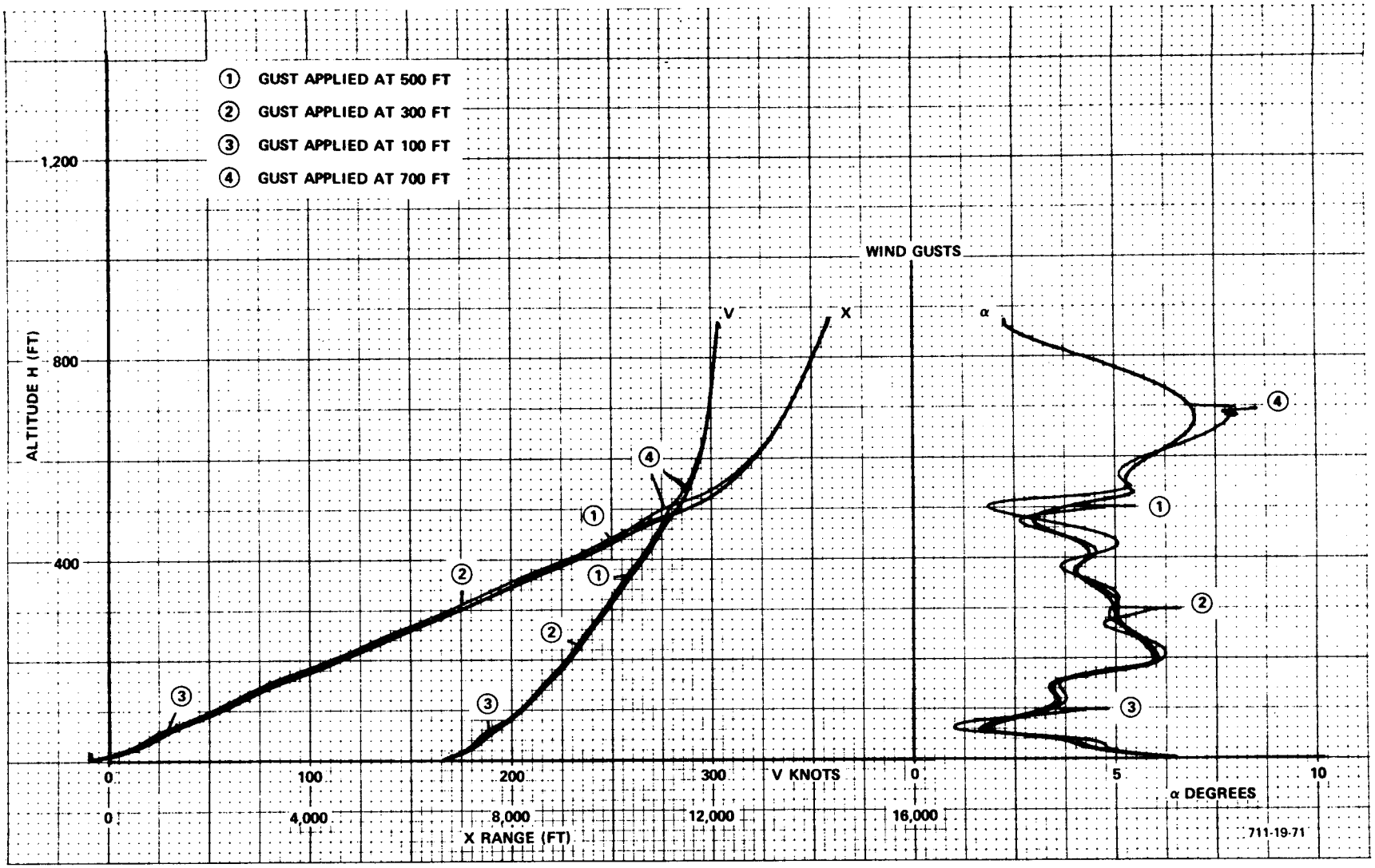

Figure 4-9
MDAC-2 LCR Orbiter Terminal Trajectories
for 10-foot-per-second Vertical Wind Gusts

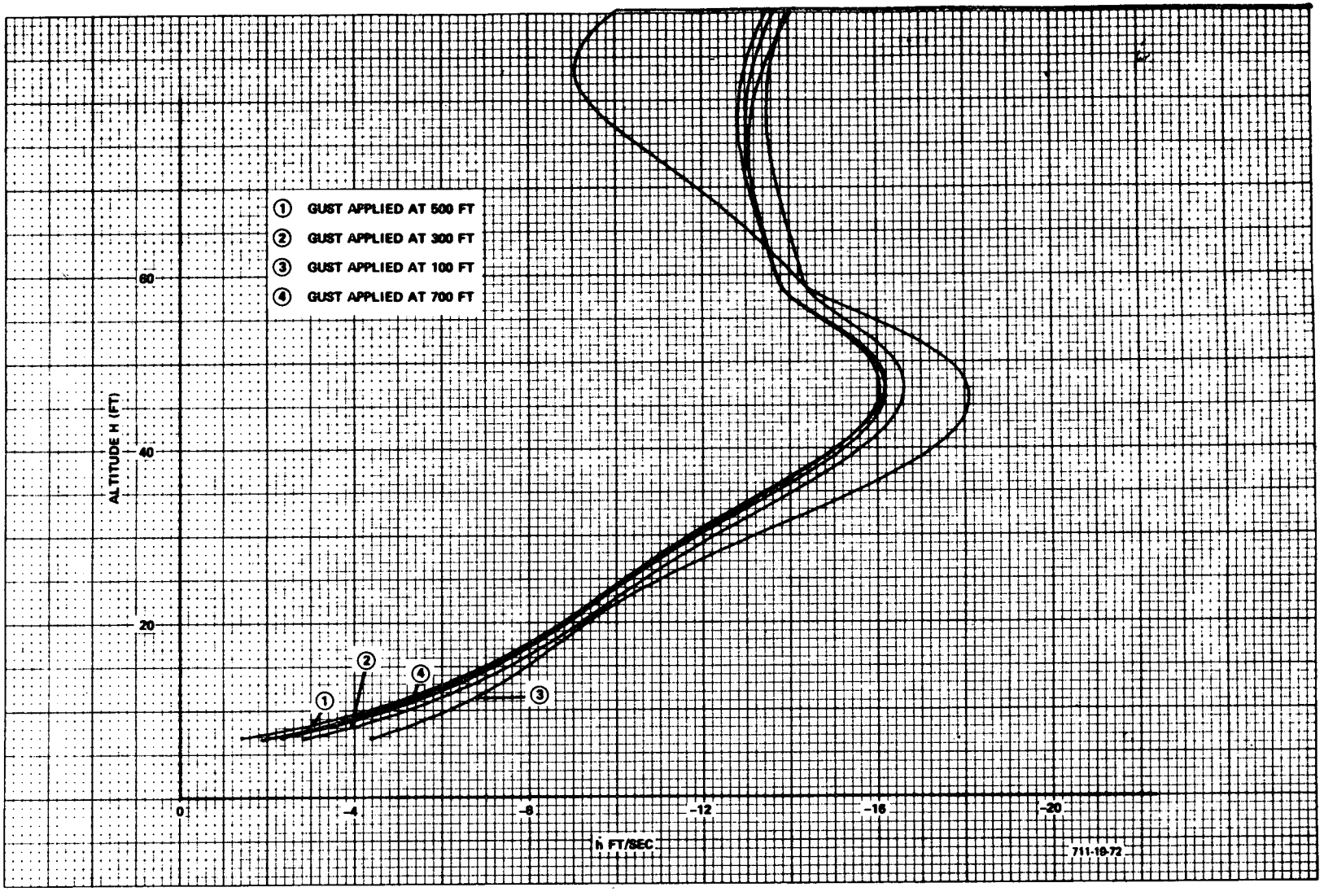

Figure 4-10
MDAC-2 LCR Orbiter, h and $\dot{h}$ Phase Plane for
10-foot-per-second Vertical Wind Gusts

The touchdown $\dot{h}$ for the different altitudes at which the severe gust was applied was:

Run (Figures 4-9 and 4-10)	Altitude at Which 10 FPS Gust (sustained) is Applied	Touchdown $\dot{h}$
1	500 feet	-1.6 ft/sec
2	300 feet	-3.0 ft/sec
3	100 feet	-4.4 ft/sec
4	700 feet	-2.4 ft/sec

The Acceleration Flareout Controller (Section III.C-4) was used. Although this performance is acceptable for vertical gusts as large as 10 feet per second; final simulations with wind and turbulence models indicated that the acceleration controller did not perform as well as an $\dot{h}$ controller.

Figure 4-11 displays the flareout trajectories for nominal and ±10 percent off-nominal velocity errors at first flare altitude and Figure 4-12 shows the corresponding h and $\dot{h}$ phase planes for a control law employing updating of the predictive commands for the velocity error. The vehicle touches down within ±0.1 foot per second of the desired rate of -2 feet per second for forward speed spreads of +10 percent and -13 percent. Range spreads are ±400 feet. This performance is achieved at the expense of an angle of attack variation of 9 degrees. The peak α for the low speed off-nominal reached the wing stall region. It is therefore apparent that a more elaborate speed control procedure prior to first flare would have been needed to avoid this penetration of an unacceptable α region. To avoid this low speed problem, the nominal landing speed could have been raised about 10 knots. This was ultimately done in the final simulator verification of LCR vehicle performance.

5. LCR Vehicle Performance Summary 100,000 Feet to Touchdown

Complete 6-degree of freedom runs from 100,000 feet to touchdown are documented in Figures 4-13 through 4-17. These runs include the blended reaction and aerodynamic controls, the transition maneuver, acquisition of the terminal glide path, first flare, shallow glide path tracking, final flare, and lateral flight path tracking. The vertical (altitude-range) profile for a straight-in approach is shown in Figure 4-13. Note that the zero range coordinate is at the

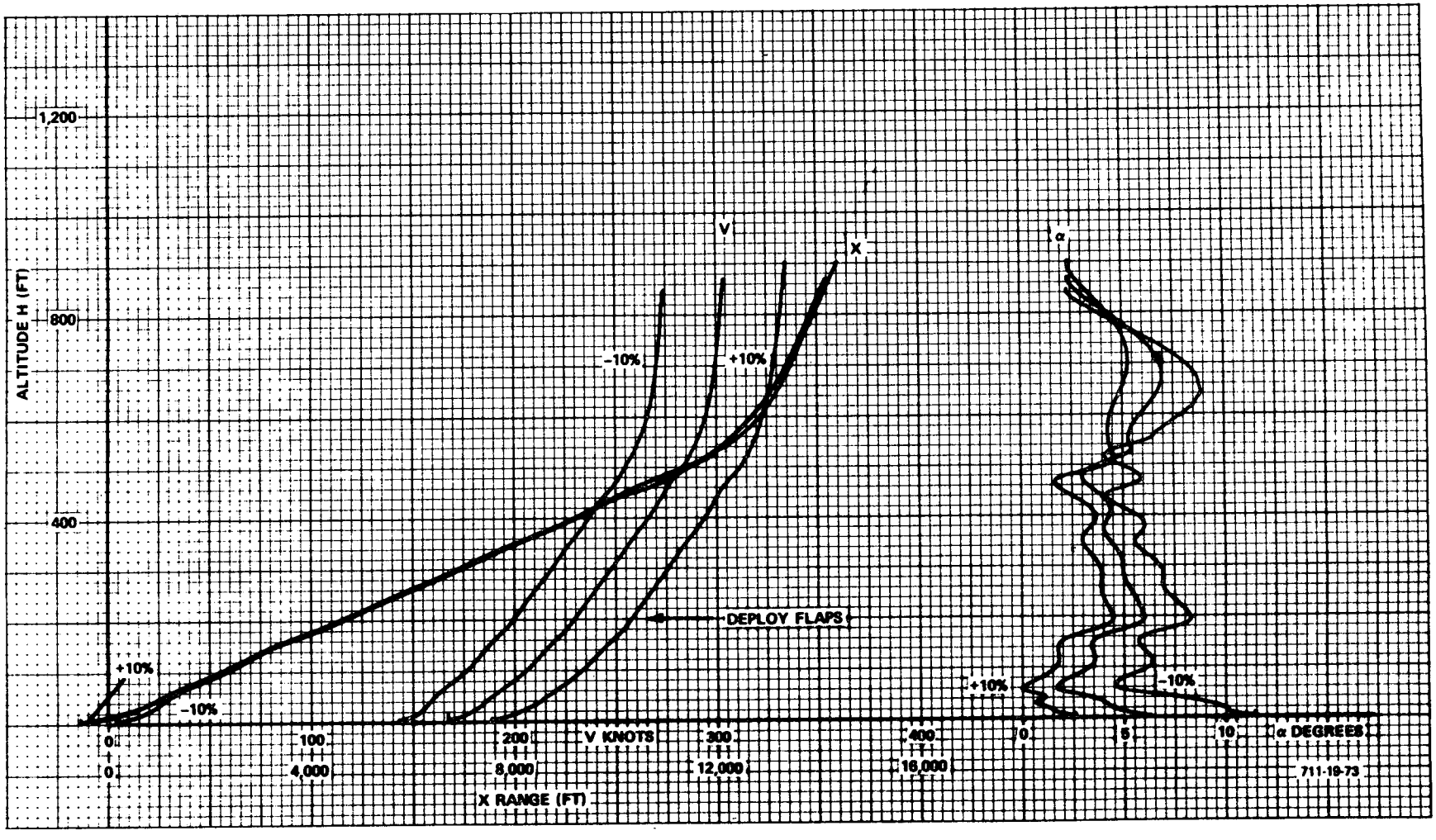

Figure 4-11
MDAC-2 LCR Orbiter Flareout Trajectories Predictive Commands
Updated for ±10 percent Initial Flare Velocity Errors

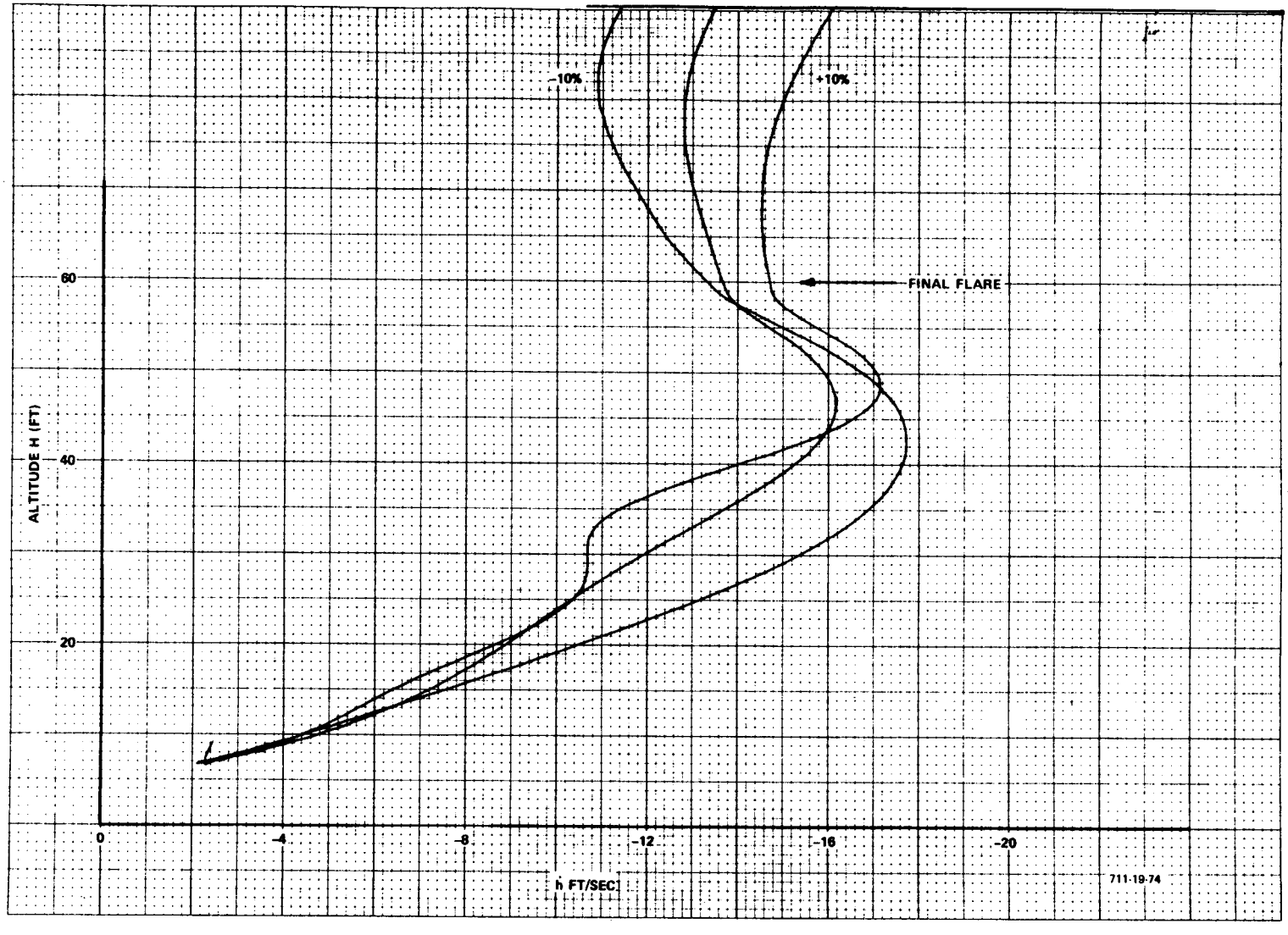

Figure 4-12
MDAC-2 LCR Orbiter, h and $\dot{h}$ Phase Plane for
±10 percent Off-Nominal Velocities

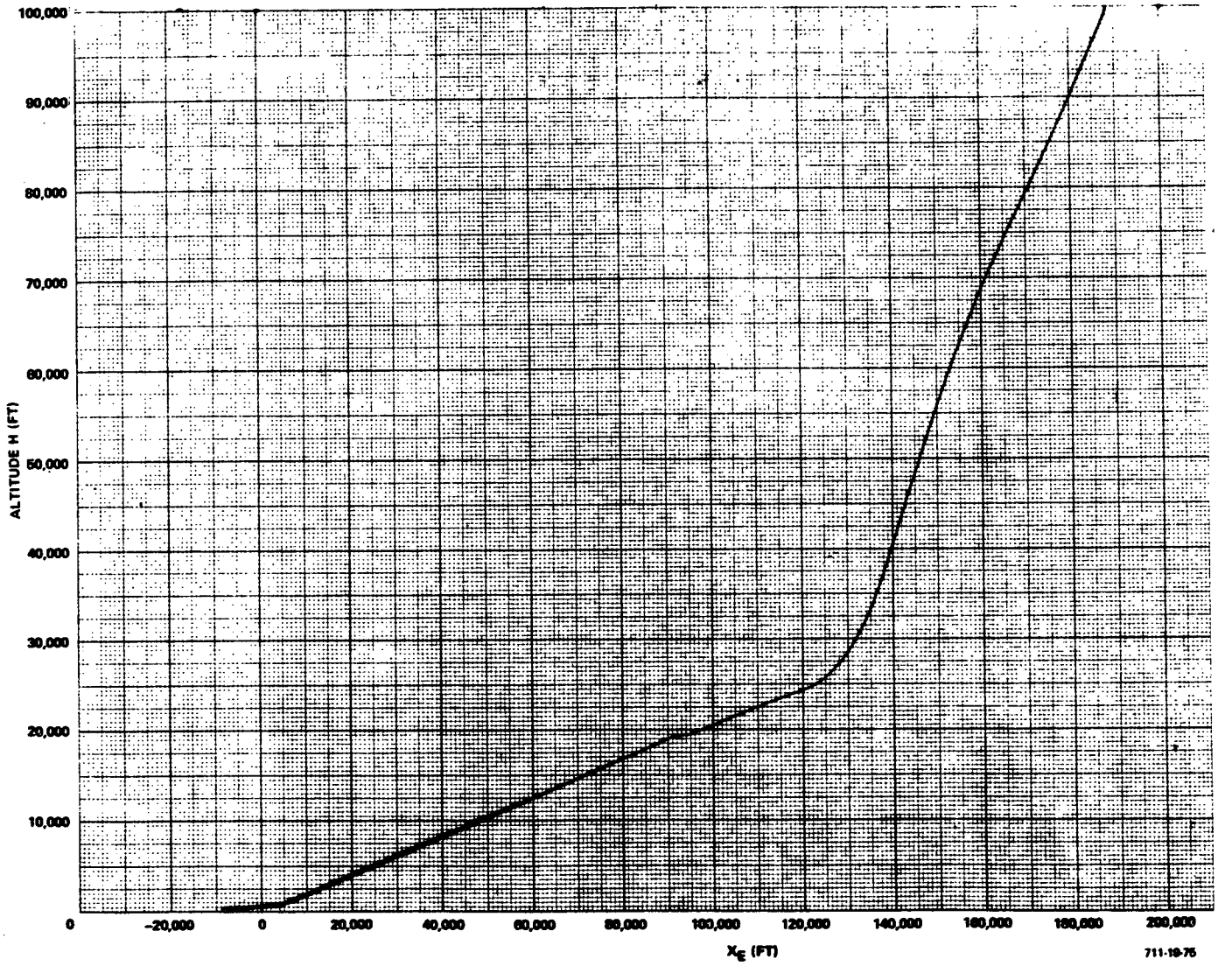

Figure 4-13
LCR (Straight Wing) MDAC-2 Orbiter Trajectory for Straight-In Flight from 100,000-Foot Altitude with Large Off-Nominal Initial γ (Altitude-Range Profile)

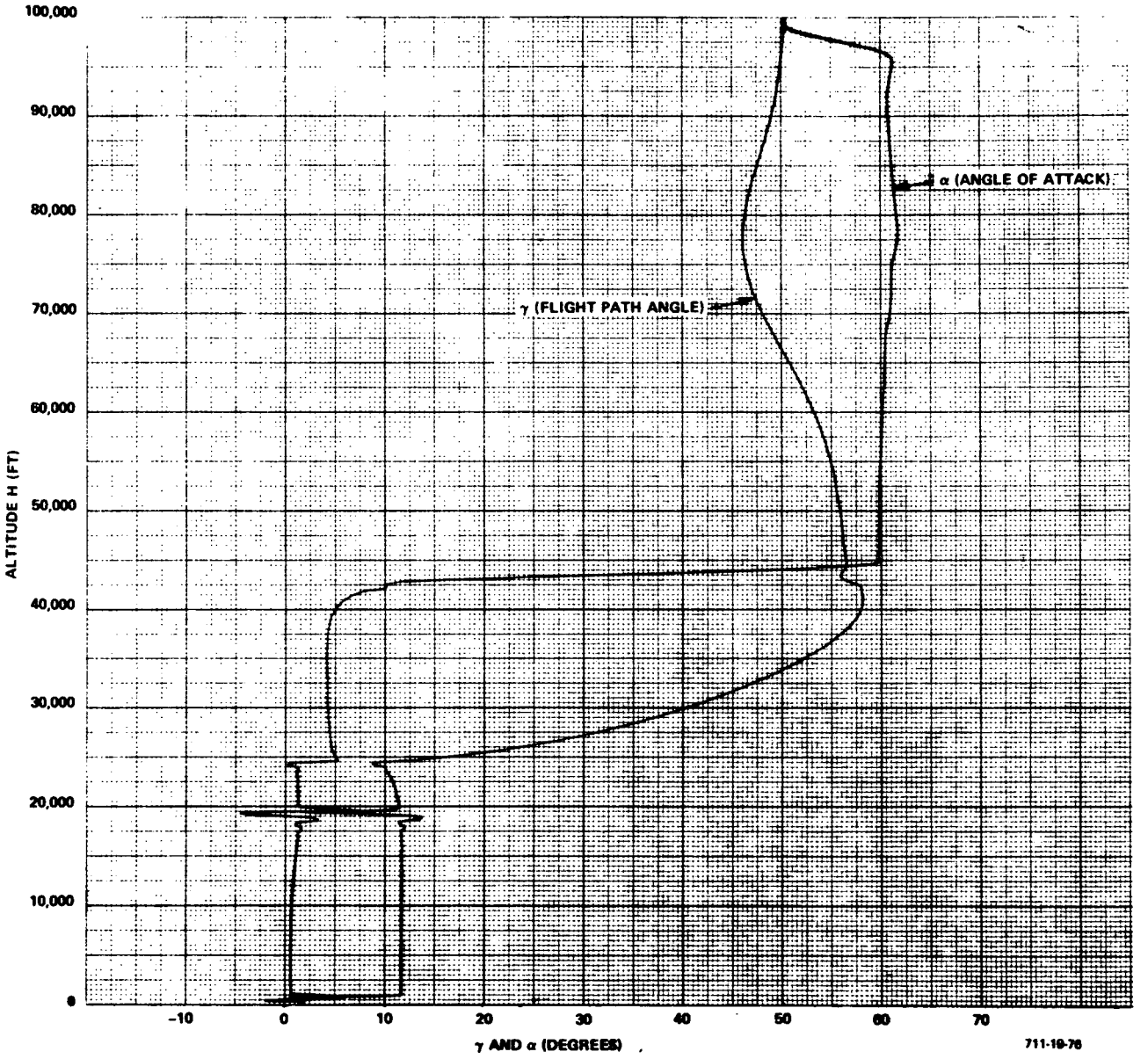

Figure 4-14
LCR (Straight Wing) MDAC-2 Orbiter Trajectories for Straight-In Flight from 100,000-Foot Altitude with Large Off-Nominal Initial γ (γ and α Profiles)

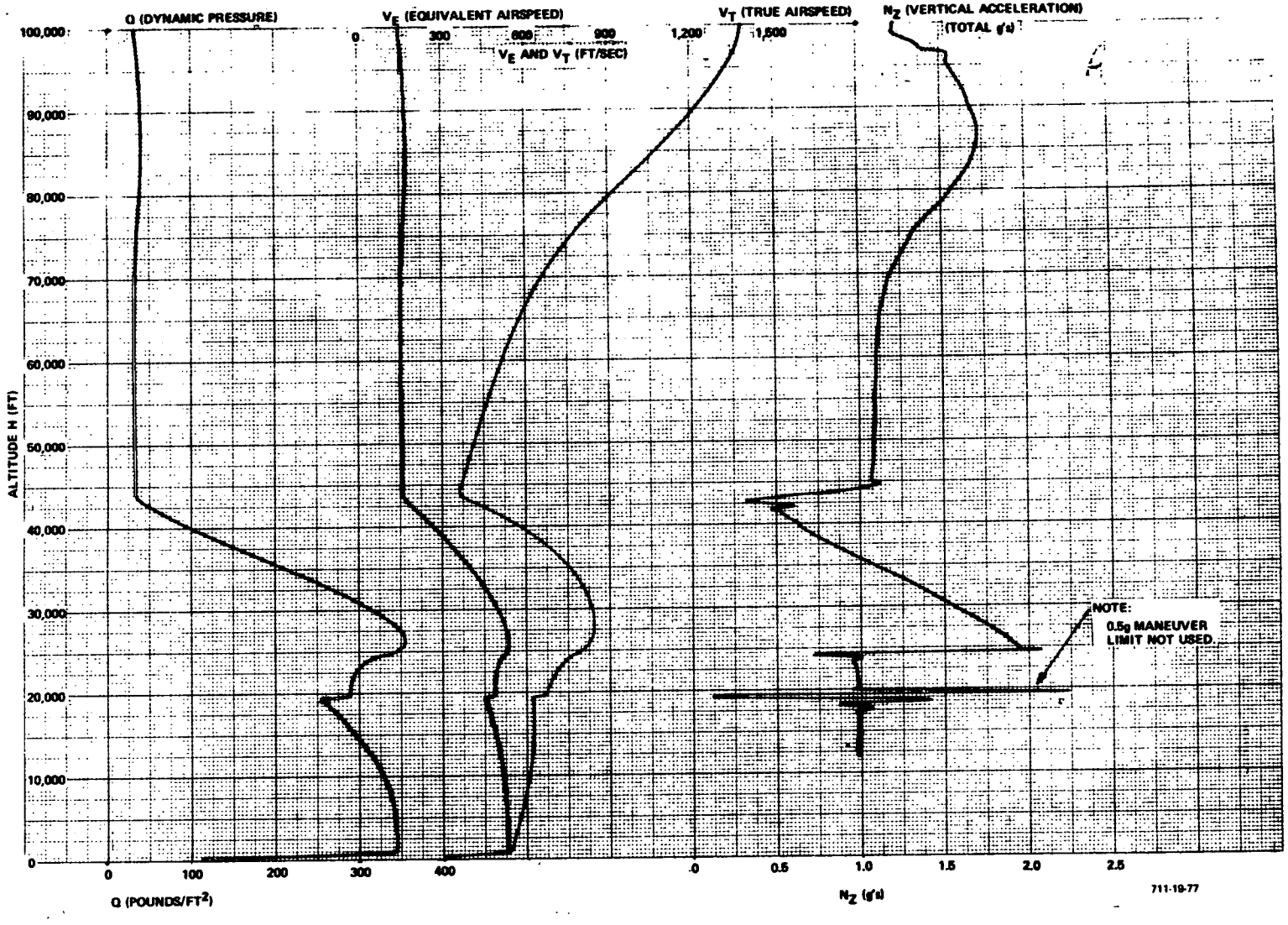

Figure 4-15
LCR (Straight Wing) MDAC-2 Orbiter Straight-In Flight from 100,000-foot Altitude to Touchdown with Large Off-Nominal Initial γ (Q, V_E, V_T, and N_Z Profiles)

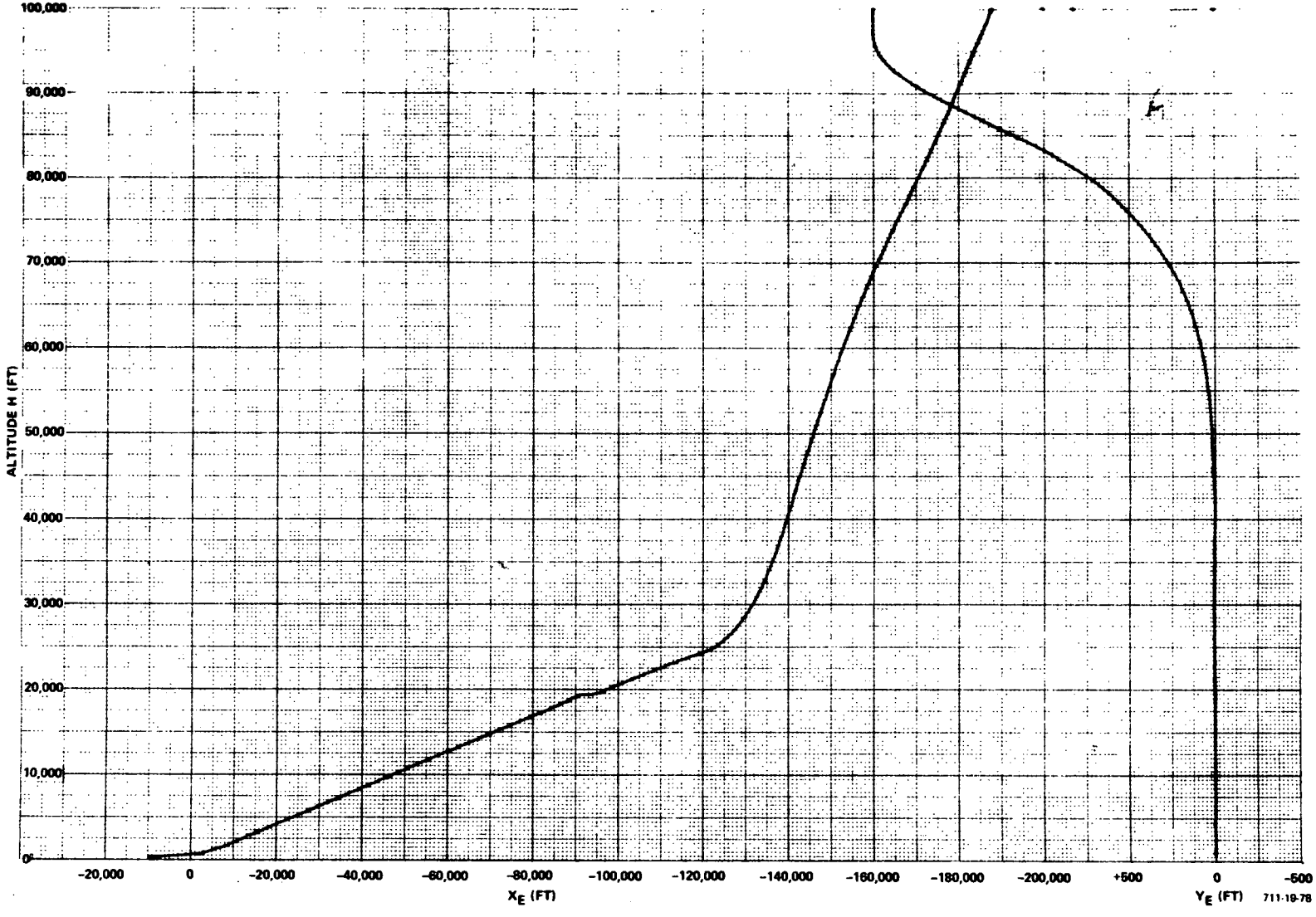

Figure 4-16
LCR (Straight Wing) MDAC-2 Trajectories for
Straight-In Approach with Lateral Offset, Altitude-
Range Profile and Lateral Error Range Profile

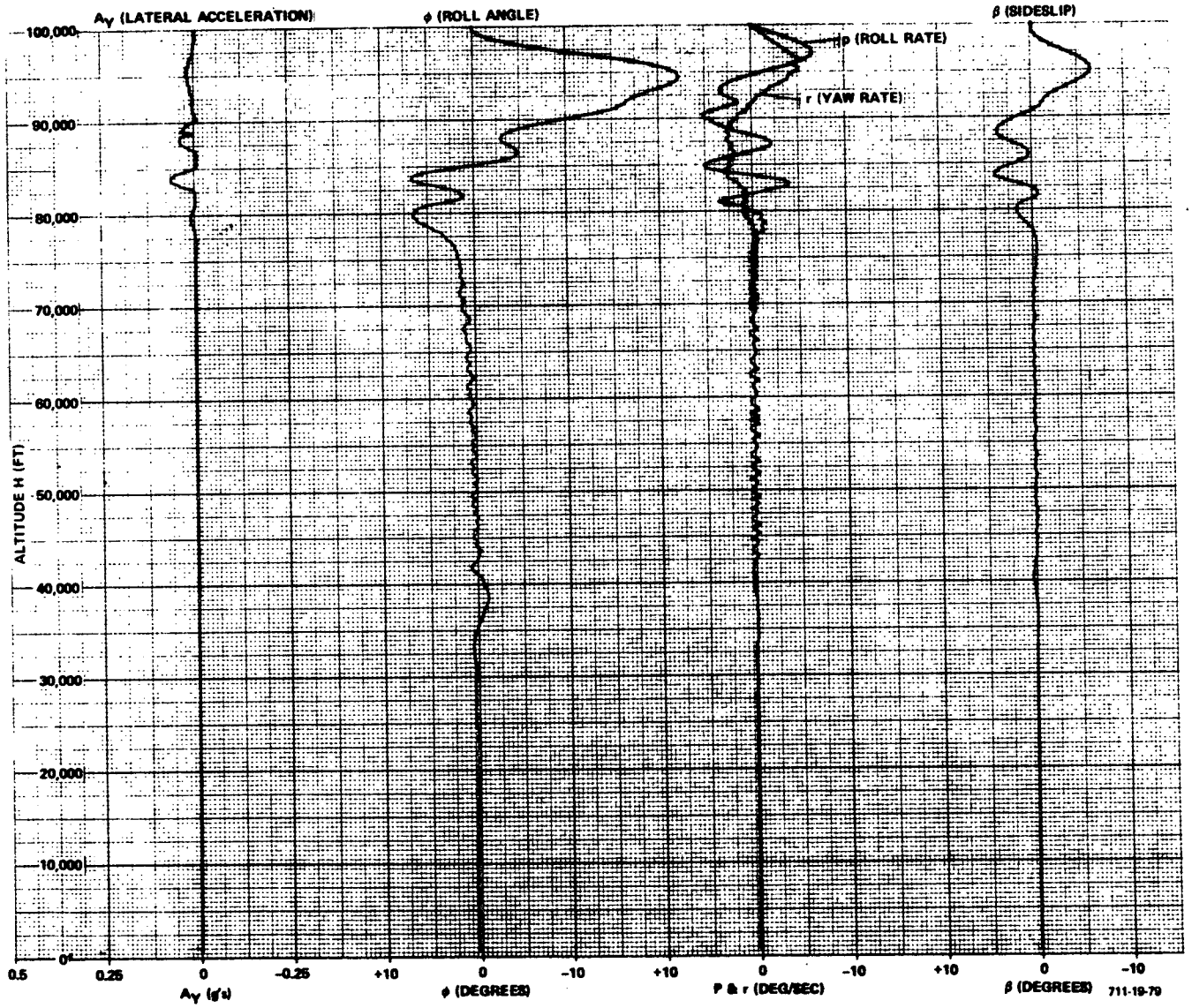

Figure 4-17
LCR (Straight Wing) MDAC-2 Orbiter Straight-In Approach with Lateral Offset Altitude History of Lateral Maneuver and Stabilization Parameters (100,000 feet to Touchdown)

steep angle glide path intercept with the ground. This trajectory is initialized with relatively severe off-nominal conditions. The initial flight path angle (γ) is about -50 degrees rather than a nominal value of about -40 degrees. The initial angle of attack (α) is about 50 degrees. The angle of attack reference is immediately changed to 60 degrees as the run starts. The α and γ histories are shown in Figure 4-14 which provides a clear picture of the transition maneuver. This maneuver starts at 45,000 feet. The angle of attack is reduced to a low value before 40,000 feet is reached and the pull-out is completed at about 25,000 feet. The trajectory approaches the terminal glide path with an offset that is eliminated as that glide path is acquired with a pull-up maneuver. For these runs the 0.5g incremental acceleration constraint was not used so that the terminal glide acquisition maneuver results in excessive g's (about 1.1g incremental). An altitude history for this trajectory showing dynamic pressure, Q, equivalent airspeed, V_E, true airspeed, V_T, and normal acceleration N_Z, is shown in Figure 4-15. Note that the landing speed has been increased to about 178 knots (300 feet per second) as suggested by the previous flareout discussion.

To complete the documentation of the LCR guidance and control performance in the descent from 100,000 feet, a set of recordings are presented that illustrate an interesting and somewhat embarassing phenomenon that has always been recognized by designers of guidance and control systems. That phenomenon is the fact that inner loops of a guidance system may be oscillatory and very objectionable from the viewpoint of handling qualities but the response of the guidance or outer loop may still be excellent. This is shown in Figure 4-16, the downrange and crossrange altitude histories of an LCR descent starting with a 2000 foot lateral offset at 100,000 feet. The lateral guidance for this initial lateral position commanded a right and then left roll maneuver to align with the desired straight-in path. As seen in Figure 4-16, the lateral guidance was precise and well damped with the reference path acquired before the nose-down transition at 45,000 feet begins. A record of the lateral-directional inner loops during the time of the turning maneuvers does not reveal the same excellent performance. As shown on Figure 4-17, roll stability is relatively poor and sideslips are excessive. All lateral-directional control is provided by the RCS (described in Section III.C) but errors in programming the control laws were not observed until the recording

of Figure 4-17 was obtained since all guidance objectives were met. The errors consisted of the following:

- The yaw control laws did not included the yaw rate washout or yaw rate command proportional to $(\frac{g}{V} \sin \phi_c \cos \theta)$. These terms are essential for sideslip minimization. The large values of β (sideslip) caused entry into poorer aerodynamic stability regions.

- The reaction control firing thresholds on the yaw and roll reaction rockets were smaller than the nominal values, thereby causing excessive limit cycle activity.

- Roll rate gains were lower than nominal.

These errors were corrected at the time that program redirection abandoned further work on LCR vehicles.

6. High Altitude Energy Management Windows

The very limited high altitude energy management window that exists for the LCR vehicle in a straight-in approach is shown in Figure 4-18. The initial heading is toward the runway. The shaded region represents the area that can be penetrated at an altitude of 100,000 feet and with the limited turning maneuvers and L/D modulation, the vehicle can be brought through transition so that it reaches alignment with the terminal glide path at 20,000 feet. The second shaded region is the area used for the transition maneuver during which no turns or range modulation is permitted. Arrows represent typical paths followed for the initial points indicated.

This window as well as the windows for other initial headings was determined empirically by varying initial conditions and running trajectories using the LCR Energy Management guidance laws described in Section III.C.

Figure 4-19 shows the shape of the window for initial headings that are oriented 90 degrees with respect to the runway. A most pessimistic view is shown of the LCR vehicle's energy management capability in Figure 4-20. As shown, an extremely small window exists for initial headings of 180 degrees with respect to the runway. (A symmetrical window also exists on the right side.) This result

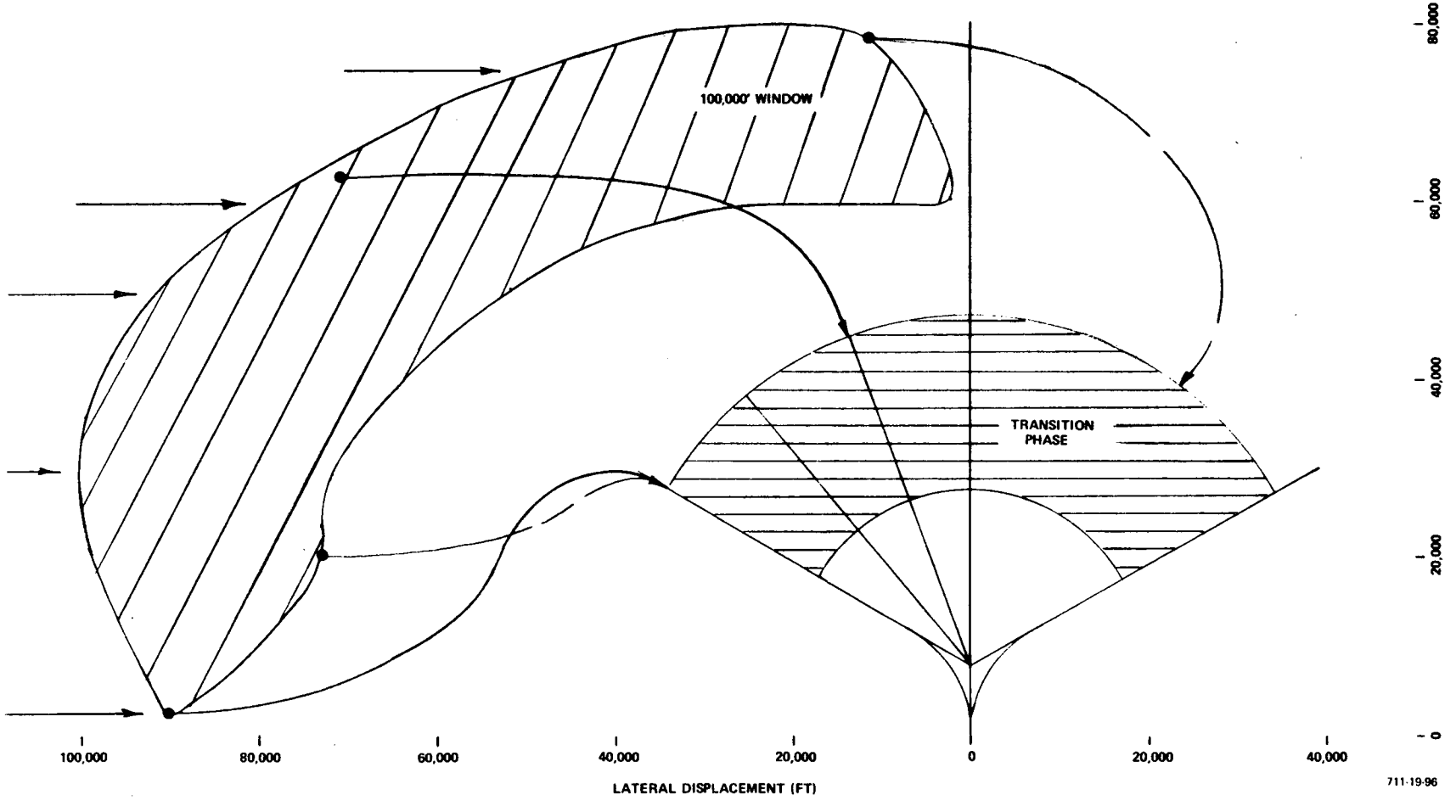

Figure 4-18
LCR Vehicle 100,000-foot Acquisition Window for Straight-In Capture

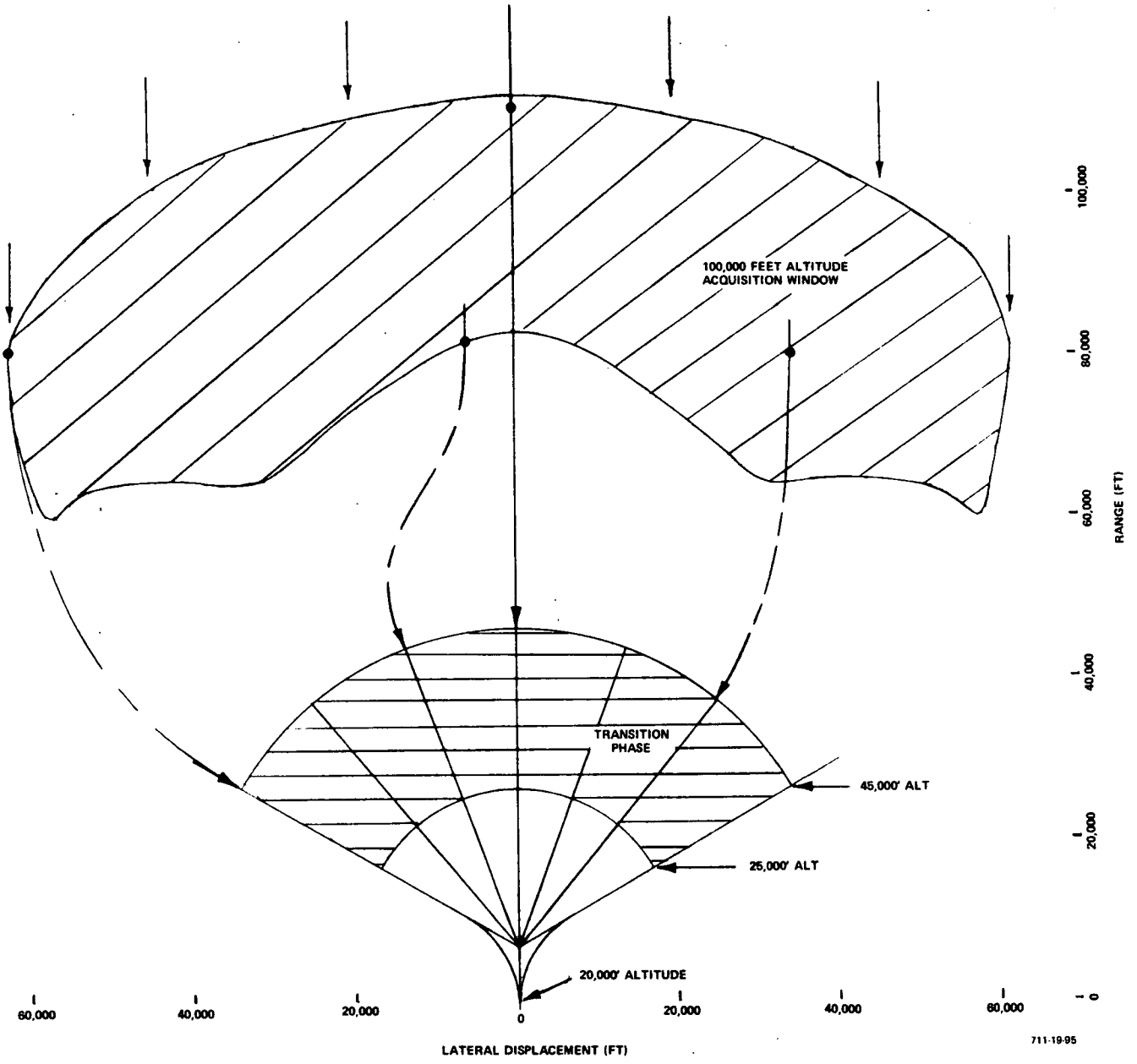

Figure 4-19
LCR Vehicle 100,000-foot Acquisition Window for Initial Heading 90 degrees with Respect to the Runway Heading

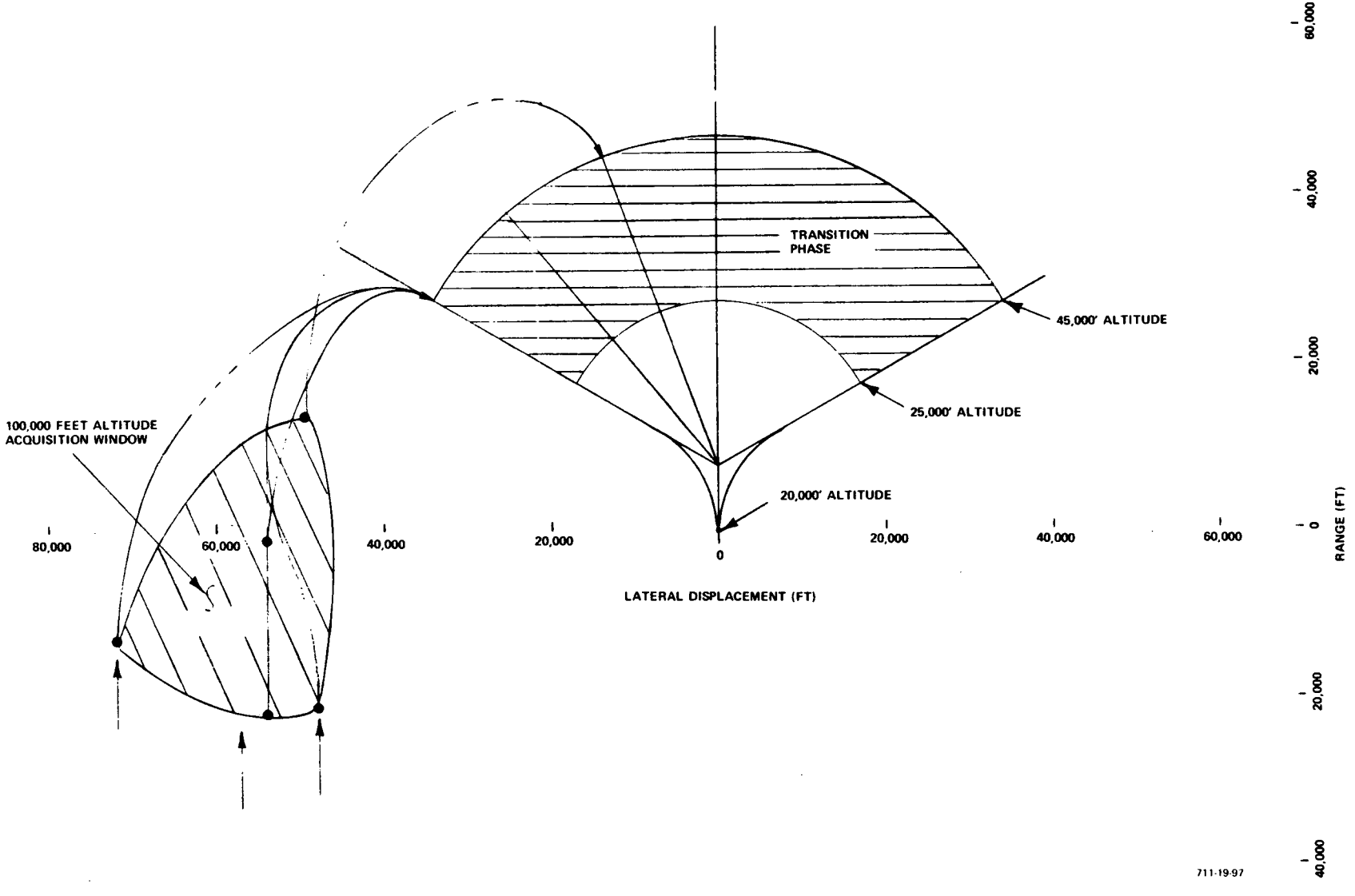

Figure 4-20
LCR Vehicle 100,000-foot Acquisition Window for Initial Heading 180 degrees with Respect to the Runway Heading

is pessimistic because the window size is smaller than the accuracy of many of the navigation devices proposed for use in this altitude region. The purpose of the energy management is to correct for navigation errors as well as other factors that produced an off-nominal trajectory. The implication of this illustration is that a 180-degree approach to the landing runway will require that all of the energy management be accomplished below 20,000 feet. This requirement reduces the range adjustment capability of the unpowered LCR vehicles to a point where unpowered landings are feasible but very marginal for some combinations of reentry errors plus adverse wind effects. This problem does not exist for HCR vehicles.

The marginal situation can be improved if we permit turning maneuvers during the latter part of the transition maneuver. During this part of the transition, a fixed angle of attack is maintained to provide a maximum pull-up maneuver consistent with vehicle acceleration limits. The pull-up g's are developed as speed and hence dynamic pressure builds up. When Q's reach about 100 pounds per square foot, reasonable aerodynamic control capability in the lateral-directional axis is available. Turning maneuvers could therefore be initiated at this time even though the pull-out has not yet been completed. If such turns are allowed, the window can be expanded by perhaps 2 NM (12,000 feet) for each of the three initial headings.

The total window for the LCR vehicle may therefore be summarized as follows:

100,000 to 25,000 feet:	Initial heading dependent per Figures 4-18 through 4-20	
25,000 to 20,000 feet:	4 NM down-range 2 NM cross-range	Estimate
20,000 to touchdown:	10 NM down-range 6 NM cross-range	Estimate

B. LMSC HIGH CROSS-RANGE, DELTA BODY ORBITER SYSTEM DESIGN STUDIES

1. Vehicle Aero Summary

Characteristics	Lockheed 8MX
	Circa 1/70
Weight (landing) - pounds	300,000
Wing Span (b) - feet	164.0
MAC (c) - feet	109.0
I_{xx} - (slug - foot^2 x 10^6)	4.7
I_{yy} - (slug - foot^2 x 10^6)	12.0
I_{zz} - (slug - foot^2 x 10^6)	15.0
I_{xz} - (slug - foot^2 x 10^6)	0.34
Ref Area (S) - foot^2	5,740
Wing Loading (W/S) - pound/foot^2	52.3
Peak L/D at Landing Condition	4.7
α for L/D_P - (degrees)	17.0
*Pitch Control Power - M_{δ_e} (1/sec^2)	-0.745
*Roll Control Power - L_{δ_A} (1/sec^2)	0.258
*Yaw Control Power - N_{δ_R} (1/sec^2)	-0.378
*For Landing Condition - Q = 150 pounds/foot^2	

The significant information (from the guidance and control viewpoint) contained in this table are the large inertias and relatively low control power. This is most important for the roll control case. A roll acceleration capability of 0.258 degree per second^2 per degree of aileron (differential elevon) will require 2-seconds to achieve a 10 degree per second roll rate for an instantaneous 20 degree δ_A deflection. This limitation would require very high surface actuator rate capability in order to achieve reasonable roll stabilization characteristics.

It is noted that the subsonic rolling moment characteristics of the rudders for this vehicle indicate that the rudders are more effective rolling moment produces than differential elevons. For example, the rolling moment due to rudder (at subsonic speeds) is:

$$C_{\ell_{\delta_R}} = 0.00027 \text{ per degree at } \alpha = 15°$$

$$C_{\ell_{\delta_R}} = 0.00065 \text{ per degree at } \alpha = 6°$$

In contrast, the rolling moment due to differential elevon at these speeds is:

$$C_{\ell_{\delta_A}} = 0.00017 \text{ per degree (at } \alpha = 0 \text{ to } 15 \text{ degrees)}$$

In the design of the lateral-directional autopilot loops, no attempt was made to exploit the rudders' rolling moment capability to improve the speed of a roll command response. The rudders are used in turn coordination and to a limited extent, when the turn coordination system attempts to yaw the vehicle into a turn, it can contribute a sideslip rolling moment that tends to speed up response. However, if the low rolling power of the differential elevons proved to be a problem, some attempt at roll maneuver augmentation through the rudders would have been attempted. This did not prove necessary.

The detailed aero characteristics for this vehicle are summarized in Reference 12. The vehicle as defined in this reference is statically and dynamically stable at all flight regimes associated with terminal control and landing. (It is also stable throughout its reentry flight regime.) The stabilization loops associated with the autopilot can nevertheless cope with considerable ranges of vehicle instability. This is discussed later in the section on parametric studies of lateral-directional stability.

The vehicle dynamic characteristics along the terminal trajectory from 100,000 feet to touchdown are summarized in Tables 4-3 through 4-6. Linearized perturbation coefficients were established for the following flight conditions:

M = 3.5, h = 100K feet

M = 1.5, h = 70K feet

M = 1.0, h = 55K feet

M = 0.5, h = 27.5K feet

M = 0.25, h = S.L.

An angle of attack of 15 degrees corresponding to the approximate peak L/D condition was used for all flight conditions. Since all coefficients are extremely dependent upon angle of attack, these linearized characteristics can only be used to provide an approximate scoping of the stabilization system design problem. Tables 4-3 through 4-6 show this vehicle to be not unlike many supersonic aircraft in regard to pitch and lateral-directional mode frequency and damping characteristics.

The status of this vehicle design was too preliminary for a detailed definition of total surface deflection or rate capability. Values for these parameters were selected in accordance with design practices in present day supersonic aircraft. These assumptions may have been somewhat optimistic in regard to differential elevon control limits and rates.

The important aerodynamic properties that establish the approach flight path equilibrium angles and speeds for the LMSC delta body vehicle are the L/D characteristics. These are converted to the glide angle VS airspeed curves as shown in Figure 4-21. The range of acceptable glide angles shown on this figure are somewhat arbitrary. The -15 degree minimum is fairly close to the peak L/D condition and leaves very little margin for glide path acquisition maneuvering. The -30 degree maximum provides a higher speed (above 275 knots) for energy management flexibility but requires a much more severe flare maneuver. The -20 degree nominal implies problems of inadequate speed margin at the time of flare but it is considered to be a reasonable compromise over the other two extremes. The basic problem with this vehicle's aerodynamic characteristics in regard to the unpowered landing problem is not so much its relatively low L/D but its high drag (C_{D_0} of equation 3-7). This causes the steep roll-off of the α vs V curve at speeds above V(L/D MAX).

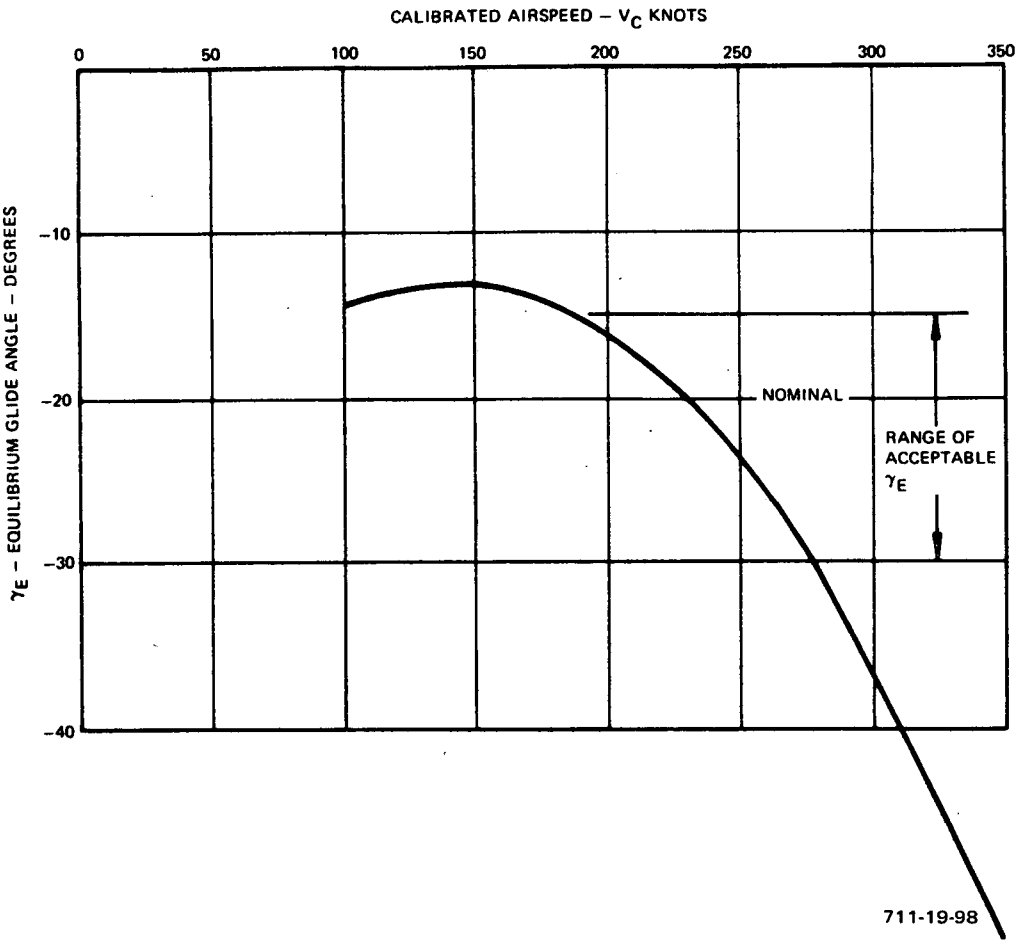

Figure 4-21
LMSC Delta Body Orbiter Equilibrium
Glide Angles versus Calibrated Airspeed

TABLE 4-3

LATERAL DIRECTIONAL TRANSFER FUNCTIONS ALONG TERMINAL TRAJCETORY

Flight Condition	$[P/\delta_A]$	r/δ_R	β/δ_A
M = 3.5 h = 100K'	$\frac{0.255(S - 0.0025)[S^2 + 2(0.05)(0.44)S + \overline{0.44}^2]}{D_1}$	$\frac{-0.147(S + 0.036)[(S^2 + 2(0.037)(0.66)S + \overline{0.66}^2]}{D_1}$	$\frac{0.00005(S + 0.037)(S + 0.01)(S + 1418)}{D_1}$
M = 1.5 h = 70K'	$\frac{0.19(S - 0.0058)[S^2 + 2(0.08)(0.63)(S + \overline{0.63}^2]}{D_2}$	$\frac{-0.347(S + 0.085)[S^2 + 1(0.11)(0.39)S + \overline{0.39}^2]}{D_2}$	$\frac{0.00009(S + 0.085)(S + 0.2)(S + 572)}{D_2}$
M = 1.0 h = 55K'	$\frac{0.278(S - 0.0086)[S^2 + 2(0.097)(0.59)S + \overline{0.59}^2]}{D_3}$	$\frac{-0.17(S + 0.12)[S^2 + 2(0.05)(0.42)S + \overline{0.42}^2]}{D_3}$	$\frac{0.00026(S + 0.13)(S + 0.026)(S + 283)}{D_3}$
M = 0.5 h = 27.5K	$\frac{0.37(S - 0.016)[S^2 + 2(0.19)(0.68)S + \overline{0.68}^2]}{D_4}$	$\frac{-0.23(S + 0.25)[(S^2 - 2(0.088)(0.92)S + \overline{0.92}^2]}{D_4}$	$\frac{0.00041(S + 0.25)(S + 0.058)(S + 237)}{D_4}$
M = 0.25 h = SL	$\frac{0.37(S - 0.024)[S^2 + 2(0.44)(0.39)S + \overline{0.39}^2]}{D_5}$	$\frac{-0.23(S + 0.44)[S^2 + 2(0.095)(1.2)S + \overline{1.2}^2]}{D_5}$	$\frac{0.00062(S + 0.44)(S + 0.1)(S + 157)}{D_5}$
$D_{1 \text{ through } 5} = \left(S^2 + 2\zeta_{DR}\omega_{DR}S + \bar{\omega}^2_{DR}\right)\left(S + 1/T_R\right)\left(S + 1/T_S\right)$		(See Table 4-4.)	

TABLE 4-4

SUMMARY OF LATERAL DIRECTIONAL DYNAMIC CHARACTERISTICS

Flight* Condition	ω_{DR} Dutch Roll Frequency	ζ_{DR} Dutch Roll Damping	$1/T_R$ Roll Subsidence	$1/T_S$ Spiral
M = 3.5 h = 100K'	0.88	0.028	0.043	0.006
M = 1.5 h = 70K'	0.85	0.058	0.095	0.0055
M = 1.0 h = 55K'	0.905	0.048	0.118	0.013
M = 0.5 h = 27.5K'	1.29	0.084	0.252	0.036
M = 0.25 h = SL	1.33	0.099	0.44	0.094
* α = 15 degrees all flight conditions.				

TABLE 4-5

LONGITUDINAL TRANSFER FUNCTIONS ALONG TERMINAL TRAJECTORY

Flight Condition	μ/δ_e	θ/δ_e	N_Z/δ_e
M = 3.5 h = 100K	$\frac{-0.67(S + 90)(S - 0.057)}{D_6}$	$\frac{-1.77(S + 0.046)(S + 0.019)}{D_6}$	$\frac{-34.2(S + 3.3)(S - 3.2)[S^2 + 2(0.149)(0.017)S + 0.\overline{017}^2]}{D_6}$
M = 1.5 h = 70K	$\frac{-1.86(S + 27)(S - 0.1)}{D_7}$	$\frac{-1.05(S + 0.1)(S + 0.07)}{D_7}$	$\frac{-33.8(S + 2.7)(S - 2.6)[S^2 + 2\ (0.21)(0.04)S + 0.\overline{04}^2]}{D_7}$
M = 1.0 h = 55K	$\frac{-5.68(S + 18.9)(S - 0.1)}{D_8}$	$\frac{-1.54(S^2 + 2)(0.93)(14)S + 0.\overline{14}^2}{D_8}$	$\frac{-54.6(S + 2.6)(S - 2.4)[S^2 + 2(0.17)(0.067)S + 0.\overline{067}^2]}{D_8}$
M = 0.25 h = SL	$\frac{-4.3(S + 54.5)(S - 1.25)}{D_9}$	$\frac{-19.8(S + 0.3)(S + 0.18)}{D_9}$	$\frac{-0.41(S + 57)(S - 79)[S^2 + 2(0.028)(0.19)S + 0.\overline{19}^2]}{D_9}$
M = 0.5 h = 27.5K			
$D_{6 \text{ through } 9} = \left(\delta^2 + 2\zeta_{SP}\omega_{SP} + \omega_{SP}^2\right)\left(S^2 + 2\zeta_{PH}\omega_{PH} + \omega_{PH}^2\right)$ (See Table 4-6.)			

TABLE 4-6

SUMMARY OF LONGITUDINAL DYNAMIC CHARACTERISTICS

Flight Condition*	ω_{SP} Short Period Frequency	ζ_{SP} Short Period Damping	ω_{PH} Phugoid Frequency	ζ_{PH} Phugoid Damping
M = 3.5 h = 100K	0.985	0.076	0.017	0.15
M = 1.5 h = 70K	1.41	0.13	0.042	0.21
M = 1.0 h = 55K	1.54	0.174	0.065	0.182
M = 0.5 h = 27.5K				
M = 0.25 h = SL	0.70	0.53	0.155	-0.001

* X = 15 degrees for all flight conditions.

2. Attitude Stabilization and Autopilot Parameters

a. Pitch Stabilization and Vertical Flight Path Control

The control equations are identical to those used for the straight wing vehicle in its aerodynamic flight regimes [equations (4-1) and (4-2)]. The gains are different for the LMSC delta body vehicle for two reasons. They are:

- Lower elevator effectiveness required increase in k_θ, pitch control static gain [equation (4-1)].
- Larger acceleration response lags (greater influence of $C_{L_{\delta E}}$) necessitated lower flight path control gains [k_h in equation (4-2)].

The gains used for the LMSC vehicle were:

$k_\theta = 3\left(\frac{300}{Q}\right)$ ... Max = 5.0

$\frac{k_q}{k_\theta} = 1.0$

$\tau = 2.0$ seconds

$k_{INT} = 0.05$ to 0.1

$k_h = 0.025\left(\frac{500}{V}\right)$ deg/ft

$a_2 = 0.05$ to 0.08

$k_\gamma = 1.0$ deg per deg

b. Lateral Directional Stabilization

The roll and yaw control equations are identical to those of the straight wing vehiclle [equations (4-4) and (4-5) respectively]. In the design of the autopilot for lateral-directional control of this vehicle, a constant gain stabilization system was synthesized. Although improvements are attainable with gain programming as a function of dynamic pressure, these were not needed for the specific aerodynamic configuration under study. (Note that guidance gains do include the velocity (V) gain programs).

Figure 4-22 is a lateral axis block diagram used to evaluate lateral control system performance. This diagram indicates all gains used and also identifies the surface rate and position limiting simulation. Referring to equations (4-4) and (4-5), the lateral directional gains used for the LMSC delta body vehicle were:

k_r = 3.0 to 5.0 deg per deg/sec

$\frac{k_p}{k_\phi}$ = 1.5 to 2.0 sec

k_ϕ = 2.0 deg per deg

k_{A_Y} = 5.0 deg per ft/sec^2

k_{RA} = 0.2 deg per deg

In comparing these control gains with the gains determined for the straight wing vehicle, a significant difference in the ratio K_p/K_{ϕ_E} is noted. The delta vehicle requires a larger rate to displacement gain than the straight wing vehicle. This is a consequence of the low aileron control power effectiveness on the delta vehicle. Lower K_p/K_{ϕ_E} gains would have allowed more rapid maneuvering responses in some cases, but sensitivity to saturation instabilities are increased. The assumption of δ_A limits of ±40 degrees and 30 degrees/seconds for $\dot{\delta}_A$ is somewhat optimistic considering that the control surfaces are elevons. Even with these limits, some degraded response was necessary.

The results obtained from 3-degree of freedom simulations at the five reference flight conditions are summarized in Table 4-7. Figures 4-23 and 4-24 are recordings of the command and disturbance responses. Sluggish roll command response is a consequence of the surface limit constraints and the need for high roll rate damping.

The sideslip experienced for the 20 degree roll command is small, ranging from 0.3 to 0.5 degrees for the typical flight conditions studied. Consequently, peak side acceleration is also reduced for this vehicle.

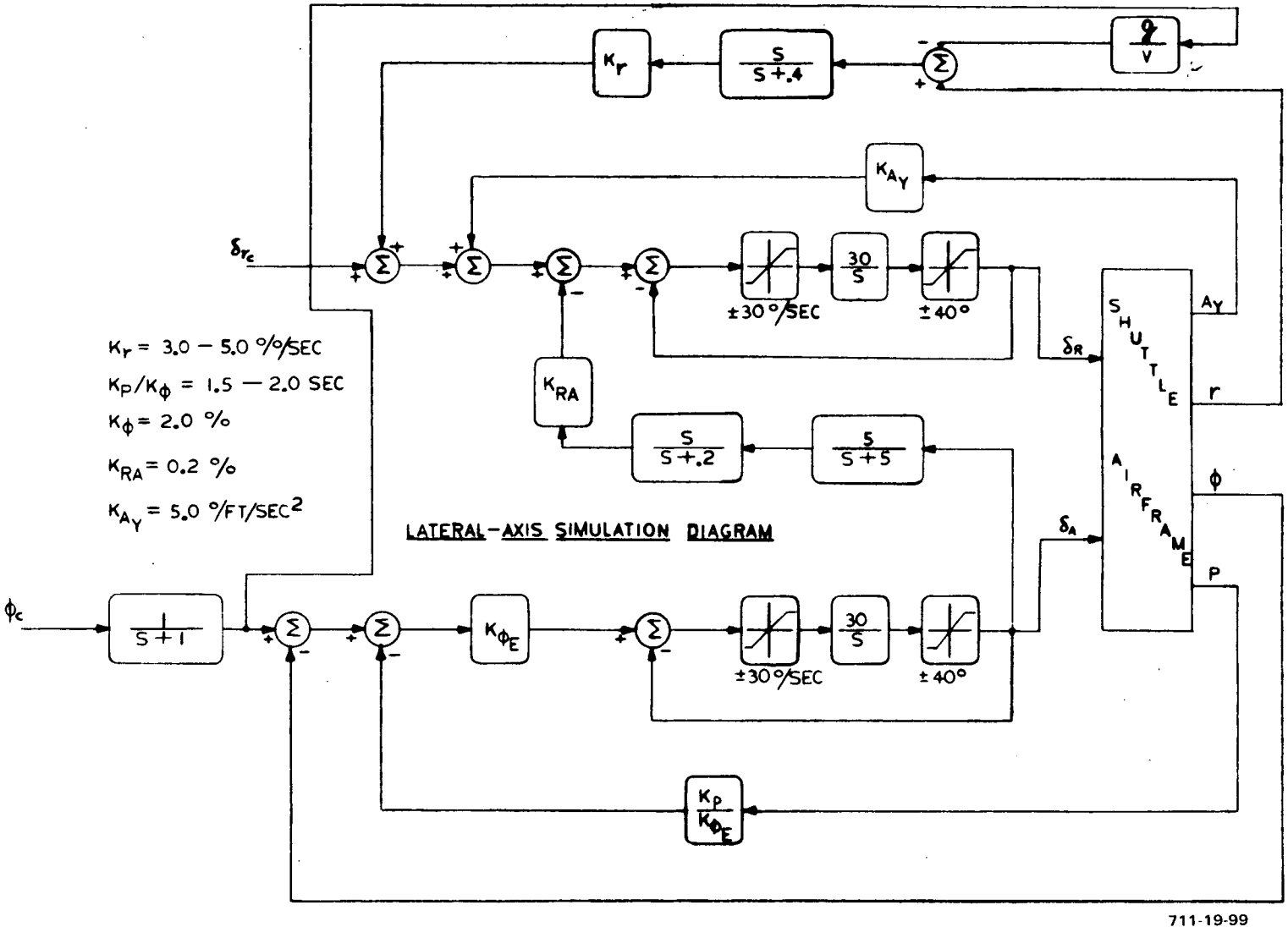

Figure 4-22
Lateral Axis Block Diagram

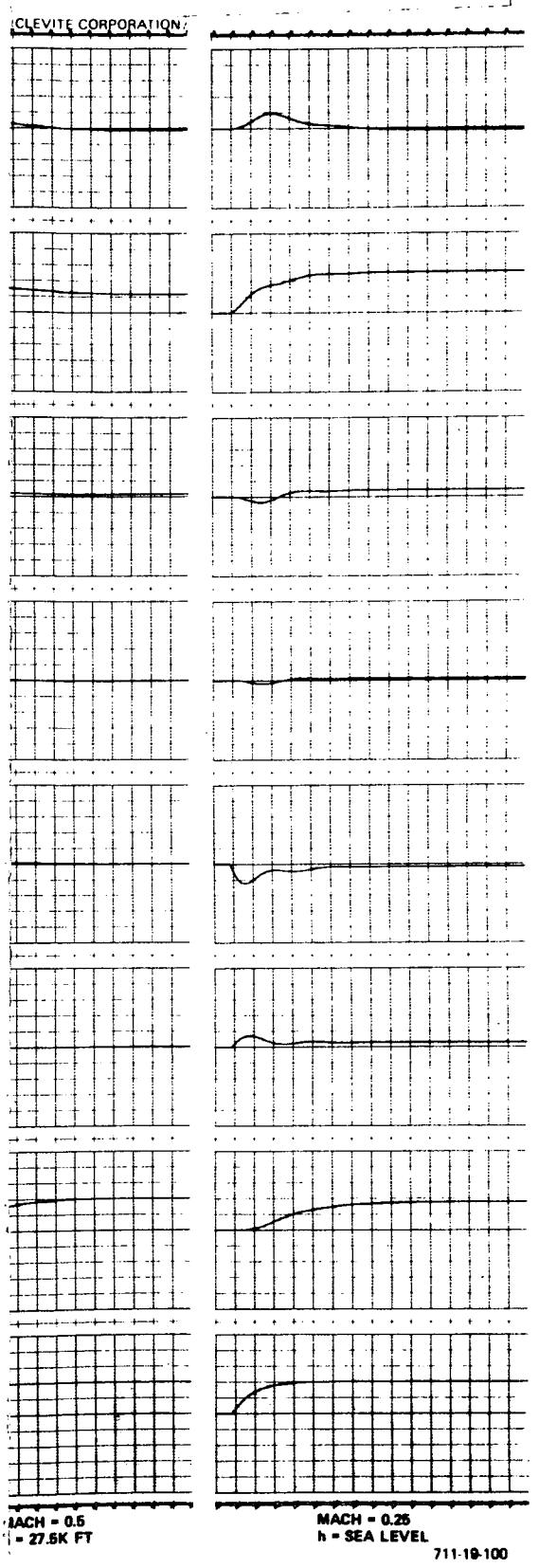

Figure 4-23
ɔmmand Responses, LMSC Delta Body Orbiter

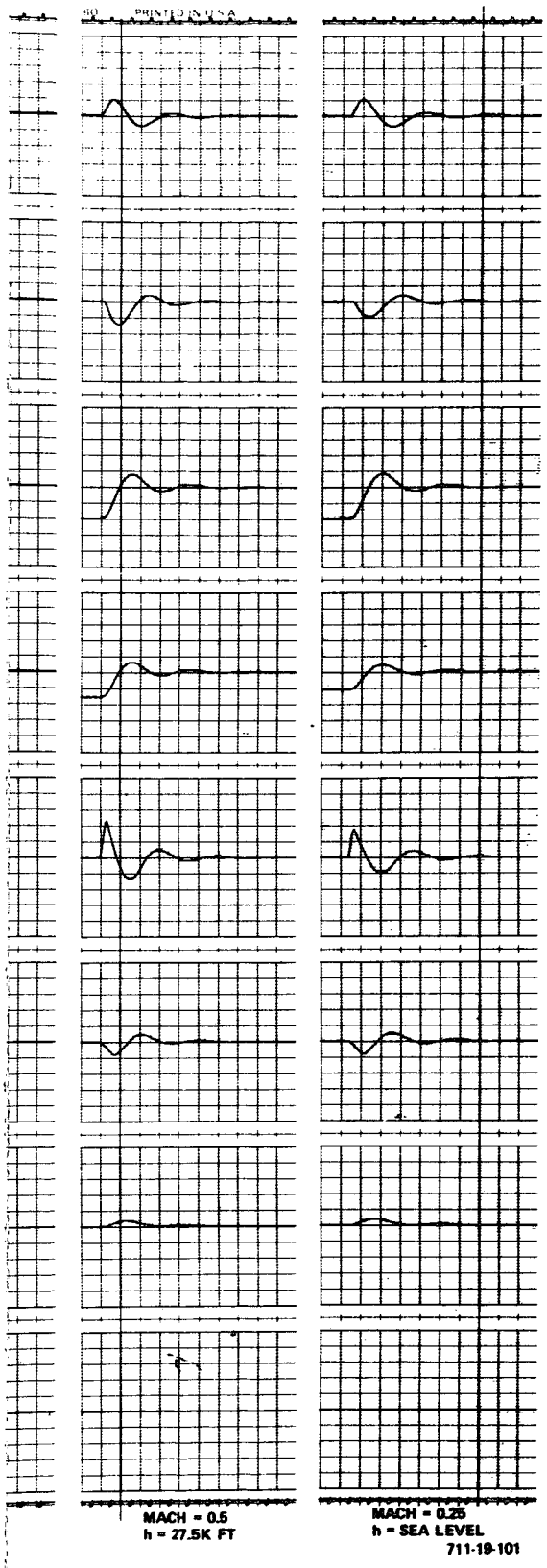

Figure 4-24
ust Responses, LMSC Delta Body Orbiter

Table 4-7 and Figure 4-24 summarize the vehicle damping for a 2 degree beta gust. In general, the vehicle responds very well to gusts with damping ranging from 0.3 to 0.4. However, larger gust inputs did tend to present some problems since actuator rate limiting began to produce instabilities. Based on these preliminary results, it appears that the rate limits are critical design parameters and in particular, the δ_A rate limit will dictate the performance attainable.

3. Final Approach and Flareout

a. Performance of Basic System

Nominal values of N_Z, Q, V, x, and α for an approach to the first flare maneuver from 20,000 feet of altitude for the delta wing orbiter are shown in Figure 4-25. The vehicle is initialized at 20,000 feet considerably out of trim. The initial response allows the closed loop steering law to establish the trim elevator. (This is done primarily by the integral term in the flight path steering law.) The vehicle is flown to the ground to demonstrate the trend in speed, Q and α. Note that the finite N_Z is due primarily to the $\dot{V}$ sin α contribution to N_Z. The equilibrium speed is about 260 knots corresponding to a Q of about 235 pounds per foot^2.

Flareout trajectories for the delta orbiter are shown in Figure 4-26 for a flare from an approach on an equilibrium glide path of -20 degrees. The first flare occurs at an altitude of 805 feet and for this 0.5g maneuver the shallow glide path is not acquired until 70 feet of altitude. Final flare employing a terminal controller occurs at 40 feet of altitude for a landing at 153 knots and α of 22 degrees with a vertical velocity of -2 feet/second. It is apparent from this performance that the segmented glide paths or two phase flareout concept is not even discernible since the shallow glide path is acquired and tracked for an altitude duration of only 30 feet.

One of the advantages of an extended run on the shallow glide path is the ability to make a final correction for position and velocity errors. The absence of a reasonable traverse time on a shallow glide path makes flareout with this vehicle sensitive to off-nominal velocities.

Figure 4-25
LMSC Delta Orbiter Nominal Glide Path Acquisition Trajectory

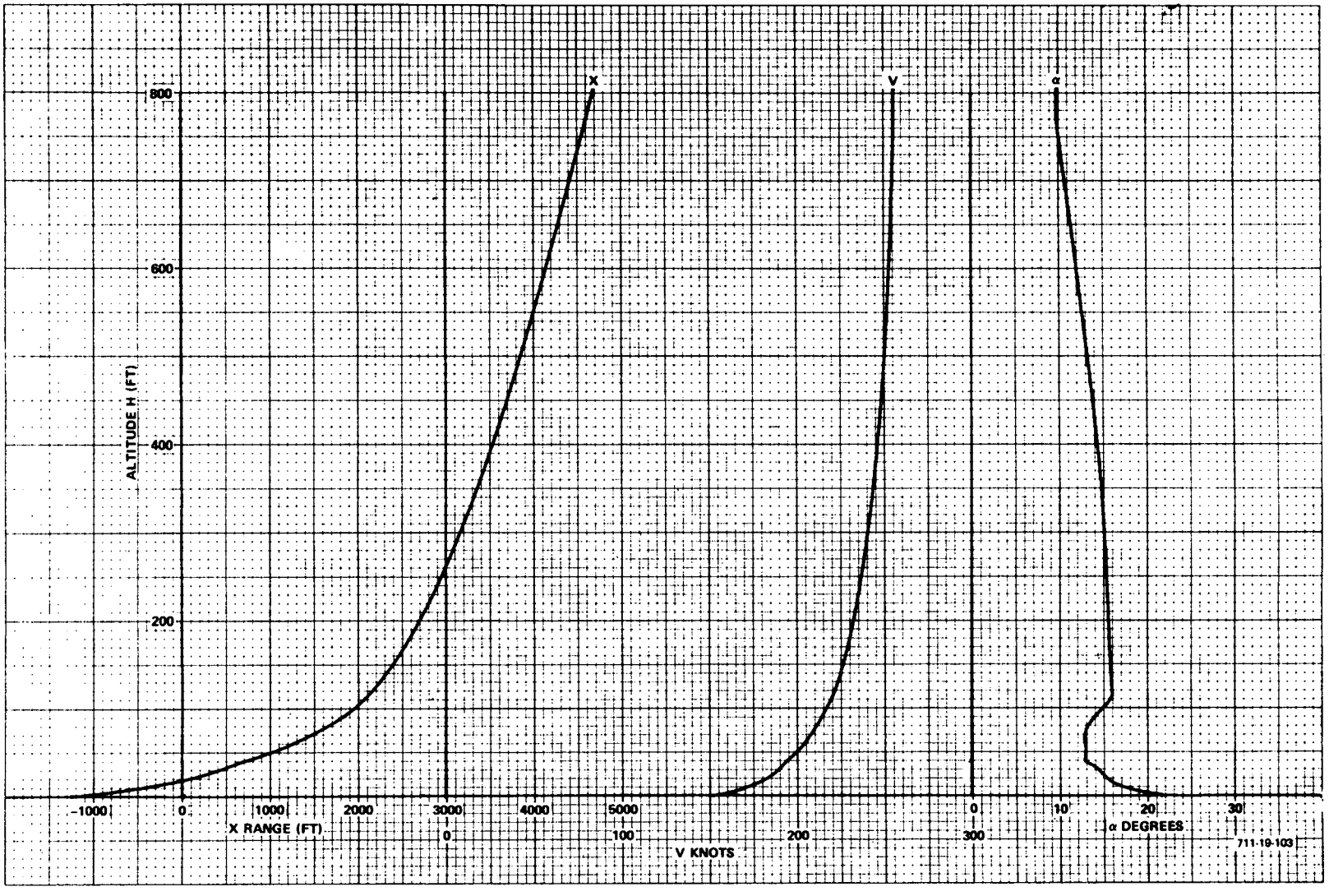

Figure 4-26
LMSC Delta Orbiter Nominal Flareout Trajectory

Figure 4-27 shows flareout trajectories for nominal and ±10 percent off-nominal velocity errors at first flare altitude with a first flare altitude correction. Whereas the touchdown range dispersions of ±300 feet are not excessive, refinements are necessary to reduce the spread of ±2.5 feet/second for vertical touchdown velocities, angle-of-attack spreads of 9 degrees, and final velocities of ±8 percent. Moreover, note that the angle of attack at touchdown for the low speed case is academic since the tail would have scraped prior to touchdown. A first flare maneuver in which 0.5g is exceeded would permit acquisition and flight on the stabilizing shallow glide slope for a longer duration.

The main problem is a consequence of the inability to acquire and sustain flight on the shallow glide path. There are two alternatives that were investigated to correct this problem. First, acquisition of the shallow path was attempted using maneuvers as high as 2.0g (incremental normal acceleration). Then, a single flare scheme was investigated with the terminal Controller guidance law initiated with this first and only flareout.

b. Performance with Single Flareout System

Landing trajectories for off-nominal initial velocities for a single flare maneuver are shown in Figure 4-28. An iterative acceleration terminal controller with ten percent integral action is employed. A predictive pitch command system acts in parallel with the closed loop terminal controller.

The pitch control laws are (as in the previous cases):

$$\delta_E = \left[\frac{3\ (2S)}{2S+1}\, q + 3\,\theta_E\right] \quad \left[1 + \frac{0.1}{S}\right] \tag{4-5}$$

where:

$$\theta_E = \theta - \theta_c$$

$$\theta_C = \left(\ddot{h}_{REF} - \ddot{h}\right)\left(0.1\right)\left(1 + \frac{0.1}{s}\right) + \theta_{C_{PREDICT}} \tag{4-6}$$

and $\ddot{h}_{REF}$ is the continuously computed vertical acceleration required to satisfy the terminal condition that the touchdown $\dot{h}$ = -2 feet per second. [The terminal controller equations were derived as equations (3-77) to (3-80) in Section IIIC].

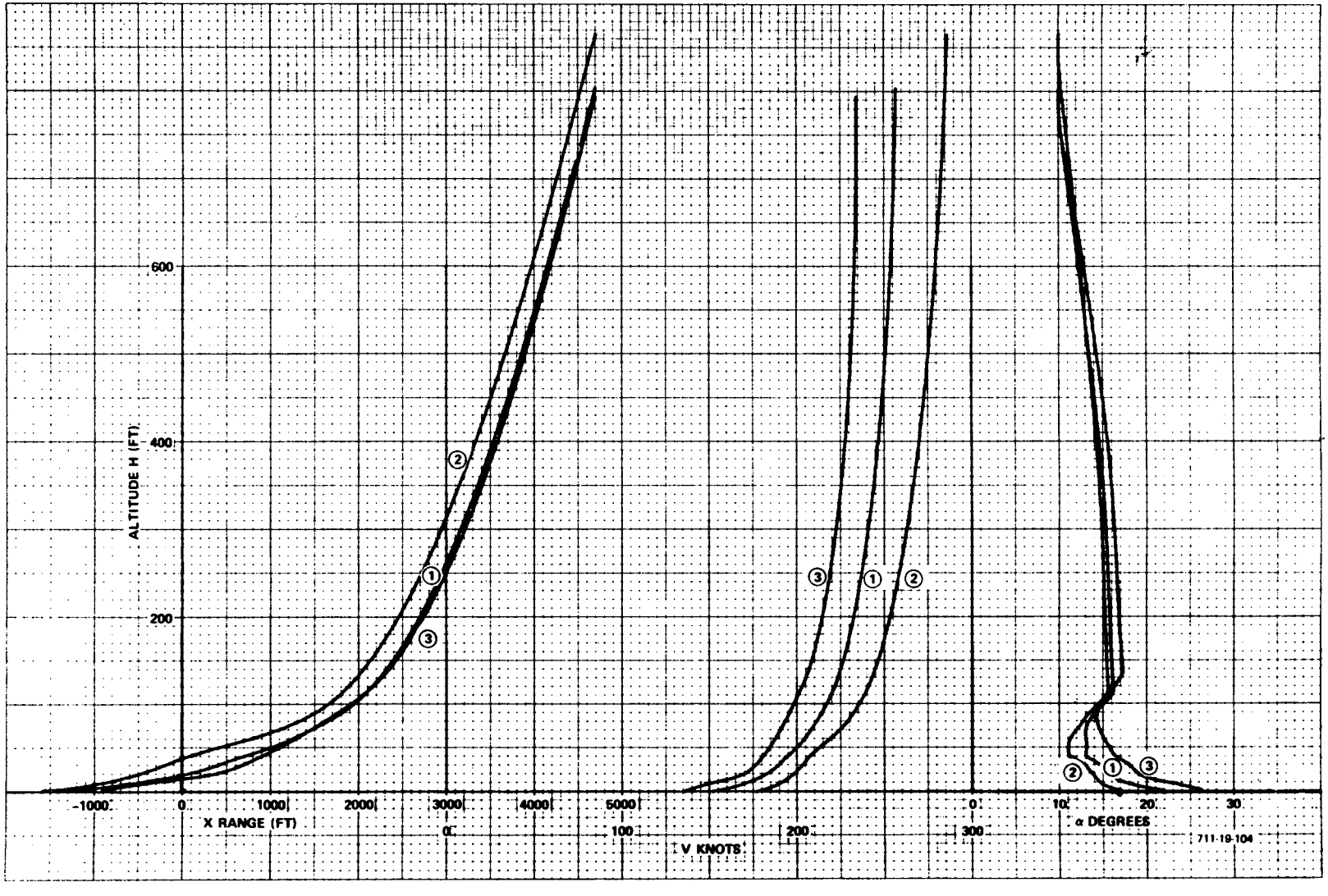

Figure 4-27
Flareout Trajectories for ±10 percent Off Nominal Initial Conditions
LMSC Delta Orbiter (Altitude Correction for Initial Flare)

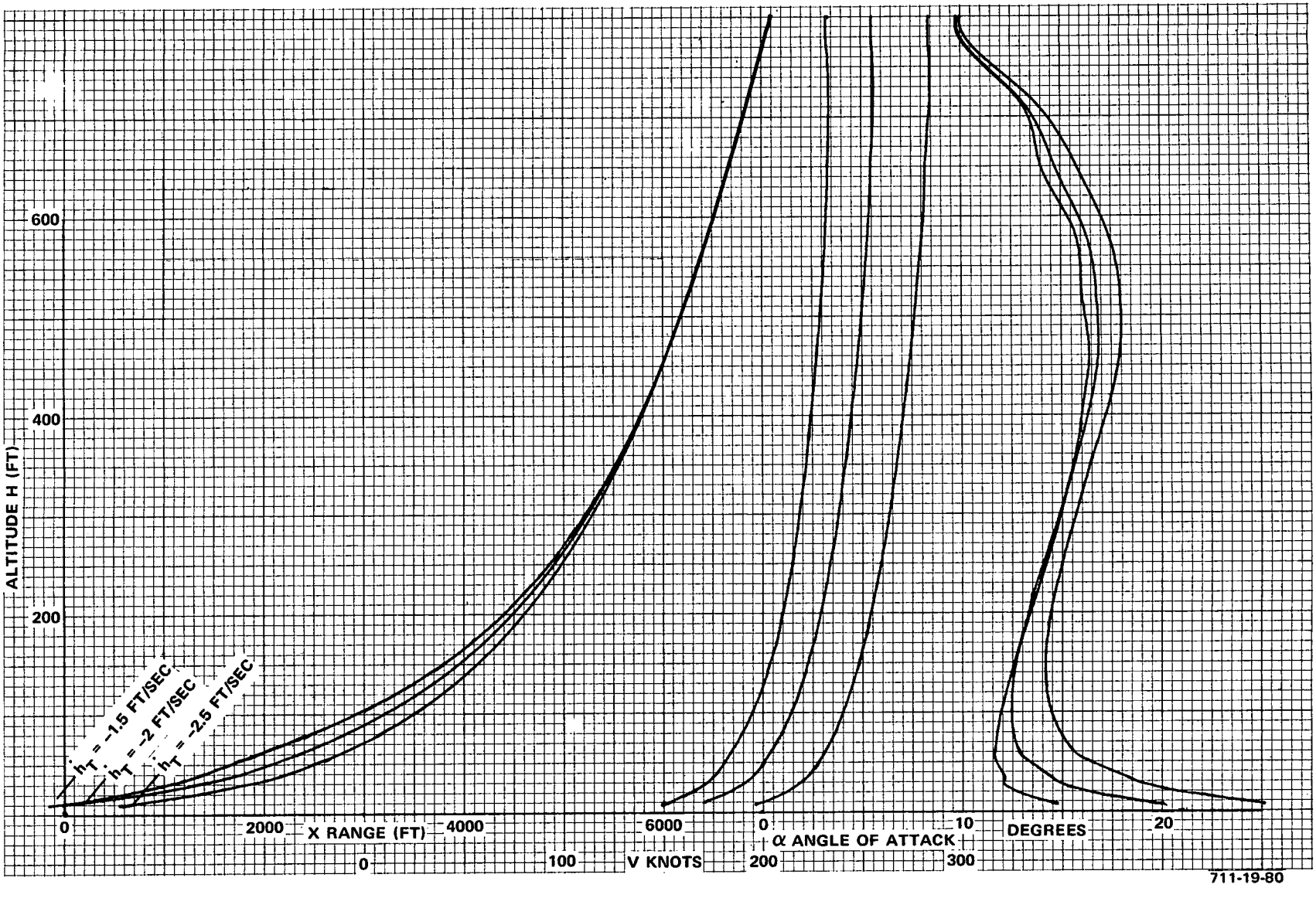

Figure 4-28
Terminal Trajectories for the LMSC Delta Orbiter,
Employing a Single Flare with Terminal
Controller for a Nominal 0.93g Peak Maneuver

As illustrated in Figure 4-28, the flare maneuver is initiated at about the same altitude that the two stage flare was initiated in Figures 4-26 and 4-27 with this vehicle. In these previous flareouts the peak incremental normal acceleration reached 0.5g whereas in the maneuvers illustrated in Figure 4-28 the acceleration level peaks at 0.93g. Compared to these previous results with a two-stage flare that did not incorporate compensations for speed errors, the single flare technique achieves good results. Touchdown vertical velocity dispersions are reduced to ±0.5 feet per second and range dispersions are ±375 feet. The nominal touchdown occurs 750 feet down-range of the intercept of the shallow glide path (if we used a shallow glide path). The nominal touchdown speed is 170 knots and the nominal angle of attack is about 20 degrees. The spread in angle of attack and landing speed is very large for off-nominal initial velocities.

c. Improved Two Phase Flareout System

The first improvement over results described by Figures 4-26 and 4-27 is obtained by adjusting the first flare initiation altitude and the predictive pitch command as a function of initial speed error. The results are summarized in Figure 4-29. A nominal 0.5g maneuver is used in the initial flare to acquire the shallow glide path. It is apparent that we are still not on that shallow path for any significant distance. However, the touchdown vertical velocity dispersion is good; (total spread of 0.6 feet per second) with the off-nominal conditions resulting in softer landings but longer runway consumptions. Also, the angle of attack and touchdown speed dispersions are considerably improved over those obtained with the single flareout system. The nominal landing speed, however, is greater than for the single flare system.

A second improvement aimed at achieving longer times on the shallow glide path was also investigated. Higher g-maneuvers were used to acquire the shallow glide path.

The altitude and range histories of Figure 4-30 depict various acquisition maneuvers from 0.5g to 1.5g in which the shallow glide slope was flown into the ground for an α_T = 15 degrees. These trajectories show that a point of diminishing returns is reached at about 1.25g. (That is, higher

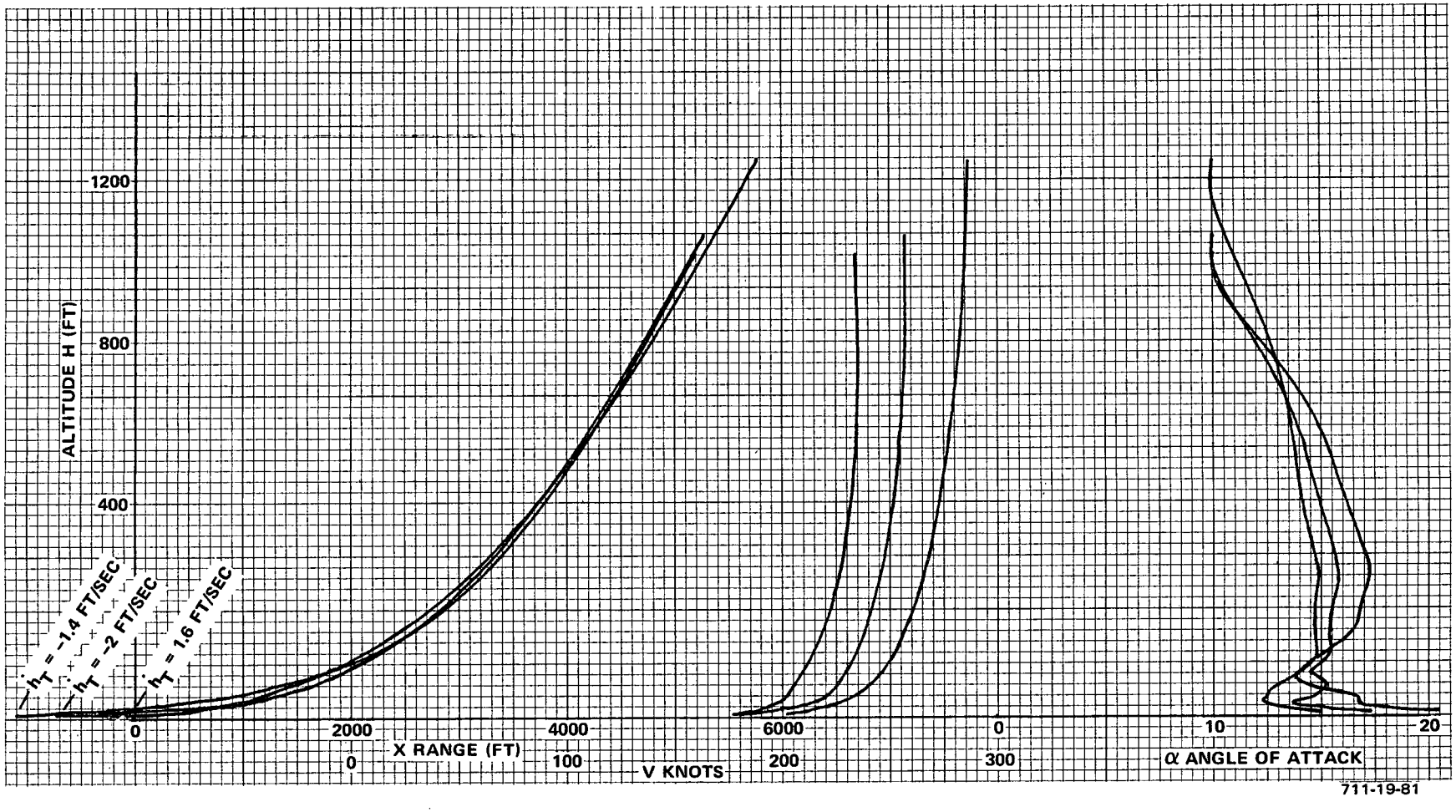

Figure 4-29
Improved Flareout Trajectories for LMSC Delta Orbiter

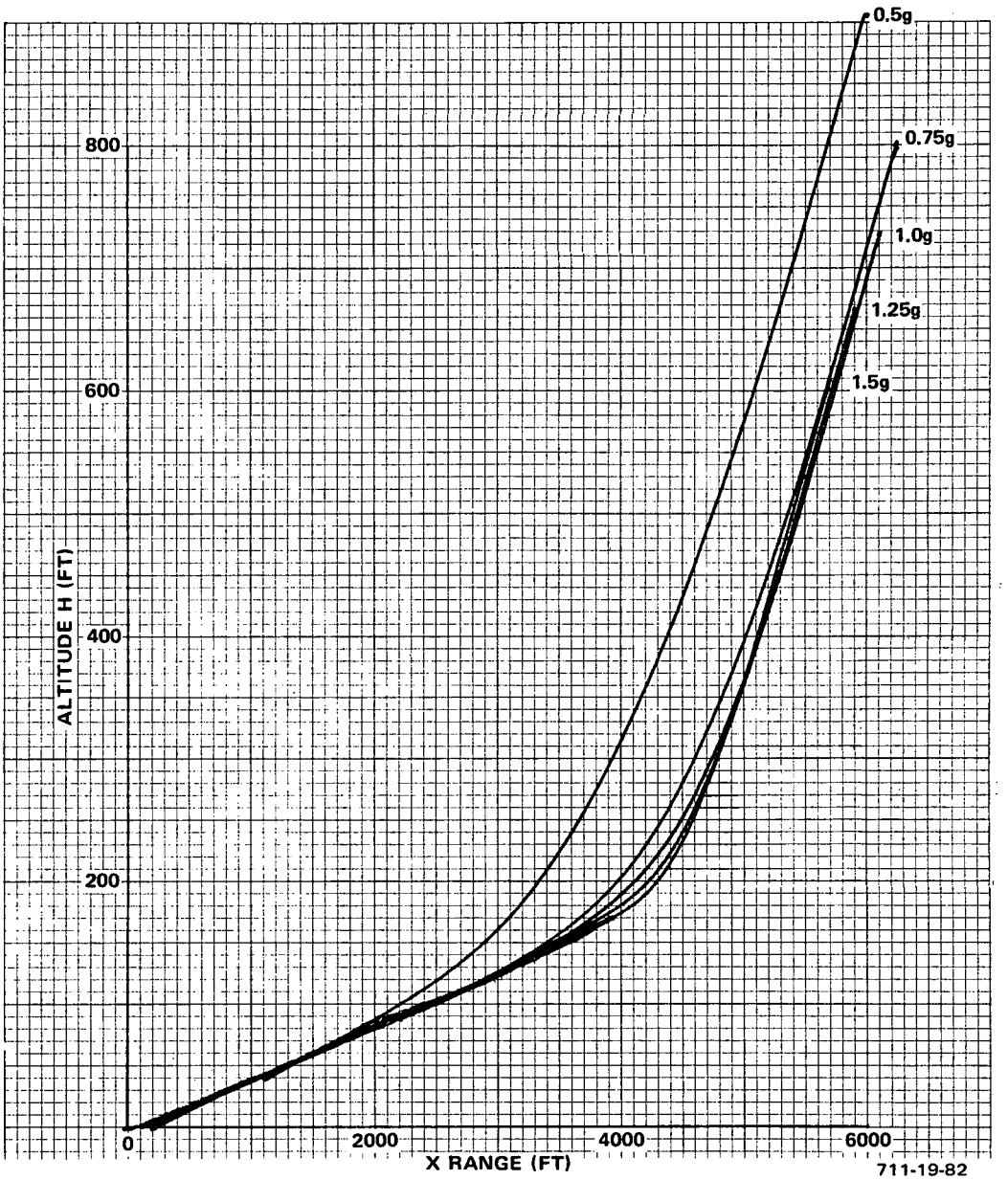

Figure 4-30
Delta Orbiter (LMSC) Flight on Shallow Glide Slope
with no Final Flare and α_T = 15 degrees
for Various Acquisition g Maneuvers

g-maneuvers permit flaring at lower altitudes but result in higher drag and therefore increased decelerations during the maneuver. The shallow glide slope is acquired at an altitude of 175 feet with a 1.5g maneuver; an increase in altitude on the shallow path of 100 feet over that obtained with the 0.5g maneuver. Figure 4-31 shows the results in touchdown performance. Vertical velocity touchdown spreads are now ±0.35 feet per second with range dispersions of ±300 feet, angle of attack spreads of 7 degrees and final velocities of ±10 percent. In conclusion, satisfactory touchdowns for the LMSC-HCR orbiter have been demonstrated which approach the performance levels achieved with the LCR-straight wing orbiters. The performance criteria on which this conclusion is based are touchdown vertical velocity and fore-aft (x) dispersion as tested by off-nominal velocity conditions at flareout. The LMSC vehicle was not tested in simulations that included turbulence, winds, and wind shears.

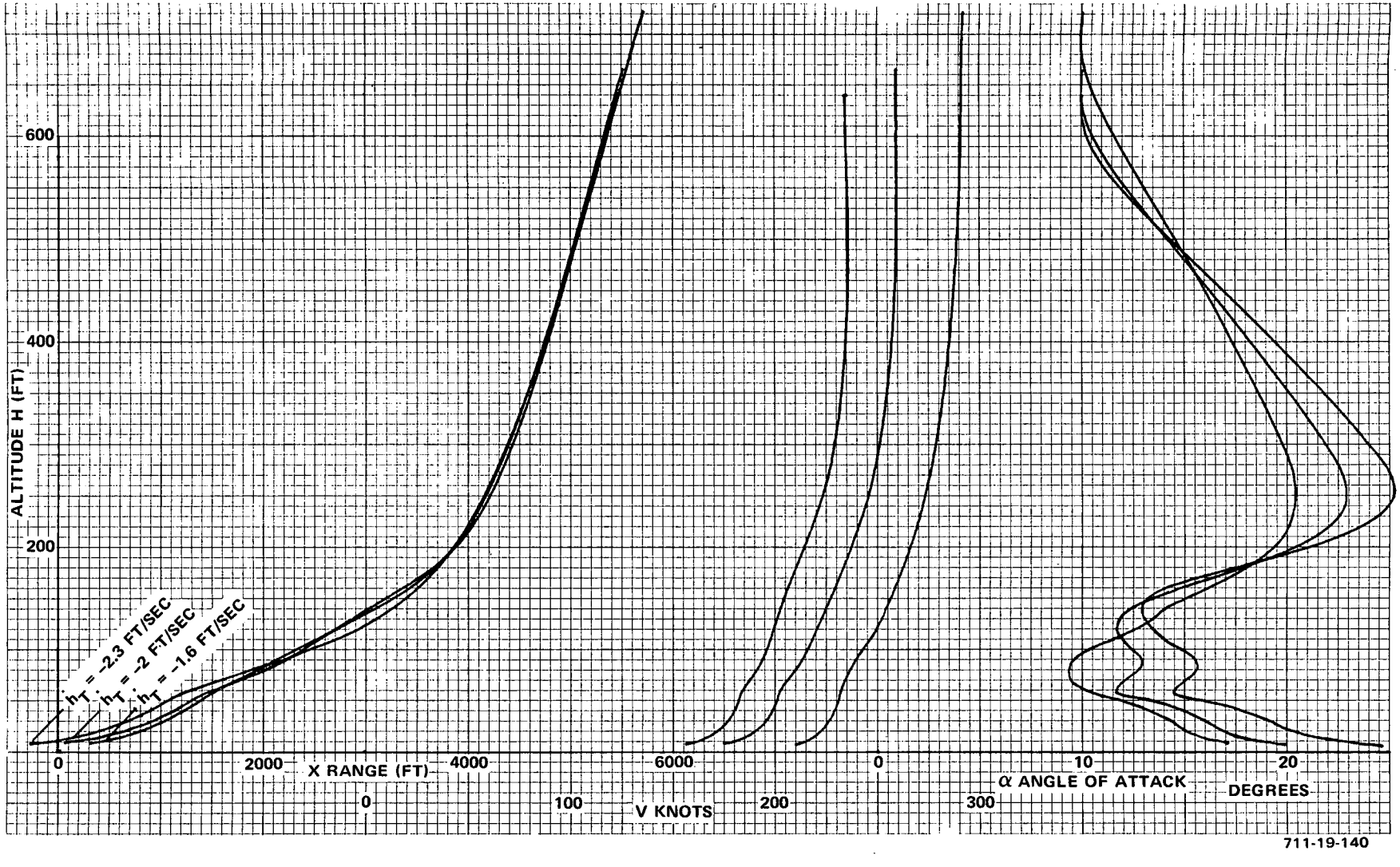

Figure 4-31
Terminal Trajectories for the LMSC Delta Orbiter Employing a 1.5g Landing Maneuver

4. Lateral Stabilization Parametric Studies

In hypersonic flight and at high angles of attack, there is a trend toward loss of static directional stability (N_β becomes negative). Whether the negative trend in N_β results from masking of vertical tail area at high values of α, or forward shift of the aerodynamic center at hypersonic speeds, it would appear that dutch roll stability can be retained if the dihedral effect, L_β, is sufficiently stable. That is, the vehicle dutch roll frequency is approximately equal to

$$\omega_D^2 = N_\beta \cos\alpha - L_\beta \sin\alpha = C_{n_\beta} \cos\alpha - \frac{I_z}{I_x} C_{l_\beta} \sin\alpha \qquad (4\text{-}7)$$

where stable L_β is negative. Recognizing this phenomenon as

$$C_{n_{\beta\,(\text{dynamic})}} = C_{n_\beta} \cos\alpha - \frac{I_z}{I_x} C_{l_\beta} \sin\alpha, \qquad (4\text{-}8)$$

aerodynamicists tended to consider a positive $C_{n_{\beta\,(\text{dynamic})}}$ as an acceptable design objective. A vehicle with positive $C_{n_{\beta\,(\text{dynamic})}}$ and negative C_{n_β} will not provide acceptable handling qualities nor will it accept conventional roll and yaw dampers to improve dutch roll damping. The relationships of the various lateral coefficients to handling quality criteria in the presence of negative C_{n_β} have been identified in many handling quality studies (See reference 31, for example.)

The problem can be described intuitively as follows:

- The yawing moment due to sideslip is divergent
- Build-up of sideslip causes a stable rolling moment that causes roll angle to build-up in a direction that tilts the lift vector to produce a corrective lateral acceleration (with respect to the velocity vector)
- The lateral acceleration integrates into a lateral velocity opposite to the lateral velocity resulting from the original sideslip build-up

- This reduces the original sideslip and with the proper combination of other lateral-directional coefficients, a convergent dutch roll oscillation results.

- A roll damper or roll attitude constraint prevents the build-up of the corrective rolling motion. The vehicle therefore diverges in yaw.

To cope with this problem artificial directional stability must be achieved by yawing the vehicle to oppose the build-up of sideslip. The lateral acceleration feedback loop achieves this objective. Thus, the acceleration loop not only serves to improve turn coordination, but it makes an essential contribution to lateral directional stability when N_β becomes negative. The LMSC delta body orbiter was used to define a baseline vehicle from which all the critical lateral-directional coefficients could be varied to determine the sensitivity and capability of the recommended lateral-directional control system. It was demonstrated that the lateral acceleration loop creates a wide stability window that permits good stabilization characteristics for a wide range of possible N_β, L_β and α variations.

Table 4-7 is a summary of figures that demonstrate the relationship between control loop parameters and vehicle lateral directional characteristics at the M = 0.5, h = 27.5K flight condition.

Figure 4-32 demonstrates the nature of the $C_{n_{\beta\,(dynamic)}}$ problem discussed above. N_β is made significantly negative (-0.5). The nominal normal value of N_β is +0.463. Figure 4-32 shows that a convergent dutch roll exists with both the yaw and roll dampers off ($K_r = K_p = 0$). This illustrates the fact that $C_{n_{\beta\,(dynamic)}}$ is positive at the 15 degree angle of attack. The damping ratio, however is below 0.1. Now if we increase the yaw damper (yaw rate feedback to rudder) by itself we only deteriorate damping. A short period oscillation becomes divergent if we increase the roll damper (roll rate feedback to roll surface) by itself. We also decrease damping; this time by making a long period oscillation divergent. The closure of both damper loops simultaneously, however,

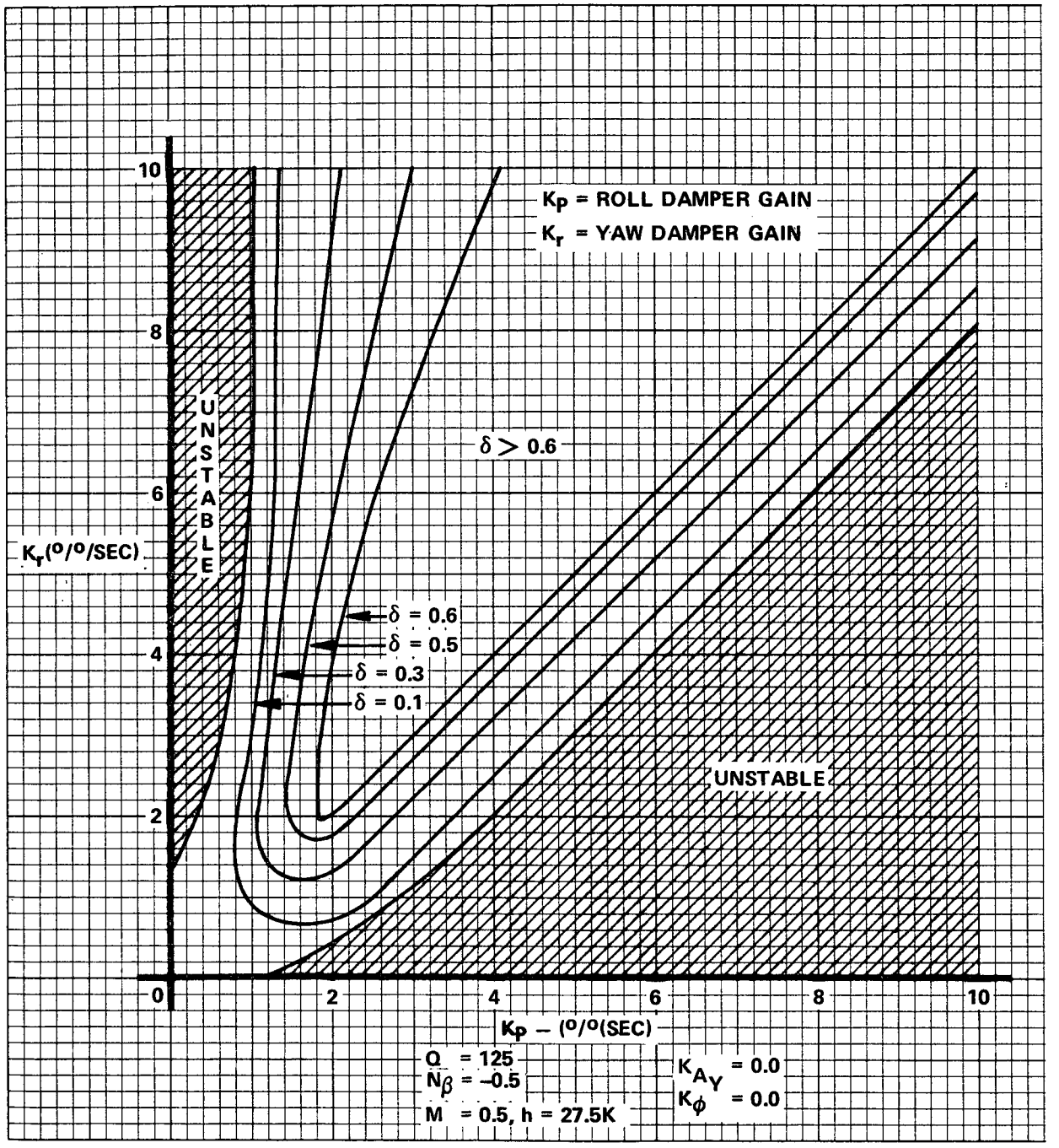

Figure 4-32
Roll and Yaw Damper Stability Regions,
Negative N_β, No Acceleration Feedback

TABLE 4-7

LATERAL DIRECTIONAL PARAMETRIC STUDY
FIGURE SUMMARY

Figure Number	Description
4-32	K_r versus K_p for $N_\beta = -0.5$, $K_{A_Y} = K_\phi = 0$
4-33	K_r versus K_p for $N_\beta = -0.5$, $K_{A_Y} = K_\phi = 2$
4-34	K_r versus N_β for $K_p = K_\phi = K_{A_Y} = 0$
4-35	K_r versus N_β for $K_p = 4$, $K_{A_Y} = K_\phi = 0$
4-36	K_r versus N_β for $K_p = 4$, $K_{A_Y} = 2$, $K_\phi = 0$
4-37	K_r versus L_β for $K_p = K_\phi = K_{A_Y} = 0$
4-38	K_r versus L_β for $K_p = 4$, $K_\phi = K_{A_Y} = 0$
4-39	K_r versus L_β for $K_p = 4$, $K_{A_Y} = 2$, $K_\phi = 0$
4-40	K_r versus L_β for $K_p = 4$, $K_{A_Y} = K_\phi = 2$
4-41	K_r versus K_p for $\alpha = 0°$, $K_\phi = K_{A_Y} = 2$
4-42	K_r versus K_p for $\alpha = 15°$, $K_\phi = K_{A_Y} = 2$
4-43	K_r versus K_p for $\alpha = 30°$, $K_\phi = K_{A_Y} = 2$

NOTES:
1. Parametric studies show curves of constant damping ratio represented by the symbol δ.
2. All figures are for M = 0.5, h = 27.5K feet where the nominal $L_\beta = -4.56$ and the nominal $N_\beta = +0.463$ and nominal $\alpha = 15$ degrees.

results in good stability. Gains of 2 or 3 for both dampers result in excellent stability. This stability is deceptive and has nothing to do with handling qualities or autopilot stability. If we now attempted to apply a roll angle constraint, even at a relatively low gain, the lateral directional system will become divergently unstable. With low gain roll constraints a long period divergent oscillation will develop. With higher gain roll constraints, a flat sideslip divergence will occur.

Figure 4-33 shows the dramatic elimination of the instability boundaries when the A_y feedback into rudder is closed. The narrow stability window of Figure 4-32 disappears. This figure includes a roll loop closure with a gain of 2.0. Such a loop was divergently unstable for any combination of K_p and K_r gains without the A_y feedback. Now some relatively high roll rate gains are needed to achieve a well damped response with a roll loop gain of 2.0 but this roll rate gain requirement can be lowered with a lower roll gain or increased A_y and yaw rate gains.

The role of the A_y feedback is illustrated in a different form with a parametric plot of stability regions for variable N_β. Figure 4-34 shows the case for zero roll control and no A_y feedback. This figure shows how low directional stability makes a sharply increasing demand on yaw damper gain until in negative N_β regions a yaw damper becomes totally ineffective. Figure 4-35 shows that the addition of a roll damper opens the stability window a little wider, but again, high yaw damper gains are needed to cope with small values of negative N_β, but, as discussed previously, this apparent stability is meaningless if we attempted to constrain roll angle. Figure 4-36 shows the wide opening of the window of acceptable unstable N_β with the addition of the A_y into rudder feedback. It is noted however, that although good stability is theoretically possible for N_β as large as -3, the yaw damper gain requirement is unrealistic. The practical limitations of high gain augmentation loops (structural instabilities, actuator limit problems, etc) preclude the consideration of these electronic augmentation systems for very unstable vehicles.

Figures 4-37 through 4-40 define the stability region characteristics when the vehicle parameter being varied is L_β. As long as L_β is not too stable,

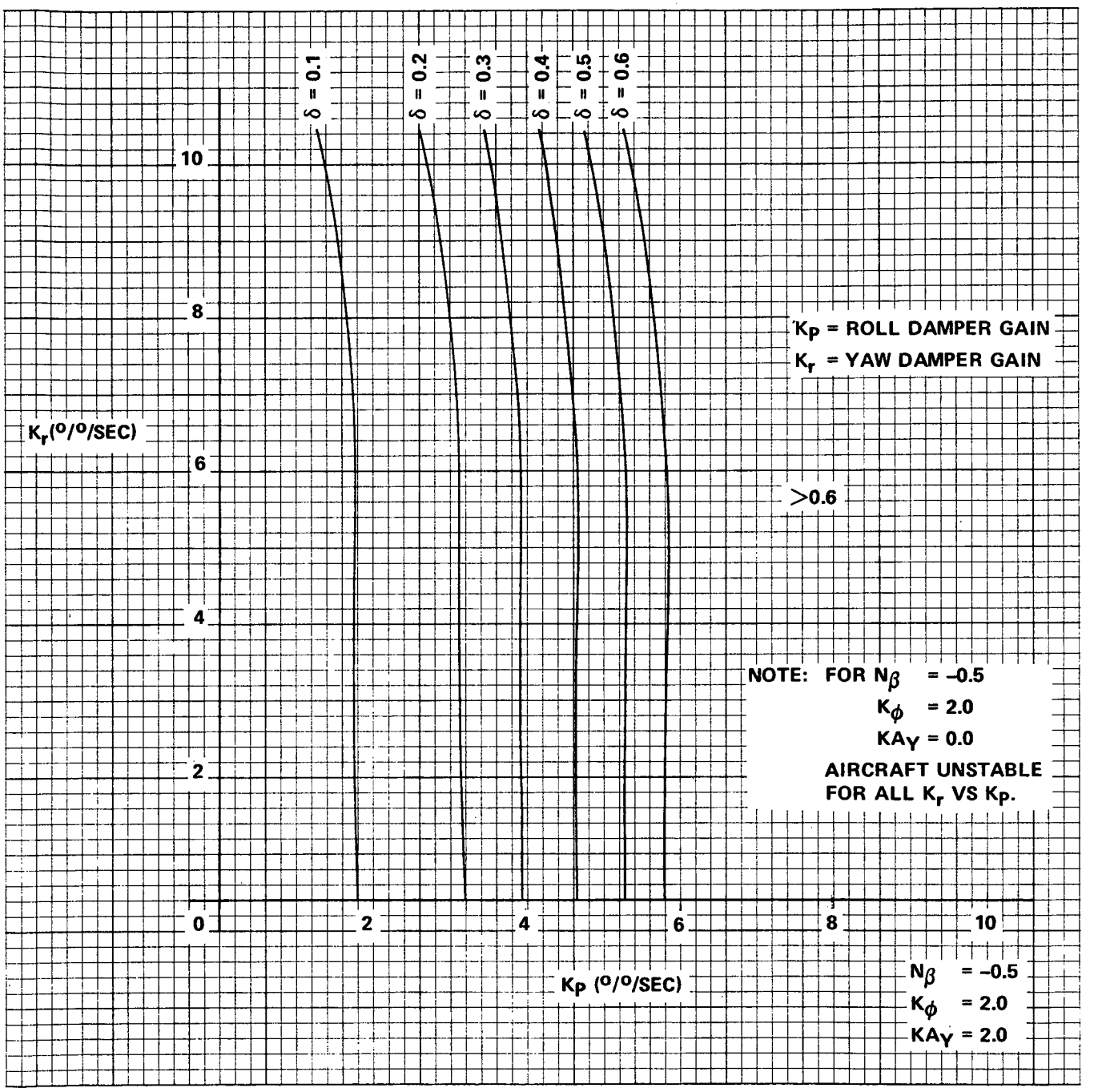

Figure 4-33
Roll and Yaw Damper Stability Regions with
A_Y Feedback, Roll Loop Closed

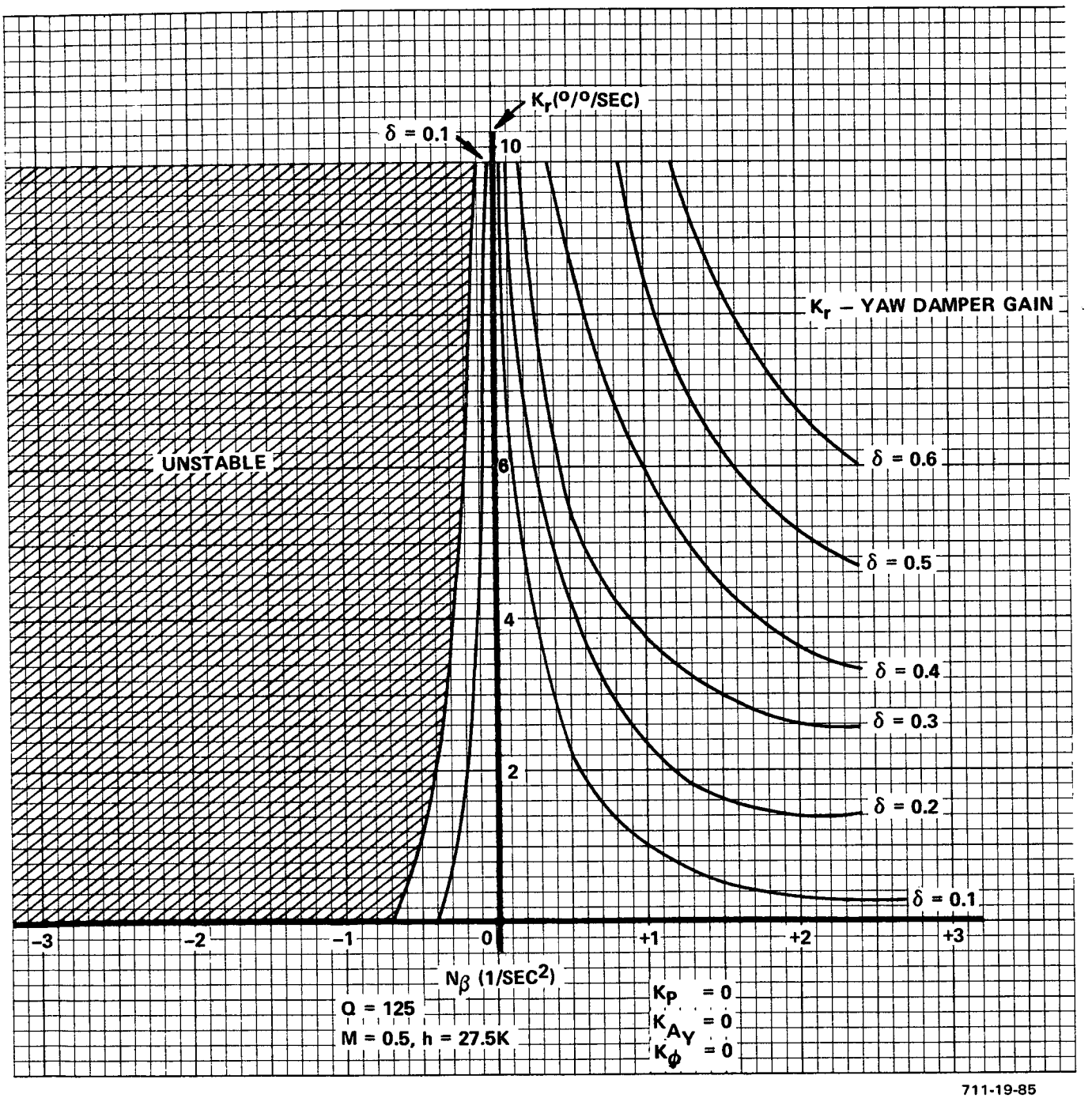

Figure 4-34
Yaw Damper Stability Regions
with Variable N_β ($K_p = K_\phi = K_{A_y} = 0$)

G

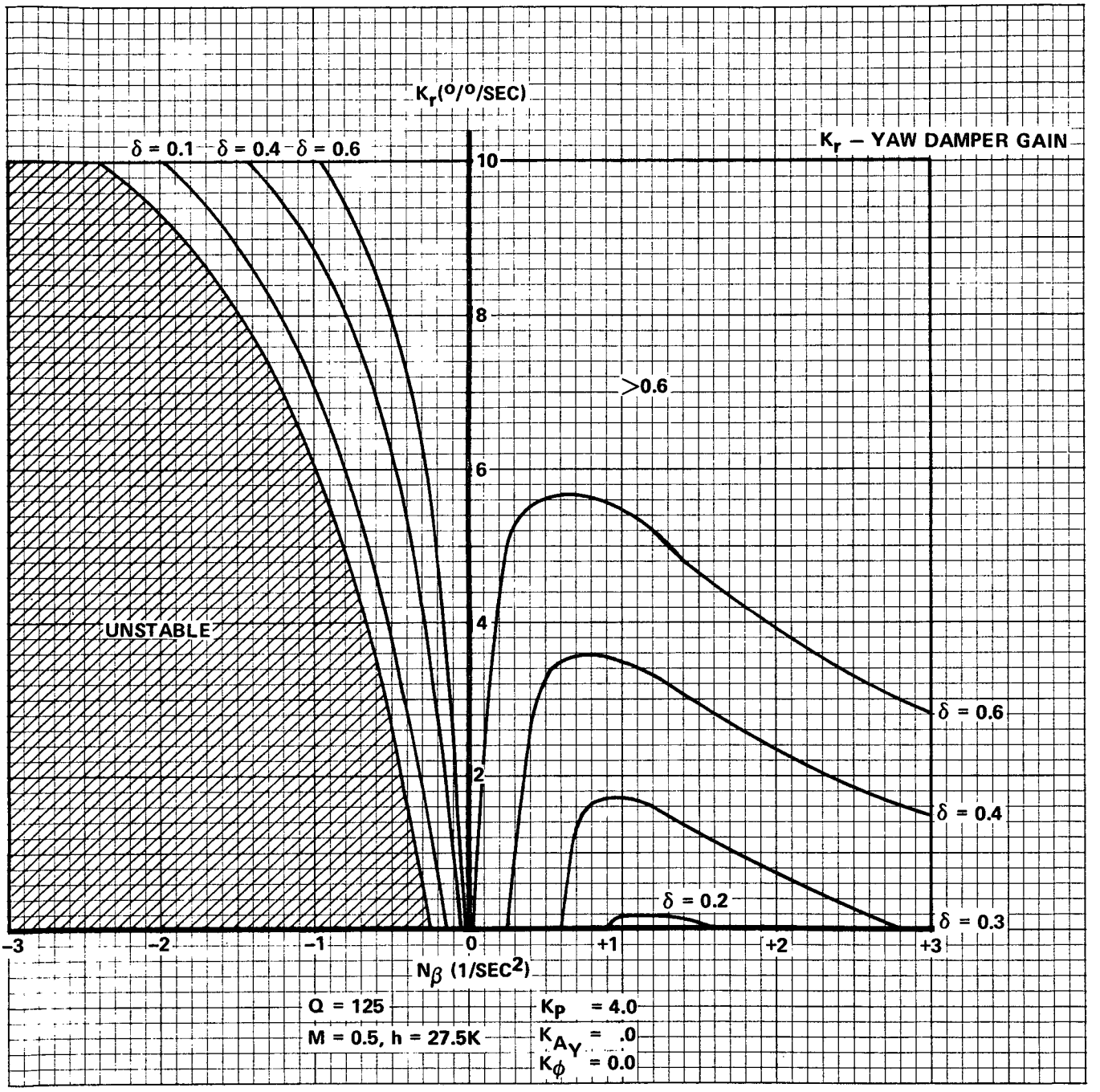

Figure 4-35
Yaw Damper Stability Regions with
Variable N_β (K_p = 4, K_{A_y} = K_ϕ = 0)

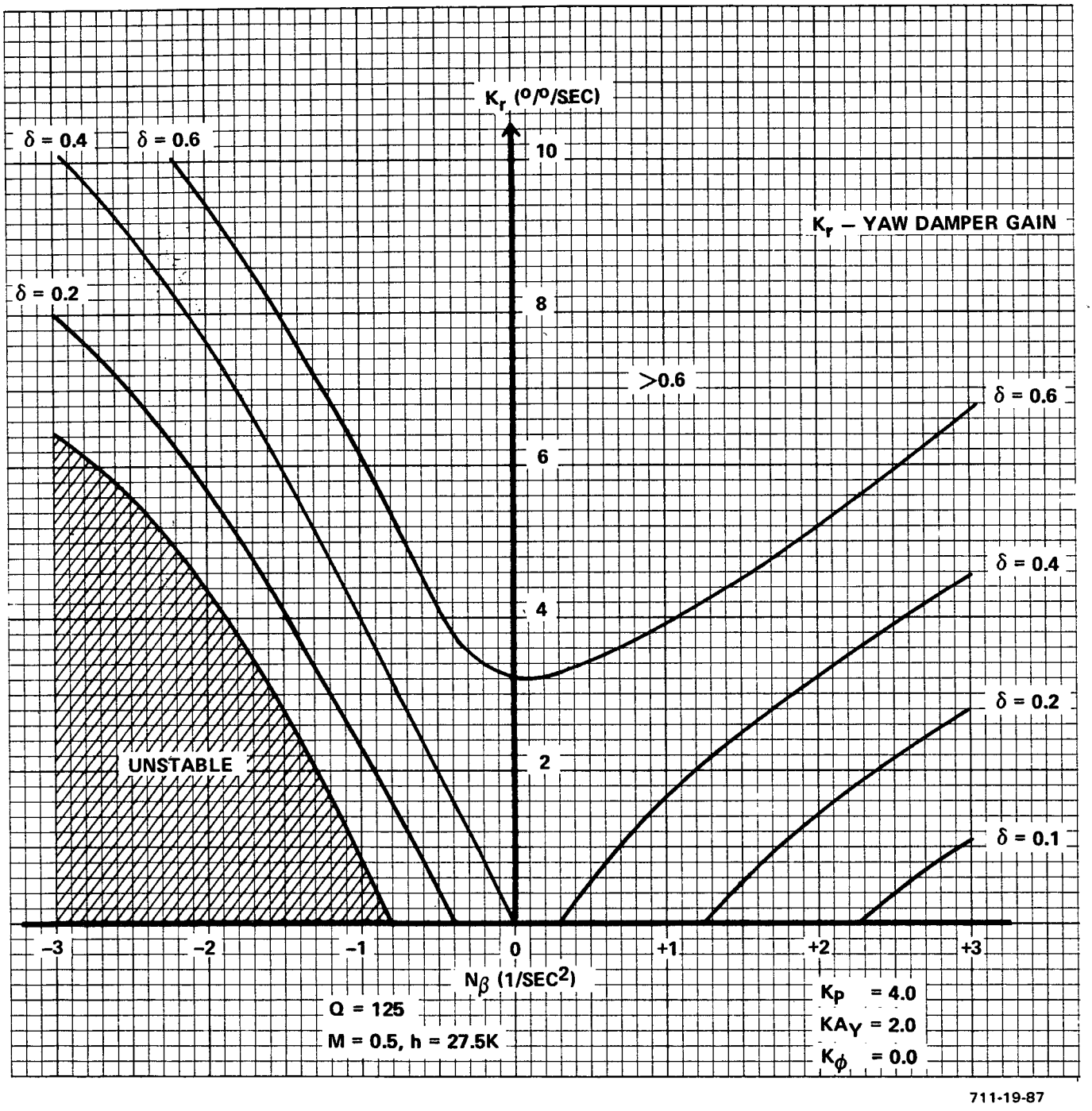

Figure 4-36
Yaw Damper Stability Regions with
Variable N_β (K_p = 4.0, K_{A_y} = 2.0, K_ϕ = 0)

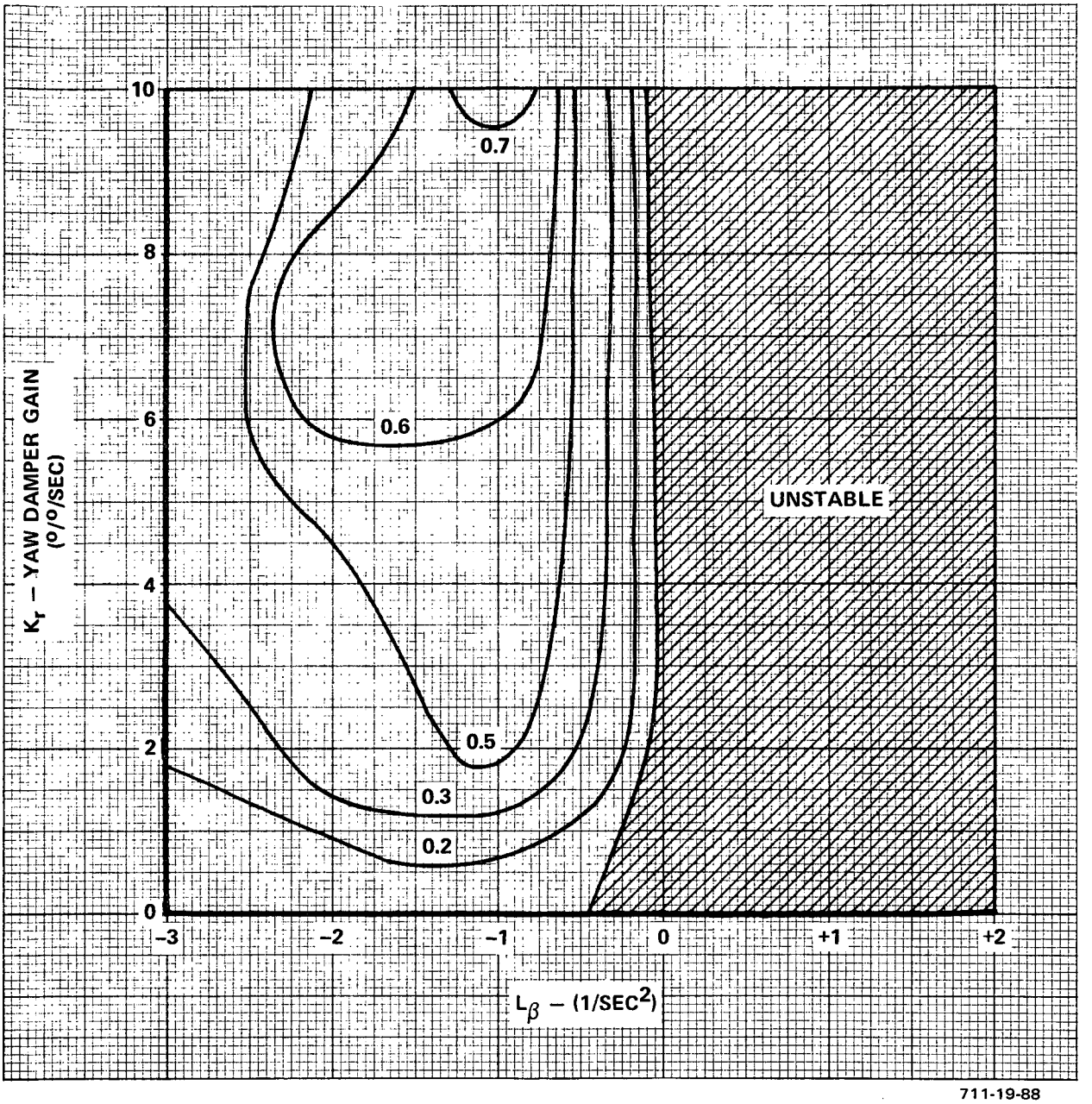

Figure 4-37
Yaw Damper Stability Regions for
Variable L_β ($K_\phi = K_p = K_{A_y} = 0$)

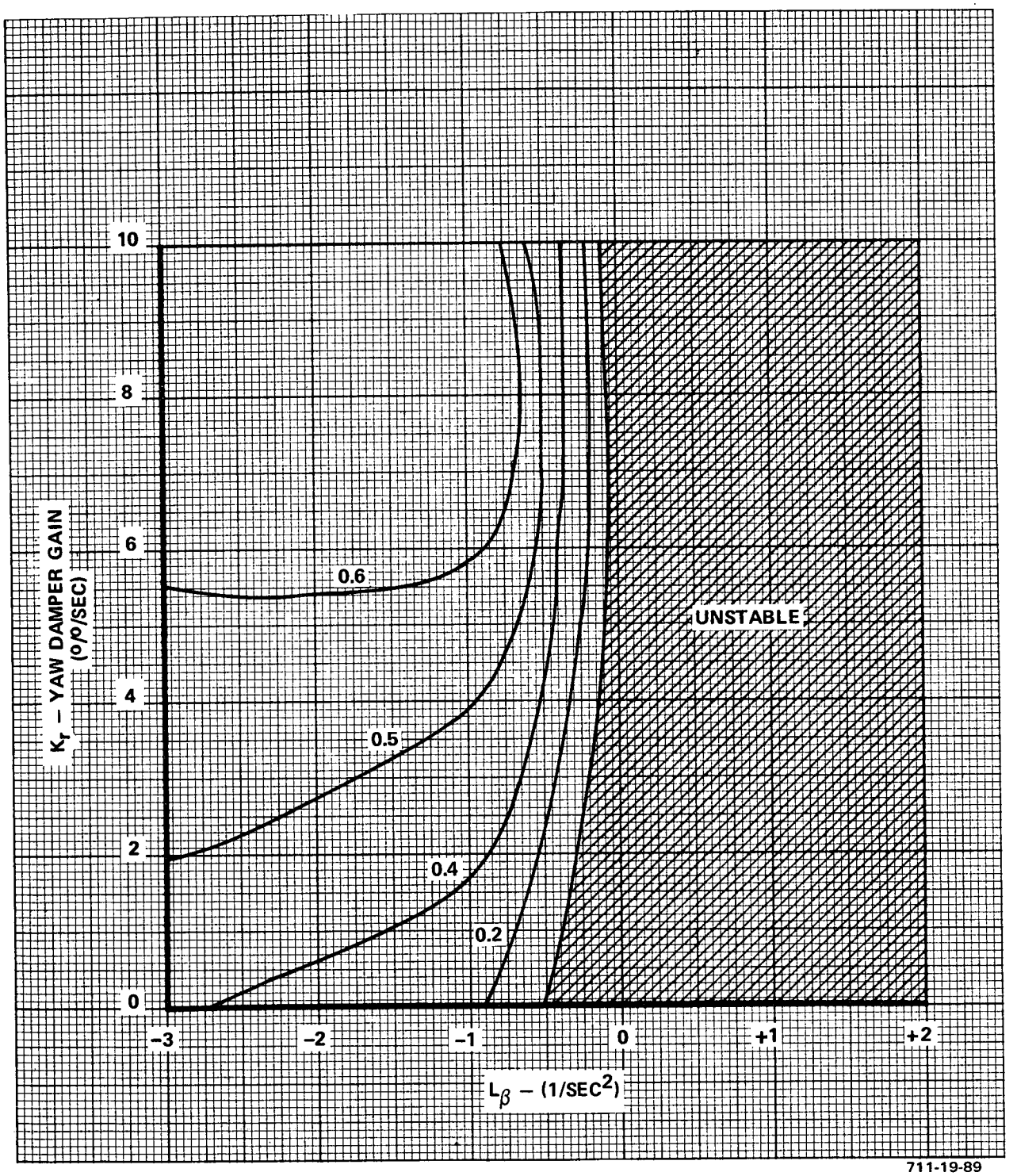

Figure 4-38
Yaw Damper Stability Regions for
Variable L_β ($K_p = 4$, $K_\phi = K_{A_y} = 0$)

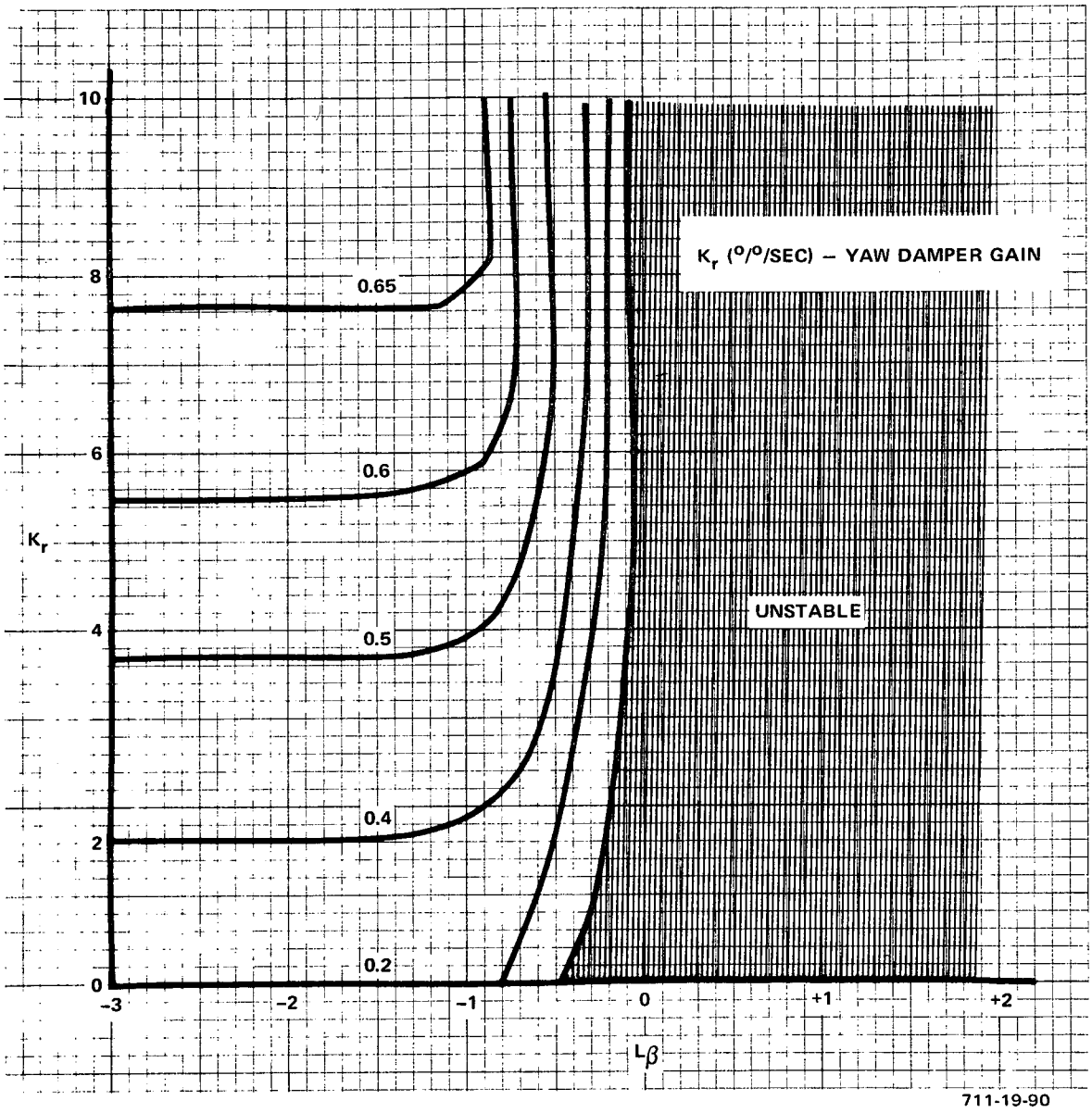

Figure 4-39
Yaw Damper Stability Regions for
Variable L_β ($K_p = 4$, $K_{A_y} = 2$, $K_\phi = 0$)

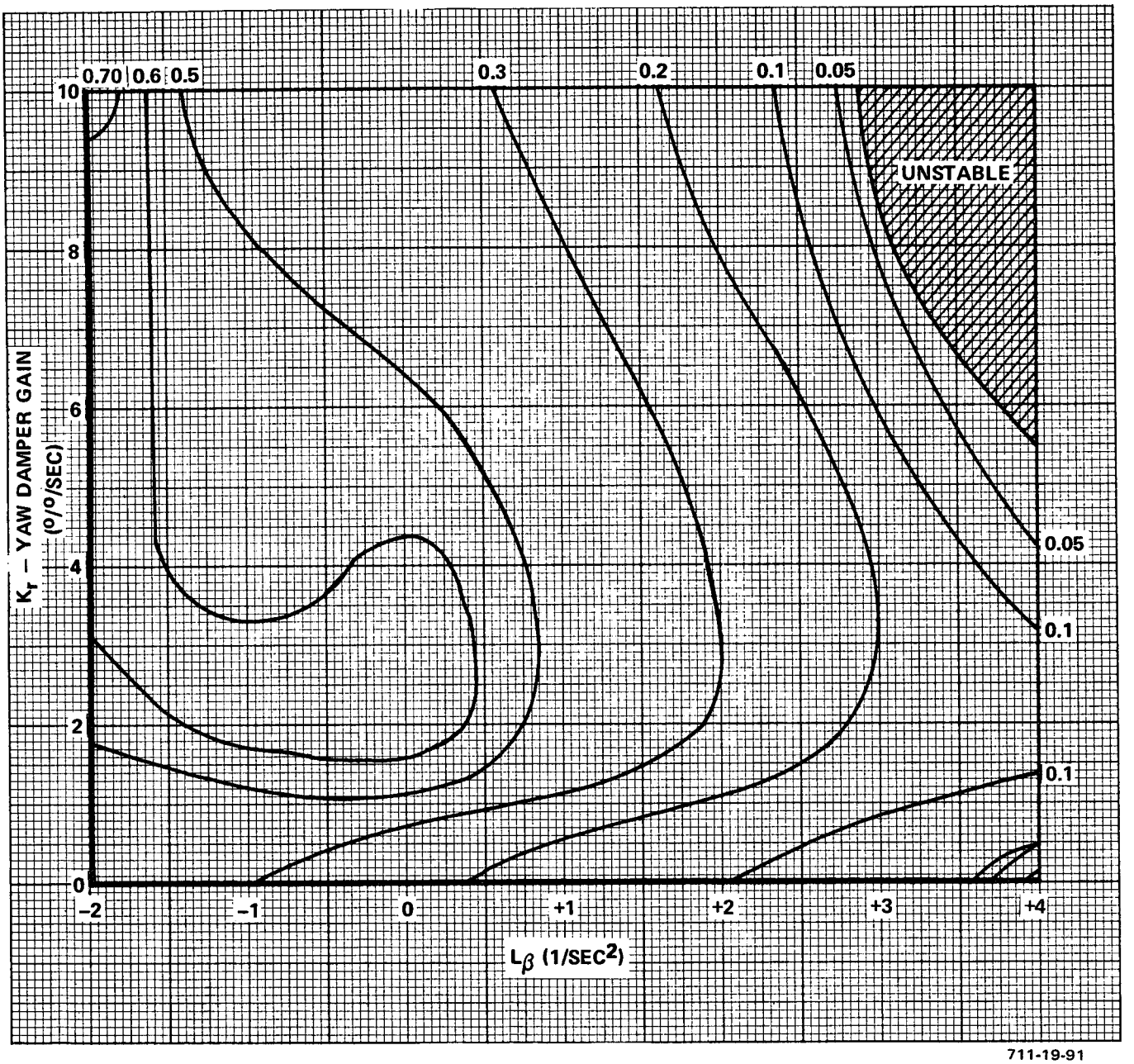

Figure 4-40
Yaw Damper Stability Regions for
Variable L_β (K_ϕ = 2, K_{A_y} = 2, K_p = 4)

a yaw damper does an excellent job of providing dutch roll stability (Figure 4-37). A roll damper allows the use of reasonably low yaw damper gains for the high stable L_β's (Figure 4-38). Lateral acceleration feedback does not help cope with an unstable L_β (Figure 4-39). What is required for unstable L_β's is an artificial roll constraint (roll spring). This is provided by the roll feedback which allows stable operation into regions of unstable (positive L_β's) (Figure 4-40). The results associated with variation in L_β are somewhat academic because obtaining stable L_β in an aircraft or reentry vehicle is not as difficult as obtaining stable N_β's.

Figures 4-41 through 4-43 show the influence of angle of attack on the dutch roll damping ratio provided by the yaw and roll controls. At the nominal gains (K_r = 3 to 5, K_p = 4.0), the performance remains adequate for the full range of α from 0 to 30 degrees although the α = 0 case gives the poorest results. At lower values of α, the reduction in the A_y gain can improve dutch roll damping. One of the problems with the use of A_y feedback is its extreme sensitivity to changing flight conditions. In the vehicle studied here, an A_y gain of 5.0 was used at the higher Mach numbers. This gain would cause stability problems at lower α's and lower speeds. In work done with the other delta configurations described later in this report, two gain controls were used on the A_y feedback: a Q control and a Mach control with the high gains used only at high Mach, low Q flight conditions.

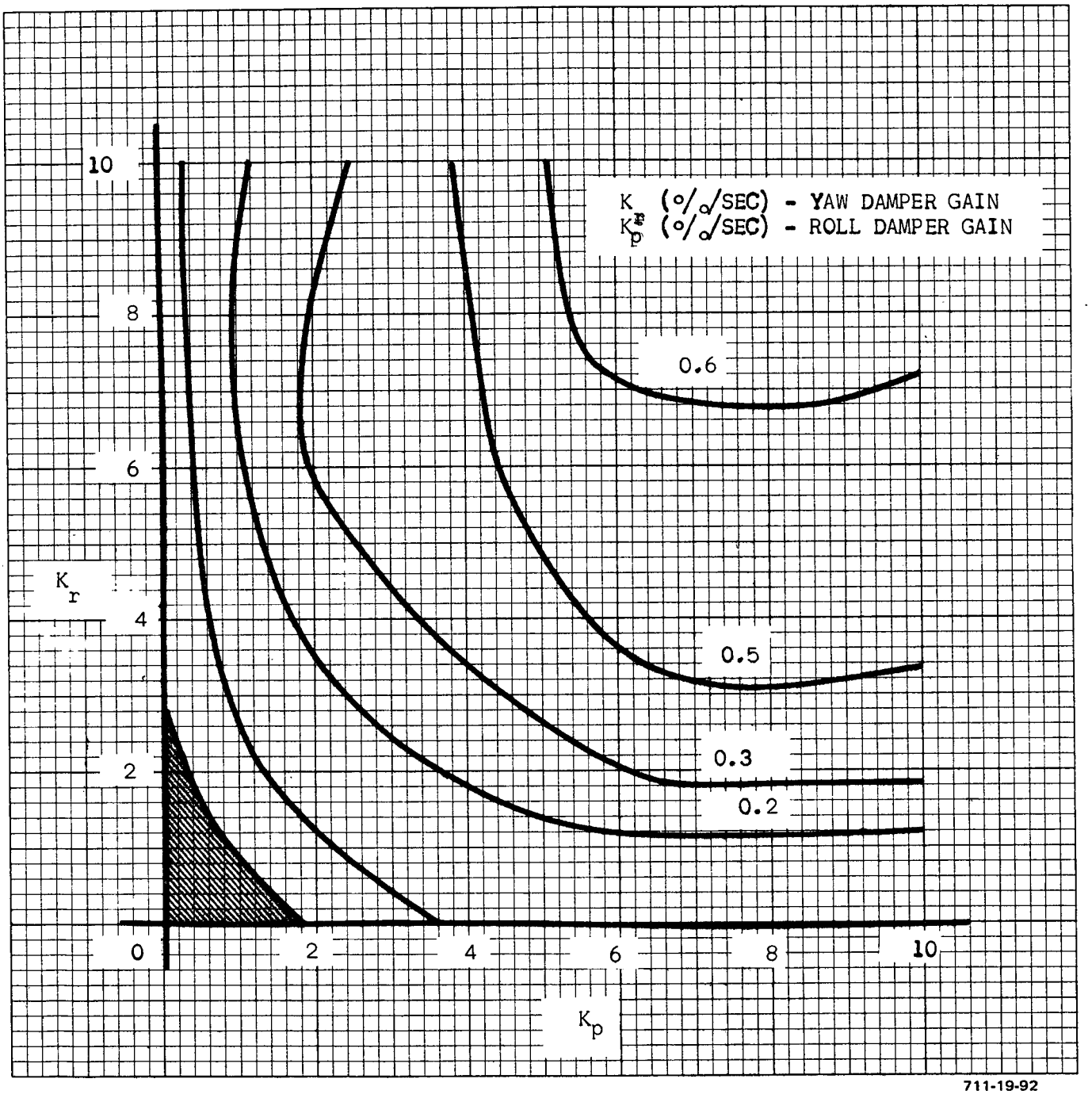

Figure 4-41
Roll and Yaw Damper Stability Regions
(K_ϕ = 2, K_{A_y} = 2, α = 0 degrees)

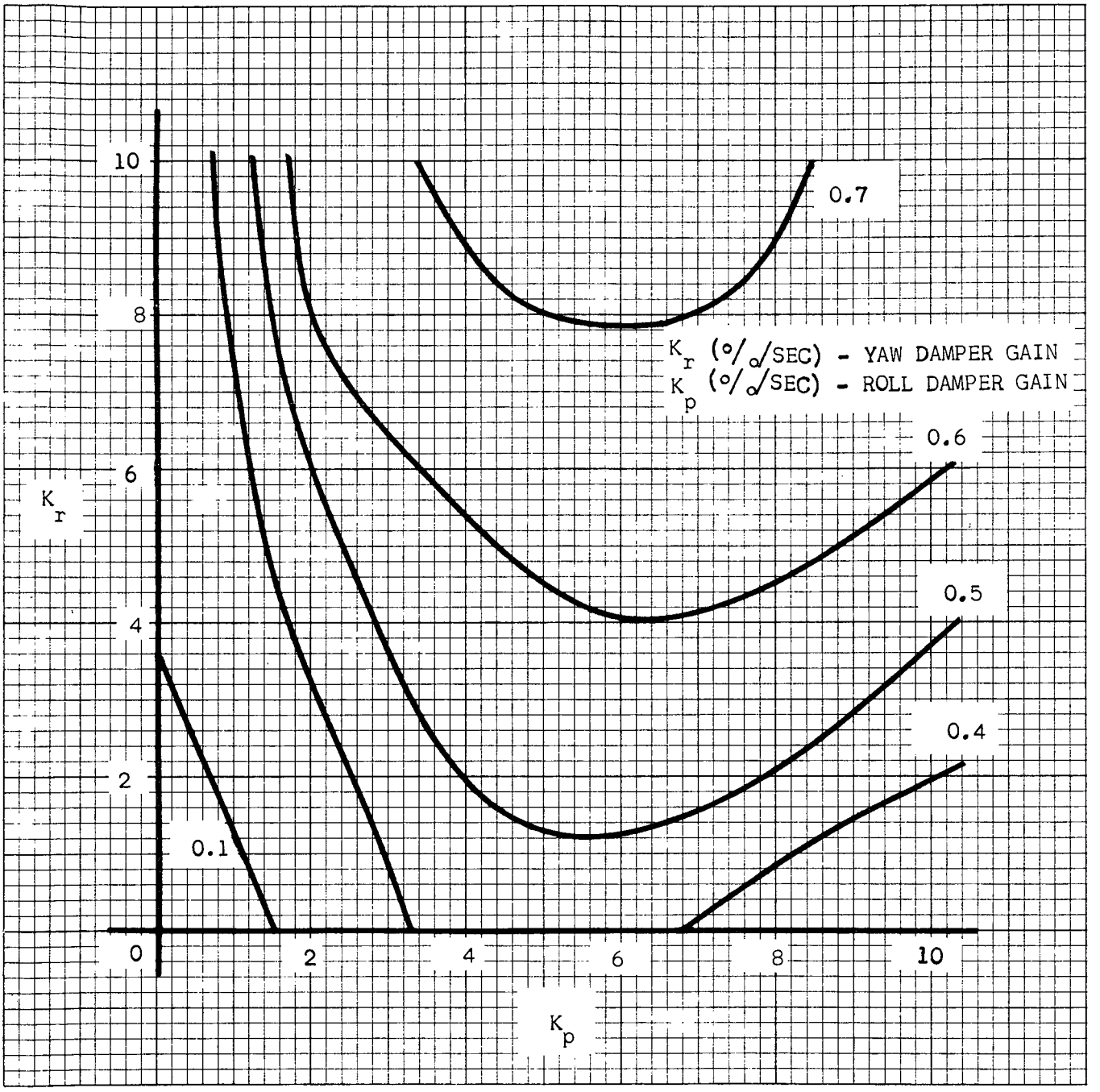

711-19-93

Figure 4-42
Roll and Yaw Damper Stability Regions
(K_ϕ = 2, K_{A_y} = 2, α = 15 degrees)

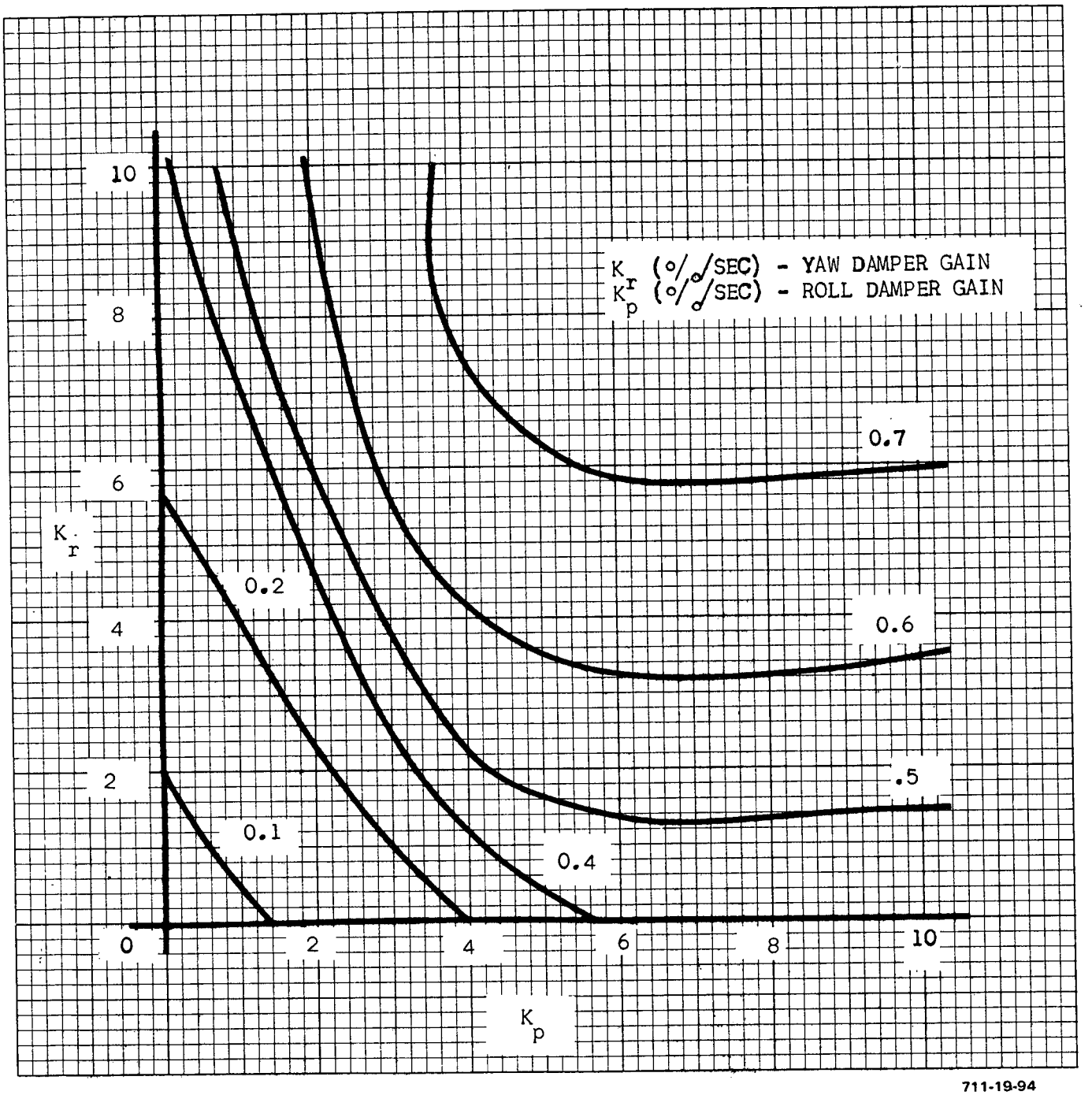

Figure 4-43
Roll and Yaw Damper Stability Regions
(K_ϕ = 2, K_{A_y} = 2, α = 30 degrees)

C. NAR HIGH CROSS-RANGE, DELTA WING ORBITER, SYSTEM DESIGN STUDIES

1. Vehicle Aero Summary

Characteristics	NAR SSV-134C
	Circa 8/70
Weight (landing) - pounds	207,000
Wing Span (b) - feet	119.3
MAC ($\bar{c}$) - feet	68.4
I_{xx} - (slug-foot^2 x 10^6)	3.35
I_{yy} - (slug-foot^2 x 10^6)	13.3
I_{zz} - (slug-foot^2 x 10^6)	14.4
I_{xz} - (slug-foot^2 x 10^6)	0.95
Ref Area (S) - foot^2	6,086
Wing Loading (W/S) - pound/foot^2	34
Peak L/D at Landing Condition	9.4
α for L/D_P - (degrees)	10.5
*Pitch Control Power - M_{δ_e} (1/sec^2)	-1.66
*Roll Control Power - L_{δ_A} (1/sec^2)	3.89
*Yaw Control Power - N_{δ_R} (1/sec^2)	-0.756
*For Landing Condition - Q = 150 pounds/foot^2	

The most interesting aerodynamic characteristic identified in the above table is the high landing L/D capability. During the early phases of study with this vehicle it became apparent that this L/D was quite optimistic because of errors in the drag data. Although North American Rockwell was continuously updating its HCR configuration and eventually even changed to a center fin configuration

in place of the twin fin design used in this study, it was decided to retain the data in its original form. The motivation to continue the design studies with a vehicle model having unrealistically high L/D (or low drag) was the recognition that high L/D's pose a unique set of problems that are different from those of the high drag, low L/D vehicle studied previously (Lockheed 8MX). The low drag vehicle does not converge rapidly to equilibrium speeds. In flaring to the shallow glide path it does not lose speed as rapidly as do the moderate or low L/D vehicles. Speed management is therefore more difficult especially without speed brakes. This vehicle did not have speedbrakes but the landing gear caused a significant drag increase. Varying the altitude of landing gear deployment could therefore have been used as a method of speed management during the final part of the landing approach. This technique was considered, but rejected after discussions with pilots experienced in unpowered landings of high performance vehicles. The consensus of these discussions was that this technique would be operationally undesirable. In general, therefore, this vehicle should have tendencies to land at excessive speeds (under tailwind conditions) and higher speed landings tend to increase longitudinal runway dispersions.

All control was done with elevons and rudders. The elevons were defined as separate "elevator" and "aileron" controls in accordance with the following definitions:

$$\delta_{EL-L} = \delta_{\substack{ELEVON \\ (left)}} = \delta_{E_{COMMAND}} + \delta_{A_{COMMAND}} \tag{4-8}$$

$$\delta_{EL-R} = \delta_{\substack{ELEVON \\ (Right)}} = \delta_{E_{COMMAND}} - \delta_{A_{COMMAND}} \tag{4-9}$$

$$\delta_E = \frac{\delta_{EL-L} - \delta_{EL-R}}{2} \tag{4-10}$$

$$\delta_A = \frac{\delta_{EL-L} - \delta_{EL-R}}{2} \tag{4-11}$$

where δ_E and δ_A are the synthetic elevator and aileron surfaces used in the simulations.

The surface rate and position constraints were:

$$\text{Range of } \delta_E = 0 \text{ to } -45 \text{ deg}; \quad \left|\dot{\delta}_{E_{MAX}}\right| = 20 \text{ deg/sec}$$

$$\delta_{A_{MAX}} = \pm 10 \text{ deg}; \quad \left|\dot{\delta}_{A_{MAX}}\right| = 20 \text{ deg/sec}$$

$$\delta_{R_{MAX}} = \pm 10 \text{ deg}; \quad \left|\dot{\delta}_{R_{MAX}}\right| = 20 \text{ deg/sec}$$

Neither speed brakes nor flaps were used. It is noted that the elevator and aileron limits should be applied to the elevon deflections of equations (4-8) and (4-9). When elevons are near their symmetrical deflection limits, the effective aileron rate limits become asymmetrical.

The stability and control characteristics of this vehicle are poor if considered from the viewpoint of manual handling qualities. The lateral-directional dynamics include such unacceptable phenomena (again from the manual handling quality viewpoint) as dutch roll poles and $\left(\phi/\delta_A\right)$ zeroes in the right half plane. The closure of the roll and yaw control augmentation loops provide a properly responsive aircraft for both the automatic guidance inputs or manual control. The key to the lateral-directional stabilization is the A_y into rudder feedback.

The L/D characteristics for this vehicle in the terminal area are summarized in terms of peak L/D (trim) at various Mach numbers along the descent trajectory:

MACH NO.	PEAK L/D_T	ANGLE OF ATTACK
0.3	9.4	10.5
0.9	5.5	10.5
1.2	3.0	11.0
2.0	2.5	11.5

The subsonic data can be used to compute the equilibrium glide angle versus airspeed. The resultant curve is shown in Figure 4-44 which also includes the corresponding curve for the MDAC high cross-range, delta wing configuration. The MDAC configuration is shown as a comparison because it is more representative of this type of delta wing configuration since it is acknowledged that the NAR aero model is in error because of its low drag/high L/D at the final approach condition. Figure 4-44 predicts an equilibrium speed (on a -10 degree glide path) of 310 knots for the higher L/D NAR vehicle model while the MDAC vehicle's equilibrium speed would be 280 knots.

2. Attitude Stabilization and Autopilot Parameters

a. Pitch Guidance and Control

The autopilot control laws for aerodynamic phases of flight are identical to those used for the previous vehicles described in Sections IVA and IVB [Equations (4-1) and (4-2)]. The gains used for the NAR vehicle are:

$$k_\theta = 2.0 \frac{300}{Q} \text{ degrees per degree}$$

$$\frac{k_q}{k_\theta} = 1.0 \text{ seconds}$$

$$k_h = 0.050 \frac{500}{V} \text{ degrees per foot to } 0.067 \frac{500}{V}$$

$$a_2 = 0.05 \text{ to } 0.08$$

$$k_\gamma = 1.5 \text{ to } 1.0 \text{ degrees } \theta_c \text{ per degree } \gamma$$

$$\tau = 2.0 \text{ to } 2.5 \text{ seconds}$$

At high altitudes, prior to attaining the final descent γ, a fixed dynamic pressure (Q) guidance loop was used as defined in Section IIIC, Equation (3-92). The energy references used in the energy management system are based on a nominal trajectory.

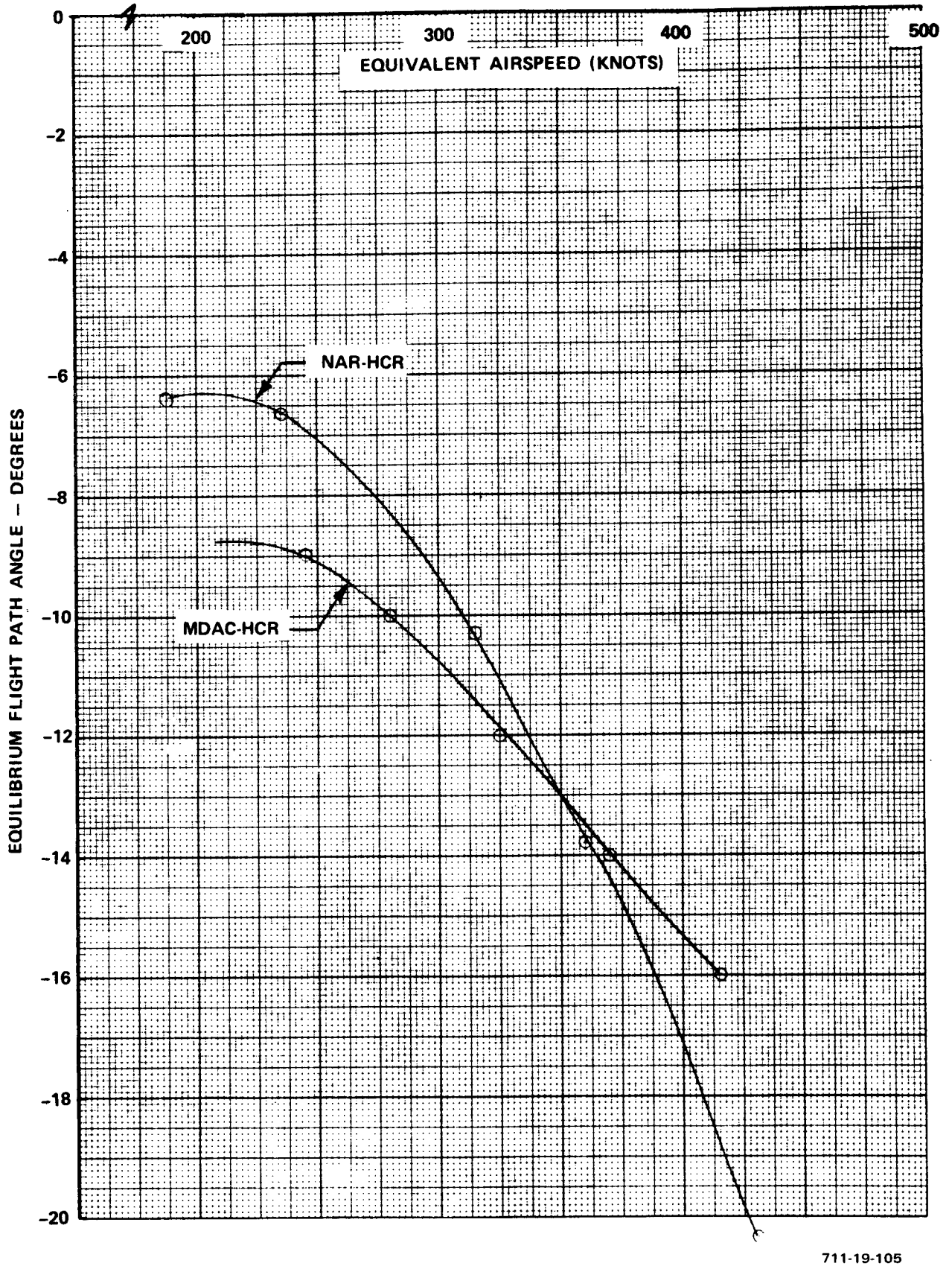

Figure 4-44
Equilibrium Flight Path versus Equivalent
Airspeed for MDAC and NAR-HCR

The potential energy reference, $C_1(D_K)$ and the kinetic energy reference, $C_2(D_K)$ as a function of the distance to the low keypoint, D_K, are given in Table 4-8.

TABLE 4-8

NOMINAL TRAJECTORY

D_K (FT)	C_1 (D_K) (FT) [h]	C_2 (D_K) (FT/SEC) [V]
0	54,000	979.2
50,000	62,800	1,180
100,000	70,000	1,450
150,000	76,300	1,720
200,000	83,000	1,950
250,000	88,000	2,160
300,000	91,000	2,400
350,000	94,200	2,660
400,000	98,500	2,990
450,000	102,000	3,150
500,000	105,500	3,276.7
550,000	109,000	3,370
600,000	112,500	3,450

b. Lateral-Directional Stabilization

The roll and yaw equations are identical to those of the straight wing vehicle and the LMSC delta body vehicle [Equations (4-4) and (4-5), respectively]. In the design of the lateral-directional control system, several iterations were needed to determine acceptable gain programs for the lateral acceleration feedback. Roll instabilities at relatively high frequency (above 2 Hz) were encountered and the cause was in a combination of servo dynamics, servo rate limiting and the digital simulation frame time. The internal simulator integration instability should not have dictated control

gains but unfortunately a complete solution to these problems could not be obtained except through the arbitrary and safe technique of lowering gains. Consequently, the autopilot gains used in the system performance verification tests accomplished on the NASA ARC simulations were somewhat lower than the gains used in the Sperry perturbation analog simulations or 6-degree of freedom digital simulations. Guidance system performance did not seem to be affected by these gain differences.

The same lateral-directional control equations that were used for the previous vehicles were also applicable to the NAR HCR vehicle. However, to show the required gain programming, these equations are rewritten in the following form:

$$\delta_{R_C} = \left[K_r \left(r - \frac{g}{V} \sin \phi_c \left(\frac{\tau_4 S}{\tau_4 S + 1} \right) + \frac{A_Y}{\tau_5 S + 1} K_{AY} \right] \frac{Q_o}{Q} \right. \tag{4-12}$$

$$\delta_{A_C} = (p - p_{com}) \; k_p + (\phi - \phi_{com}) \; K_\phi \tag{4-13}$$

where:

K_p = 2.5 deg/deg/sec — Roll rate gain

K_ϕ = 2.5 deg/deg — Roll gain

K_{AY} = M + 1 $\frac{\text{deg rud}}{\text{ft/sec}^2}$ — Lateral acceleration gain

K_r = 4 deg/deg/sec — Yaw rate gain

τ_4 = 2.5 sec — Yaw rate wash out

τ_5 = 0.1 sec — Acceleration noise filter

Q_o = 130

Q = Dynamic pressure

M = Mach number

c. Autopilot Performance Summary

Lateral-directional stabilization system performance with step gust excitations and roll command responses at Mach 0.3, 0.6 and 3.0 is shown in Figures 4-45, 4-46 and 4-47. Also shown in these figures is the free aircraft transient response for each of these flight conditions. The free aircraft is unstable in every case. In general the roll command responses are adequate for the guidance loops. (The command incorporates a 1.0 second lag). Roll rates that occur during these command responses reach only about 4.0 degrees per second. For roll rates as low as this the sideslip performance is not outstanding; sideslip angles reaching as high as 1.0 degree. The main cause of the sideslip is the fact that at the angles of attack involved, a significant body axis yaw rate is needed to roll about the velocity vector (zero sideslip roll). The yaw damper opposes this yaw rate but does not oppose the steady state yaw rate of the turn ($g/_V \sin \phi_c$). A number of solutions are used in practice. The yaw rate gyro can be tilted so that the input axis is rotated an amount equal to the average α. Another approach is to compute the body axis yaw rate required to roll at the desired rate about the velocity vector. Neither of these approaches were used at this time since performance was adequate for the automatic and manual steering tasks being evaluated.

Pitch command responses at various Mach numbers along the nominal trajectory are shown on Figure 4-48. In every case, the responses are well damped and sufficiently rapid to meet all required automatic or manual steering requirements.

Tables 4-9 and 4-10 summarize the autopilot performance obtained at five reference points along the terminal control trajectory. Table 4-9 describes the manual mode and automatic mode pitch response characteristics while Table 4-10 summarizes the manual and automatic roll response characteristics.

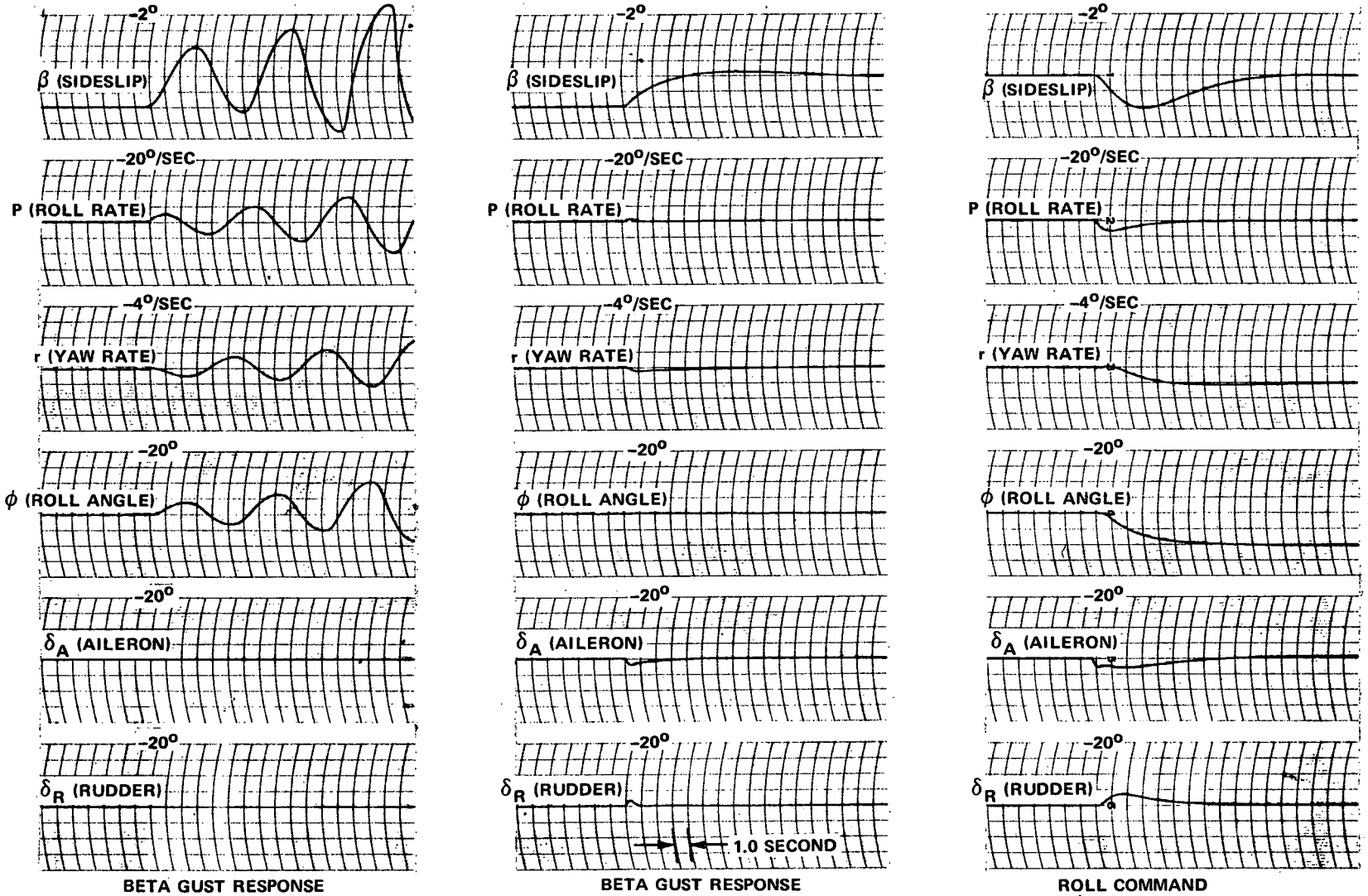

BETA GUST RESPONSE
HCR ORBITER
FREE VEHICLE
M = 0.3, h = S. L.

BETA GUST RESPONSE
HCR ORBITER
CLOSED LOOP CONTROL
M = 0.3, h = S. L.

ROLL COMMAND
HCR ORBITER
CLOSED LOOP CONTROL
M = 0.3, h = S. L.

711-19-106

Figure 4-45
HCR Orbiter Lateral Stability
(M = 0.3, h = Sea Level)

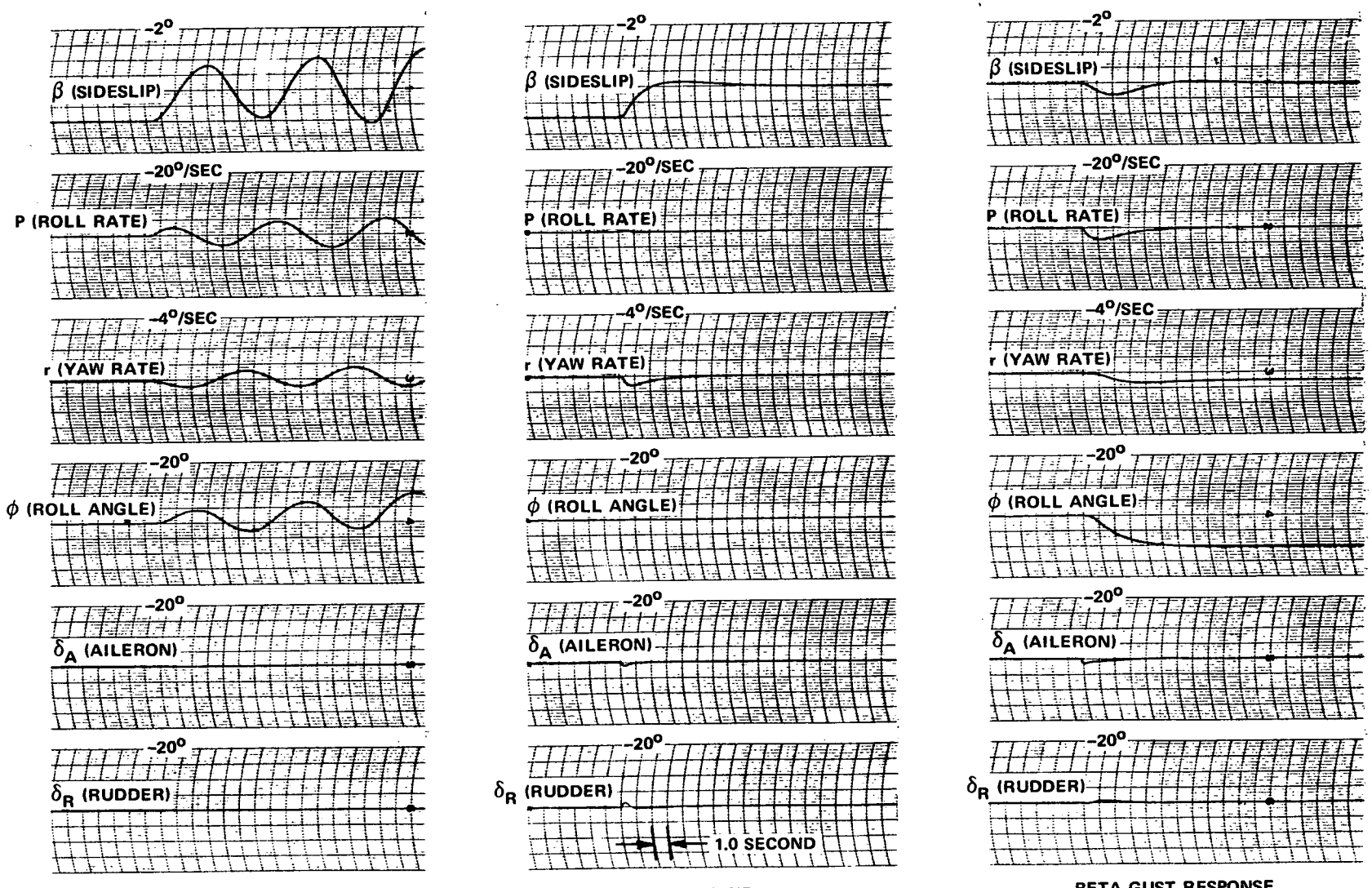

FREE VEHICLE GUST RESPONSE
HCR ORBITER
M = 0.6, h = 20,000 FEET

ROLL COMMAND
HCR ORBITER
CLOSED LOOP CONTROL
M = 0.6, h = 20,000 FEET

BETA GUST RESPONSE
HCR ORBITER
CLOSED LOOP CONTROL
M = 0.6, h = 20,000 FEET

711-19-107

Figure 4-46
HCR Orbiter Lateral Stability
(M = 0.6, h = 20,000 feet)

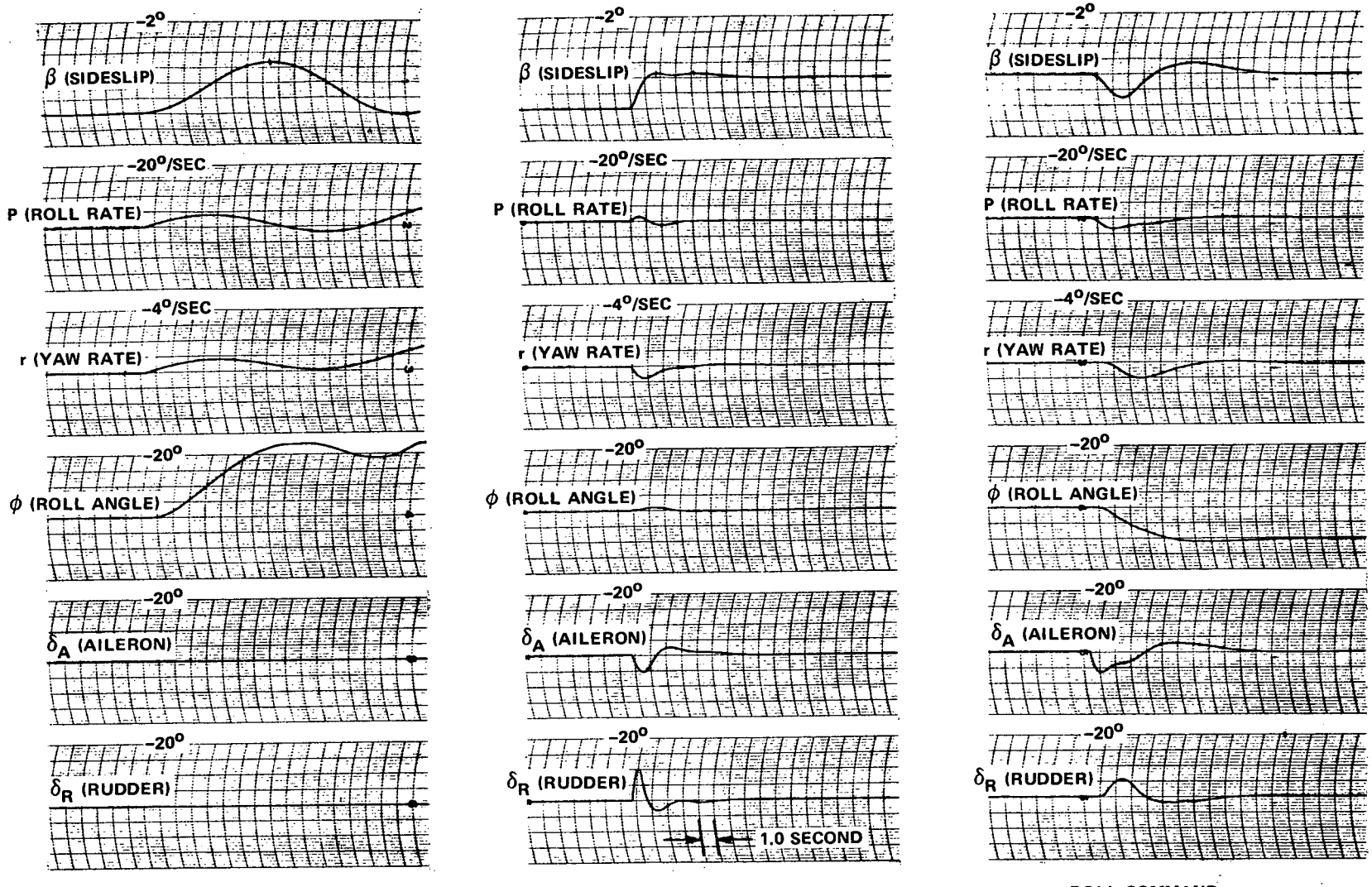

Figure 4-47
HCR Orbiter Lateral Stability
(M = 3, h = 100,000 feet)

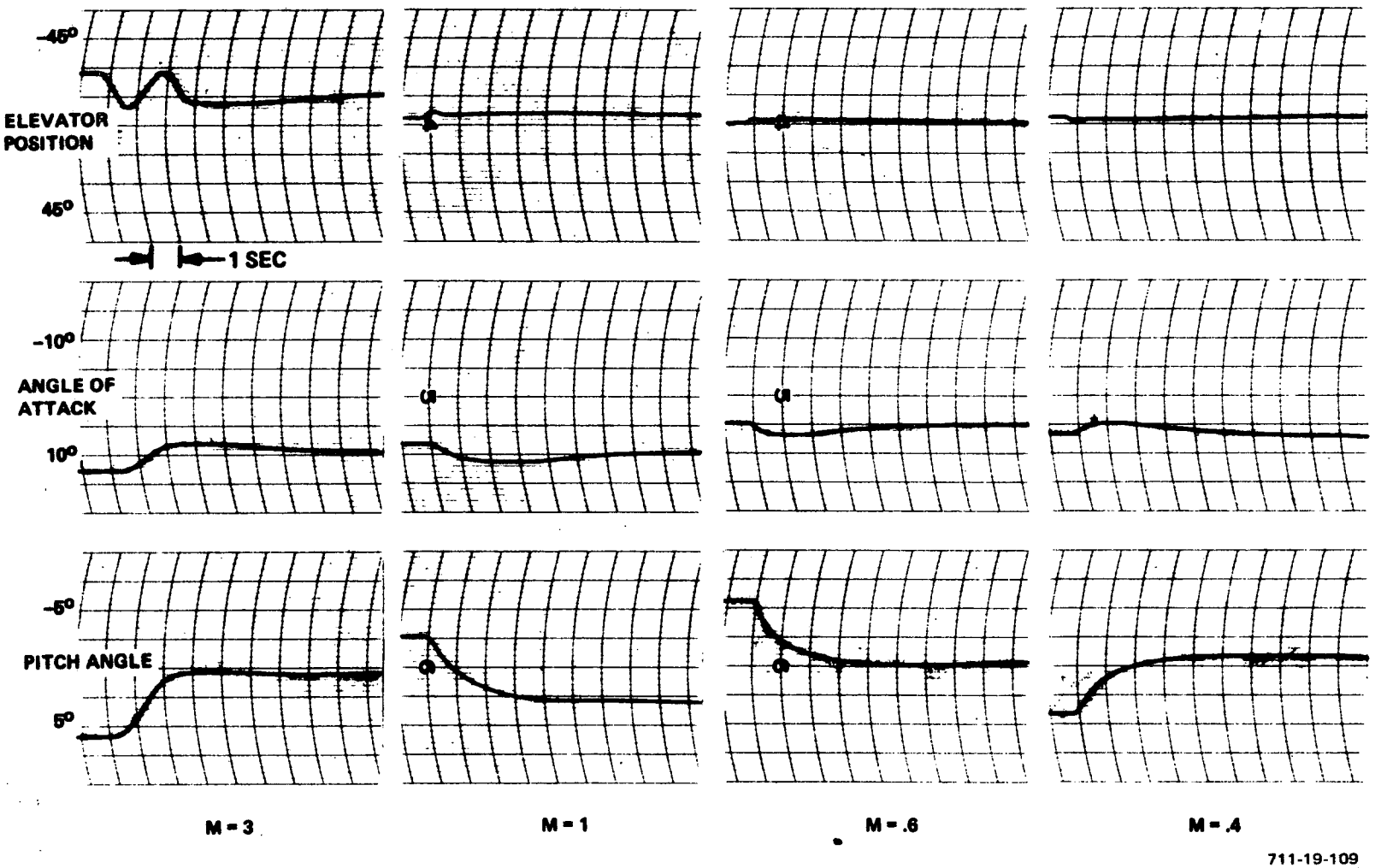

Figure 4-48
HCR Vehicle Response to Step Pitch Commands

TABLE 4-9

AUTOPILOT PERFORMANCE SUMMARY,
HCR VEHICLE, PITCH

PARAMETER		MACH NUMBER				
		M = 3.0 h = 100,000 FT	M = 2.0 h = 82,000 FT	M = 1.0 h = 52,000 FT	M = 0.6 h = 10,000 FT	M = 0.4 h = 400 FT
$\left(\frac{\dot{\theta}}{\dot{\theta}_C}\right)$ MANUAL MANEUVER RESPONSE	t_{90} PERCENT (SEC)	0.4	0.3	0.2	0.2	0.2
$\dot{\theta}_C$ PROPORTIONAL TO STICK DISPLACEMENT FROM DETENT	ζ_{MIN} FOR $\omega < 6$ RAD/SEC	0.7	0.8	0.8	0.7	0.8
	MAXIMUM SURFACE RATES REQUIRED (DEG/SEC)	<20	<20	<20	<20	<20
$\left(\frac{\theta}{\theta_C}\right)$ AUTOMATIC GUIDANCE RESPONSE (g CONSTRAINTS ARE APPLIED SO THAT RESPONSE TIMES REFER TO LINEAR OPERATING REGIONS)	t_{90} PERCENT (SEC)	2	2.5	2	2	2
	PERCENT OVERSHOOT (%)	5	5	0	5	0
	ζ_{MIN} FOR $\omega < 6$ RAD/SEC	0.7	0.8	0.8	0.7	0.8
	MAXIMUM SURFACE RATES REQUIRED (DEG/SEC)	<20	<20	<20	<20	<20

TABLE 4-10

AUTOPILOT PERFORMANCE SUMMARY,
HCR VEHICLE, LATERAL

PARAMETER		MACH NUMBER				
		M = 3.0 h = 100,000 FT	M = 2.0 h = 82,000 FT	M = 1.0 h = 52,000 FT	M = 0.6 h = 10,000 FT	M = 0.4 h = 400 FT
$\left(\frac{\dot{\phi}}{\dot{\phi}_C}\right)$ MANUAL MANEUVER RESPONSE	t_{90} PERCENT (SEC)	1	0.7	0.5	0.5	0.5
(MAXIMUM COMMAND TIMES 15 DEG/SEC) INCLUDES FULL LATERAL DIRECTIONAL STABILIZATION SYSTEM	ζ_{MIN} FOR $\omega < 6$ RAD/SEC	0.4	0.5	0.6	0.7	0.7
	MAXIMUM SURFACE RATES REQUIRED (DEG/SEC)	AILERON < 40 RUDDER < 30	AILERON < 40 RUDDER < 30	AILERON < 40 RUDDER < 30	AILERON < 40 RUDDER < 30	AILERON < 40 RUDDER < 30
$\left(\frac{\phi}{\phi_C}\right)$ AUTOMATIC GUIDANCE RESPONSE INCLUDES FULL LATERAL DIRECTIONAL STABILIZATION SYSTEM	t_{90} PERCENT (SEC)	3.5	3.2	3.0	3.0	3.0
	PERCENT OVERSHOOT (MAXIMUM) (%)	6	0	0	0	0
	β_{MAX} FOR 25 DEG ϕ_C (DEG)	1.2	1.5	1	1	2.5
	ζ_{MIN} FOR $\omega < 6$ RAD/SEC FOR ALL COMMAND OR GUST DISTURBANCES	0.4	0.5	0.6	0.7	0.7
	MAXIMUM SURFACE RATES REQUIRED (DEG/SEC)	AILERON < 40 RUDDER < 30	AILERON < 40 RUDDER < 30	AILERON < 40 RUDDER < 30	AILERON < 40 RUDDER < 30	AILERON < 40 RUDDER < 30

3. Final Approach and Flareout

a. Terminal Approach Paths

Section IIIB, discussing the theory of the equilibrium glide path as a means of satisfying the energy and position requirements of an unpowered landing, illustrated glide path acquisition and tracking with the NAR HCR orbiter (Figures 3-18 and 3-19). Those figures showed a 12.5 NM window at 20,000 feet based on velocity convergence to within ±10 percent of nominal by the time the first flareout altitude is reached. In these figures dive acquisitions are arbitrarily limited to a maximum flight path angle of -25 degrees. Airspeed and dynamic pressure converge toward the nominal value after the glide path is captured but the speed convergence is not as rapid as it was for the lower L/D, higher drag vehicles that were studied. The effects of speed limiting are to be noted for dive approach number (5) on Figure 3-18 and 3-19. Dynamic pressures were permitted to range from 100 to 575 pounds/foot^2. Closed loop constraints per equations (3-38) through (3-41) prevented α, γ and Q from exceeding the specified limits.

b. Flareout

Flareout trajectory trade-offs showing landing speed versus initial flare altitude are shown in Figure 4-49. The vehicle acquires the shallow glide slope with a 0.5g maneuver and landing gear is deployed at 300 feet of altitude. A final flare maneuver occurs at an altitude of 60 feet and the nominal touchdown vertical velocity is -2 feet/second.

This figure illustrates four successful landings using different steep glide slope, shallow glide slope geometries. The first flare starts at various altitudes. The resultant trajectories ride the shallow glide path for

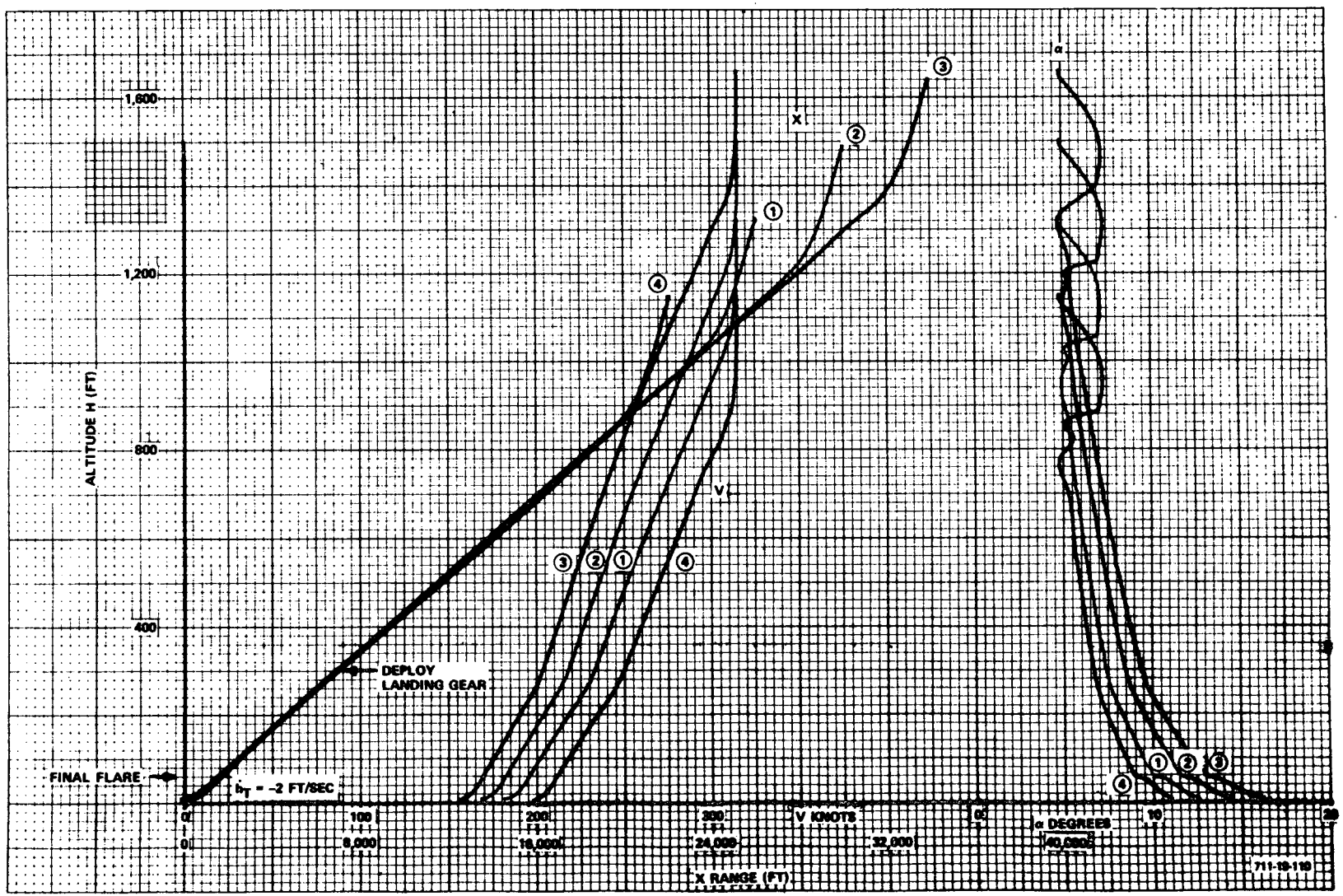

Figure 4-49
HCR (Delta Wing) NAR Flareout Trajectory
Tradeoffs for Various Altitudes

varying durations and as a consequence touchdown with different velocities and α's as summarized below:

Run No.	First Flare Altitude	Touchdown Velocity	Touchdown α	
(3)	1660 ft	156 kt	16 deg	
(2)	1500 ft	168 kt	14.5 deg	
(1)	1320 ft	182 kt	12.5 deg	NOMINAL
(4)	1150 ft	198 kt	11.0 deg	

The selection of a nominal trajectory specifies the two glide path geometrical relationships. The trajectories shown on Figure 4-49 are for a no-wind case. If we had to cope with headwinds, it is apparent that case (3) which gives the longest shallow glide path traverse would be unacceptable. Moreover, nominal touchdowns at α = 16 degrees are excessive. In addition to tail scrape margins, the high α condition causes degradation in the lateral-directional dynamics. Although lateral maneuvering is minimized during the final phase of flight the decrab maneuver could be seriously compromised by poor lateral-directional stability.

Trajectory (1) with a landing speed of 182 knots is selected as the nominal trajectory.

It is noted that in the final 6-degree-of-freedom, full-trajectory simulations to verify system performance, the nominal trajectory had to be modified slightly. These final simulations used aero data in their table look-up routines that incorporated a drag coefficient error as large as 20 percent below Mach 0.6. This drag coefficient error did not exist in the simulation that produced Figure 4-49. The result of the lower drag in the final simulations was a nominal speed increase at touchdown to about 195 knots. Also, the first flare altitude had to be raised about 180 feet.

Runs for nominal and ±10 percent off-nominal velocities at flare in which no updating of the predictive commands is employed are shown in Figure 4-50.

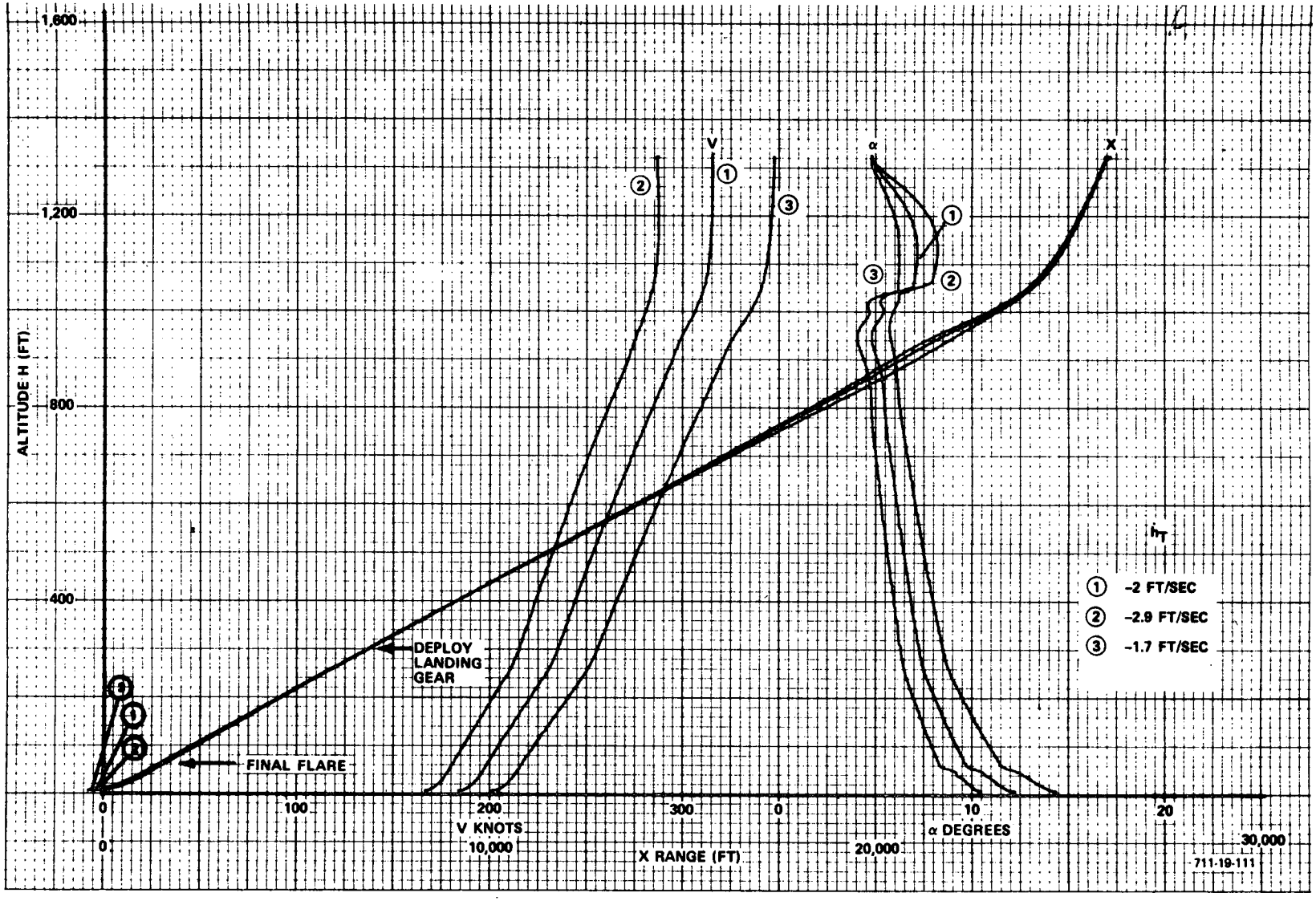

Figure 4-50
HCR-NAR Orbital Terminal Trajectories,
Nominal and Off-Nominal Flare Velocities

Vertical touchdown speed spreads are a little larger than desired at 1.2 feet/second. Angle of attack spreads are 4 degrees. Forward speed variations are ±10 percent, and range dispersions are ±175 feet. Updating of predictive commands for the velocity errors improves landing performance. Figure 4-51 displays terminal trajectories in which updating of the predictive commands for the ±10 percent off-nominal velocities has been employed. Range, angle of attack, and forward velocity spreads are comparable, but vertical touchdown rate spreads are reduced to 0.6 foot/second. Figure 4-52 shows the rapid convergence to the nominal for ±50 foot flare altitude errors. The system's ability to tolerate a large error in the first flare initiate altitude is a consequence of the sustained flight on the shallow glide path where sufficient time exists for correcting the initial position error. If the shallow glide path were acquired below 300 feet, this capability would not have been as good (note problems with LMSC vehicle, Section IV.B.3).

The flareout control law used in Figure 4-49 through 4-52 was the Acceleration Terminal Controller described in Section IIIC [Equations (3-77) through (3-80)]. Off-nominal velocities were used in these runs to partially predict the system's capability of handling headwind and tailwind conditions. In the final simulations the winds and turbulence were added. The acceleration controllers ability to cope with the turbulence was not as good as expected. Consequently, the flareout system was changed to the Vertical Velocity Flare Controller [See discussion in Section IIIC and Equations (3-81) through (3-83.)] The specific flare equation found optimum for the NAR HCR vehicle model (with the low drag error) was:

Final flareout is initiated when the following equation is satisfied:

$$h + \dot{h} - 45 \lesseqgtr 0$$

At that time, the following flareout control equations is initiated:

$$\theta_c = K_{\dot{h}}\left(\dot{h}_{REF} - \dot{h}\right)\left(1 + \frac{K_1}{S}\right) - K_{\ddot{h}}\,\ddot{h} + \theta_p\,(t,\ h) \qquad (4\text{-}14)$$

Figure 4-51
HCR-NAR Orbiter Terminal Trajectories, Guidance Laws Updated for Off-Nominal Flare Velocities

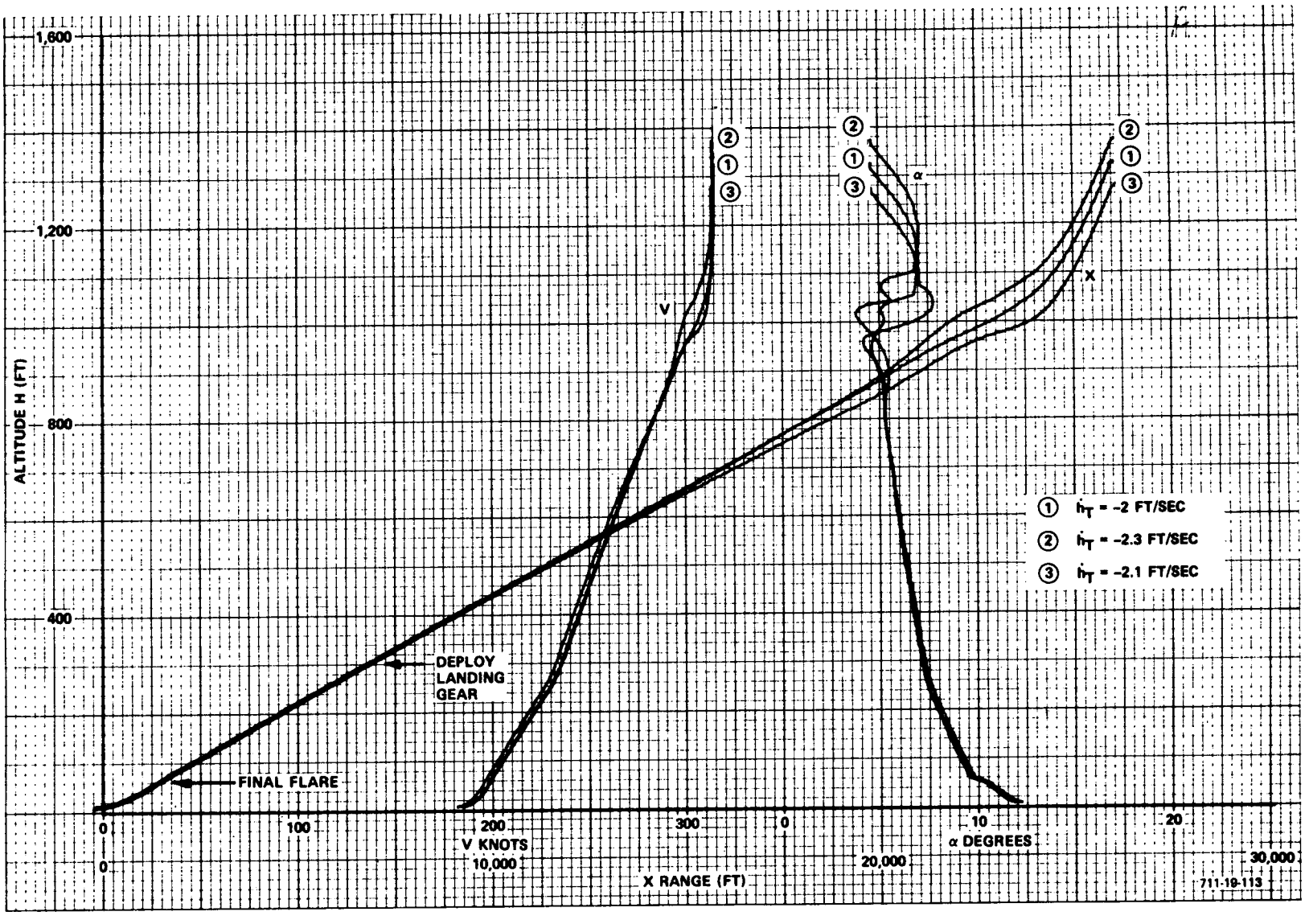

Figure 4-52
HCR-NAR Orbiter Terminal Trajectories,
Nominal and ±50 feet Errors in Flare Altitude

where:

K_1 = 0 until $\dot{h}_{REF} - \dot{h} \leq 3$ feet/second (4-15)

$\dot{h}_{REF}$ = -2 feet/second

K_1 = 0.5 or 0 as defined above

$K_{\dot{h}}$ = 0.25 degree/foot/second

$K_{\ddot{h}}$ = 0.1 degree/foot/second^2

$$\theta_p\ (t,\ h) = \frac{1.5}{0.5\ S + 1} + 0.16 \int_o^t dt \qquad (4\text{-}16)$$

The predictive term is written as a function of time and height, t and h. Only the time function, however, has been used thus far. A maximum constraint is placed on the integral (ramp) part of the θ_p term by limiting t of the integration to one second above the nominal flareout time.

4. High Altitude Energy Management

Section IIIC, Figures 3-34 and 3-35 describe the theoretical 100,000 feet window for the North American vehicle. This window is based on vehicle limitations and on certain ground rules for the system but is not a function of the guidance laws. The ground rules used include the following:

- Bank angles not to exceed 45 degrees.
- Operation is restricted to the front side of the L/D curve with sufficient margin so that the vehicle will remain on the front side for 45 degree bank turns.
- The aircraft will be on the terminal glide path by 20,000 feet.

The guidance system described by Equations (3-92) through (3-101) has been evaluated to determine its capability to meet the theoretical window.

Trajectories were run from a variety of directions and initial positions. The window achieved, which is shown in Figure 4-53, is based on the assumption that the vehicle is initially aimed at the target point and is at nominal speed at 100,000 feet. The window also does not include the effect of winds, off-nominal air density conditions, or off-nominal vehicle characteristics. The shaded area represents the window area included in the theoretical window but not achieved with the guidance system. This area represents about 2 percent of the entire window. The small circular area in the center is excluded in both the theoretical and achieved window since a vehicle in that region at 100,000 feet would be in a non-recoverable overshoot condition.

Note that the shaded area in Figure 4-53 is not symmetrical. This condition is the result of the restriction in the guidance equations that require clockwise turning circles. By providing the capability in the guidance laws for counterclockwise turns as well as clockwise, the realizable window could be increased by about 0.7 precent.

Trajectories from a variety of initial positions are shown in Figures 4-54, 4-55 and 4-56. In each case the vehicle is initially headed toward the aiming point. These runs are typical of the runs used to determine the realizable window. They illustrate typical turning patterns used to provide energy management. Run C in Figure 4-54 illustrates the problem for an overshoot case. Because the vehicle turn rate is low due to the initial high speed, a large overshoot of the target circle results. Runs in which the initial heading is 180 degrees from the runway heading are shown in Figure 4-54; trajectories with the vehicle heading due west, in Figure 4-55 and performance with the initial vehicle heading equal to the runway heading in Figure 4-56.

In every case these trajectories terminate with the final flareout and touch down on the runway. The lateral error is always zero at the time the trajectory is terminated. The few cases in these figures that show small deviations from runway alignment result from calibration errors in the recorder. The digital printout for these runs shows approximately zero lateral error in all cases.

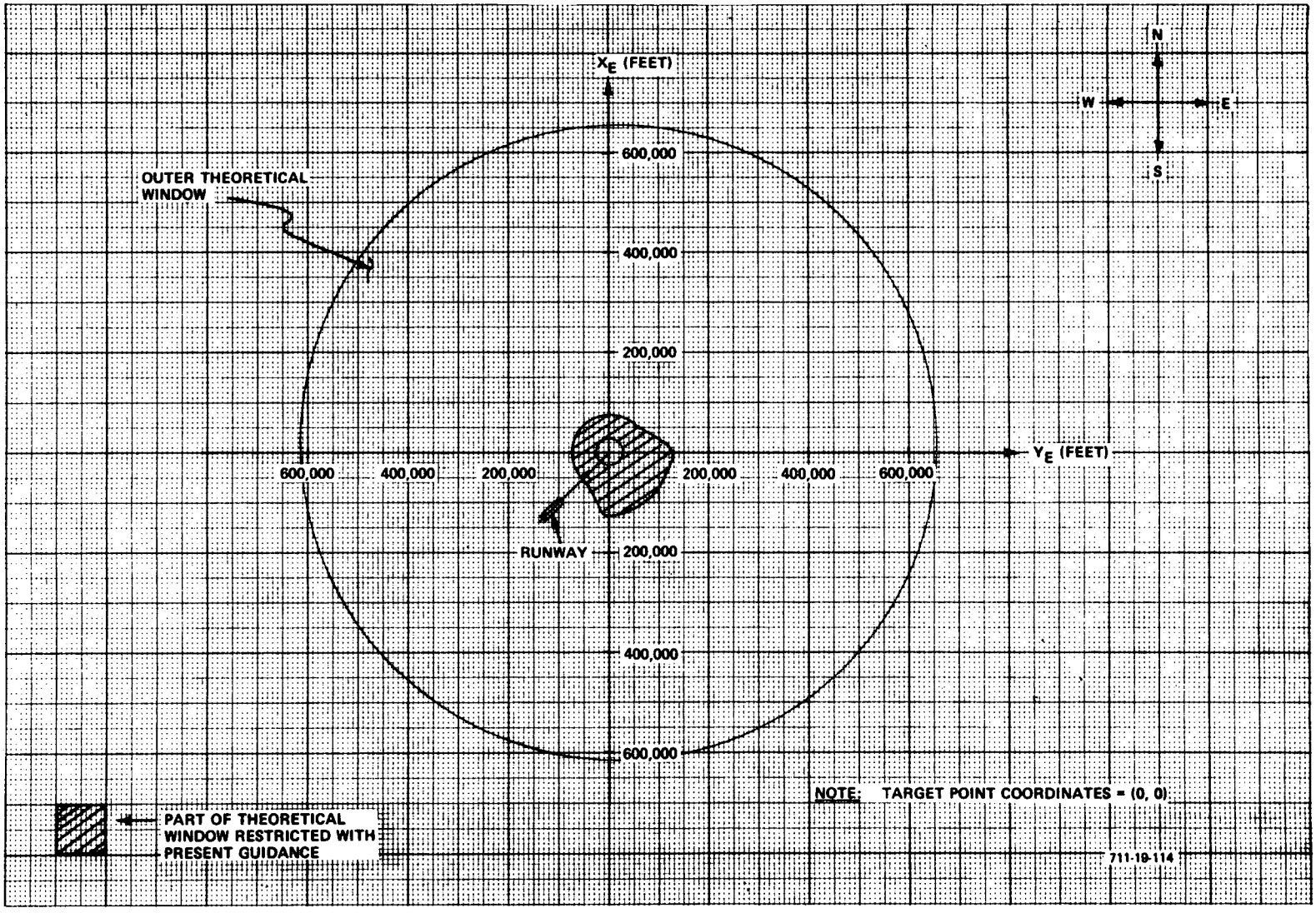

Figure 4-53
Window for HCR Orbiter at 100,000 feet
(Assuming Vehicle Initially Aimed at Target Point)

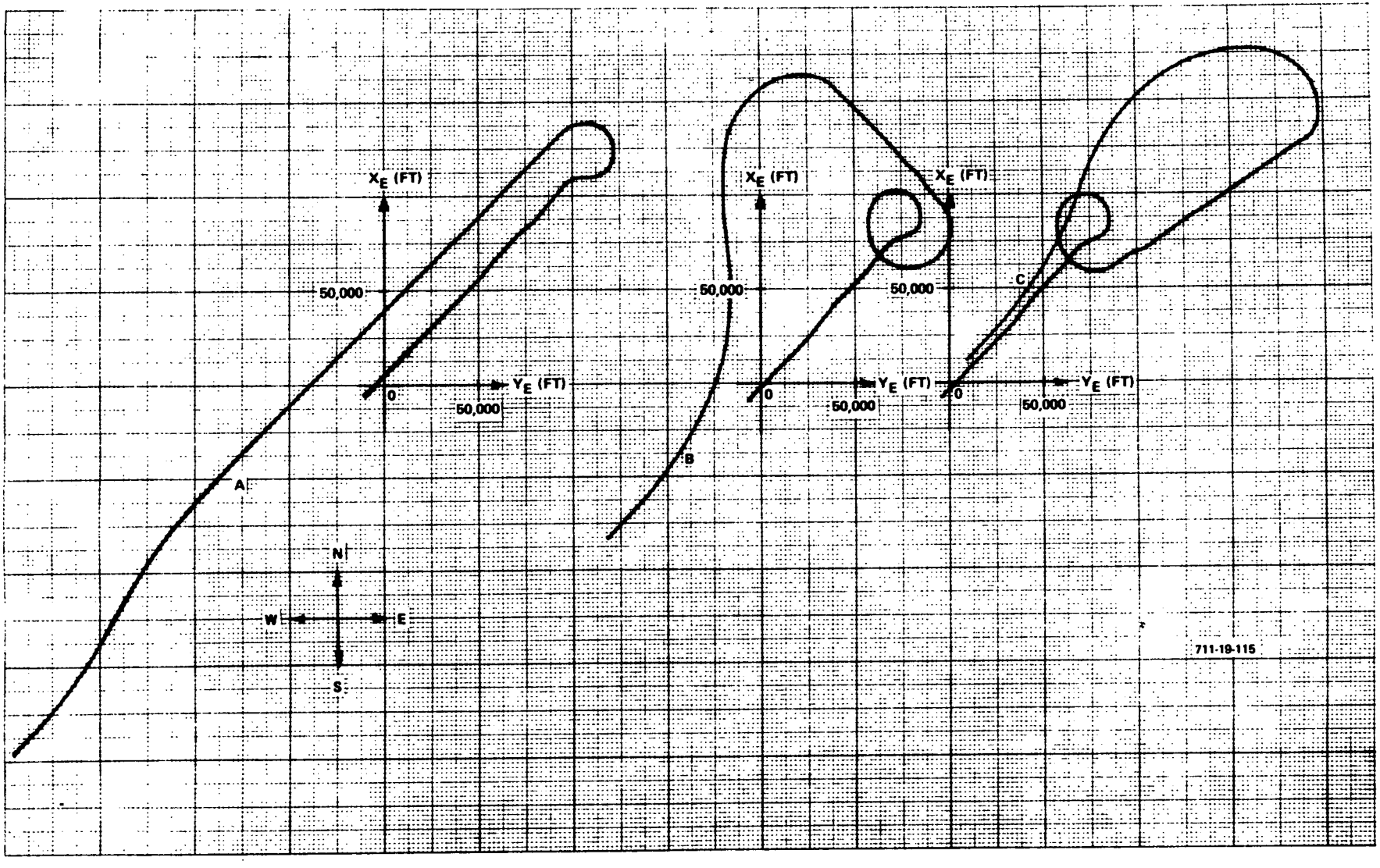

Figure 4-54
HCR Orbiter Energy Management Steering (Horizontal View)
for Various Initial Ranges to Target Point
(Initial Heading = Runway Heading +180 degrees)

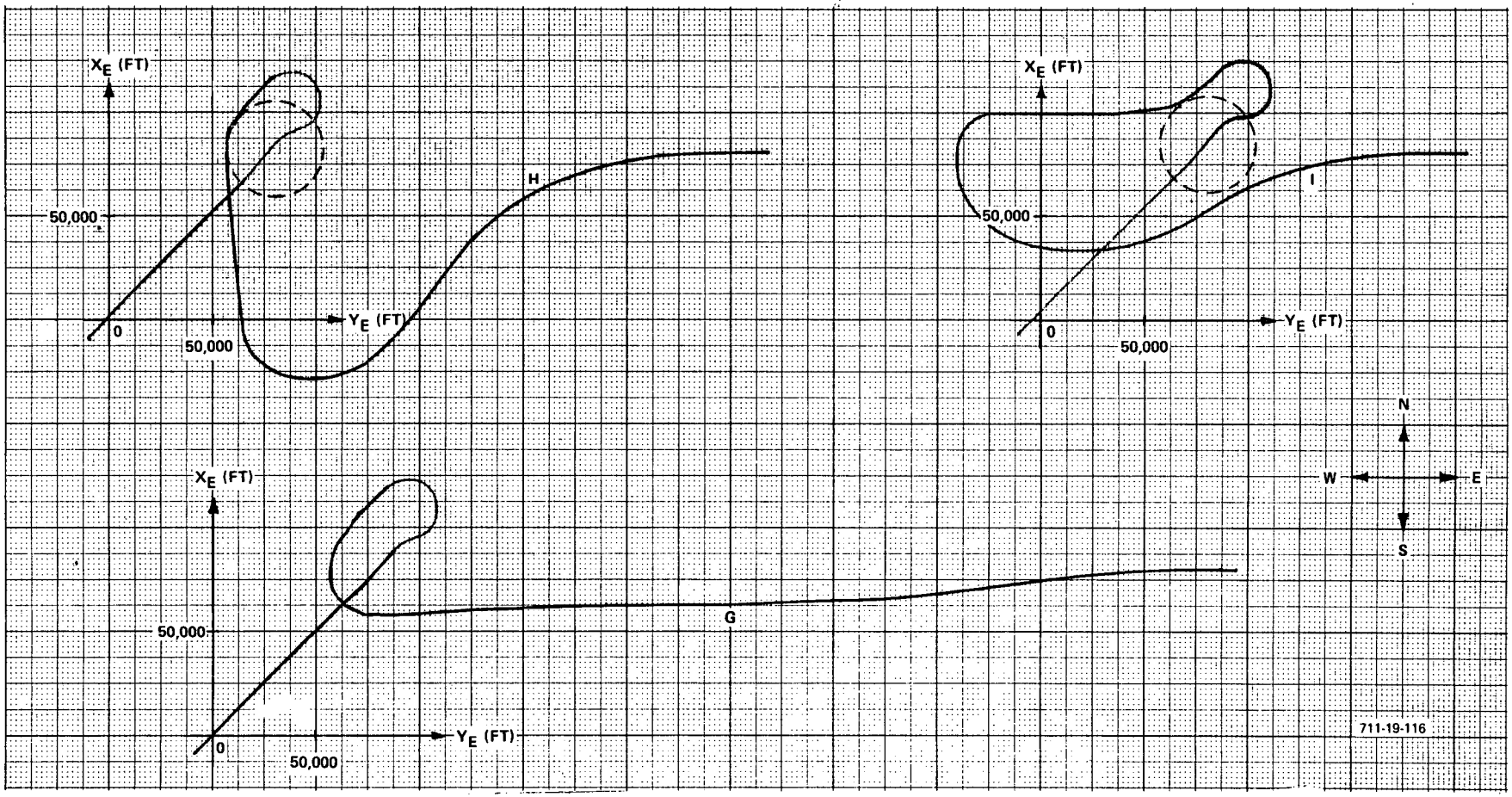

Figure 4-55
HCR Orbiter Energy Management Steering (Horizontal View)
for Various Initial Ranges to Target Point (Initial
Heading = Due West, Runway Heading = 224 Degrees)

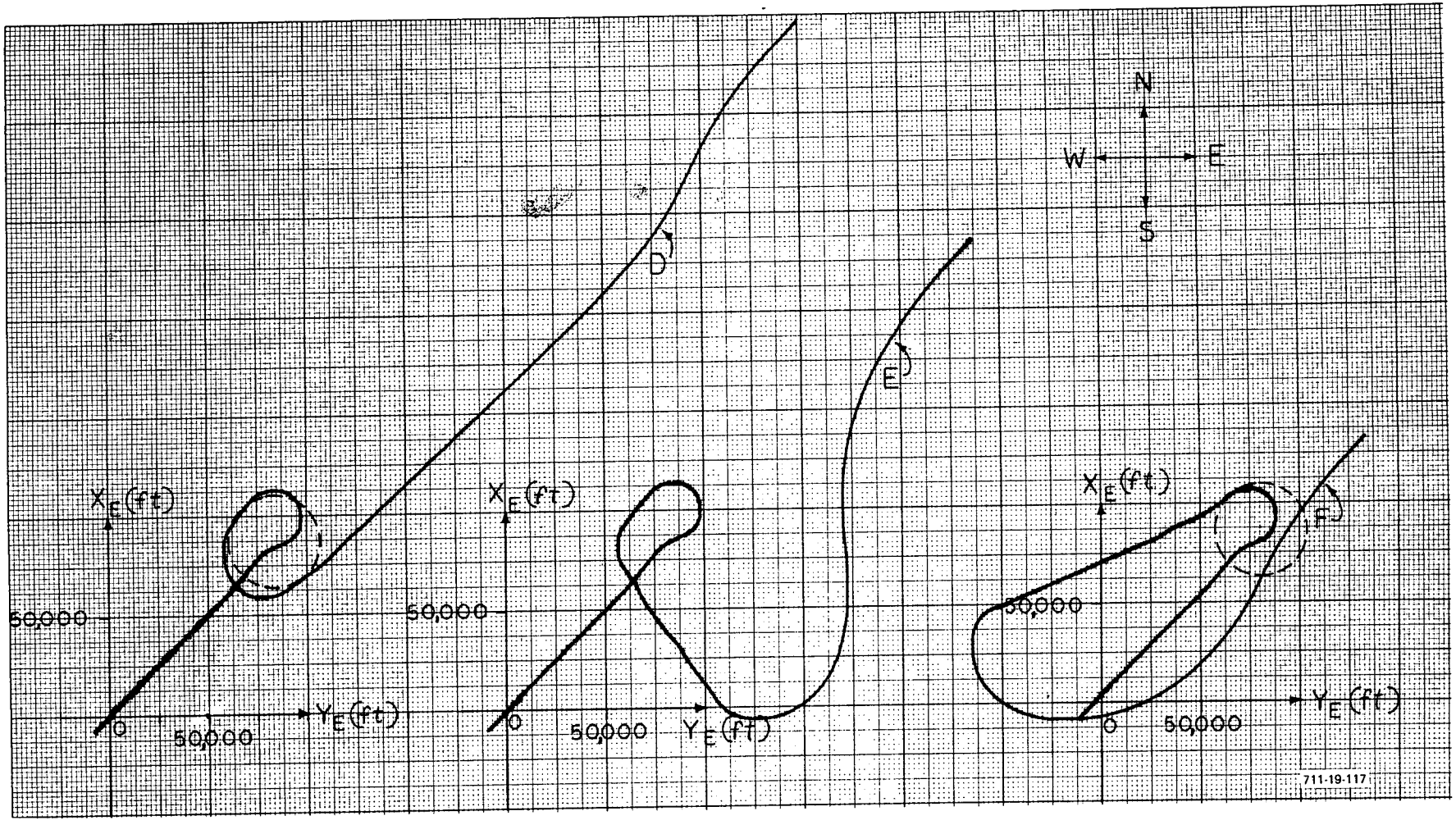

Figure 4-56
HCR Orbiter Energy Management Steering (Horizontal View)
for Various Initial Ranges to Target Point
(Initial Heading = Runway Heading)

A typical view of these energy management trajectories in the vertical plane is illustrated by Figure 4-57. This figure shows vertical views of the trajectories illustrated in Figure 4-56 (initial heading = runway heading). It is seen that the final approach glide path is acquired somewhat below 20,000 feet. This was a consequence of using an approximate guidance computation that defined the final turn onto the glide path. A more accurate turn prediction could result in a near perfect capture of the glide path at altitude above 20,000 feet. In subsequent work not documented in this report the final turn was cued on the basis of distance from the glide path center and velocity. The guidance computations used to obtain the trajectories of Figure 4-57 used a crude approximation of the correct altitude for starting the final turn onto the glide path.

In Figure 4-58, the velocity-altitude histories for the three trajectories of Figure 4-56 and 4-57 are illustrated. Note that D is the undershoot case, F is an overshoot case and E may be considered nominal. Figure 4-58 shows that the undershoot case (D) flew a higher Q than the nominal (E) which in turn had a higher Q than (F). Since the Q loop attempted to maintain Q at the reference value, the source of the deviations must be the result of a bias in the Q error Equation (3-92). The source of this bias is the lift compensation term of Equation (3-92). At a 45 degree bank angle, the lift compensation term commanded a nose-up pitch attitude of over 2.0 degrees. This corresponds to a bias error in the Q loop of near 50 pounds per foot^2 (speed reduction). Thus, the more turning there is in a trajectory, the lower the average Q as verified by the different h - V trajectories in Figure 4-58.

The time of flight from 100,000 feet to touchdown is approximately 11 minutes. A recording of altitude and incremental normal acceleration versus time is given in Figure 4-59. The various accelerations prior to reaching 20,000 feet are those associated with the turning maneuvers to achieve the high altitude energy management. Other acceleration transients mark glide path acquisition, first flare and final flare.

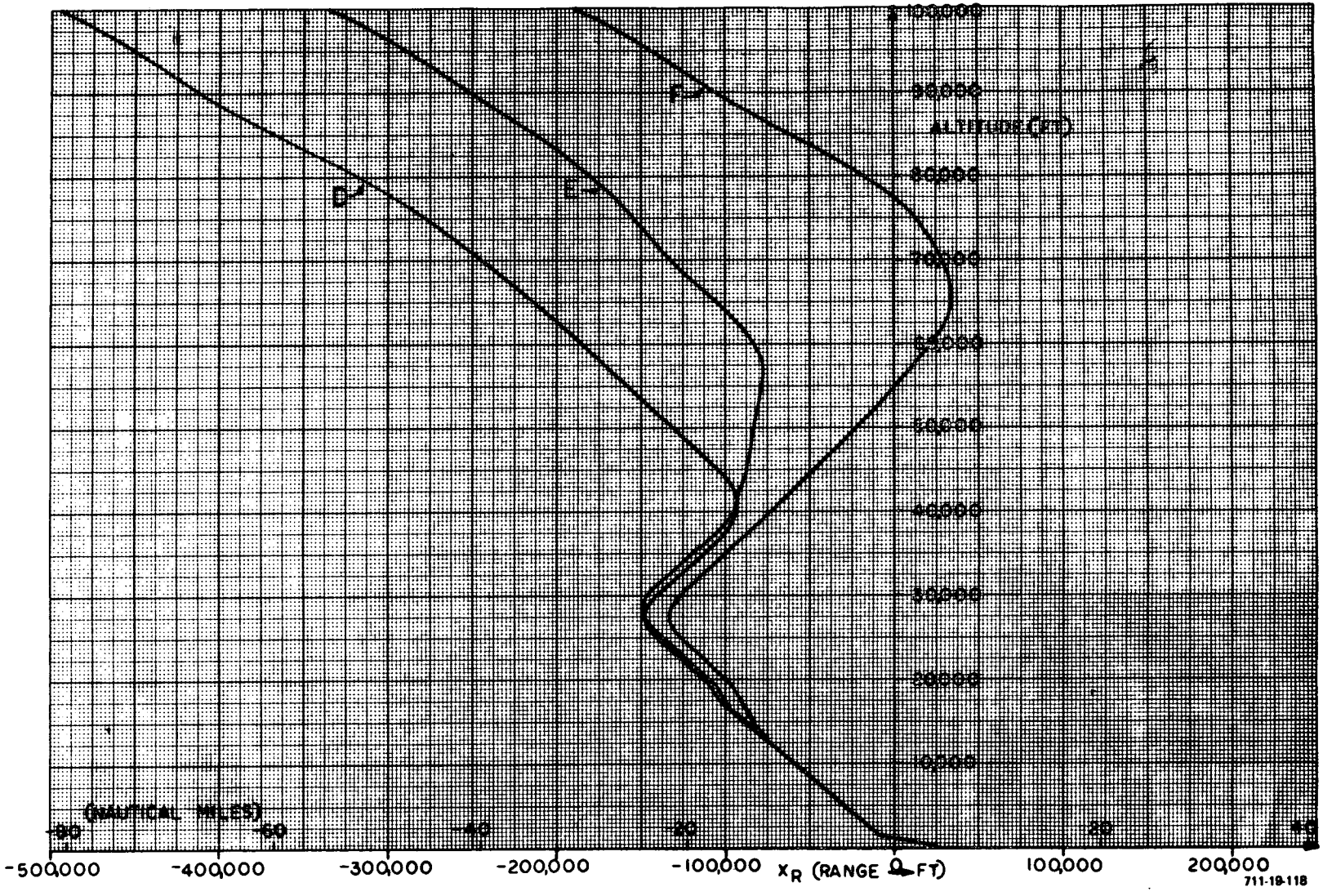

Figure 4-57
HCR Orbiter Altitude versus Range Histories for
Various Initial Ranges to Target Point
(Initial Heading = Runway Heading)

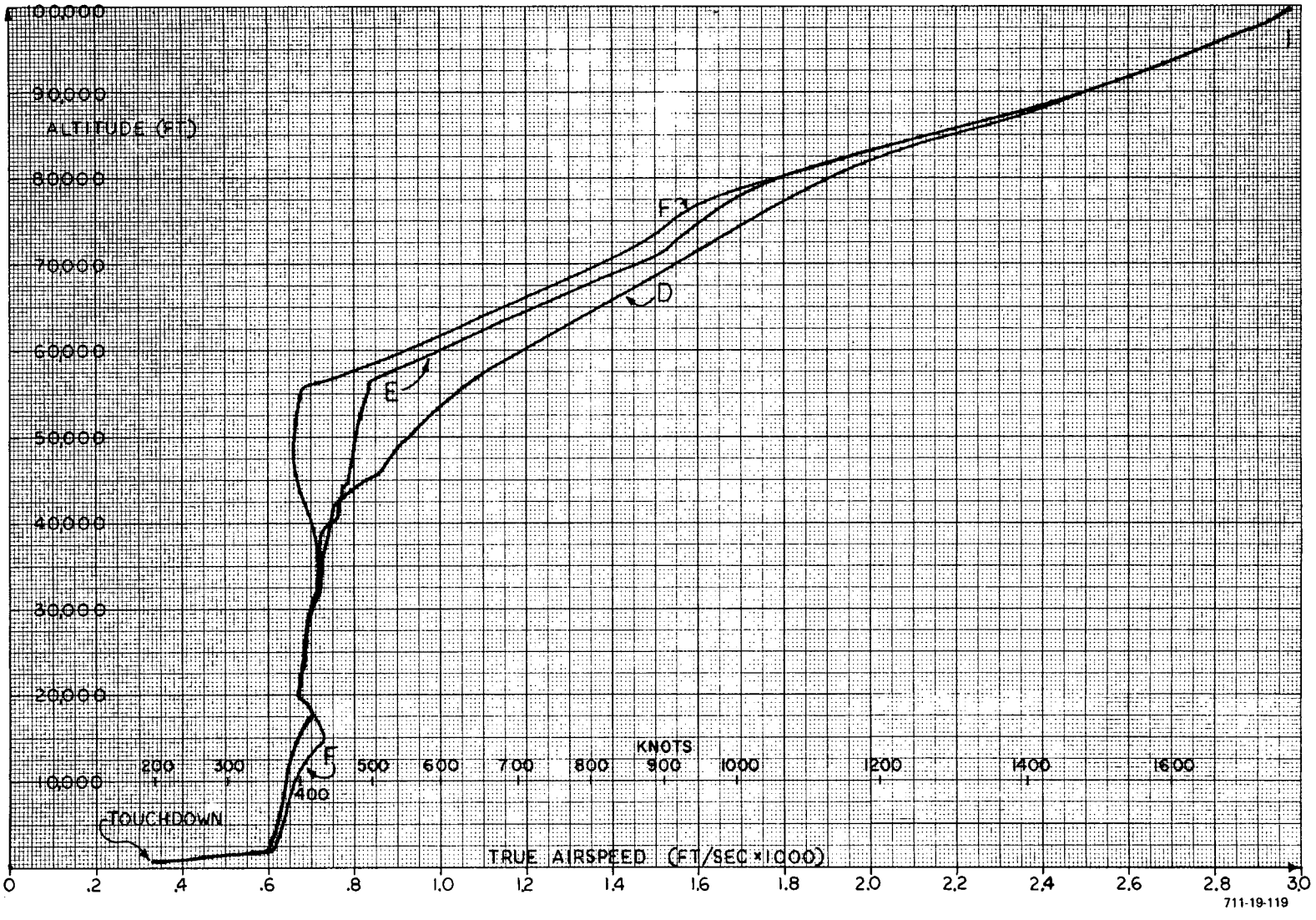

Figure 4-58
HCR Orbiter Velocity Histories for Various Initial Ranges
to Target Point (Initial Heading = Runway Heading)

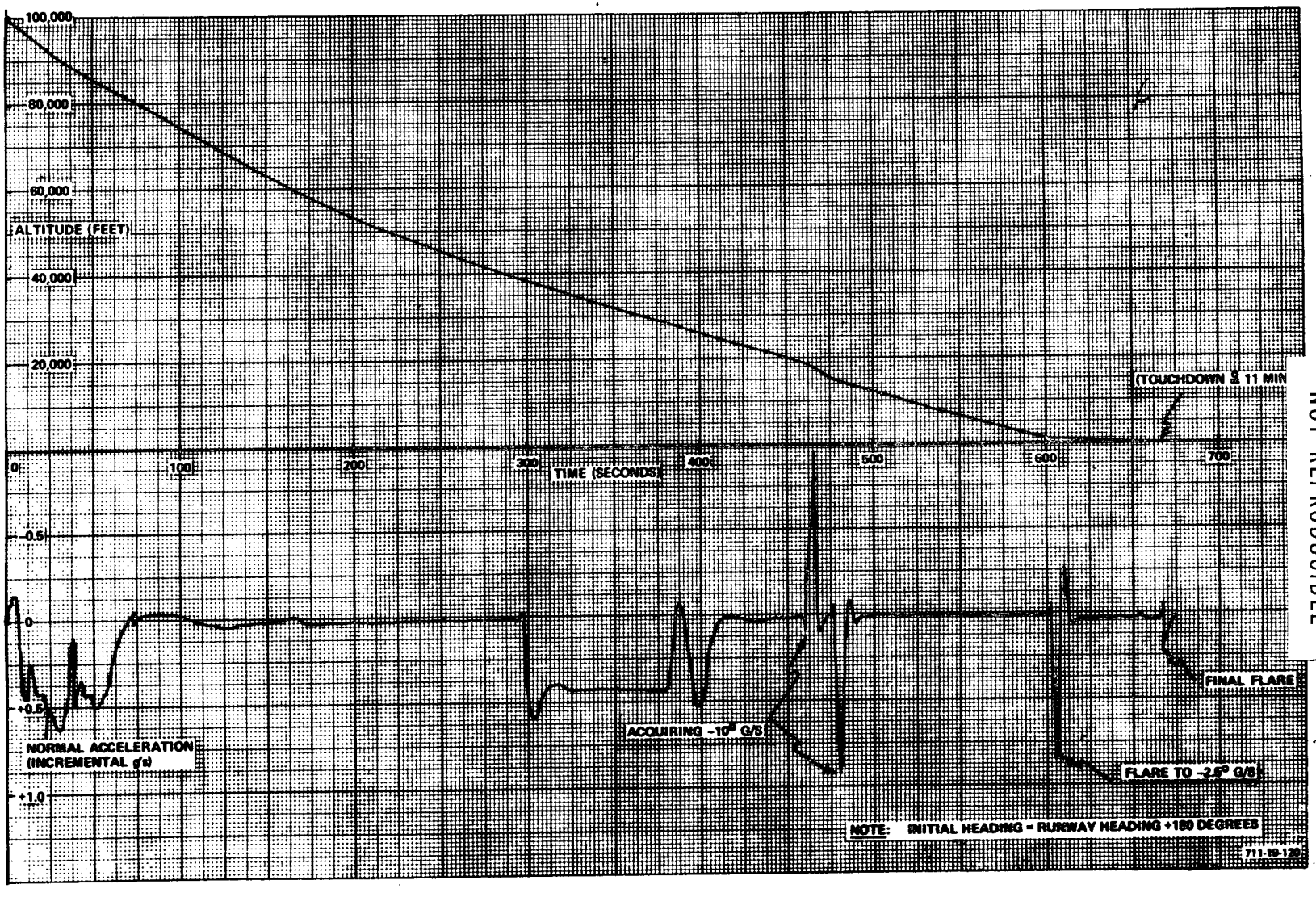

Figure 4-59
HCR Orbiter Altitude and Acceleration Time Histories from 100,000 feet

SECTION V

SIMULATOR VERIFICATION

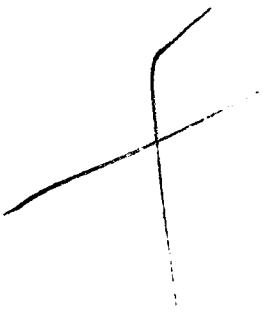

SECTION V

SIMULATOR VERIFICATION

A. SUMMARY OF SIMULATOR PROGRAMS

As discussed in Section IV, Introduction, there were various simulation techniques and simulators used in the performance of this study. Table 5-1 summarizes the simulation programs that were performed by identifying each vehicle studied and the types of simulation used. It is seen from this table that only the MDAC-2 low cross-range vehicle and the NAR high cross-range vehicle were flown and evaluated in the NASA ARC simulator. The NASA ARC simulator was the only one equipped and programmed for evaluation of the manual modes. This section is concerned with the evaluations that were performed in the NASA ARC simulator only and the primary subject of this section is the manual control investigations and the pilot evaluations of the automatic system performance (from their viewpoint in the cockpit).

TABLE 5-1

SIMULATION SUMMARY

Vehicle Studied	Simulations Used			
	Sperry 3 Degree of Freedom - Perturbation Equations (Analog Computer)	Sperry 5 Degree of Freedom - Wind Axis Aero Equations (Analog Computer)	Sperry 6 Degree of Freedom - Body Axis Aero Equations (Digital Computer)	NASA ARC 6 Degree of Freedom - Body Axis Aero Equations (Digital Computers) Plus Cab and Visual Scene
MSC 245 (LCR)				
Autopilot Design	X			
Approach and Landing Trajectories		X		
MDAC-1 (LCR)				
Autopilot Design	X			
Approach and Landing		X		
MDAC-2 (LCR)				
Approach and Landing		X	X	X
Transition	X	X	X	X
Energy MGMT		X	X	
Complete Trajectory			X	
LMSC-HCR				
Autopilot Design	X			
Approach and Landing		X		
NAR HCR				
Autopilot Design	X		X	
Approach and Landing		X	X	X
Energy MGMT		X	X	X
Complete Trajectory			X	X
MDAC HCR*			X	

*Results will be documented in Supplementary Technical Report.

B. SIMULATOR INSTRUMENTATION

A photograph of the displays and controls used in the NASA ARC simulator is given in Figure 5-1. Shown on the figure are:

- Sidestick Controller (X-15 Controller) with adjustable preload characteristics....This controller was always used in the pitch and roll rate control augmentation modes defined by equations (3-116) through (3-126) of Section III.D.
- Electronic Attitude Director Indicator (EADI) (with TV superposition capability)....The symbology shown on the figure includes horizon, pitch scale, aircraft symbol, flight path deviation window, digital airspeed, digital altitude, roll scale, azimuth scale, cross pointers and flight path angle symbol.
- Airspeed Indicator
- Altimeter
- Angle of Attack (α) Meter
- Flight Path Angle (γ) Meter
- Mach Indicator
- Vertical Speed indicator
- Flap or Surface Position Indicator
- Tactical Situation Display (Electro-Mechanical-Optical Projection Map display) and associated mode controls....Capable of fixed map/moving aircraft presentation with variable map scales.

  Note that this display was eventually removed and replaced with an X-Y plotter in lieu of the desired horizontal situation and moving map presentation.
- Gear Down Lever
- Flap Extension Lever
- Throttle Lever (not used)

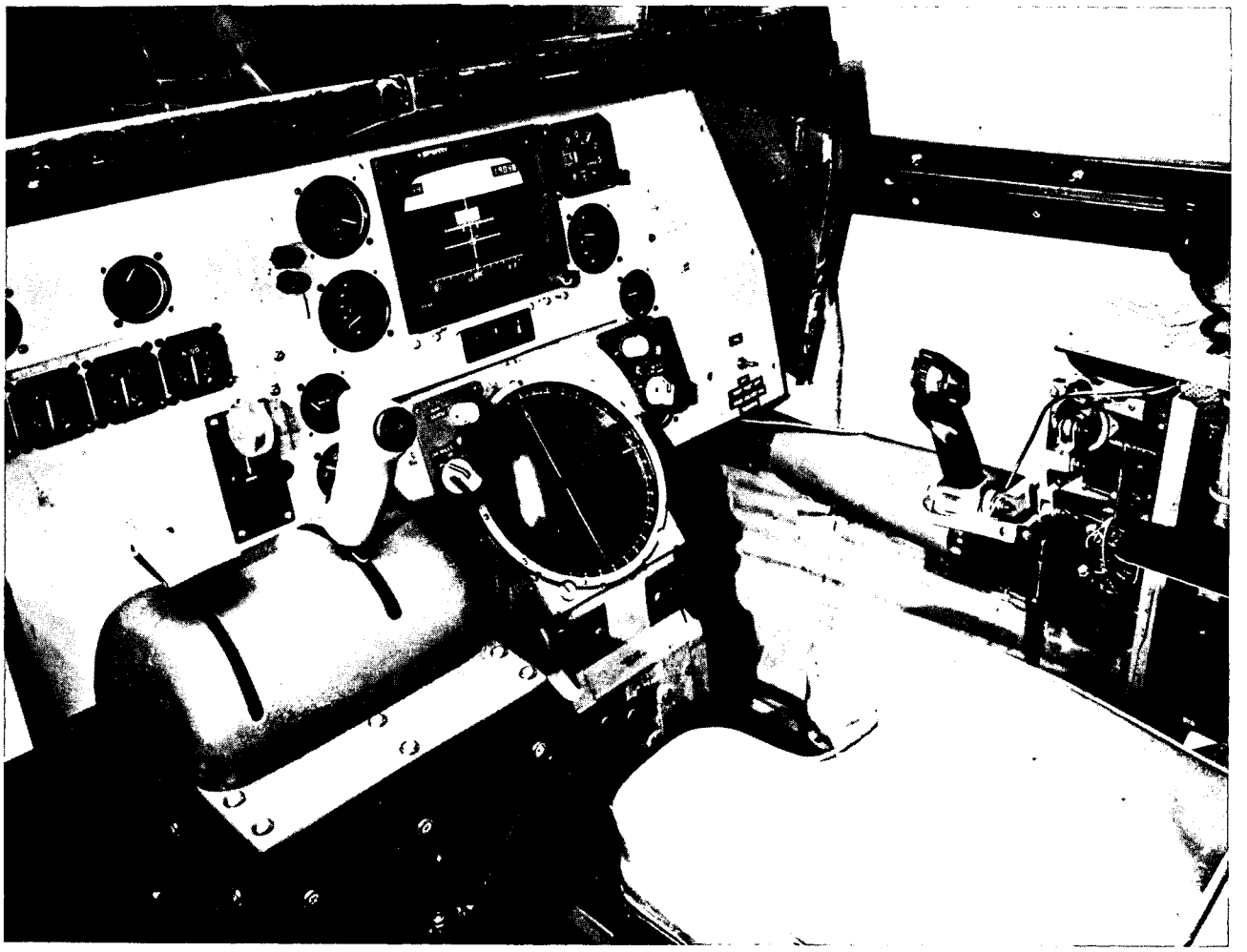

711-19-121

Figure 5-1
NASA Space Shuttle Simulator Cab

It is apparent from Figure 5-1 that the display layout did not have the benefit of an optimization study based on the latest human factors expertise, but nevertheless, this simple approach did not prevent the gathering of very useful information. The EADI had an extensive symbology repertoire, a large part of which did not prove to be useful because too much information tended to clutter and confuse the presentation. The actual EADI scales used were summarized in Section III.D, Figure 3-57. Table 5-2 summarizes all of the other available symbols and their characteristics. In early work the EADI's altitude "tape" presentation was used. This provided a moving altitude scale (against a fixed index) on the right side of the EADI. For the high rate of descent of the space shuttle, the moving "tape" display was found to be disconcerting. The digital altitude readout was retained but the resolution (availability of last digits) was changed with altitude to improve the readability when altitude is changing rapidly or slowly.

Two displays that are essential for a pilot-monitored automatic mode are an approach progress annunciator and a map display with trend vector (predicted trajectory). The former should be an adaptation of the approach progress annunciators used in conventional transport automatic approach and landing systems. It displays the phase of the automatic sequence presently engaged (green) and the phase which is armed (amber) and will be advanced to the next phase automatically at an upcoming mode switching sequence. The trend vector display is especially desirable for the high altitude energy management display where the pilot requires some indication of what type of turning trajectory the automatic system has computed. The cockpit shown in Figure 5-1 provided neither of these displays but it was recognized that future work should incorporate this capability.

TABLE 5-2

EADI SYMBOL CHARACTERISTICS

Symbol	Scale Factor	Reference	Dynamics	Travel Limits
Reference Airplane	-	-	Fixed*	-
Horizon Line	Same as Pitch	Ref Airplane	Pitches and Rolls	-
Horizon Shaping	Same as Pitch	Ref Airplane	Pitches and Rolls	-
Normal Pitch Scale	10 deg/in.	Ref Airplane	Pitches and Rolls	-
Expanded Pitch SCale	5 deg/in.	Ref Airplane	Pitches and Rolls	-
Pitch Reference Bar	10 deg/in.	Ref Airplane	Pitches and Rolls	Normal Scale
Roll Reference Marks	-	-	Fixed	0,±10,±20,±30 deg
Roll Marker	deg/deg	Roll Ref Marks	Rotates around Ref Airplane	±180 deg
Airspeed	-	-	Digital Readout	0 to 999 kt
Airspeed Error	15 kt/in.	Ref Airplane Left Wing Tip	Moves Vertically High Means Fast	±1 in.
Normal Azimuth Scale	20 deg/in.	Heading Index	Moves Horizontally	3.5-in. window
Expanded Azimuth Scale	10 deg/in.	Heading Index	Moves Horizontally	3.5-in. window
Pitch Command Bar	15 deg/in.	Ref Airplane	Moves Vertically	±1 in.
Roll Command Bar	30 deg/in.	Ref Airplane	Moves Horizontally	±1 in.
Single Cue Command	15 deg/in. vertical 30 deg/in. horizontal	Ref Airplane	Moves Vertically and Horizontally	±1 in. vertical ±1 in. horizontal
Flight Path Marker	Same as Pitch	Ref Airplane	Pitches and Rolls	-
Potential Gamma	16 ft/sec^2/in.	Flight Path Angle	Pitches and Rolls	±1 in.
ILS Window: Lateral Path Deviation	0.64 deg/in.	Ref Airplane	Moves Horizontally	±1 in.
ILS Window: Vertical Path Deviation	0.604 deg/in.	Ref Airplane	Moves Vertically	±1 in.
Selected Heading	Same as Azimuth	Azimuth Scale	Moves with Scale	-
Selected Course	Same as Azimuth	Azimuth Scale	Moves with Scale	-
Heading Index	-	-	Fixed	-
Altitude Scale: Cruise	450 ft/in.	Alt Index	Moves Vertically	3-in. window
Altitude Scale: Climb/Descent	900 ft/in.	Alt Index	Moves Vertically	3-in. window
Altitude Scale: Below 1000 ft	180 ft/in.	Alt Index	Moves Vertically	3-in. window
Altitude Scale: Below MDA +100 ft	45 ft/in.	Alt Index	Moves Vertically	3-in. window
Altitude Window	-	-	Digital Readout	-
Minimum Decision Altitude	-	-	Digital Readout	-
Altitude Index	-	-	Fixed	-

*Reference airplane is vertically positionable with controls on symbol generator.

C. LCR (MDAC-2) VEHICLE PERFORMANCE SUMMARY

This vehicle was flown in both the automatic and flight-director manual mode from 20,000 feet to touchdown on the NASA ARC simulator. The flights were with and without winds (see Appendix B for wind model description). The flareout guidance system used the acceleration controller described in Section III.C although later work with the HCR vehicles indicated the desirability of changing to a different flareout control law.

Even in conventional powered aircraft, a flight director display for flareout has never been satisfactorily verified as acceptable. Although many flareout flight director modes have been studied and tested, considerable controversy remains regarding the desirability of such a mode or the effectiveness of the command cues. In the case of the steep angle approach with unpowered shuttlecraft, the problem is magnified because there is far less margin for error than in conventional aircraft. Initial attempts with flight director displays for final flare used the same pitch command presentation technique shown in Figure 3-58 of Section III.D. In final flare, the closed-loop pitch commands were derived from the vertical acceleration control loop and the high gain terminal $\ddot{h}$ controller. If the pilot does not follow the nominal commands properly or if he entered final flare with large vertical velocity or speed errors, then he becomes dependent upon the acceleration loop for corrective action. The automatic system uses a considerable amount of pitch rate damping to keep this loop stable. It is apparent that the pilot requires some additional compensation to handle this loop. The addition of pitch rate compensation or revision of the flareout system to a straight vertical velocity control loop could have corrected the problem. In subsequent work with the HCR vehicle, the vertical velocity flareout guidance system provided adequate cues for the flight director mode.

Many flight director landings were attempted with the LCR vehicle. Whereas the automatic system always touched down with a vertical speed of about -2 feet per second, the softest flight director landings were about -4 feet per second with -6.5 feet per second typical.

Figure 5-2 shows time responses for a flight director landing for the critical period from prior to first flare to touchdown. (Compare this run with Figure 5-3 which shows a complete automatic run to touchdown.) Lateral and longitudinal flight director control during the steep glide slope phase presented no problems. This run, by an inexperienced pilot, shows a 50-foot overshoot in capturing the shallow glide slope and the digital printout (not included) showed a vertical velocity of -6.7 feet/second at touchdown. Note that this run was made without flap deployment; hence, the high landing speed of about 220 knots. Manual flap deployment proved to be a difficult task with the mechanization of the manual lever. A modification was made to permit a 5-degree-per-second rate of deployment rather than a step change in flap position when the lever is set at a given position but its effect on manual performance was not evaluated.

If we compare the manual landing (Figure 5-2) with the latter part of the automatic run (Figure 5-3), it is apparent that the pilot was following the flight director commands during the first flare but he attempted to terminate the maneuver too soon. This caused a dip in the normal acceleration which was again increased but the average acceleration was too low so that he penetrated the shallow glide path, thereby generating a 50-foot overshoot error. He attempted to correct the shallow glide path offset but never quite returned to zero error. In the flareout, the flight director manual response is considerably different from the automatic response.

The 50-foot overshoot is just on the edge of the vertical error specification defining acceptable guidance errors, but the -6.7 foot/second touchdown rate of descent exceeds the 4-foot/second which is considered maximum allowable. It is expected that the overshoot on the shallow glide slope can be reduced significantly with a little pilot experience, but the final flare requires some changes in the control laws in addition to pilot experience, as discussed previously.

A comparison of the nominal LCR vehicle final approach with no winds (Figure 5-3) and the identical approach trajectory with the standard wind model (Figure 5-4) shows that despite the relatively severe turbulence, position excursions rarely reach as high as 20 feet and flight path angle and pitch angle variations do not exceed about 1 degree.

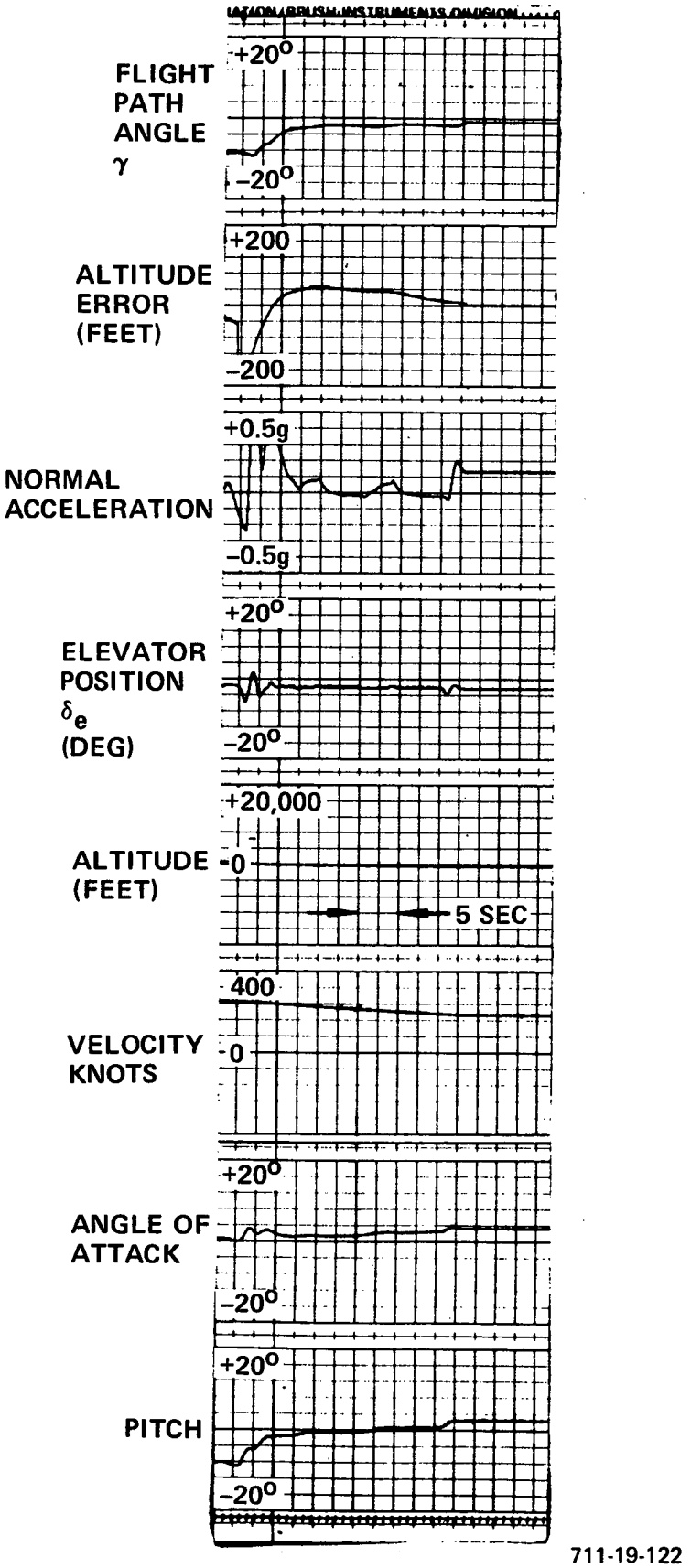

Figure 5-2
LCR Vehicle Flight Director Landing, NASA Simulation

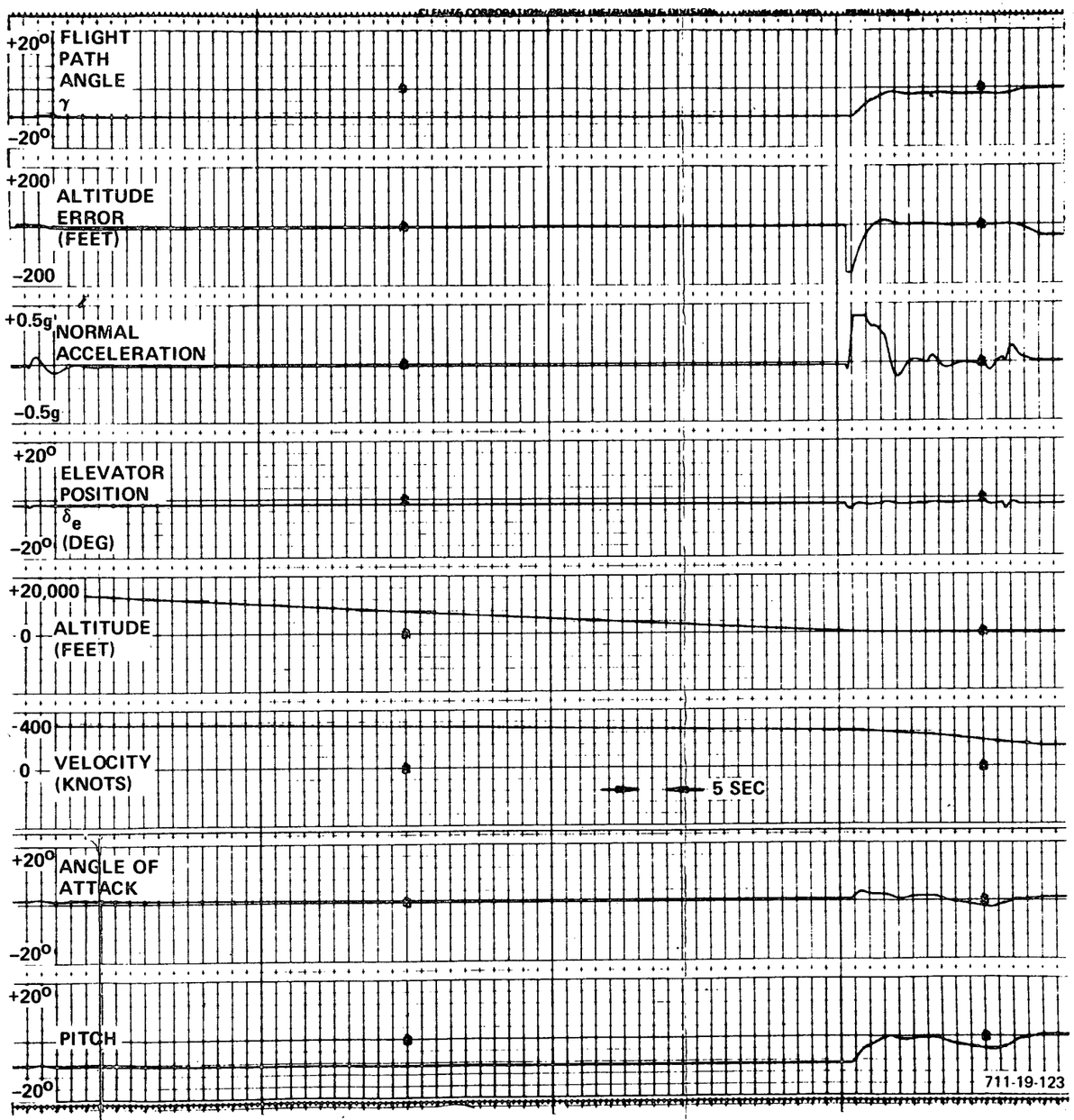

Figure 5-3
LCR Vehicle Automatic Mode, 19,000 feet
to Touchdown, NASA Simulation

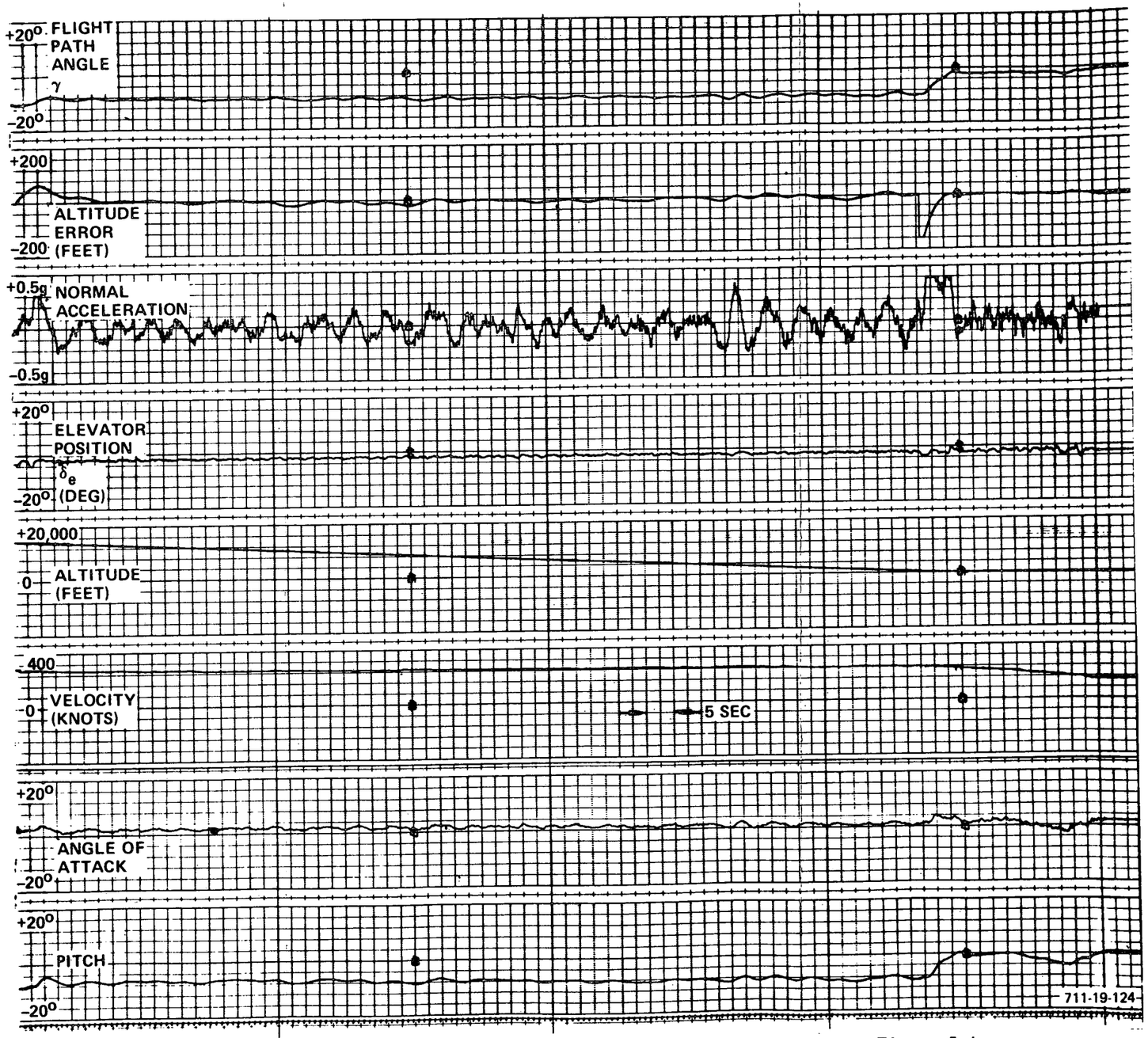

Figure 5-4
LCR Vehicle Automatic Mode with Wind Model,
20,000 feet to Touchdown, NASA Simulation

Although no formal procedure was used to gather and tabulate statistical data on landing performance with the LCR vehicle, results obtained in about 30 automatic landings were digested into Table 5-3 which summarizes performance for different conditions of disturbance.

TABLE 5-3

GUIDANCE AND CONTROL ACCURACY LANDING PERFORMANCE
FOR LCR VEHICLE

TOUCHDOWN PARAMETER	NOMINAL	VARIATION FOR ±20 KT SPEED DEVIATION AT FIRST FLARE	VARIATION FOR HEADWINDS AND TAILWINDS ±20 KT	2σ VARIATION FOR WIND MODEL (TURBULENCE AND SHEAR)
$\dot{h}_T$	-2 FT/SEC	-1.7 TO -2.2 FT/SEC	-1.5 FT/SEC	-1.4 TO -4.0 FT/SEC
x_T (FROM AIM POINT)	1000 FT	$1000^{+400\ FT}_{-300\ FT}$	$1000^{+500\ FT}_{-400\ FT}$	$1000^{+700\ FT}_{-500\ FT}$
V_T (AIRSPEED)	175 KT	175 ±15 KT	175 ±20 KT	175 ±25 KT
Δy_T (LATERAL DISPLACEMENT)	0	0	0	±20 FT

D. HCR VEHICLE PERFORMANCE VERIFICATION AND PILOT EVALUATION

1. Introduction

During the period between March 24 and April 2, 1971, a group of flight research pilots participated in the evaluation of the automatic and manual modes as mechanized on the NASA ARC visual scene simulator. The pilot evaluators included Apollo astronauts and research pilots experienced in unpowered landing techniques for high speed aircraft. They were:

Col. Edwin E. Aldrin, Jr.	Astronaut
Maj. Donald H. Peterson	Astronaut
Maj. Karol J. Bobko	Astronaut
Stan Cobb	Technical Pilot, Space Shuttle Pan American Airways
Walter Smith	Test Pilot McDonnell Douglas
Donald Germaraad	Test Pilot Lockheed Space and Missile Company
Fred Drinkwater	Research Pilot NASA ARC
Gordon Hardy	Research Pilot NASA ARC

The vehicle simulated was the particular model of the NAR HCR (delta wing) vehicle described in Section IV.C. They flew the manual modes and flight director modes and observed and monitored the automatic modes. A complete description of these three modes in terms of guidance laws and displays is given in Section III.D. Note that all manual modes including the so-called manual raw data mode used the control augmentation system which provided attitude rate maneuvering of a stabilized vehicle.

2. Simulator Results

The performance of different evaluation pilots on the manual modes depended upon many factors such as familiarity with the simulator and system concepts plus their inquisitiveness relating to how far they can improvise a solution that deviated from the system design. It would have been most desirable to allow each pilot evaluator two days on the simulator. The first day would provide for familiarity with system, simulator, and vehicle idiosyncracies. The

second day would be used for accumulating statistical performance data. Unfortunately, this amount of time was not available so that the pilot performance statistics are not too significant. Nevertheless, it was apparent that all of the pilots participating could become very proficient in the manual modes after one day of simulator experience.

A summary of results obtained during one day of simulator flights (3/29/71) is given in Table 5-4. The two participating pilots are identified as Pilots A and B. Runs are numbered in the sequence in which they occurred. Run numbers omitted correspond to cases where the problem was aborted prior to landing; usually because of simulator problems or the desire of the pilot to experiment with handling qualities or some aspect of the system other than landing performance. The HDG, X, and y columns correspond to the heading and coordinates of the vehicle when initialized at 100,000 feet. When an initial condition other than 100,000 feet was used, it is noted in these columns. The wind column indicates the presence or absence of the NASA standard wind (with turbulence) and the direction of the wind. The final four columns represent the touchdown x, y, coordinates, vertical speed, $\dot{h}$, and forward speed V. The x coordinate is measured from the beginning of the runway which is about 1600 feet forward of the intersection of the shallow glide path with the ground. The mode column identifies automatic mode (AUTO), flight director mode (FD), and back-up manual mode or raw data mode (RD).

Table 5-3 only shows the touchdown performance, but the performance during other phases of flight are of equal or greater significance. All pilots did an excellent job in acquiring and controlling to the high energy glide path. The techniques for flareout with flight director are always a source of controversy. Manual flareouts using the visual scene are dependent upon getting used to the simulator. However, arriving at the flareout point with the proper position and velocity is always essential and this task was readily achieved with both manual modes. Figure 5-5, for example, is an x-y recording of Col. Aldrin's simulator flights using the back-up manual mode. The procedure followed was the one described in Figure 3-59 of Section III.D. That flight terminated near the runway (0, 0 coordinate) with a relatively soft touchdown.

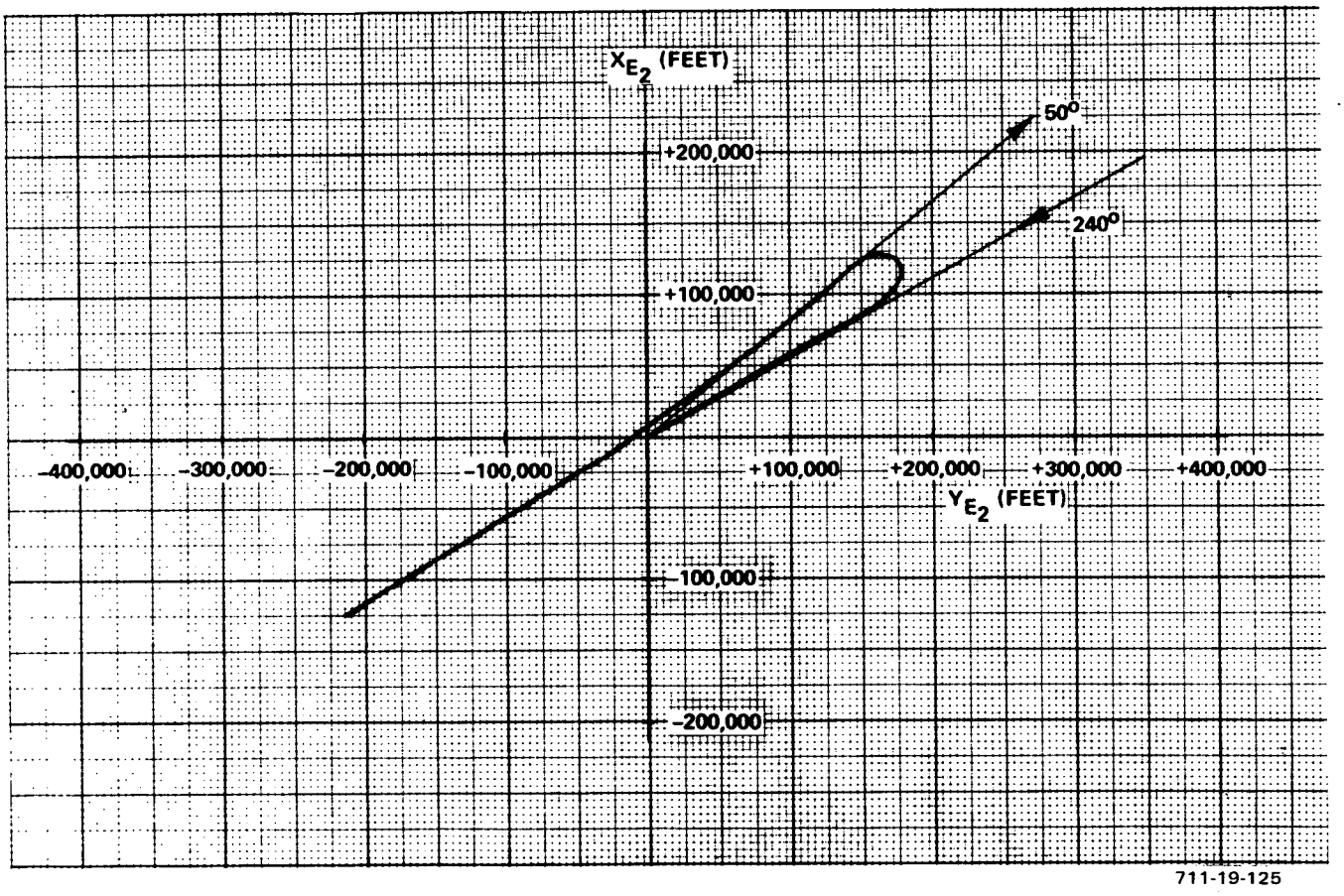

Figure 5-5
HCR Vehicle Raw Data Mode, 100,000 feet to Touchdown, Pilot - Colonel Edwin E. Aldrin

TABLE 5-4

SUMMARY OF SIMULATOR RUNS, PILOTS A AND B

Run No.	HDG	X	Y	Winds	Mode	$*X_{TD}$	Y_{TD}	$\dot{h}_{TD}$	V_{TD}	Remarks
1	60 deg	257K	0	341.4 deg	Auto	3815	-18	-1.8	192.8	
14	60 deg	257K	0	No	Auto	3923	0	-1.8	195	
15		20,000 ft		No	Auto	4029	0	-1.8	196	
16		20,000 ft IC		No	FD	6580	16	-1.4	176	X Offset + 500 ft Pilot A Y Offset + 1000 ft Pilot A
17		6,000 ft IC		No	FD	4978	18	-2.2	189	X Offset + 500 ft Pilot A Y Offset + 1000 ft Pilot A
19		20,000 ft IC		330 deg	FD	4442	-30	-21	192	Pilot B
20		20,000 ft IC		330 deg	FD	4480	-21	-2.6	183	Pilot B
22		5,000 ft IC		330 deg	FD	5132	-9	-3.2	182	Pilot B
23		5,000 ft IC		330 deg	FD	4162	-23	-2.4	186	Pilot B
24		5,000 ft IC		330 deg	FD	6130	-27	-11.7	170	Pilot B
25		5,000 ft IC		330 deg	FD	3687	-24	-7.1	186	200 ft Breakout Pilot A
26		5,000 ft IC		No	FD	6492	13	-8.1	171	500 ft Breakout Pilot A
27		5,000 ft IC		No	FD	1676	4	-4.1	195	Pilot A
28		20,000 ft IC		No	FD	5556	29	-2.3	186	700 ft Breakout Pilot A
29		5,000 ft IC		No	FD	4451	68	-5.4	187	700 ft Breakout Pilot A
30		5,000 ft IC		330 deg	FD	6634	43	-8.6	166	500 ft Breakout Pilot A
31		5,000 ft IC		330 deg	RD					500 ft Breakout Pilot A Abort
32		5,000 ft IC		330 deg	RD	6076	-83	-8.6	167	200 ft Breakout Pilot A
33		5,000 ft IC		330 deg	RD	6013	-50	-7.5	169	200 ft Breakout Pilot A
34		20,000 ft IC		No	RD	2791	25	-5.6	199	700 ft Breakout Pilot B
35		20,000 ft IC		330 deg	RD	1396	-37	-14.4	192	700 ft Breakout Pilot B
36		5,000 ft IC		330 deg	RD	-746	-46	-17.9	214	500 ft Breakout Pilot B
37		5,000 ft IC		150 deg	RD	3687	26	-5.6	191	200 ft Breakout Pilot B
38		5,000 ft IC		150 deg	RD	6787	62	-7.6	163	100 ft Breakout Pilot B
39	150 deg	-137K	393K	240 deg	FD	1338	0	-2.4	179	700 ft Breakout Pilot B
40	60 deg	0	0	240 deg	FD	1338	22	-8.4	189	700 ft Breakout Pilot A
41	60 deg	0	0	240 deg	FD	2340	42	-5.9	170	200 ft Breakout Pilot A
42	150 deg	-137K	393K	240 deg	RD		-25	-9.5	158	500 ft Breakout Pilot B

*Glide slope intercept coordinate ≈ 1600 ft.

As mentioned previously, the coordinates of x, the downrange distance at touchdown on Table 5-3, are offset from the intersection of the shallow glide path by about 1600 feet. Nevertheless, this indicates that the nominal touchdown point (as represented by automatic mode performance) is about 2300 feet downrange of the shallow glide path intersect point. This is considered an excessive distance. In the Sperry simulations, the identical control parameters resulted in a nominal downrange touchdown point of about 1900 feet from the shallow glide path intersect. This discrepancy has been traced to a difference in the vertical speed loop response. It may be that slight differences in the aero simulation model could account for the discrepancy, but this was never resolved. Of greater significance is the fact that even the 1900-foot downrange touchdown is excessive. This undesirable consumption of runway is partially a consequence of the flareout system that favors a soft touchdown over runway dispersion. The changeover to the vertical speed control flareout scheme in place of the acceleration control scheme tended to sacrifice longitudinal runway consumption prior to touchdown. However, in more recent work with the McDonnell Douglas high cross-range orbiter, the vertical velocity flareout controller was designed to give consistent touchdown $\dot{h}$'s of -2 feet/second while achieving a nominal longitudinal position at touchdown which is 800 feet from the intersection of the shallow glide slope and the ground. This work will be described in the Supplement to the present report.

Detailed descriptions of the manual mode evaluation runs were recorded and printed in a summary format. That format described the vehicle state and the control commands at altitude intervals of 10,000 feet and during critical mode transition times (first flare, final flare, decrab, touchdown, for example). An examination of some typical print outs provides many insights into system capabilities, idiosyncracies and potential problem areas.

Consider two runs made by Major Peterson; one in the raw data mode and one in the flight director mode. Tables 5-5 and 5-6 are the computer printouts for these runs. They both start at about 100,000 feet heading initially at 150 degrees. (The runway heading is 240 degrees.) Figure 5-6 is a plot of the horizontal view of these two trajectories. Note that the evaluation pilot, Major Peterson is flying these trajectories with no previous simulator practice.

TABLE 5-5

COMPUTER PRINTOUT OF RAW DATA MODE FLIGHT

SSV FLIGHT DATA DATE MM/DD/YY

RUN NUMBER 23

CONSTANT WIND DIRECTION = 240.000 DEG
INITIAL MEAN WIND VELOCITY = 0.830 FT/SEC

VARIABLE	EVENT 1 I.C.	2 90 K-FT	3 80 K-FT	4 70 K-FT	5 60 K-FT	6 50 K-FT	7 40 K-FT	8 30 K-FT	9 20 K-FT	10 10 K-FT
ALTITUDE) FROM	99986.	90011.	80004.	70007.	60008.	50006.	40010.	30001.	20004.	10002.
X POSITION) RUNWAY	-137000.	-143703.	-151562.	-159640.	-191759.	-232133.	-251253.	-203212.	-135695.	-79865.
Y POSITION) IN FT	393000.	288432.	155745.	80506.	28193.	18518.	-14587.	-15911.	-224.	144.
ROLL RATE)	0.00	0.22	0.00	-0.96	-0.08	2.26	0.57	0.56	0.00	-0.16
PITCH RATE)DEG/S	0.00	0.13	0.08	1.58	1.01	3.22	2.77	1.14	0.03	0.06
YAW RATE)	0.00	0.09	-0.00	-0.74	-1.15	2.22	1.68	1.07	0.01	-0.17
BETA) DEG	-1.51	0.06	0.02	0.17	-0.04	0.42	0.11	0.50	-0.18	0.09
ALFA)	14.61	13.13	9.19	11.26	11.22	10.31	11.61	9.15	5.58	4.04
THETA)	9.68	7.08	1.27	1.44	-4.00	-9.94	-5.89	3.93	-3.75	-4.62
THETA COMMAND) DEG	9.68	7.72	3.58	4.34	-4.80	-8.04	-5.87	4.33	-3.87	-4.53
PHI) DEG	0.00	0.37	0.38	-39.82	-42.03	45.15	49.45	15.67	1.15	-0.59
PHI COMMAND) DEG	0.00	0.57	0.43	-39.17	-42.10	46.05	49.68	15.71	1.06	-0.56
PSI	150.00	148.34	148.97	134.48	80.64	78.23	206.52	259.92	244.74	240.17
ELEVATOR DEFL)	-35.63	-25.95	-19.27	-27.17	-11.42	-8.99	-8.96	-7.25	-3.65	-2.76
AILERON DEFL) DEG	0.00	0.02	0.12	2.78	0.03	1.10	-0.05	0.17	-0.17	0.00
RUDDER DEFL)	-0.00	0.14	0.01	0.32	-0.00	-0.41	-0.27	-0.08	-0.15	0.09
FLIGHT PATH DEG	-4.92	-0.07	-7.92	-7.25	-12.20	-17.26	-13.66	-5.16	-9.38	-9.00
AIR SPEED) KNOTS	1787.7	1569.3	1192.5	958.1	680.1	580.2	466.2	379.0	374.0	357.4
EQUIV A/S)	209.8	232.7	224.7	230.4	208.5	228.6	231.2	231.8	273.0	307.2
QBAR LBS/FT.SQ	149.3	183.8	171.4	180.2	144.6	177.4	181.5	182.4	252.9	320.2
LOAD FACTOR	1.08	1.29	0.89	1.33	1.46	1.51	1.76	1.14	0.90	1.00
LATERAL ACCL FT/S2	2.64	-0.09	-0.03	-0.15	0.10	-0.74	-0.25	-0.68	-0.00	-0.01
ALTITUDE ERROR FT	-79796.22	-68653.77	-57261.28	-46365.20	-30175.45	-19057.40	515.99	1860.51	-49.91	106.86
GAMMA ERROR DEG	5.08	3.93	2.09	2.75	-2.20	-7.25	-3.69	4.84	0.63	0.19
VERT VELOCITY FT/S	-259.2	-278.8	-278.2	-204.1	-242.5	-292.7	-186.2	-57.0	-134.0	-103.2
PSI-PSI RUNWAY DEG	-90.0	-91.7	-91.0	-105.5	-159.4	-161.8	-33.5	19.9	4.7	0.2

TABLE 5-5 (cont)

COMPUTER PRINTOUT OF RAW DATA MODE FLIGHT

EVENT

VARIABLE	11 8000-FT	12 6000-FT	13 4000-FT	14 2000-FT	15 1000-FT	16 800-FT	17 600-FT	18 400-FT	19 200-FT	20 100-FT
ALTITUDE) FROM	8002.	6001.	4002.	2001.	1000.	801.	601.	400.	200.	101.
X POSITION) RUNWAY	-68421.	-56780.	-45292.	-33797.	-22182.	-18905.	-12906.	-8474.	-2476.	-754.
Y POSITION) IN FT	-31.	-28.	100.	-14.	-7.	49.	19.	5.	35.	29.
ROLL RATE)	0.77	-0.16	-2.29	0.26	-0.26	-0.09	-2.29	0.42	0.07	0.22
PITCH RATE) DEG/S	0.18	0.10	-0.02	-0.13	-0.00	0.26	0.32	1.58	-1.47	0.75
YAW RATE)	0.03	0.14	-0.32	0.07	-0.25	-0.15	-0.04	0.30	-0.03	-0.12
BETA) DEG	0.03	0.29	-0.66	0.44	-0.31	0.58	-0.56	-0.11	1.46	1.30
ALFA)	5.11	4.35	4.69	5.06	5.76	6.87	7.31	9.42	9.34	12.72
THETA)	-5.10	-5.03	-4.74	-4.65	2.25	4.81	6.18	5.92	7.59	9.71
THETA COMMAND) DEG	-5.01	-5.09	-4.82	-4.46	2.45	5.22	6.46	6.60	8.19	10.45
PHI) DEG	0.94	1.50	-2.07	0.64	-0.13	-0.46	-0.74	0.71	1.47	2.34
PHI COMMAND) DEG	0.92	1.53	-2.06	0.65	-0.22	-0.26	-0.68	0.81	2.05	3.34
PSI	239.84	241.04	240.76	239.68	240.57	239.53	240.33	239.44	239.57	238.52
ELEVATOR DEFL)	-2.84	-2.22	-2.46	-3.02	-3.66	-4.56	-5.79	-7.84	-6.96	-8.27
AILERON DEFL) DEG	0.18	0.34	0.14	0.25	0.05	0.79	-0.36	0.32	2.02	2.37
RUDDER DEFL)	0.01	-0.05	0.37	-0.05	-0.06	-0.06	0.49	-0.12	0.19	-0.07
FLIGHT PATH DEG	-9.87	-9.10	-9.20	-9.66	-3.66	-2.50	-1.70	-3.40	-1.45	-2.96
AIR SPEED) KNOTS	351.5	340.8	332.6	318.3	276.5	266.6	249.3	236.4	206.6	199.1
EQUIV A/S)	311.6	311.6	313.6	309.0	274.6	265.5	247.1	235.6	206.0	198.8
QBAR LBS/FT.SQ	329.5	329.4	333.7	324.1	256.1	239.2	207.3	187.5	144.0	134.2
LOAD FACTOR	1.09	0.87	1.04	1.04	0.94	1.17	1.01	1.25	0.96	1.05
LATERAL ACCL FT/S2	-0.22	-0.55	2.40	-1.03	0.56	-1.17	1.21	0.13	-1.51	-1.69
ALTITUDE ERROR FT	90.08	58.71	12.26	-13.56	32.63	91.05	27.17	34.46	-27.45	-3.92
GAMMA ERROR DEG	0.12	0.97	0.80	0.34	1.16	-0.00	-0.80	0.90	-1.07	0.46
VERT VELOCITY FT/S	-101.8	-91.7	-89.8	-91.2	-30.6	-16.8	-12.3	-22.5	-6.9	-15.4
PSI-PSI RUNWAY DEG	-0.2	1.0	0.8	-0.9	0.6	-0.5	0.3	-0.6	-0.4	-1.5

TABLE 5-5 (cont)

COMPUTER PRINTOUT OF RAW DATA MODE FLIGHT

VARIABLE	EVENT 21 CAPTURE RZERO	22 PROCEDURE TURN	23 LATERAL CAPTURE	24 VERTICAL CAPTURE	25 FIRST FLARE	26 SHALLOW G/S TRACK	27 LANDING GEAR	28 FINAL FLARE	29 DECRAB	30 TOUCHDOWN
ALTITUDE) FROM	40000.	20004.	19998.	0.	1663.	1377.	101.	50.	26.	16.
X POSITION) RUNWAY	-251253.	-135695.	-135695.	0.	-31693.	-30093.	-754.	1667.	2322.	4407.
Y POSITION) IN FT	-14587.	-224.	-224.	0.	-92.	-92.	28.	3.	-9.	-25.
ROLL RATE)	0.58	0.00	0.00	0.00	-0.61	0.76	0.22	0.99	1.08	0.09
PITCH RATE)DEG/S	2.74	0.03	0.05	0.00	0.09	2.05	0.75	0.95	2.20	0.05
YAW RATE)	1.68	0.01	0.02	0.00	0.17	0.14	-0.12	-0.04	0.00	0.27
BETA) DEG	0.06	-0.18	-0.30	0.00	-0.16	0.89	1.30	1.30	2.38	2.09
ALFA)	11.69	5.58	5.57	0.00	4.74	6.30	12.72	12.79	14.84	14.25
THETA)	-5.86	-3.75	-3.75	0.00	-4.57	-1.26	9.71	10.42	12.98	12.29
THETA COMMAND) DEG	-5.84	-3.87	-3.87	0.00	-4.46	-1.03	10.43	11.07	14.56	13.12
PHI) DEG	49.46	1.13	1.13	0.00	2.75	1.80	2.34	1.85	4.00	5.00
PHI COMMAND) DEG	49.70	1.06	1.06	0.00	2.77	1.80	3.34	2.96	5.70	6.45
PSI	206.69	244.74	244.74	0.00	239.90	239.90	238.52	238.00	238.11	239.50
ELEVATOR DEFL)	-8.92	-3.65	-3.61	0.00	-2.74	-5.01	-8.27	-14.85	-15.62	-12.90
AILERON DEFL) DEG	-0.00	-0.17	-0.17	0.00	-0.83	0.76	2.37	3.61	4.07	3.34
RUDDER DEFL)	-0.28	-0.15	-0.15	0.00	-0.08	-0.43	-0.87	-1.12	-2.53	-0.11
FLIGHT PATH DEG	-13.66	-9.38	-9.38	0.00	-9.25	-7.49	-2.98	-2.13	-1.74	-1.92
AIR SPEED) KNOTS	466.2	374.0	374.0	0.0	317.0	319.0	199.1	176.4	170.7	157.9
EQUIV A/S)	231.2	273.0	273.0	0.0	309.4	312.7	198.8	176.3	170.6	157.9
QBAR LBS/FT.SQ	181.5	252.9	252.9	0.0	324.8	331.9	134.2	105.5	98.8	84.0
LOAD FACTOR	1.76	0.90	0.90	0.00	0.99	1.21	1.35	0.85	0.95	0.92
LATERAL ACCL FT/S2	-0.27	-0.00	-0.00	0.00	0.06	-2.81	-1.89	-1.82	-3.05	-1.72
ALTITUDE ERROR FT	325.66	-49.91	-44.50	0.00	-16.87	-2.81	-3.92	-57.52	-63.00	-145.19
GAMMA ERROR DEG	-3.66	0.63	0.62	0.00	0.74	4.99	0.48	-0.37	0.76	0.70
VERT VELOCITY FT/S	-185.9	-104.0	-104.2	0.0	-86.9	-69.5	-15.4	-12.0	-8.8	-9.5
PSI-PSI RUNWAY DEG	-33.3	4.7	4.7	0.0	-0.0	-0.0	-1.5	-2.0	-1.9	-0.0
SGB										

TABLE 5-6

COMPUTER PRINTOUT OF FLIGHT DIRECTOR MANUAL MODE FLIGHT

SSV FLIGHT DATA DATE MM/DD/YY

RUN NUMBER 20

CONSTANT WIND DIRECTION = 240.000 DEG
INITIAL MEAN WIND VELOCITY = 0.630 FT/SEC

VARIABLE	EVENT 1 I.C.	2 90 K-FT	3 80 K-FT	4 70 K-FT	5 60 K-FT	6 50 K-FT	7 40 K-FT	8 30 K-FT	9 20 K-FT	10 10 K-FT
ALTITUDE) FROM	99986.	90005.	80003.	70005.	60009.	50003.	40002.	30003.	20005.	10002.
X POSITION) RUNWAY	-137000.	-157349.	-173011.	-189975.	-205618.	-161882.	-129440.	-119016.	-157183.	-194006.
Y POSITION) IN FT	393000.	290087.	217431.	133408.	60050.	1005.	-21536.	14735.	-5151.	-1/.
ROLL RATE)	0.00	-1.36	-0.79	-0.13	-0.08	2.76	0.23	0.20	0.46	-0.05
PITCH RATE)DEG/S	0.00	-0.48	-1.94	-0.03	0.10	0.27	0.36	0.96	1.69	-0.07
YAW RATE)	0.00	-0.22	-0.72	-0.02	0.06	1.16	0.92	1.57	1.74	-0.01
BETA) DEG	-1.51	-0.36	0.79	0.00	-0.03	0.51	-0.35	0.21	-0.08	0.25
ALPA)	14.60	7.43	8.70	8.44	8.40	8.49	7.68	7.53	6.42	5.90
THETA)	9.67	0.17	3.45	2.20	-1.66	-2.15	-3.15	-3.78	-5.66	-4.07
THETA COMMAND) DEG	9.67	-9.72	-7.55	0.99	-1.66	-2.09	-3.16	-3.52	-5.60	-4.06
PHI , DEG	0.00	-3.68	18.46	0.65	1.46	20.54	22.16	33.70	44.05	-0.09
PHI COMMAND) DEG	0.00	-4.48	19.42	0.60	1.42	20.89	22.16	33.82	44.20	-0.09
PSI	150.00	139.09	154.12	155.87	156.84	170.47	205.47	354.86	192.84	240.04
ELEVATOR DEFL)	-35.18	-12.73	-20.30	-14.11	-8.19	-6.71	-4.86	-5.30	-4.45	-3.10
AILERON DEFL) DEG	0.00	1.50	4.24	0.22	0.10	0.64	-0.54	-0.14	-0.85	0.12
RUDDER DEFL)	0.00	0.95	-1.96	-0.06	-0.15	-0.40	0.22	0.00	-0.07	0.02
FLIGHT PATH DEG	-4.92	-7.23	-5.00	-6.25	-9.92	-10.44	-10.30	-9.85	-10.36	-9.56
AIR SPEED) KNOTS	1787.7	1473.8	1198.9	944.9	696.0	546.1	470.5	422.5	415.7	345.9
EQUIV A/S)	209.8	216.6	225.9	227.3	219.0	210.0	233.4	250.4	303.4	297.2
QBAR LBS/FT.SQ	149.3	162.2	173.2	175.3	155.5	154.0	184.8	220.6	312.4	299.6
LOAD FACTOR	1.08	0.58	0.82	1.02	1.09	1.06	1.09	1.23	1.40	1.03
LATERAL ACCL FT/S2	2.63	0.86	-1.70	-0.03	-0.08	-0.74	0.56	-0.19	0.20	-0.06
ALTITUDE ERROR FT	-79796.23	-66243.67	-53473.08	-44010.30	-34746.50	-25435.34	-21153.17	-12990.63	-3736.88	27.48
GAMMA ERROR DEG	5.08	2.77	5.02	3.75	0.08	-0.43	-0.30	0.14	-0.36	0.44
VERT VELOCITY FT/S	-259.2	-316.0	-177.3	-173.7	-202.9	-167.8	-142.8	-122.4	-126.1	-97.3
PSI-PSI RUNWAY DEG	-90.0	-106.9	-85.9	-84.1	-81.2	-69.5	25.5	114.9	-47.2	0.0

TABLE 5-6 (cont)

COMPUTER PRINTOUT OF FLIGHT DIRECTOR MANUAL MODE FLIGHT

VARIABLE	EVENT 11 8000-FT	12 6000-FT	13 4000-FT	14 2000-FT	15 1000-FT	16 800-FT	17 600-FT	18 400-FT	19 200-FT	20 100-FT
ALTITUDE) FROM	8001.	6004.	4002.	2004.	1001.	800.	600.	400.	200.	100.
X POSITION) RUNWAY	-67855.	-56628.	-45291.	-34053.	-22684.	-17874.	-12291.	-7318.	-3460.	-1009.
Y POSITION) IN FT	-18.	-4.	-0.	-23.	6.	-19.	4.	-37.	-17.	-20.
ROLL RATE)	-0.78	0.09	-0.11	0.27	-0.04	0.24	0.15	-0.37	-0.11	-0.10
PITCH RATE) DEG/S	0.18	0.22	-0.09	0.15	-0.15	0.46	0.10	0.36	0.38	0.46
YAW RATE)	-0.05	0.10	-0.11	0.05	-0.11	0.03	-0.10	0.05	0.04	0.05
BETA) DEG	0.03	0.37	-0.03	0.17	-0.35	-0.92	0.32	-0.05	0.64	-0.20
ALFA)	4.45	4.89	4.81	4.82	6.50	6.98	7.44	7.68	9.84	11.03
THETA)	-4.56	-4.93	-4.62	-4.36	3.55	4.79	5.72	5.65	7.24	8.41
THETA COMMAND) DEG	-4.74	-5.02	-4.62	-4.32	3.94	5.16	6.08	6.13	7.96	8.78
PHI) DEG	0.43	-0.40	-0.49	0.23	-0.67	0.74	-0.77	1.79	-0.34	1.05
PHI COMMAND) DEG	0.43	-0.32	-0.54	0.23	-0.79	0.66	-0.53	1.66	0.15	1.04
PSI	240.68	240.14	240.25	240.07	240.17	240.74	239.47	240.14	240.03	240.46
ELEVATOR DEFL)	-2.22	-3.10	-2.98	-2.56	-4.43	-4.84	-5.69	-6.29	-8.52	-8.84
AILERON DEFL) DEG	-0.50	0.40	-0.23	-0.14	-0.22	-0.81	0.59	-0.96	1.38	0.12
RUDDER DEFL)	-0.13	-0.09	0.02	0.04	0.02	0.17	-0.07	-0.05	0.03	-0.12
FLIGHT PATH DEG	-9.42	-9.43	-9.28	-9.38	-2.96	-2.06	-1.74	-2.40	-2.63	-2.04
AIR SPEED) KNOTS	341.5	336.3	326.5	316.1	270.2	259.1	240.5	225.9	210.9	200.4
EQUIV A/S)	302.7	307.4	307.0	306.9	274.3	256.1	238.5	224.6	210.3	200.2
QBAR LBS/FT.SQ	311.1	320.8	321.2	319.7	251.0	222.7	193.0	171.2	150.2	139.0
LOAD FACTOR	0.91	0.97	1.03	0.99	1.07	1.06	0.98	0.91	1.04	1.08
LATERAL ACCL FT/S2	-0.28	-1.21	0.02	-0.35	0.64	1.70	-0.37	0.31	-0.67	0.04
ALTITUDE ERROR FT	-8.27	9.21	12.42	29.01	54.75	45.99	0.34	-16.99	16.05	9.51
GAMMA ERROR DEG	0.58	0.57	0.72	0.63	0.46	-0.44	-0.76	-0.10	0.13	-0.10
VERT VELOCITY FT/S	-94.9	-92.6	-88.0	-87.4	-23.9	-15.7	-12.6	-16.5	-16.2	-13.4
PSI-PSI RUNWAY DEG	0.7	0.1	0.2	0.0	0.2	0.7	-0.5	0.1	0.0	0.5

TABLE 5-6 (cont)

COMPUTER PRINTOUT OF FLIGHT DIRECTOR MANUAL MODE FLIGHT

VARIABLE	EVENT 21 CAPTURE RZERO	22 PROCEDURE TURN	23 LATERAL CAPTURE	24 VERTICAL CAPTURE	25 FIRST FLARE	26 SHALLOW G/S TRACK	27 LANDING GEAR	28 FINAL FLARE	29 DECRAB	30 TOUCHDOWN
ALTITUDE) FROM	51192.	28003.	20005.	19998.	0.	1380.	100.	47.	26.	10[illegible]
X POSITION) RUNWAY	-162460.	-128362.	-157183.	-157183.	0.	-30156.	-1009.	369.	887.	1336[illegible]
Y POSITION) IN FT	8080.	22314.	-5151.	-5151.	0.	-8.	-20.	-7.	-2.	0.
ROLL RATE)	-0.18	0.38	0.48	0.17	0.00	0.04	-0.10	1.21	-0.20	-0.91
PITCH RATE)DEG/S	-0.12	1.56	1.69	1.73	0.00	1.75	0.39	0.59	2.33	0.06
YAW RATE)	0.09	1.78	1.74	1.71	0.00	0.12	0.05	-0.15	-0.09	-0.14
BETA) DEG	0.06	0.06	-0.08	-0.20	0.00	0.24	-0.20	-1.69	0.27	-0.23
ALFA)	8.09	7.43	6.42	6.45	0.00	7.44	11.03	10.77	13.78	12.08
THETA)	-2.23	-3.84	-5.66	-5.65	0.00	2.00	8.22	9.37	11.40	11.09
THETA COMMAND) DEG	-2.48	-3.69	-5.60	-5.60	0.00	2.56	8.78	10.06	12.45	13.05
PHI) DEG	1.22	40.41	44.05	44.04	0.00	0.10	1.05	-1.16	-0.95	-1.07
PHI COMMAND) DEG	1.12	40.52	44.20	44.20	0.00	0.24	1.01	-1.31	-0.99	-1.74
PSI	165.01	30.06	192.84	192.97	0.00	240.21	240.48	240.37	240.05	239.69
ELEVATOR DEFL)	-5.62	-5.40	-4.45	-4.37	0.00	-6.26	-8.84	-9.82	-9.88	-11.60
AILERON DEFL) DEG	0.08	0.05	-0.83	-0.05	0.00	0.23	0.12	0.13	0.40	2.66
RUDDER DEFL)	-0.16	-0.20	-0.07	-0.02	0.00	-0.02	-0.12	0.07	-0.03	0.00
FLIGHT PATH DEG	-10.26	-9.68	-10.38	-10.38	0.00	-5.40	-2.34	-2.03	-2.50	-0.59
AIR SPEED) KNOTS	562.8	421.9	415.7	415.7	0.0	313.7	200.4	190.3	181.9	178.9
EQUIV A/S)	213.4	267.6	303.4	303.4	0.0	307.4	200.2	190.2	181.9	178.9
QBAR LBS/FT.SQ	154.6	245.1	312.4	312.4	0.0	320.8	136.0	122.6	112.3	108.6
LOAD FACTOR	1.03	1.26	1.40	1.40	0.00	1.57	1.08	0.97	1.32	1.04
LATERAL ACCL FT/S2	0.00	-0.47	0.20	0.19	0.00	-0.49	0.04	1.21	-0.40	-0.23
ALTITUDE ERROR FT	-26522.27	-9339.26	3736.88	3743.44	0.00	-0.96	9.51	2.26	0.57	-9.91
GAMMA ERROR DEG	-0.26	0.32	-0.38	-0.38	0.00	2.90	-0.16	-0.47	-0.07	1.95
VERT VELOCITY FT/S	-168.4	-120.7	-126.1	-126.1	0.0	-47.5	-13.4	-11.3	-12.6	-2.4
PSI-PSI RUNWAY DEG	-75.0	-209.9	-47.2	-47.0	0.0	0.2	0.5	0.4	0.0	-0.1

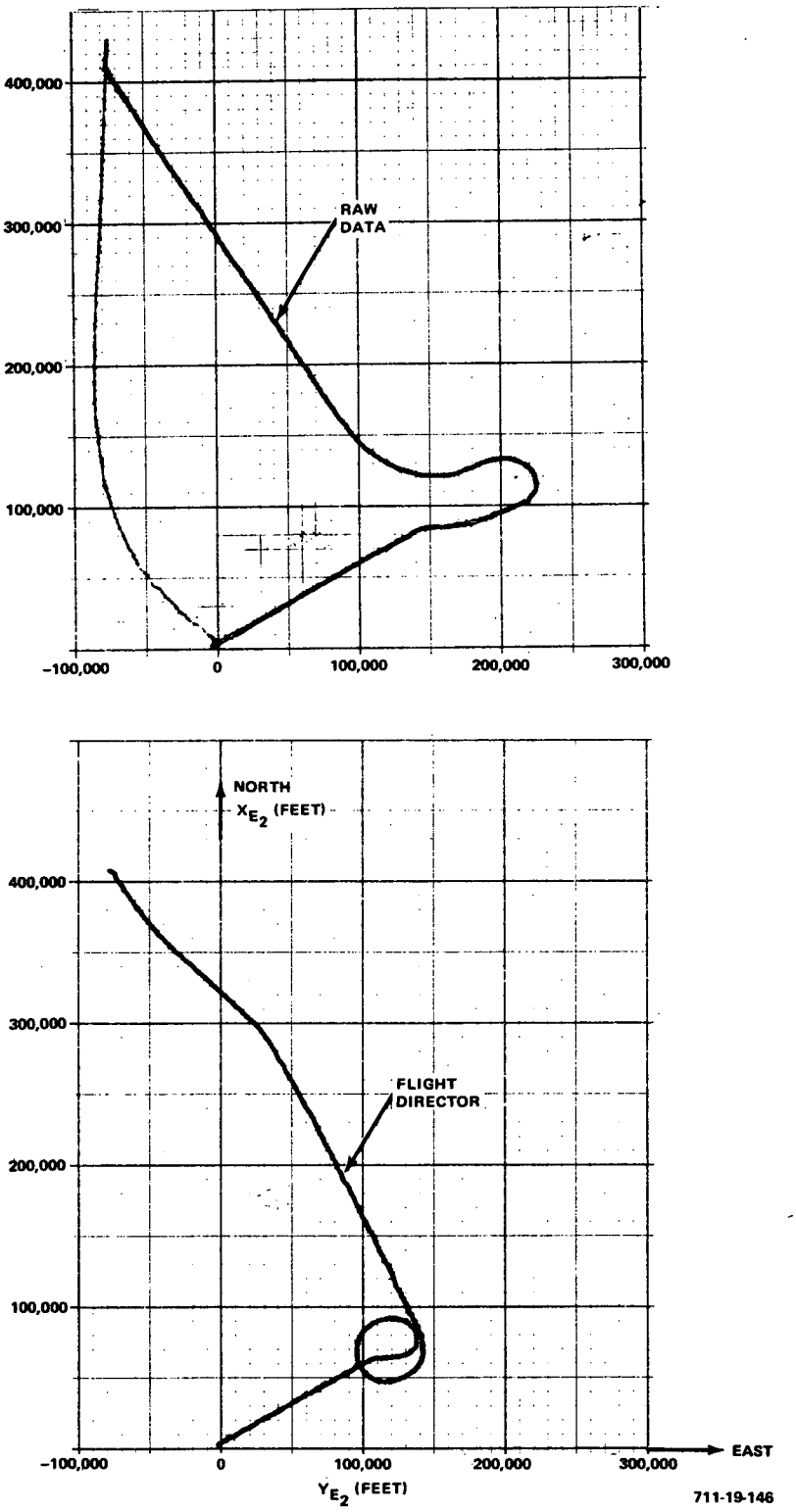

Figure 5-6
HCR Vehicle Manual Modes,
Raw Data and Flight Director,
Pilot - Major Donald H. Peterson

His familiarity with the system and the simulator was based on a short briefing and a few trials at the simulator controls. Let us first examine the raw data mode (Table 5-5). The vehicle is maintained at the initial heading until an altitude of about 70,000 feet is reached. At that time a left bank (phi) is initiated in an attempt to align the vehicle with the outbound radial (50°C). This bank is started somewhat late. The cue to start this bank was nothing more than the presentation of position information to the pilot. If a ground controller had used tracking information to communicate the turning cue, he would have directed that the bank start sooner because of his knowledge of the vehicle's turn rate limitation. If the pilot had a few more familiarity flights, he too would have learned to accommodate better to turn rate restrictions. In this flight he tries to get turned around with a bank angle that reaches over 40 degrees at 60,000 feet. Before he can reach the outbound radial, the glide path capture cue appears. He immediately starts the procedure turn (right) but he overshoots the center of the reference lateral flight path. He penetrates the reference lateral flight path with an intercept angle of about 90 degrees. He now increases his bank angle to about 50 degrees attempting to turn the vehicle back toward intercept of the reference lateral path. By the time an altitude of 30,000 feet is reached, the bank angle is moderated to about 15 degrees and a reasonable intercept path (about 20 degrees) has been established. At that time a reasonable acquisition of the glide slope (within 1,800 feet) has been accomplished. When the altitude reaches 20,000 feet, the altitude error (from the glide slope) has been reduced below 50 feet and the lateral error is only 224 feet (Note that "y position" in the printout represents lateral error since the x, y coordinates given in this table are runway coordinates.)

From the terminal flight path acquisition results using the raw data mode, one concludes that the preciseness of the acquisition maneuvers are not critical. This is certainly a desirable attribute of a raw data system. Continuing the examination of Table 5-5, it is seen that Major Peterson maintained reasonably tight glide slope and localizer tracking (altitude error and y position) until flareout. Since the raw data mode does not provide information for flareout this phase of the flight is performed using the visual cues as defined by the visual scene. Here the problem of the fidelity of the visual scene arises. A pilot's performance using cues obtained from the visual scene was very dependent upon his experience with that specific simulator. NASA ARC

research pilots who had considerable experience on the simulator and visual scene used in this study made the best manual landings. As seen on Table 5-5, Major Peterson's manual landing was "hard" (-9.5 feet/second vertical velocity at touchdown). After he transitioned to VFR control he maintained lateral alignment quite well but drifted off 25 feet in the final seconds prior to touchdown.

A manual flight with flight director steering cues resulted in better landing performance. Table 5-6 presents the printout of this run and the horizontal view of the trajectory is also contained in Figure 5-6. The flight director steering cues are the same as those used in the automatic mode. As seen in Figure 5-6, the vehicle is steered toward intercept of the R_o circle, starts to turn around that circle (or cylinder) and then, when it is about 180 degrees outbound from the runway, determines that additional turning on that circle is no longer possible. It then makes the procedure turn aimed at simultaneous interception of the glide path and lateral flight path (localizer). As seen in Table 5-6, the final acquisition of the glide path and "localizer" occurs later than with the raw data mode. At 20,000 feet, the vehicle is still in a 45 degree bank attempting to capture the lateral path. Also, at 20,000 feet, the glide slope capture is not yet complete. However, below 20,000 feet, flight path precision is good. Touchdown vertical speed is -2.4 feet/second and the lateral eroor at touchdown is zero.

3. Pilot Comment

Pilot comment on automatic system performance was generally good but they all confirmed the need for a horizontal situation display that provided some clues regarding the intent of the high altitude energy management turning maneuvers. A trend vector on a moving map display was considered to be the ideal solution to this problem. A mode annunciator was also suggested.

Handling qualities for the manual modes were generally rated as excellent. There was some criticism of the large banking maneuver associated with the high altitude energy management. The fact that a different guidance scheme was used for the raw data and automatic modes was considered undesirable.

The EADI was considered to be a definite improvement over equivalent electromechanical displays and there were many suggestions for improving EADI symbology and other characteristics. Some of the suggestions are:

- Incorporate vertical speed display....if possible, place the index for such a display on the bezel, not on the CRT face.... likewise, incorporate other fixed indices on the bezel.
- Change aircraft symbol....remove landing gear symbology.
- Provide runway proximity bar that rises to meet the aircraft symbol....same as present day electromechanical ADI's.
- Provide additional bank angle indices (to 45°).

The raw data mode was considered to be an acceptable minimum back-up system (with experience and a reasonable HSI display).

Flight director modes were considered satisfactory but some additional pitch smoothing was desired for critical maneuvers such as flareout. This implies the need for some pitch rate in the flight director computations.

On the question of what is the minimum acceptable altitude for transition from instruments to visual control, there were no conclusions obtainable from the simulator work done thus far. The utility of the visual scene as a means of making judgments in this area was questioned and some comment indicated a preference for flying the flareout heads-down rather than attempt a transition near the ground.

4. General Comment on Simulator Evaluation of Energy Management System

The success of the back-up, raw data mode in providing energy management capability without the computation of the turning descent trajectories (as used in the automatic mode) raised some interesting questions. From the time that the high altitude guidance was first being designed it was apparent that almost any turning trajectory could be made to end up on the desired final approach path. This fact was reported in an interim progress report where it was noted that a non-pilot, and relatively uncoordinated engineer could use a simple display to maneuver the vehicle to a near perfect intercept with the final approach path.

The unusual aspect of his performance was that for the same initial conditions he flew a different trajectory every time and always arrived at his desired terminal state. With the infinity of solutions to this problem some techniques will no doubt provide a larger window than others and there may very well be an optimum from the standpoint of window size.

Although the system that steers toward interception of target cylinders has been documented in this report as providing an excellent energy management capability, we have concluded that a simpler system that avoids excessive banking maneuvers can be implemented using the concept of flying outbound on a fixed radial from the coordinate defined by the intercept of the steep glide path and ground. Referring to Figure 5-5, for example, the energy management system would always steer the vehicle to intercept the 50-degree radial (for a right turn) or the 70-degree radial (for a left turn). Energy management would be accomplished by controlling the distance flown on these outbound radials. The initial phase of the energy management guidance computation is the determination of the best path to intercept and acquire one of these outbound radials. Such a system was designed after the study reported herein was completed.

SECTION VI

NAVIGATION AND GUIDANCE SYSTEM MECHANIZATION AND FLIGHT TEST REQUIREMENTS

SECTION VI

NAVIGATION AND GUIDANCE SYSTEM MECHANIZATION AND FLIGHT TEST REQUIREMENTS

A. INTRODUCTION

Task 3 of NASA Ames Research Center Specification No. 15698 which is the statement of work for this study required the recommendation of systems and equipment, both airborne and ground based, necessary to flight test the guidance and control concepts for shuttlecraft terminal approach and landing. Included in this requirement was the recommendation of an aircraft which can be configured to simulate a space shuttle vehicle, both in its aerodynamic characteristics and in its ability to accommodate the required avionics and control systems. The candidate aircraft identified in the NASA specification were:

- F-102
- F-104
- F-106
- F-111
- F-4
- B-58
- CV 990
- Any other suitable aircraft available to NASA

A study was performed in response to this work statement requirement and the results of that study were reported in a separate document (Reference 32). This section presents a summary of that study plus some updating of the original conclusions.

The results of the original study indicated that the F-104 or a drag plate modified F-106 were the most suitable aircraft for flight testing approach and landing systems for unpowered shuttlecraft. Their selection was based on their excellent match with the key aerodynamic characteristics of the candidate space shuttle vehicles. It was possible to compensate for the significant size discrepancy between the large shuttle vehicles and the relatively small simulator

aircraft by adjusting the control system characteristics of the flight test aircraft.

Since completion of the original study report (Reference 32), a second look at the Convair 990 based on additional CV 990 aero data plus new data on more recent space shuttle candidates revealed that the CV 990 is also a very good choice as a flight test vehicle. Its recommendation as a flight test aircraft is further enhanced by its availability to NASA.

There are several equipment mechanizations that can be used to implement the shuttlecraft guidance and control concepts defined thus far. In the high altitude region (100,000 to 20,000 feet) the navigation problem is not critical in that several types of devices offer adequate accuracy with equivalent weight and cost penalties. The Inertial Navigation System (INS) plus air data information for vertical navigation may be sufficient in this region. Area navigation techniques using VOR/DME or TACAN can improve this accuracy, although conventional DME has a velocity limit between Mach 2 and 3. Long range tracking radars with up-data links can also be used to provide this additonal accuracy improvement. From 20,000 feet to about 1,000 feet, the navigation information must converge to an accuracy improvement of about two orders of magnitude. The choice candidate for this phase of flight is a microwave scanning beam system sited at the aim point (forward of the touchdown point). The microwave scanning beam used in this manner offers a unique capability in that raw data and a simple cross pointer display could be used to fly a manually controlled descent though a cloud layer. From 1,000 feet to about 50 feet another set of criteria applies for vertical guidance. Conventional UHF Glide Slopes (ILS), a second microwave scanning beam, or multilateration beacons could provide the required information for automatic guidance. The final flareout occurs in the remaining 50 feet. A radio altimeter or the microwave scanning beam is the choice in this region. The INS is used throughout for data smoothing or as a primary data reference.

A preferred mechanization would be:

Altitude Region	Guidance/NAV References
• 100,000 feet to 20,000 feet	INS, Air Data, VOR/DME
• 20,000 feet to 1,000 feet	Microwave, Scanning Beam (MSB). Glide Path sited at aim point plus MSB Localizer and DME at end of runway. Plus INS.
• 1,000 feet to 50 feet	Second microwave scanning beam sited behind nominal touchdown point. Plus INS. Plus MSB localizer.
• 50 feet to touchdown	Same as above or with additional radio altimeter.

This preference cannot be based on conclusive verification of superior performance in all regions of flight. Also, there are sufficient operational uncertainties in shuttlecraft to preclude the elimination of other navigational devices at this time. It is therefore recommended that the flight test program make provision for evaluating system mechanizations based on the above recommended complement of equipment but the basic avionics complex should also be capable of accommodating other navigational references that are considered to be reasonable candidates for space shuttle applications.

B. NAVIGATION AND GUIDANCE SYSTEM MECHANIZATION

1. Requirements

The terminal trajectory may be divided into four phases as follows:

- 100,000 to 20,000 feet - high altitude energy management and steering along turning or spiral descent paths aimed at acquiring the terminal glide (or equilibrium glide path) by the time an altitude of 20,000 feet is reached.

- 20,000 to 1,000 feet - equilibrium glide path descent where lateral and vertical position errors are converged to a few feet by the time an altitude of 1,000 feet is reached. Also velocity is converged to a fixed nominal value at this lower altitude.

- 1,000 feet to about 50 feet – flareout to the shallow glide path where the vehicle decelerates while aligning for the final flareout.

- About 50 feet to touchdown – final flareout to touchdown.

The navigational accuracy existing at 100,000 feet is assumed to be the INS error at that altitude. This is variously estimated to be anywhere between 2 and 20 nautical miles depending on alignment and updating prior to de-orbit. The maximum INS error normally exists in the vertical plane (estimation of altitude). The INS altitude measurement will probably use some knowledge of vehicle aerodynamics and the trajectory to update the altitude measurement. The initiation of the terminal navigation should not, however, depend upon the altitude measurement to transfer to ground based navigation devices. Vehicle velocity may be a better indicator of the vehicle's penetration of the terminal area.

The specification of navigation accuracy requirements can start from the terminal glide (equilibrium) path at 20,000 feet. This may be referred to as a low key point. The guidance and control system can accommodate errors of about ±5 nautical miles to ±8 nautical miles downrange and cross-range from this low key point. It can accommodate a downrange and cross-range window of about ±50 nautical miles at 100,000 feet and reduce errors to zero at the low key point if the high cross-range orbiter is the vehicle under consideration. The energy management capability of the low cross-range vehicle in this high altitude, pre-transition region is much smaller but this is an academic point at this time. These estimates do not include the effects of high altitude winds which modify the shape of the window as a function of wind direction with respect to the vehicles initial direction of flight.

2. General Description of Navigation/Guidance System Mechanization

Figure 6-1 illustrates the basic avionics configuration that should be used for a shuttle landing flight research program. The heart of the system is the general purpose digital computer and its data adapter that permits interfacing with other airborne equipment. The computer provides state estimation from various navigation inputs, guidance and control law computation, display generation and system test, and status appraisal. The data adapter talks to the

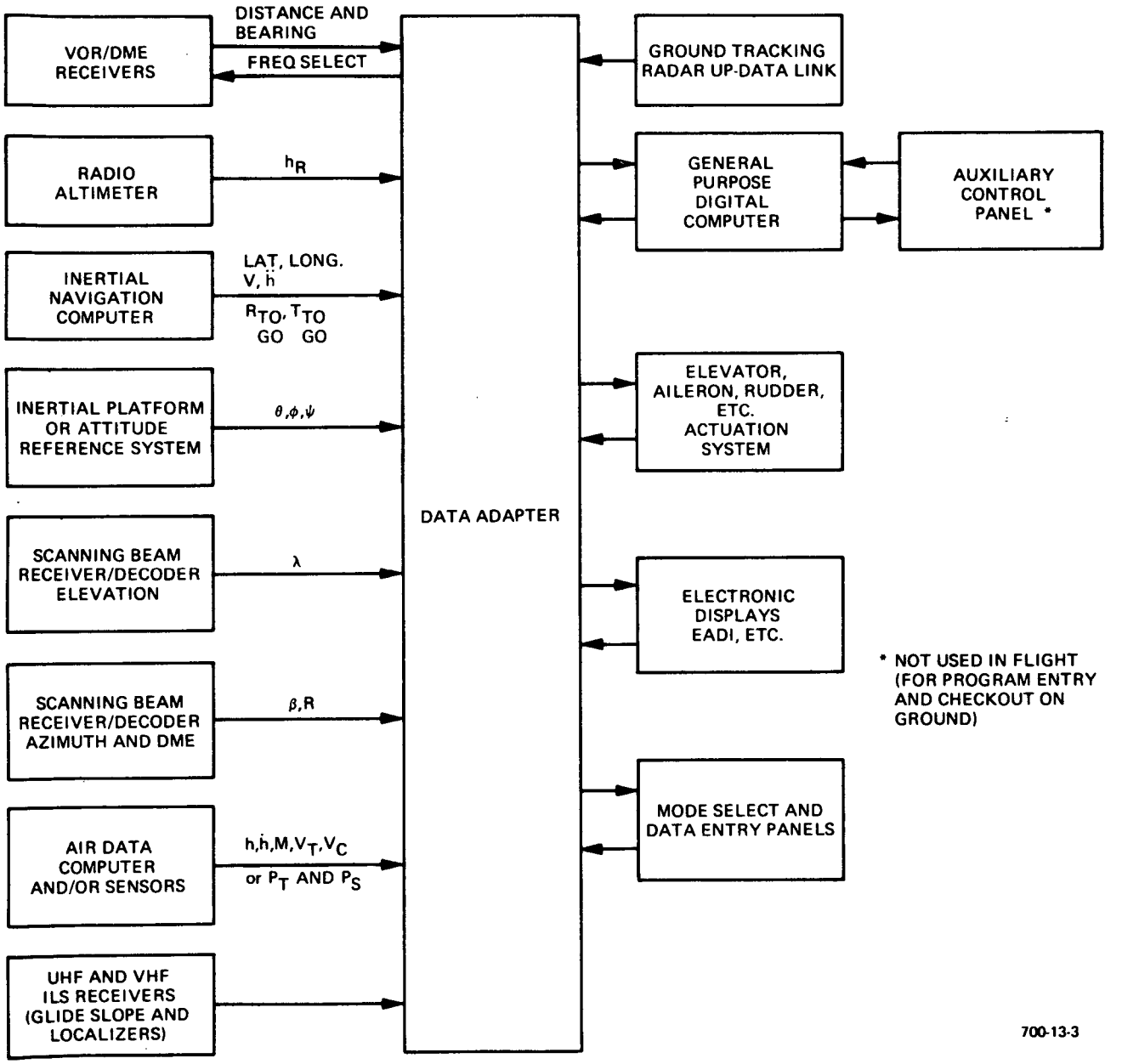

Figure 6-1
Avionics Configuration for Shuttle Landing Flight Research Program

computer in a fast, parallel data transfer interface. It also provides the signal conditioning for all associated devices including the usual elements of an autopilot. It provides A/D, D/A and D/D conversion. The D/D conversion is associated with the receipt of serial digital data from the INS and other forms of digital data from airborne receiver/decoders. The D/D conversion is also associated with remote tuning of receivers if that feature is available in the VHF and UHF receivers used in the flight test aircraft. The data adapter also includes the servo amplifiers and electronics which drive the autopilot servos and excite the various autopilot transducers.

A state of the art INS can be used on this program and subsequent evaluations of candidate configurations assume the characteristics of a commercially available INS such as the ARINC 561 (Carousel IV, etc). The air data computer and sensors could be limited to only a remote static and total pressure sensor. The central computer can provide the necessary computations to obtain altitude, altitude rate, Mach number, airspeed, etc.

Mode select and data entry panel functions are shown in Figure 6-1. Ideally, a single, integrated panel should be used to optimize cockpit operating procedures and to minimize the use of cockpit real estate. An integrated data entry and mode select panel would have to be specially developed for the flight test program. An alternative is to mechanize this function using several panels associated with existing subsystems.

A number of radio navigation devices are shown on Figure 6-1. These are not restricted to only those sensors or devices that are the leading contenders for application in a shuttle landing avionics system. Figure 6-1 shows most of the navigation devices that are in general use in military and commercial aircraft plus some that are special purpose for the specific requirements of the shuttle landing. The on-board computer programs and interfacing electronics should make provision for evaluating more than one navigation technique for a given phase of flight. For example, VOR/DME, INS and air data may be one method of achieving the high altitude, long range navigation. An alternate could be the tracking radar and up-data link. The avionics test system should make provision for both methods if the flight tests are conducted at a facility where the tracking radar system is applicable. Likewise provision should be made to interface

receivers for the trilateration beacon system and appropriate software developed to permit the use of that data for navigation computations.

3. Description of Candidate Navigation Sensors and Subsystems

The paragraphs that follow provide a brief description and appraisal of the various navigation devices which have been considered as a source of shuttle landing system navigation data. Table 6-1 summarizes these descriptions in terms of accuracies and coverage.

a. VORTAC and TACAN

VORTAC is the most widely used system today for domestic enroute navigation and in many cases, approach. Courses are presently restricted to radials with baro altitude sensing for aircraft separation. Stations are configured in three coverage types: H (high altitude) frequencies protected to 130 nautical miles up to 45,000 feet, 100 nautical miles to 60,000 feet; L (low altitude) protected to 40 nautical miles up to 18,000 feet; and T (terminal protected to 25 nautical miles up to 12,000 feet. These are guaranteed frequency protection volumes; generally the coverage extends much further. Individual VORTAC's may be analyzed and/or measured for coverage beyond these limits. Both VORTAC and TACAN are limited to elevation angles less than 50 degrees for accurate azimuth sensing; the DME portion (slant range) is omnidirectional. Advantages are the wide and increasing deployment of these stations, the availability of low cost, reliable airborne equipment, and the extensive experience obtained with them by all types of air carriers from general aviation through the airlines and the military. Additionally, the techniques of coupling to instruments, flight directors, and autopilots have been highly developed over the years.

The disadvantage is the marginal accuracy. Depending on the particular ground and air installation, these accuracies may vary from 1 to 4 degrees for azimuth and 0.2 to 0.5 nautical mile in slant range.

TACAN provides essentially the same service as VORTAC except the angular accuracy is improved slightly.

TABLE 6-1

SYSTEM COVERAGES AND ACCURACIES

	Coverage	System Accuracy
VOR (Bearing)	Omnidirectional in azimuth, but accuracy degrades within ±40 degrees of zenith. Line of sight limited. "H" facility guaranteed to 130 nm at 45,000 feet. 100 nm radius to 60,000 feet.	Varies with both ground and air installation. Typical good sites and modern airborne equipment produce less than ±3 degrees overall (2 σ). Poor facilities up to ±4 degrees or more.
TACAN (Bearing)	Same as VOR.	Typically better than VOR. +3 degrees maximum, typically ±1 degree overall (2 σ).
TACAN/DME (Slant Range)	Same as VOR, TACAN, except has no overhead dead zone (operates at all elevation angles).	±0.5 nm or 3 percent (2 σ) guaranteed, ±0.2 nm typical in modern equipment.
VHF Localizer (Azimuth)	To 25 nm within ±10 degrees of front course line, at an elevation angle up to 7 degrees maximum.	RSS of ground and airborne instrumentation errors, 2 σ, Category II System: At threshold: ±36 feet At Point C (100 feet decision height): ±40 feet At Point B (3500 feet from threshold): ±48 feet Subject to overflight, ground vehicle, reflection perturbations.
UHF Glide Path (Elevation)	To 10 nm minimum from 1.2 to 5 degrees elevation, (2.8 degrees nominal glide path) within ±8 degrees of localizer center line.	RSS of ground and airborne instrumentation errors, 2 σ, Category II: Threshold: ±4.5 feet Point C: ±9 feet Point B: ±19 feet
Microwave Scanning Beam ILS (Azimuth)	±20 degrees	±0.3 degree at reference course.
(Elevation)	0 to +20 degrees	±0.15 degree at reference glide path.
(Range)	To 50 nm clear weather. To 10 nm guaranteed in 10 mm/hour rainfall.	±100 feet

TABLE 6-1 (cont)

SYSTEM COVERAGES AND ACCURACIES

	Coverage	System Accuracy
Range Instrumentation Radar - MPS-19, FPS-16, etc.	Line of sight only. Typically 50 nm at 10,000 feet 80 nm at 20,000 feet 150 nm at 40,000 feet 200 nm at 60,000 feet 300 nm at 100,000 feet All azimuths, all elevations. (Gimbal lock, tracking rate problems near zenith.)	±0.5 milliradian in azimuth and elevation. Subject to elevation angle perturbations at low elevation angles. ±5 yards in range.
Optical Trackers (Az and El)	Short range, clear weather, line of sight, all azimuth and elevation angles (low angle fill-in for radar).	0.1 to 0.5 milliradian. Use in conjunction with radar range only.
Tri-Lateration Systems (Cubic CR-100-3)	20 nm maximum range, omnidirectional.	±1.5 foot position errors claimed at 20 nm. Subject to multipath and geometric dilution of precision errors.)
Low Altitude Radar Altimeters (Absolute Altitude)	0 to 2500 feet (ARINC 552) 0 to 5000 feet (AN/APN-171)	±2 feet or 2 percent (not including indicator).
Air Data	-1,000 to +50,000 feet (ARINC 565). To 70,000 feet available.	-1,000 feet to sea evel ±15 feet Sea Level to +10,000 feet ±20 feet 10,000 to 30,000 feet ±40 feet 30,000 to 50,000 feet ±80 feet Subject to further aircraft static port errors. Correlation of pressure altitude with true altitude depends upon atmospheric conditions.
Inertial Navigation Systems (INS)	Unlimited; depends upon time from initialization or updating.	±1.0 to 2.0 nm per hour (horizontal plane - latitude and longitude) ±20,000 to 40,000 feet per half hour (vertical plane - altitude)

b. VHF/UHF ILS

VHF/UHF ILS is the standard approach guidance system for both civil and military flying. Virtually all systems are qualified for Category I (200 feet DH, 2,400 feet RVR). Many, particularly at the larger, busier airports are being replaced or upgraded to Category II (100 feet DH, 1,200 feet RVR). No Category III (to touchdown and beyond) has been implemented. Approximately 300 Category I runways are in use but only a dozen or so Category II (1969). Thousands of airborne receivers, of various degrees of quality, are in use by all classes of aircraft.

Like VORTAC, the great advantage of this system is its wide deployment, the vast experience with it, availability of reliable inexpensive airborne equipment, and the proven coupling techniques.

Accuracy of ILS can be quite good down to the 100 or 200 foot decision height, but the system is subject to severe siting problems and interference from moving ground aircraft or vehicles and overflying aircraft.

c. Microwave Scanning Beam Landing Systems

Because of the inherent limitations of any VHF/UHF landing system due to the wavelength-antenna size-beamwidth problem, much developmental activity has taken place in the last few years in this area. It is the stated intention of the FAA to accelerate development of microwave landing systems (RTCA SC-117). By using wavelengths of an order one or two magnitudes shorter, these systems can achieve freedom from site effects by use of narrow beams with reasonable antenna sizes while achieving greatly improved accuracies. By rapid wide angle scanning of these beams, much greater angular coverage can be achieved which allows a wider range of approach paths in both elevation and azimuth. By addition of DME service, complex approach paths are possible with airborne computation. However, raw data alone may be used.

FAA measurements at NAFEC of a prototype system show angular accuracies of 0.03 to 0.05 degree and DME accuracy of 100 feet.

The disadvantage of the system is its present low availability and the uncertain nature of its future due to possible funding limitations. Experience is limited to experimental sites and military deployment. (Navy AN/SPN-41, AN/TRN-28, and AN/ARA-63.)

d. Range Instrumentation (Radar Optics, Computers, Data Links, etc)

Range instrumentation includes an extremely wide range of equipment and a large number of operating personnel. Books can and have been written on the subject. Examples of the complexes available are those at Cape Kennedy, Wallops Island, Kwajelain, Edwards, Ames, White Sands, P.M.R., Vandenberg, SPASUR and Spacetrack, NASA and Air Force tracking ships, NASA near space and deep space instrumentation facilities, and others of both nature. Their present deployment is almost exclusively limited to government-owned test facilities.

For orbital and earth escape missions these systems are indispensable but may be limited to coverage during terminal navigation and approach guidance.

Where adequate facilities are located in close proximity to the landing area, the high quality of this instrumentation and the trained personnel associated with them can provide almost unexcelled precision and coverage. A good radar-optics-computer-data link combination can provide accuracies to a fraction of a milliradian in angle and a few yards in range. For test purposes a particular value is the ability of this type of ground complex to simulate almost any conceivable sensor combination (ILS, VORTAC, altimeters, etc) by means of proper computer programming and data up-link means.

The disadvantage of these systems is the lack of low altitude coverage unless the facility is located at or directly adjacent to the intended operational landing site.

e. Barometric Altitude

Pressure altitude can be routinely measured to excellent accuracies. ARINC 565 specs, for example, run from ±15 feet at sea level to ±80 feet at 50,000 feet. Even when one or two hundred feet are added for static port errors,

this is sufficient for aircraft separation purposes, the primary use in civil aviation at high altitudes (over 18,000 feet).

Pressure altitude is based on 29.92 inches Hg standard day so that all aircraft in the same vicinity experience nearly equal errors and thus maintain their separation. But separation is not the problem in the SSV. The problem is elevation sensing with respect to the landing area for guidance purposes. Conversion to mean altitude above sea level is easily made by compensating for the ground reference pressure referenced to sea level. A further correction to absolute altitude (above the landing site) may be made with a knowledge of the landing site altitude. (Alternatively, both these corrections may be combined into one.) Thus an elevation accuracy (for an idealized atmosphere) of 200 to 300 feet should be possible at altitudes of 40,000 to 60,000 feet with an increased accuracy at lower altitudes. This is more than sufficiently accurate to guide the SSV to the 20,000-foot key point to acquire radio NAVAIDS. It will not be sufficient for elevation positioning at lower altitudes, say below 1,000 feet, however. At these altitudes atmospheric anomalies, static source errors, and instrument errors could cause errors of about 100 feet. Altitude determination accuracy of about ±10 feet at 1,000 feet is a desired objective with ±25 feet appearing to be an allowable error if good performance in the presence of off-nominal conditions is to be achieved.

f. Radar Altimeters

Over the past 6 years, low altitude (0 to 2,500 feet) radar altimeters have come into wide commercial use as a complement of aircraft equipment for Category II approaches. Thus they are reliable, widely available, and reasonably priced. (Military versions up to 5,000 feet are also available.) Their use has been necessitated largely by the inadequacies of the conventional ILS glide path below 100- to 200-foot height, and to pinpoint the Category II 100-foot decision height.

Accuracies are typically 2 feet or 2 percent, but obviously they may incur errors because of the particular terrain directly under the aircraft on the approach path.

High altitude radar altimeters (200 to 70,000 feet) are available but much less widely used. They have been used for military reconnaissance, aerial surveying, and pressure pattern flying over water, not as a vertical guidance sensor. At high altitudes, terrain variations can lead to serious errors.

g. LORAN C/D

LORAN C/D has no coverage in western U.S. at present. Four "D" stations might be made available. Three of these are in present use in the Eglin AFB area and a fourth is in storage. The system is usable at altitudes in excess of 100,000 feet, possibly up to 50 miles altitude. Recommended deployment for testing at Edwards AFB would be:

Master	Northwest Nevada
Slave 1	Los Angeles
Slave 2	Western Oregon

Another slave would be needed to give the altitude coordinate since three stations provide only two-dimensional measurement.

Accuracies claimed are in the order of 100 or at most a few hundred feet. The system is subject to geometric dilution of precision when at great distances from the baseline but this generally can be minimized by careful choice of station siting.

h. Inertial Navigation Systems (INS)

These systems include a wide spectrum of combinations of Inertial Measurement Units (IMU's) and computers. The IMU's may be of the gimballed platform type in which rate sensors and accelerometers are stabilized on a fixed coordinate frame or strap down configurations, where vehicle body rates and accelerations are sensed, and the computer determines the instantaneous direction cosine matrix for the desired navigation coordinate frame. The state of the art in terms of accuracy, size, weight and cost is very dependent upon the specific application. The space shuttle vehicle will have its own unique requirements that are not met by an existing inertial navigation systems. The space shuttle, for example, has considered a strapdown approach where a duodecahedron orientation of rate sensors is a leading candidate. This orientation is featured not

because of any inherent accuracy advantages but because of the unique and interesting properties it provides in regard to redundancy and reliability. The commercial INS equipment, on the other hand, are gimballed systems using local vertical coordinate frames but they are not capable of providing navigation for most of the space shuttle phases of flight. (They cannot provide the ascent, orbit, and reentry phases.) Various military inertial navigators are available but they are usually oriented toward specialized problems (fire control and weapon delivery) although their IMU's could be usable with other computer programs.

All inertial navigators have their own specialized problems in regard to alignment, initializing and in-flight calibration or cancellation of bias errors. The development of a multipurpose inertial navigation system for space shuttle vehicle is a technology task of the space shuttle program that is largely independent of the landing navigation/guidance problem. A landing avionics flight research program can achieve its objectives by using an INS that provides only those functions associated with aerodynamic flight. Although provision should be made for the actual initializing errors prior to de-orbit, a state-of-the-art commercial INS could provide the desired capability at minimum cost.

4. Definition of Candidate Systems

a. Definition of Candidates

Five candidate systems are defined to permit an evaluation of different methods of synthesizing navigation information during the various phases of flight. These candidates employ different sensors in the four specified regions of terminal flight (100,000 to 20,000 feet; 20,000 to 1,000 feet; 1,000 to 50 or 60 feet; and 60 feet to touchdown). There are obviously permutations on the five candidates where the navigation devices for different regions may be interchanged. It will be apparent from the subsequent system description that combinations of two of the candidate configurations result in the best approach for a flight test program.

The following is a summary of the five candidate systems. (Table 6-2 defines the airborne equipment size and weight for various candidate devices.)

TABLE 6-2

AIRBORNE SIZE AND WEIGHT

	Size ($in.^3$)	Weight (lb)
TACAN	1000	40
VHF/UHF Navigation Receiver	700	25
DME	825	37
Marker Beacon	225	5
C-Band Beacon	300	8
Command Receiver	200	10
Radar Altimeter	500	15
Tri-Lateration Interrogator (Cubic CR-100-3)	720	20
Scanning Beam Receiver (ARA-63)	370	15
Air Data Sensor	100	4
Airborne Computer	1500	45
Data Adapter	500	25
Inertial System	2000	75

- Candidate No. 1 (Figure 6-2, and Table 6-3 and 6-4)

This system is selected as a combination of standard, contemporary sensors in proper combinations to cover the various flight regimes. It is composed of VOR, DME, Air Data, ILS, etc. The main advantage of the system is its economy with respect to ground-based equipment. These have been widely deployed for many years and long operational experience has been acquired. Additionally, reliable, low-cost airborne equipments are available for this same reason. The disadvantages of the system are the varying locations, coverage and accuracy of the ground stations from one landing site to another. Because of the lack of coverage under certain conditions (for instance, in the 80-degree cone over a VOR OR TACAN station) inertial fill-in will be required. The stations have been developed and deployed assuming straight line, radial, point-to-point navigation of the present civil system (Rho-Theta). Thus, off-course, complex, three-dimensional paths must be computed leading to higher errors under unfavorable conditions.

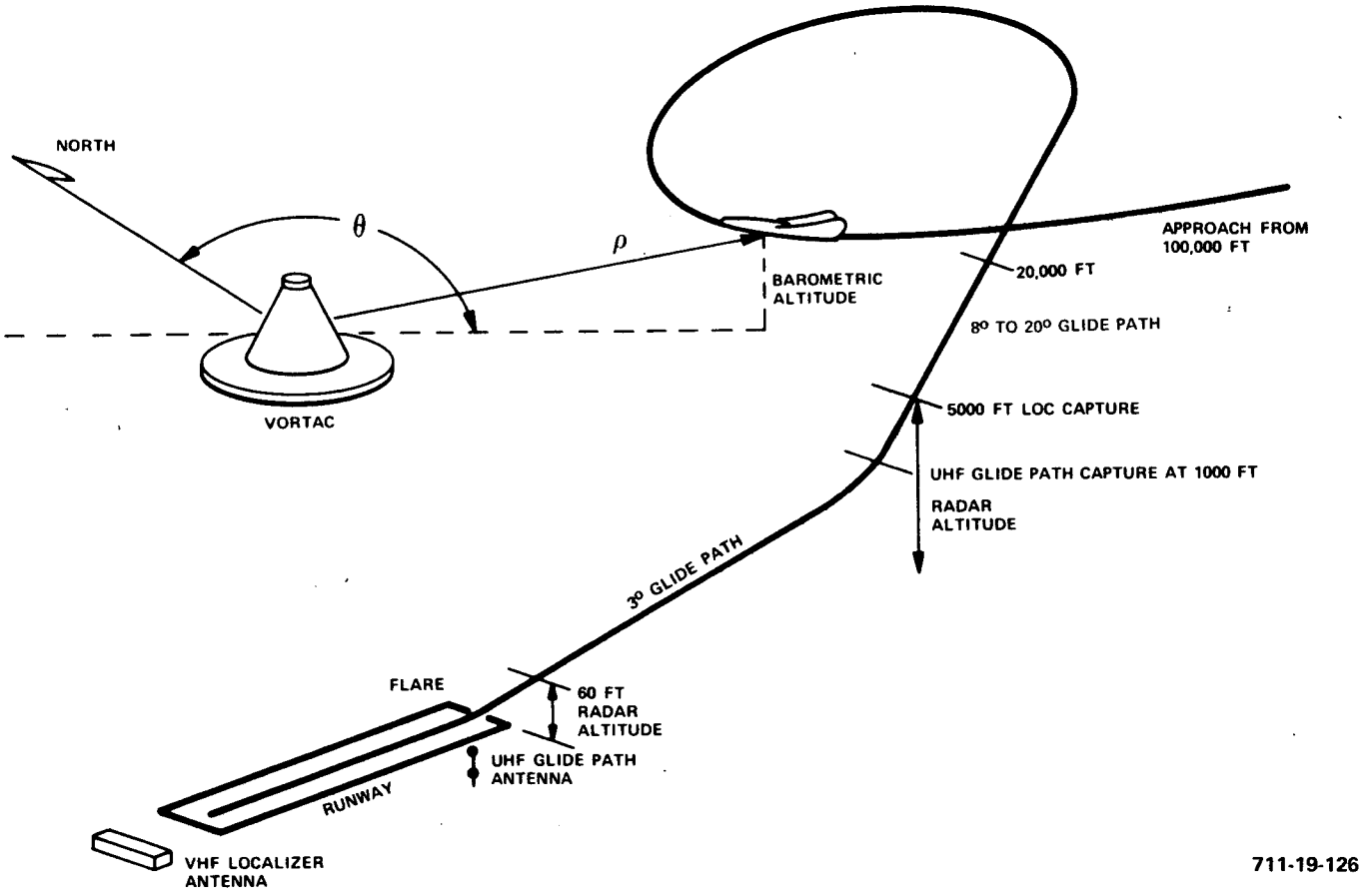

Figure 6-2
Candidate No. 1

TABLE 6-3

SYSTEM CANDIDATE NO. 1 CHARACTERISTICS

100,000 to 20,000 feet	
Lateral	VORTAC or TACAN + off-course computer and slant range correction using baro data. INS for rates, attitudes, data fill-in during non-coverage periods.
Vertical	Barometric + INS smoothing.
20,000 to 1,000 feet	
Lateral	Same as (a) except switch to localizer below approximately 10,000 feet.
Vertical	Computation of glideslope by DME-Baro, switch to DME-radar altimeter at 5,000 feet or at appropriate altitude determined by terrain characteristics.
1,000 to 60 feet	
Lateral	VHF localizer
Vertical	UHF glidepath to 200 to 300 feet, G/P extension (inertial-baro computed) and radar altimeter to 60 feet.
60 to 0 feet	
Lateral	VHF localizer
Vertical	INS glidepath extension, radar altimeter flare (+INS smoothing).

TABLE 6-4

AIRBORNE EQUIPMENT REQUIRED, CANDIDATE 1

Item	Weight, Pounds	No. Antennas
VHF/UHF Nav Receiver	25	2
DME	37	1
Radar Altimeter	15	2
Marker Beacon Receiver	5	1
Subtotal Radio Sensors	82	6
Air Data Sensor	4	-
Airborne Computer	45	-
Data Adapter	25	-
INS	75	-
Subtotal Others	149	-
Grand Total	231	6

- Candidate No. 2 (Figure 6-3, and Tables 6-5 and 6-6)

This is similar to Candidate No. 1 except that the 20° glide path portion now uses a high angle, microwave scanning beam ILS. This adequately solves the accuracy problem during this phase of flight but incorporates a system with less operational experience behind it. The other advantages and disadvantages of Candidate No. 1 are retained.

It is the stated intention of the civil aviation community to rapidly implement microwave scanning ILS systems. Yet much testing remains to be done and the uncertainity of the funding of the project leads to the conclusion that operational civil use is at least five years away. However, such systems will inevitably come into being, with vastly increased coverage and accuracy compared to conventional VHF/UHF ILS. From this standpoint alone, consideration of the system becomes attractive.

This candidate continues to use conventional ILS, radar altimeters, and conventional glide slope extension and flare during the last two flight regimes, 1000 to 60 feet and 60 to zero feet.

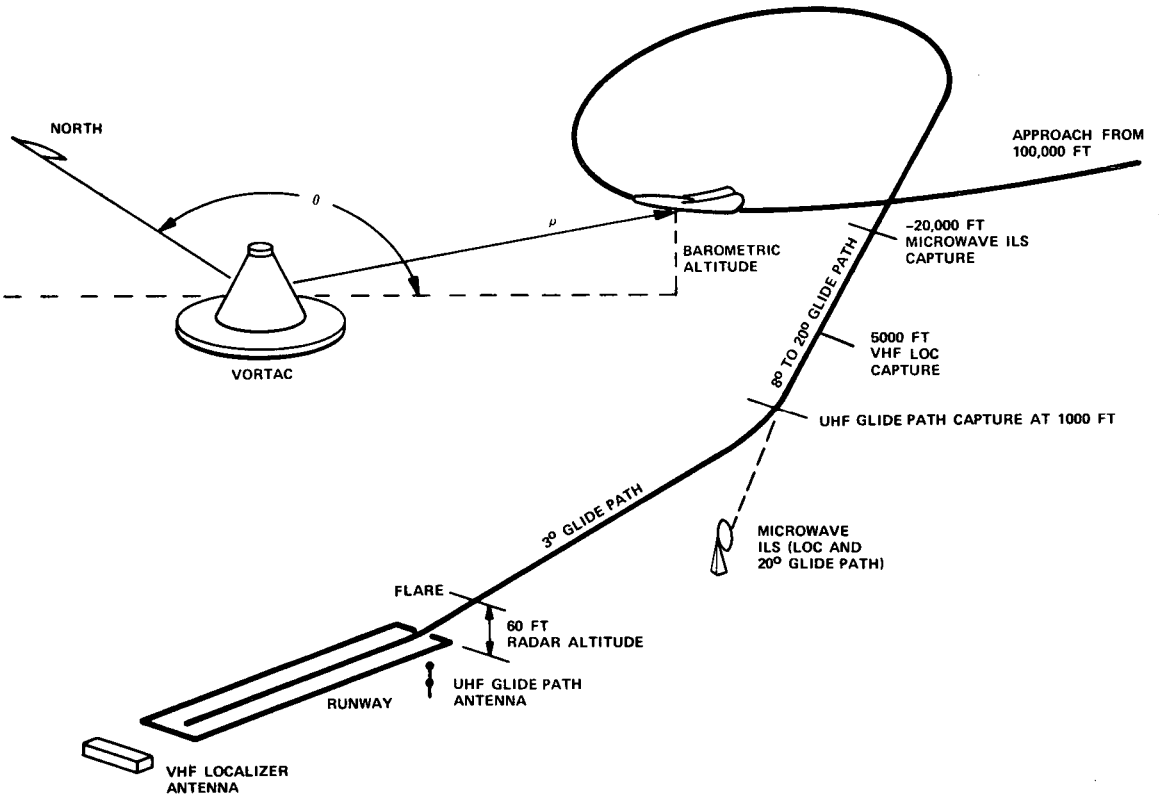

Figure 6-3
Candidate No. 2

TABLE 6-5

SYSTEM CANDIDATE NO. 2 CHARACTERISTICS

100,000 to 20,000 feet	
Lateral	VORTAC or TACAN + off-course computer and slant range correction using baro data. INS for rates, attitudes, data fill-in during non-coverage periods.
Vertical	Barometric + INS smoothing
20,000 to 1,000 feet	
Lateral	Microwave scanning localizer
Vertical	Microwave scanning glidepath properly sited up range
1,000 to 60 feet	
Lateral	VHF localizer
Vertical	UHF glidepath to 300 feet; G/P extension and radar altimeter to 60 feet.
60 to 0 feet	
Lateral	VHF localizer
Vertical	INS glidepath extension; radar altimeter flare

TABLE 6-6

AIRBORNE EQUIPMENT REQUIRED, CANDIDATE 2

Item	Weight, Pounds	No. Antennas
VHF/UHF Nav Receiver	25	2
DME	37	1
Marker Beacon Receiver	5	1
Radar Altimeter	15	2
AN/ARA-63	15	1
Subtotal Radio Sensors	97	7
Air Data Sensor	4	-
Airborne Computer	45	-
Data Adapter	25	-
INS	75	-
Subtotal Others	149	-
Grand Total	246	7

- Candidate No. 3 (Figure 6-4, and Tables 6-7 and 6-8)

Whereas Candidates 1 and 2 have the great advantages of prepaid ground equipment, the high altitude coverage of VORTAC may be inadequate. Candidate No. 3 puts its dependence upon precision range radar instrumentation, ground-based computation, and telemetry up-link of simple displacement, position, or command signals. High and medium altitude coverage and accuracy problems are virtually non-existent. Low altitude coverage is obtained by conventional ILS. For light traffic and only a few landing sites, this system seems excellent. It does require highly trained ground operators and an expensive array of elegant ground equipment. At high altitudes this is nothing more than an extension of manned orbiting or lunar vehicle techniques and has successfully proven itself for high angle glide paths at Edwards AFB with test vehicles.

On the other hand, many landing sites or high traffic will drive up the cost of ground equipment and maintenance/operating personnel.

Additionally, the ground facility must be located in close proximity to the landing area (within a few miles) to assure accurate tracking down to glide path capture.

An alternative to ILS is to switch to optical angle tracking at very low angles where radars will suffer from multipath. (Continue radar ranging.) This requires even more highly skilled operators and has no all-weather capability. It should only be considered as a back-up or flight test device.

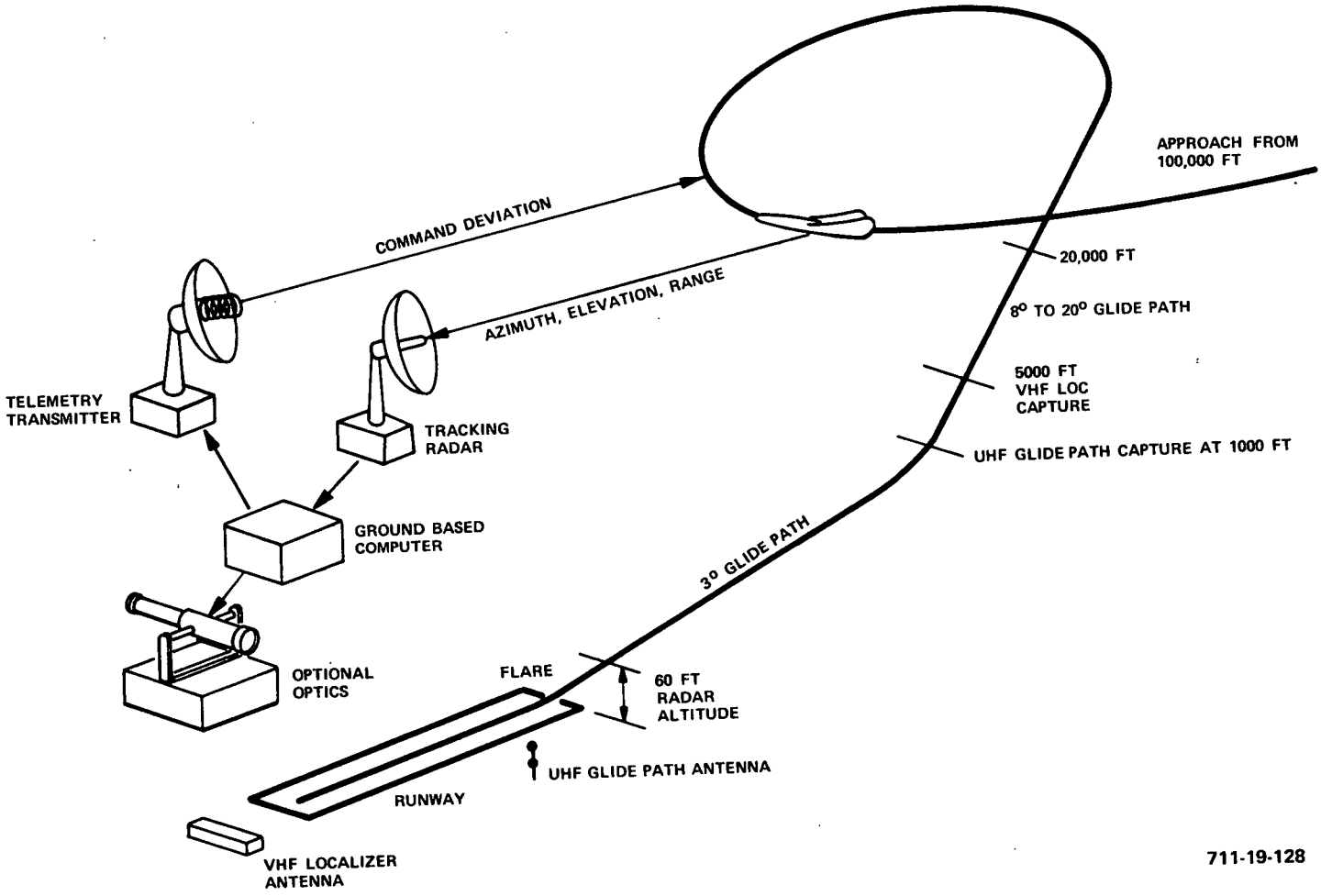

Figure 6-4
Candidate No. 3

TABLE 6-7

SYSTEM CANDIDATE NO. 3 CHARACTERISTICS

100,000 to 20,000 feet	
Lateral and Vertical	Range instrumentation radar, ground based computer, and telemetry up-link (INS smoothing)
20,000 to 1,000 feet	
Lateral and Vertical	Range instrumentation radar, ground based computer, and telemetry up-link
1,000 to 60 feet	
Lateral	VHF localizer
Vertical	UHF glidepath to 300 feet; G/P extension and radar altimeter to 60 feet.
60 to 0 feet	
Lateral	VHF localizer
Vertical	INS glidepath extension, radar altimeter flare

TABLE 6-8

AIRBORNE EQUIPMENT REQUIRED, CANDIDATE 3

Item	Weight, Pounds	No. Antennas
C-Band Beacon	8	1
Telemetry Receiver	10	1
VHF/UHF Nav Receiver	25	2
Radar Altimeter	15	2
Marker Beacon Receiver	5	1
Subtotal Radio Sensors	63	7
Air Data Sensor	4	-
Airborne Computer	45	-
Data Adapter	25	-
INS	75	-
Subtotal Others	149	-
Grand Total	212	7

- Candidate No. 4 (Figure 6-5, and Tables 6-9 and 6-10)

This is similar to No. 3 except that the requirement to site the range instrumentation radars in close proximity to the landing site is relieved by use of a microwave scanning beam ILS (with precision DME) from 20,000 feet down to zero. Thus a single range instrumentation radar and associated equipment could service the high altitude region for numerous landing sites within a 100 NM or greater radius. High traffic and/or the desire for redundancy might dictate two or three installations however.

Other advantages and disadvantages of instrumentation radar and microwave ILS remain. The system has the advantages of overlapping coverage by the two sensor types during the critical 20,000 to 1,000 feet region if siting is selected properly.

The system preferably uses a single microwave localizer with precision DME and two microwave glide path transmitters, one in line with the steep angle path and the second in line with the low angle path. This provides further redundancy and back-up modes by allowing either airborne path computation via DME and the second glide path scanner, or the flying of raw data and switching from the first to second glide path scanner at the transition from steep to low angle glide path.

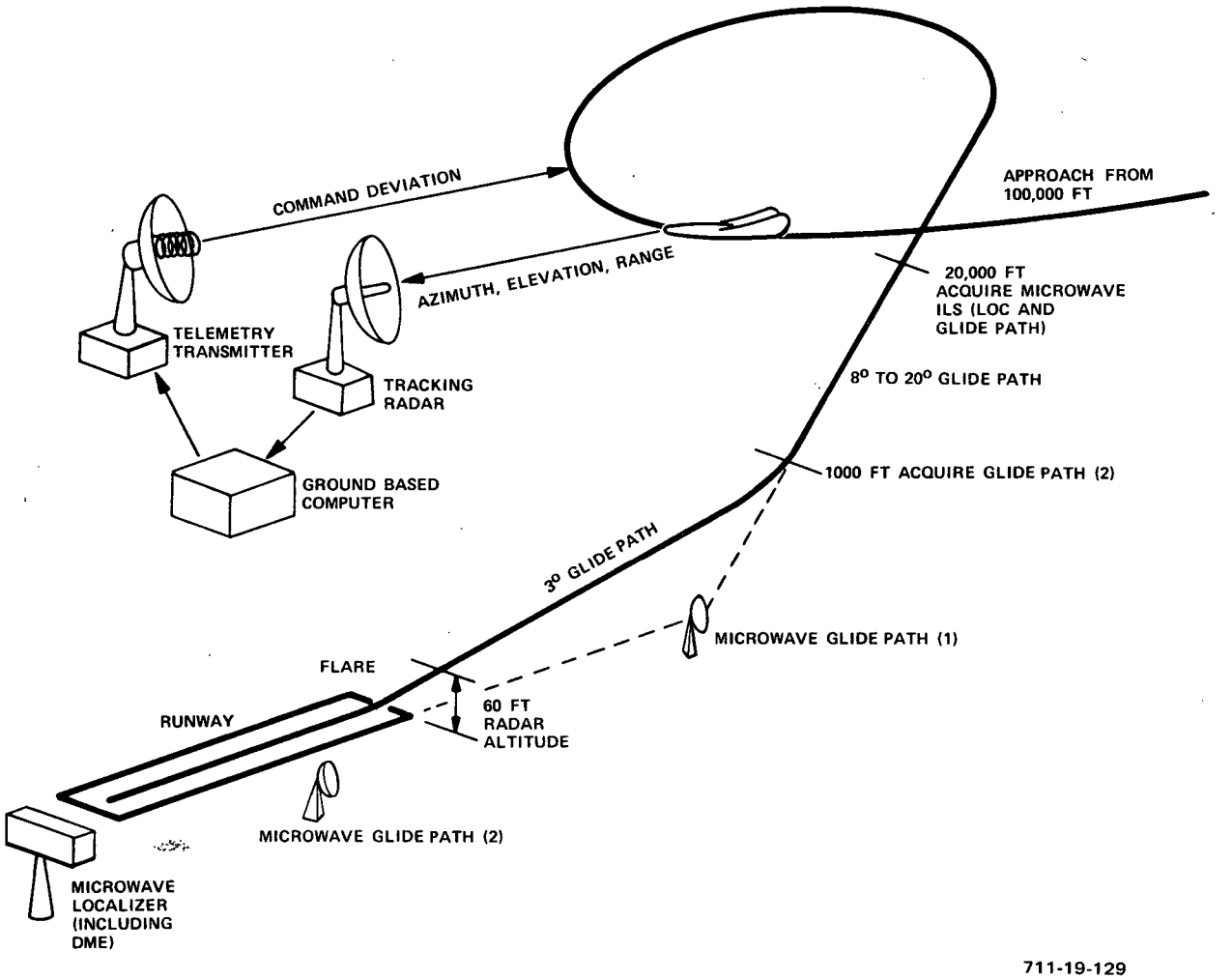

Figure 6-5
Candidate No. 4

TABLE 6-9

SYSTEM CANDIDATE NO. 4 CHARACTERISTICS

100,000 to 20,000 feet	
Lateral and Vertical	Range instrumentation radar, ground based computer, and telemetry up-link (INS smoothing).
20,000 to 1,000 feet	
Lateral and Vertical	Microwave scanning localizer, including precision DME. Microwave scanning glidepath.
1,000 to 60 feet	
Lateral	Microwave scanning localizer, including precision DME
Vertical	Second microwave scanning glidepath
60 to 0 feet	
Lateral	Microwave scanning localizer, including precision DME
Vertical	Second microwave scanning glidepath (radar altimeter as backup).

TABLE 6-10

AIRBORNE EQUIPMENT REQUIRED, CANDIDATE 4

Item	Weight, Pounds	No. Antennas
C-Band Beacon	8	1
Telemetry Receiver	10	1
ARA-63	15	1
Radar Altimeter	15	2
Subtotal Radio Sensors	48	5
Air Data Sensor	4	-
Airborne Computer	45	-
Data Adapter	25	-
INS	75	-
Subtotal Others	149	-
Grand Total	197	5

- Candidate No. 5 (Figure 6-6, and Tables 6-11 and 6-12)

This candidate introduces the concept of an omni-directional tri-lateration airborne sensor-computer complex for below 20,000 feet. The range instrumentation radar concept is retained above 20,000 feet since the short base line tri-lateration system has excessive errors at long range and would require much higher powers to work reliably beyond 20-nautical mile slant range.

The tri-lateration system has proven accurate in some applications, notably geodesy and aerial surveying. It is a low traffic density system but does not require human operators. Being omni-directional and narrow band, it is subject to multipath errors unless siting is done with care. It has not had the wide operational experience of conventional VHF/UHF systems nor does it seem destined for such wide adoption as microwave scanning beam ILS. It is considered to embody some technical risk and little eventual economy.

An alternate is two tri-lateration ground systems, one deployed in close proximity to the landing site to cover 20-nautical mile range as above, and the second widely deployed and of higher power (including dual purpose, switchable airborne higher power interrogators) to give coverage to 100,000 feet and 150 to 200-nautical miles.

The multi-lateration system has the further disadvantage that raw data is not available in a form that may be used directly.

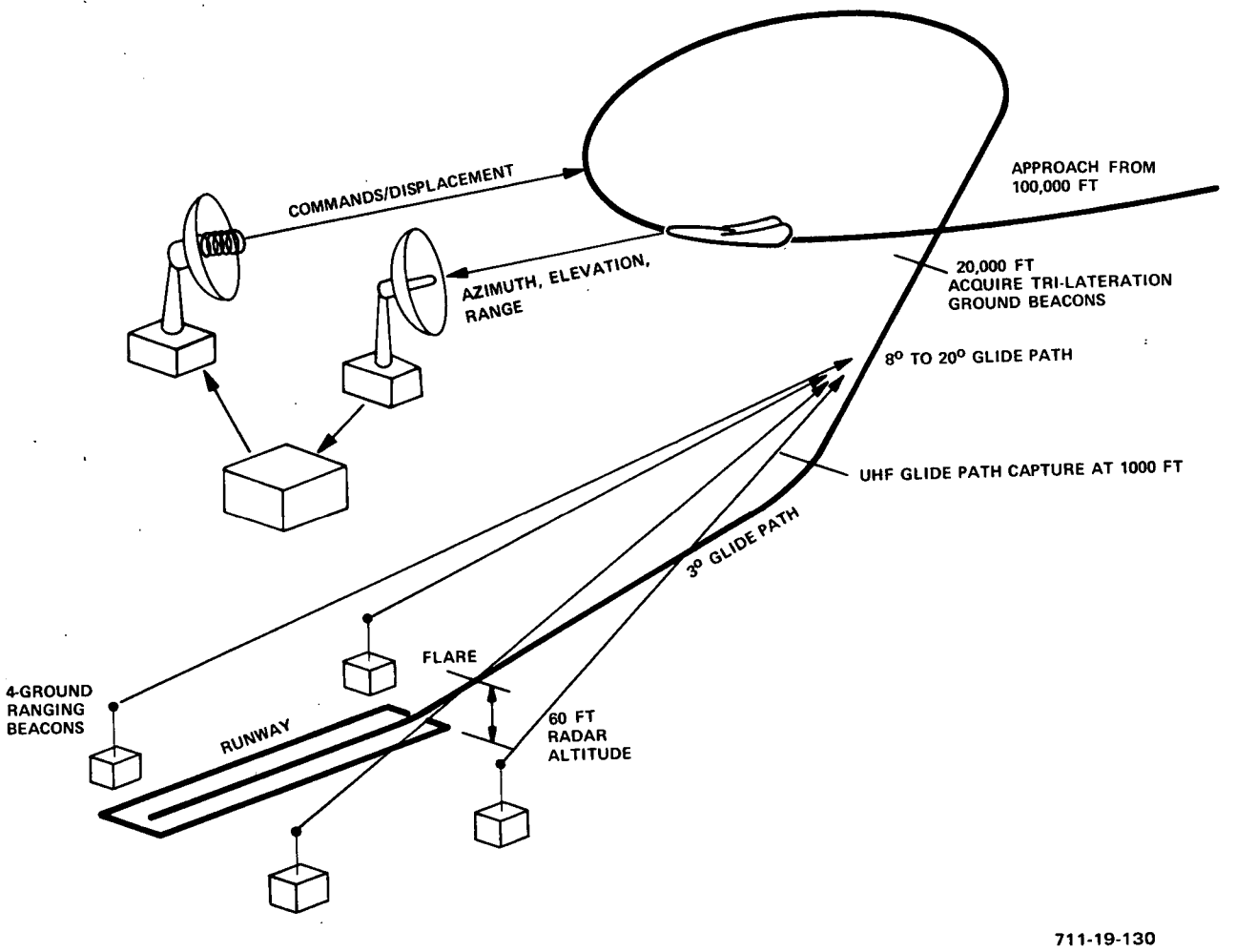

Figure 6-6
Candidate No. 5

G

TABLE 6-11

SYSTEM CANDIDATE NO. 5 CHARACTERISTICS

100,000 to 20,000 feet	
Lateral and Vertical	Range instrumentation radar, ground based computer, and telemetry up-link.
20,000 to 1,000 feet	
Lateral and Vertical	Tri-lateration interrogator (air), transponders (ground), and airborne computer.
1,000 to 60 feet	
Lateral and Vertical	Tri-lateration interrogator (air), transponders (ground), and airborne computer.
60 to 0 feet	
Lateral and Vertical	Tri-lateration system. Tri-lateration (radar altimeter backup for flare).

TABLE 6-12

AIRBORNE EQUIPMENT REQUIRED, CANDIDATE 5

Item	Weight, Pounds	No. Antennas
C-Band Beacon	8	1
Telemetry Receiver	10	1
Tri-Lateration Interrogator	20	1
Radar Altimeter	15	2
Subtotal Radio Sensors	53	5
Air Data Sensor	4	-
Airborne Computer	45	-
Data Adapter	25	-
INS	75	-
Subtotal Others	149	-
Grand Total	202	5

b. Conclusions

Candidate system No. 4 was selected as the best method of performing operational space shuttle approach and landing guidance, but perhaps with additional VOR/DME capability for high altitude as in Candidate 2. This system, which has adequate accuracy, a low technical risk, and reasonable costs, is capable of being flight tested at Edwards in the near future (less than one year) without excessive expense.

During the Edwards flight test however, serious consideration should be given to VORTAC use for the high altitude (above 20,000 feet) region with a view to eventual economics should space shuttle traffic become more frequent than one or two operations a month. Tests should be directed to this end. Specifically, high altitude (above 60,000 feet) VORTAC tests for accuracy, coverage, and interference should be made. Offset navigation techniques by airborne computation of VORTAC signals with barometric altitude should be verified. Should the results of these tests prove favorable, it is envisioned that the ultimate system would be a combination of candidates 2 and 4; VORTAC/Baro down to 20,000 feet and microwave scanning ILS from 20,000 feet to full stop on the runway.

C. CANDIDATE AIRCRAFT REQUIREMENTS FOR SPACE SHUTTLE SIMULATION

1. Introduction

A study of the seven aircraft listed below and shown in Figure 6-7 was made to determine which aircraft could best be used for investigating unpowered Space Shuttle Vehicle (SSV) terminal area and landing approach problems.

F-104
F-106
F-111
F-4
T-38
CV-990
B-52

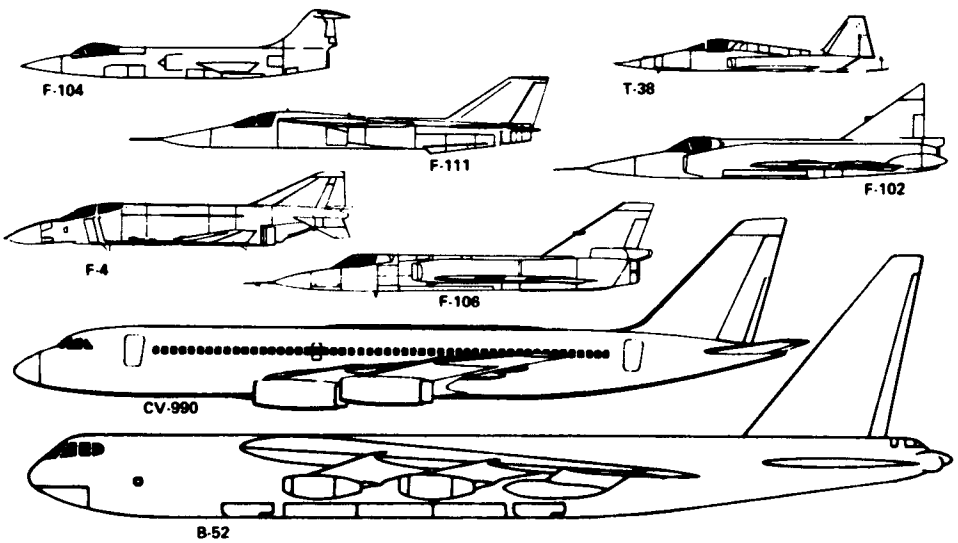

Figure 6-7
Candidate Aircraft to Simulate Space Shuttlecraft Vehicle

This list includes two aircraft which were not listed in the statement of work (T-38 and B-52) and does not include the F-102 and B-58 which were listed. For the purposes of selecting an aircraft to simulate an SSV the F-102 would have similar idle thrust lift-to-drag characteristics as the F-106 since the wing area is identical. The B-58 was eliminated from the study because of predicted high operational costs, high maintenance costs, and the fact that all aircraft except one are in "moth balls" at Davis Monthan AFB. The T-38 aircraft was added as a candidate vehicle because it exhibited many of the desirable qualities such as low operating cost and low maintenance cost. The B-52 aircraft was included because it is representative of the size and gross weight of many of the SSV's.

Both high and low cross-range vehicle configurations were considered in seeking an aircraft to simulate space shuttle vehicle characteristics. At the time this study was performed, the LCR vehicle was still a strong space shuttle candidate. Many of the conclusions reached in the original study (Reference 32) were based on matching LCR vehicle characteristics. One of the criticisms of the CV-990 as reported in Reference 32, for example, was the fact that it could match the reference HCR vehicle better than it could match the LCR vehicle. It will be shown later that the second look at the CV-990 revealed an excellent match for both the MDAC and NAR HCR vehicles that were studied on this program.

2. Performance Criteria for an Aircraft to Simulate an SSV

a. L/D Versus Speed

In order to best simulate the performance of the SSV, the most important criteria for the selection of an aircraft is the ability to match the front side of the equilibrium lift-to-drag (L/D)* versus equivalent airspeed curve. A match of these curves provides the same flight path angle, the same airspeed, the same speed stable energy management response, and thus the same flight path trajectory.

---

*The L/D data is defined as the lift divided by drag minus idle thrust.

$$L/D = \frac{L}{D - T_{idle}}$$

b. Handling Qualities - Difference Between Large and Small Aircraft

Related to the problem of manual handling quality simulation is the basic question of whether a small aircraft can adequately simulate the flight path control characteristics of a large aircraft. The previous discussion stated that duplicating L/D versus airspeed curve will result in the same trajectory at the same speeds. Will control response dynamics to these trajectories be the same for large and small aircraft? There are two factors that determine the flight path control dynamics:

- Lag in flight path angle change following pitch change
- Dynamics of pitch response to pitch command

The first of these lags is the time constant τ_γ given by

$$\tau_\gamma = \left(\frac{mv}{Q}\right)\left(\frac{1}{C_{L_\alpha} S}\right) = \left(\frac{W}{S}\right)\left(\frac{V}{Q}\right)\left(\frac{1}{gC_{L_\alpha}}\right) \qquad (6\text{-}1)$$

It is seen that at a given speed that would be flown by both the large and small aircraft, the lag is proportional to wing loading W/S. Ideally, therefore, to simulate a space shuttle vehicle, we should also match wing loading and lift curve slope characteristics (C_{L_α}). A small aircraft and a large aircraft can produce a good match and in the various simulator aircraft that were considered the match of the SSV's τ_γ was relatively good.

The second factor, the pitch response dynamics shows a larger variation between large and small aircraft. The ability to obtain a responsive pitch to pitch command (θ/θ_C) characteristic depends upon the torque-to-inertia ratio (pitch angular acceleration per degree of elevator). Figure 6-8 shows this parameter for various aircraft (normalized to 280 knots at about 5000 feet). It is interesting to note from this figure that lifting bodies have the controllability of very large aircraft but because of their small size they have the gust response of the small aircraft. The conclusion we can draw from this figure is that it would be very difficult (if not impossible) to make a large aircraft respond like a small aircraft. Fortunately, in the problem under

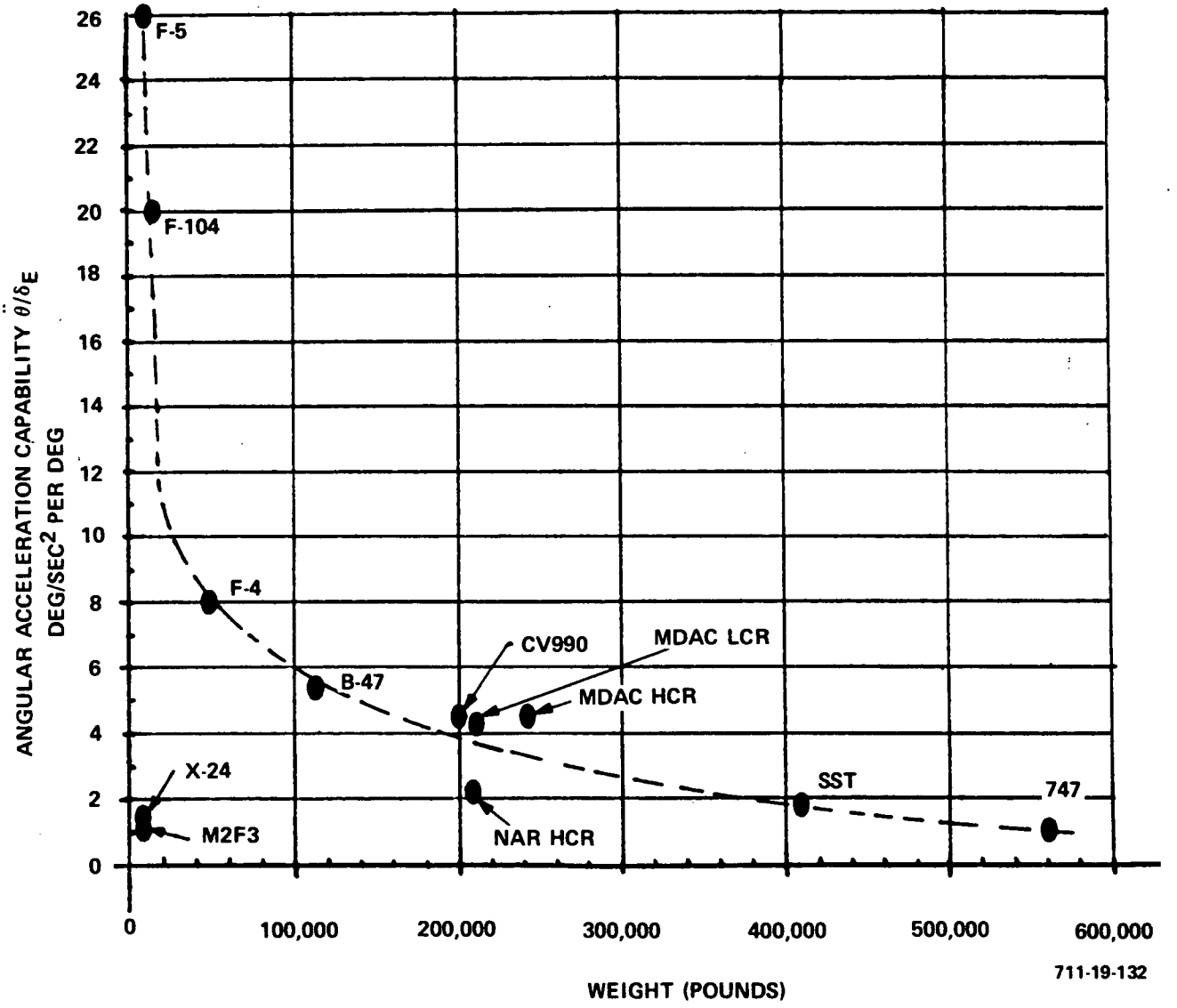

Figure 6-8
Pitch Acceleration Capability of Aircraft as Function of Weight

consideration we must achieve the reverse effect if we intend to use an aircraft such as an F-104 to represent the much larger SSV. (It is noted, however, that the CV-990 is quite representative of candidate space shuttle vehicles.) Slowing down an attitude response is readily accomplished by inserting the necessary lags into the autopilot or augmentation system.

c. Multiple Seat Capability

It is important to have an SSV simulator that has two seats to allow for evaluation of simulated IFR operation. One pilot could fly the manual steering mode while the other pilot monitored the flight.

3. Analysis of Flight Test Candidate Aircraft

In Reference 32, the L/D versus airspeed characteristics for the various candidate aircraft in various configurations of flap, landing gear, and speed brake deployment were compared with the L/D versus airspeed curves for two candidate space shuttle vehicles. The representative space shuttle characteristics were those of the LMSC Delta body HCR orbiter and the MDAC-1, Straight Wing, LCR Orbiter. Both of these vehicles were described in Sections III and IV of this report. As stated previously, the F-104 was found to give the best match for both of these vehicles. Figure 6-9 shows the F-104A characteristics superimposed on the straight-wing orbiter characteristics, and Figure 6-10 shows the F-104A curves superimposed on the delta-wing orbiter curve. The nominal L/D or operating point is shown in both figures. For the straight-wing orbiter, full flaps will not be deployed until final flare and touchdown; therefore, this will be a transient situation for which an equilibrium glide path will not be established. The F-104A is a good match for either the straight-wing or delta-wing orbiter. Other versions of the F-104 such as the two seat version (F-104B) would have identical L/D characteristics.

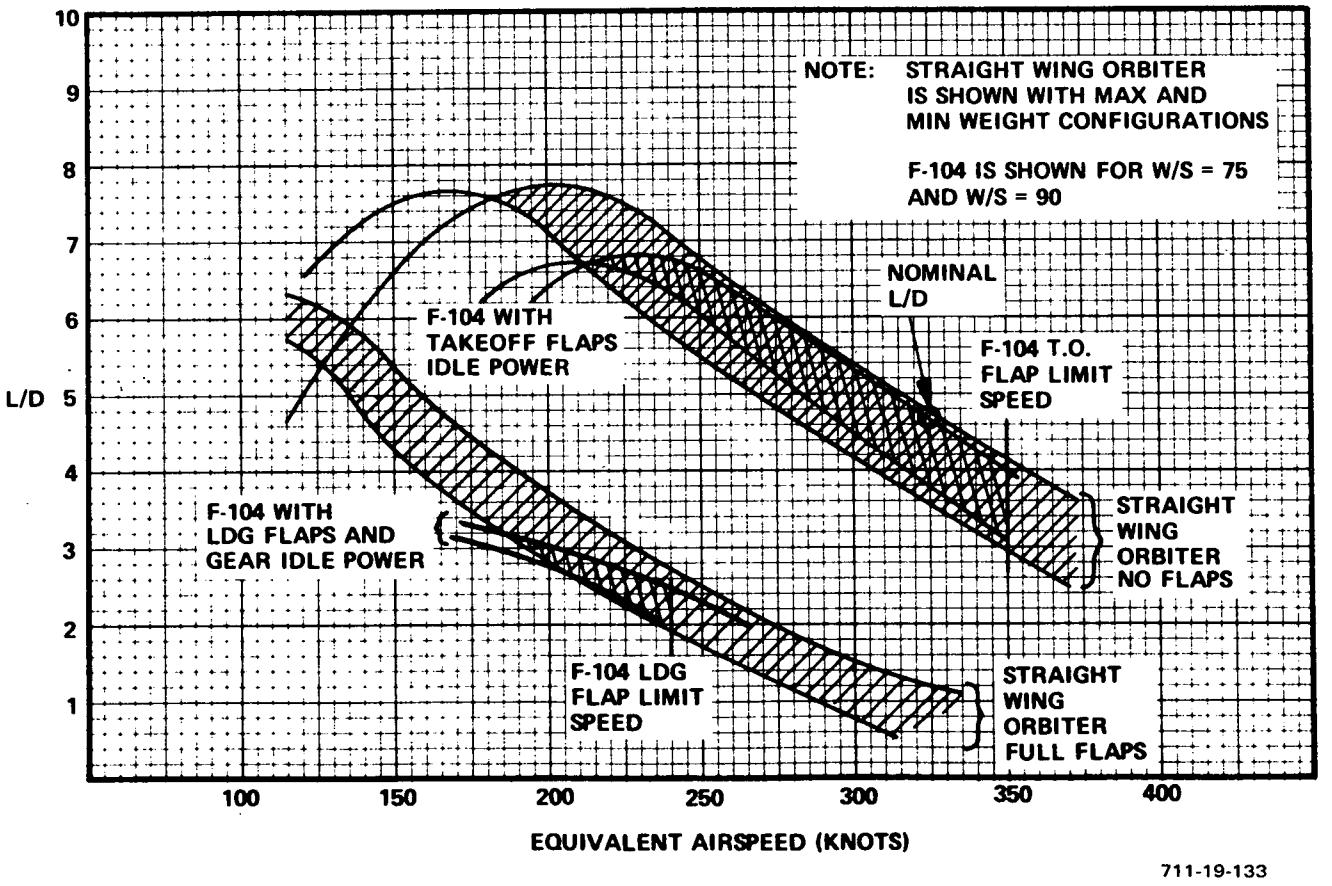

Figure 6-9
Comparison of F-104A with the Straight-Wing Orbiter L/D Data

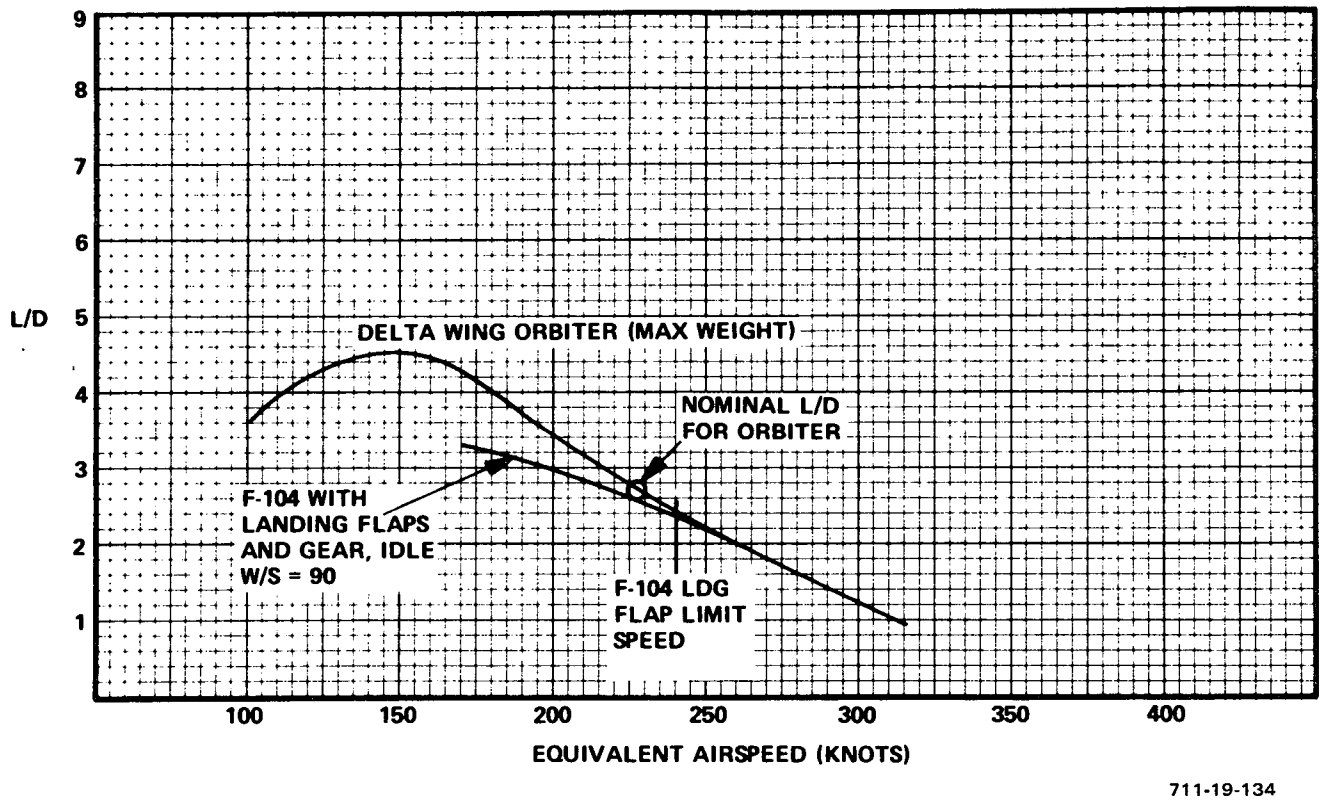

Figure 6-10
Comparison of F-104A with the Delta Wing Orbiter L/D Data

Subsequent to the analyses that produced reference 32, the CV-990 was studied in great depth to determine whether it can be made representative of some of the newer SSV configurations. The fact that the CV-990 had been used to demonstrate simulated SSV unpowered approaches at Edwards AFB was a strong motivation to take a closer look at that aircraft. Figures 6-11 and 6-12 show an extremely good matching capability when the CV-990's spoilers are deflected symmetrically in the speedbrake configuration. Figure 6-11 illustrates the high altitude part of the descent trajectory. The CV-990's aero data for Mach 0.84 was used to generate the L/D versus airspeed curves. At Mach 0.84 the aircraft would be at 40,000 feet, the start of the descent trajectory. At that altitude it would be in the high altitude energy management phase of the terminal guidance. It will therefore be operating near (L/D) maximum of the space shuttle. From Figure 6-11, it is seen that a perfect match with the MDAC vehicle is obtained with a 10-degree speedbrake deflection.

In the terminal glide region (assuming a -10 degree glide path), the CV-990 with 20 degrees of speedbrake deflection again is a near perfect match of the MDAC HCR orbiter as shown in Figure 6-12. This figure also shows the spoiler blow-down limit and demonstrates that adequate speed margin exists with the speedbrake requirement for simulating either the MDAC or NAR vehicles.

Figures 6-11 and 6-12 therefore demonstrate that the CV-990 would be an excellent choice as an SSV approach and landing simulator. To verify the capability of that aircraft and to determine whether any unique control requirements may exist, the CV-990 was flown on Sperry's 6-degree-of-freedom digital simulator using the recommended SSV energy management and terminal approach and landing guidance and control system. The complete CV-990 aero model including the tab/elevator hinge moment equations were included in the simulations. Figures 6-13, 6-14, and 6-15 illustrate one of the trajectories obtained. Figure 6-13, the horizontal view of the trajectory, shows that it starts in the final phase of the high altitude energy management guidance, moving outbound from the runway, and about 7 nautical miles from the final turn, onto the terminal approach flight path. Note that the CV-990 is in its maximum speed descent configuration; that is: gear down but zero speed brakes. The descent on the

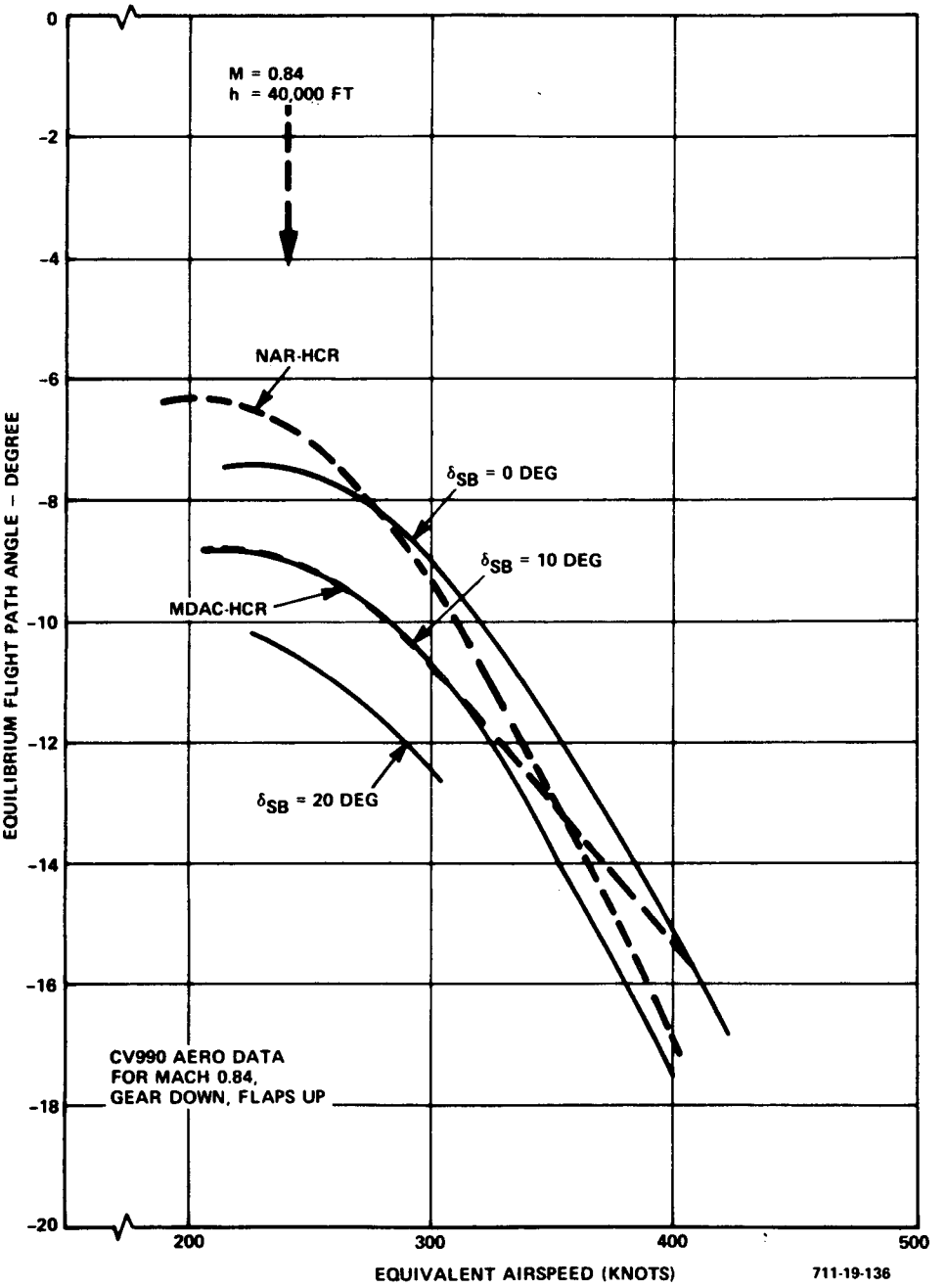

Figure 6-11
CV990 with Speedbrakes, γ versus V_E, Match to
MDAC and NAR HCR Orbiters (High Altitude)

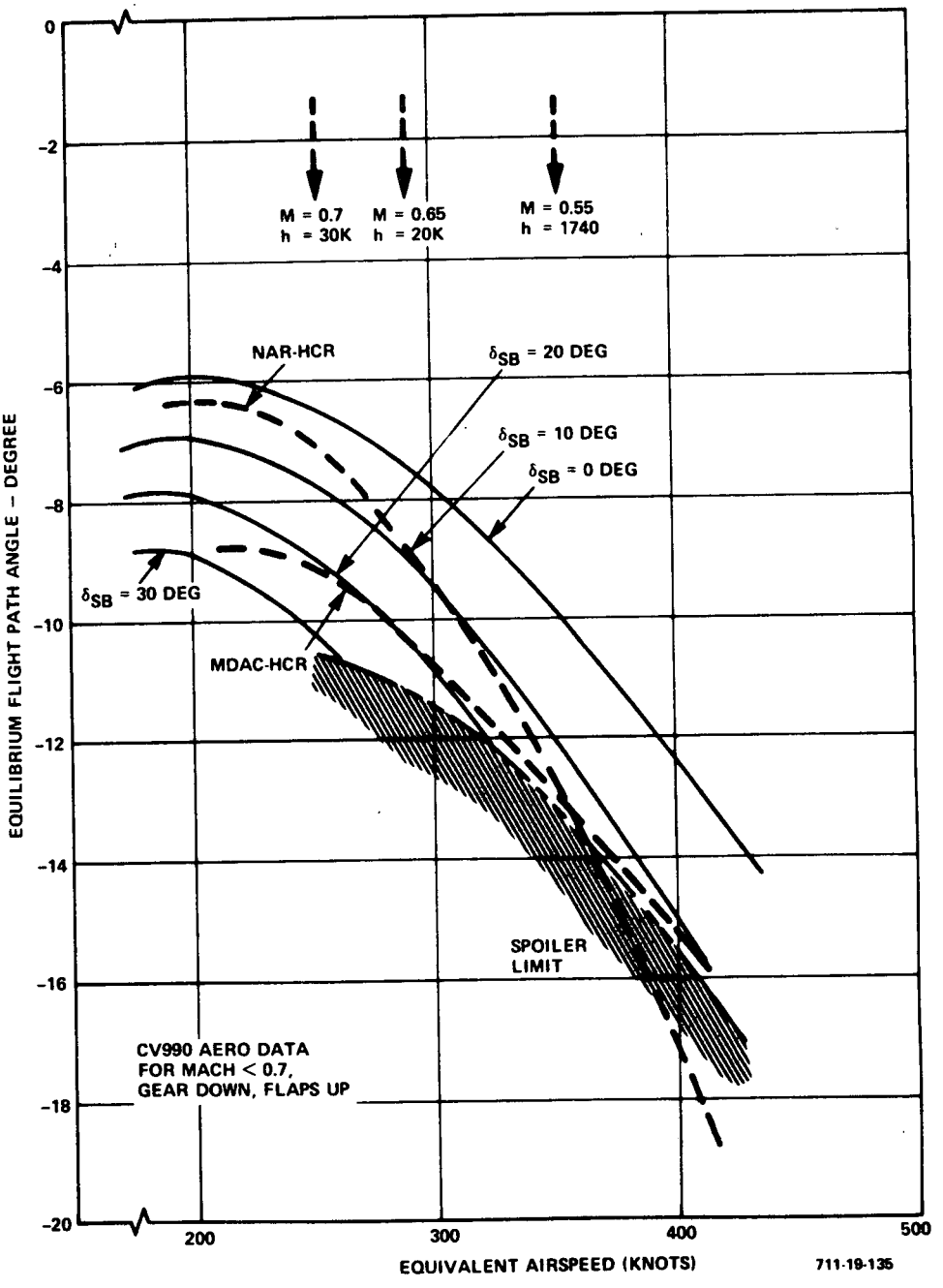

Figure 6-12
CV990 with Speedbrakes, γ versus V_E, Match to
MDAC and NAR HCR Orbiters (Terminal Glide)

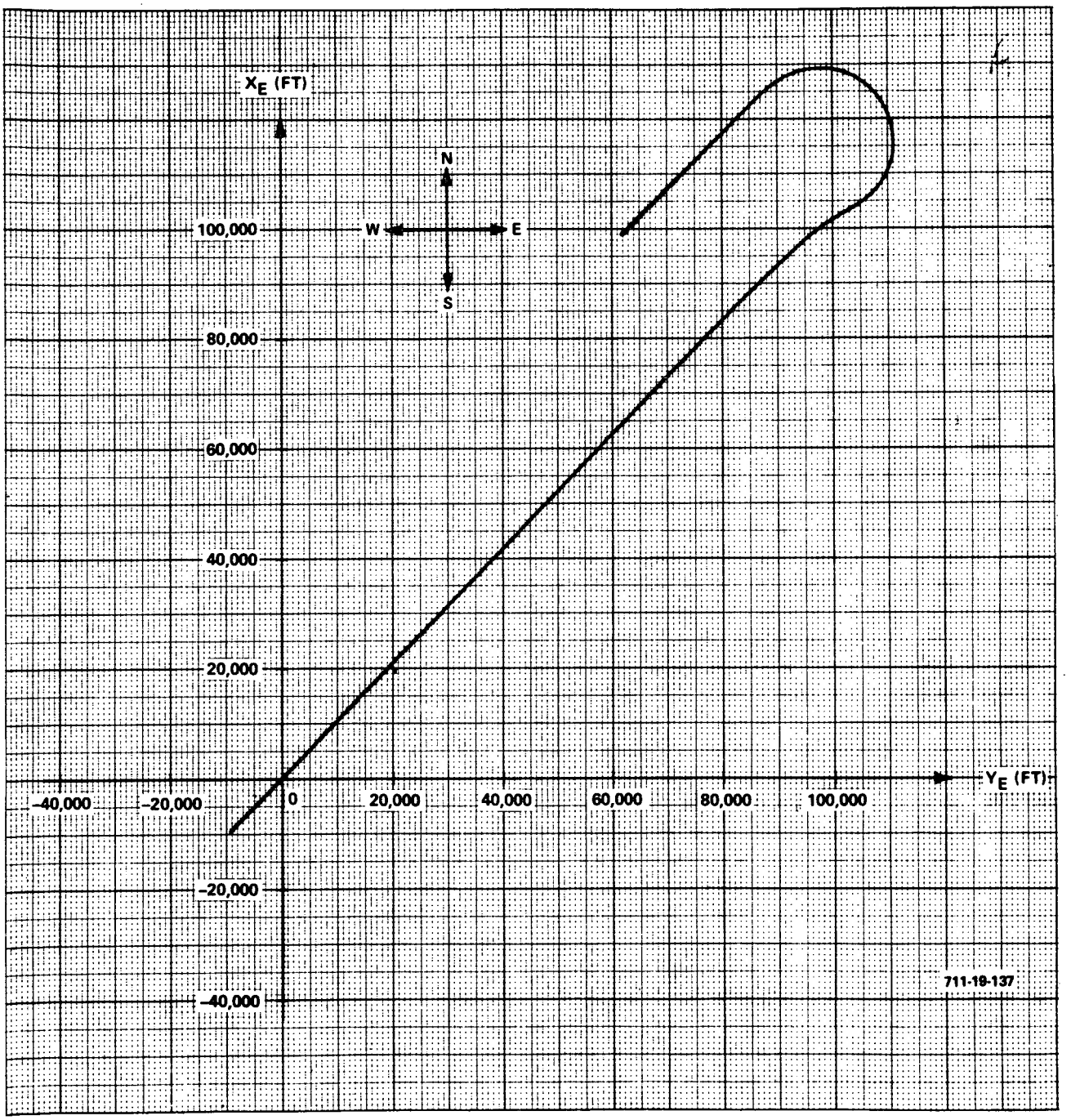

Figure 6-13
Horizontal Plane Trajectory from 40,000-foot Altitude to Touchdown for CV990 SSV (0, 0), Intercept of -10-degree Glide Slope with Ground

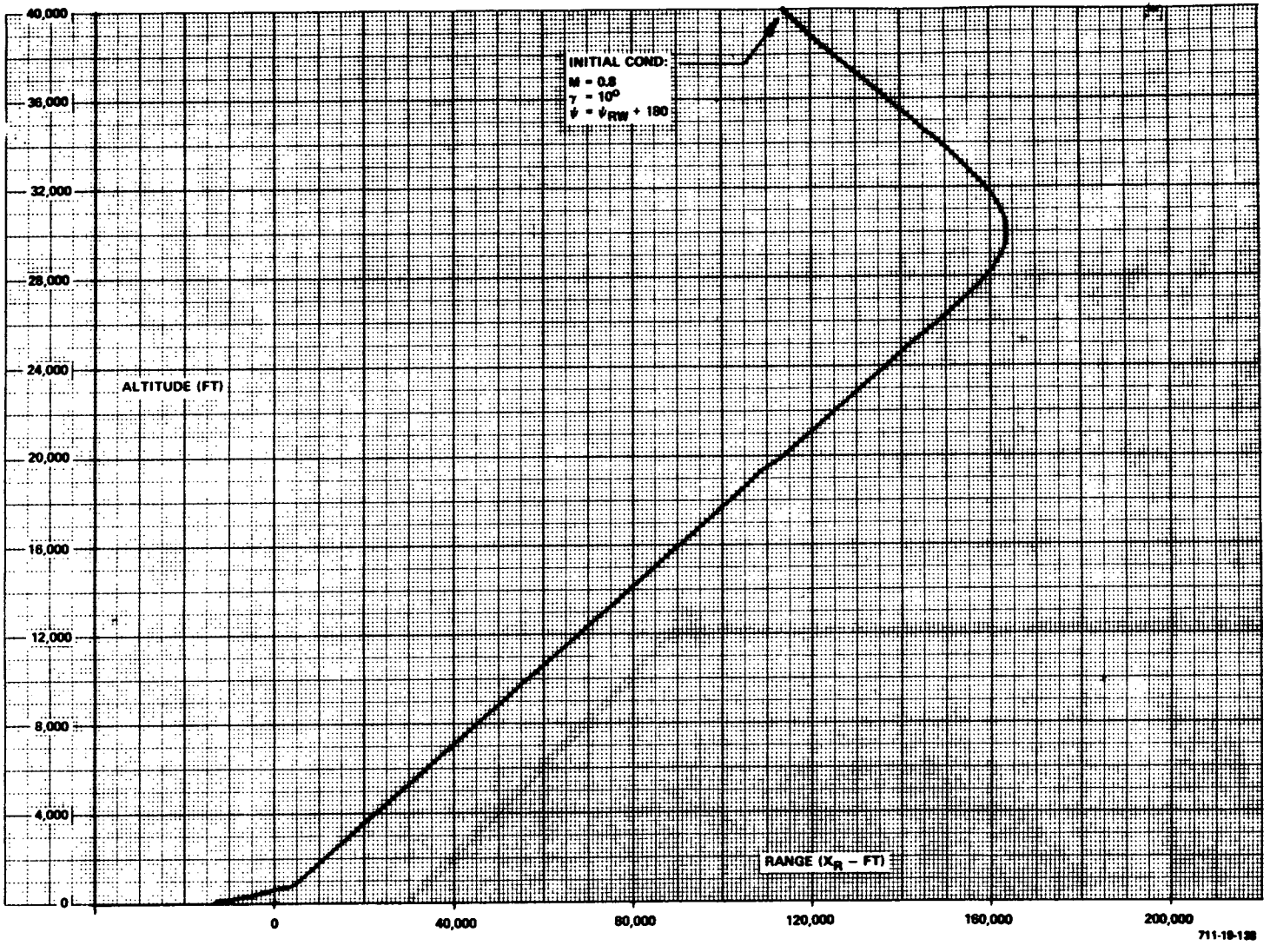

Figure 6-14
Altitude versus Range History for CV990 SSV from 40,000 feet to Touchdown, First Flare Altitude = 1,000 feet, No Speed Brakes or Flaps Deployed, Landing Gear Down at 40,000 feet

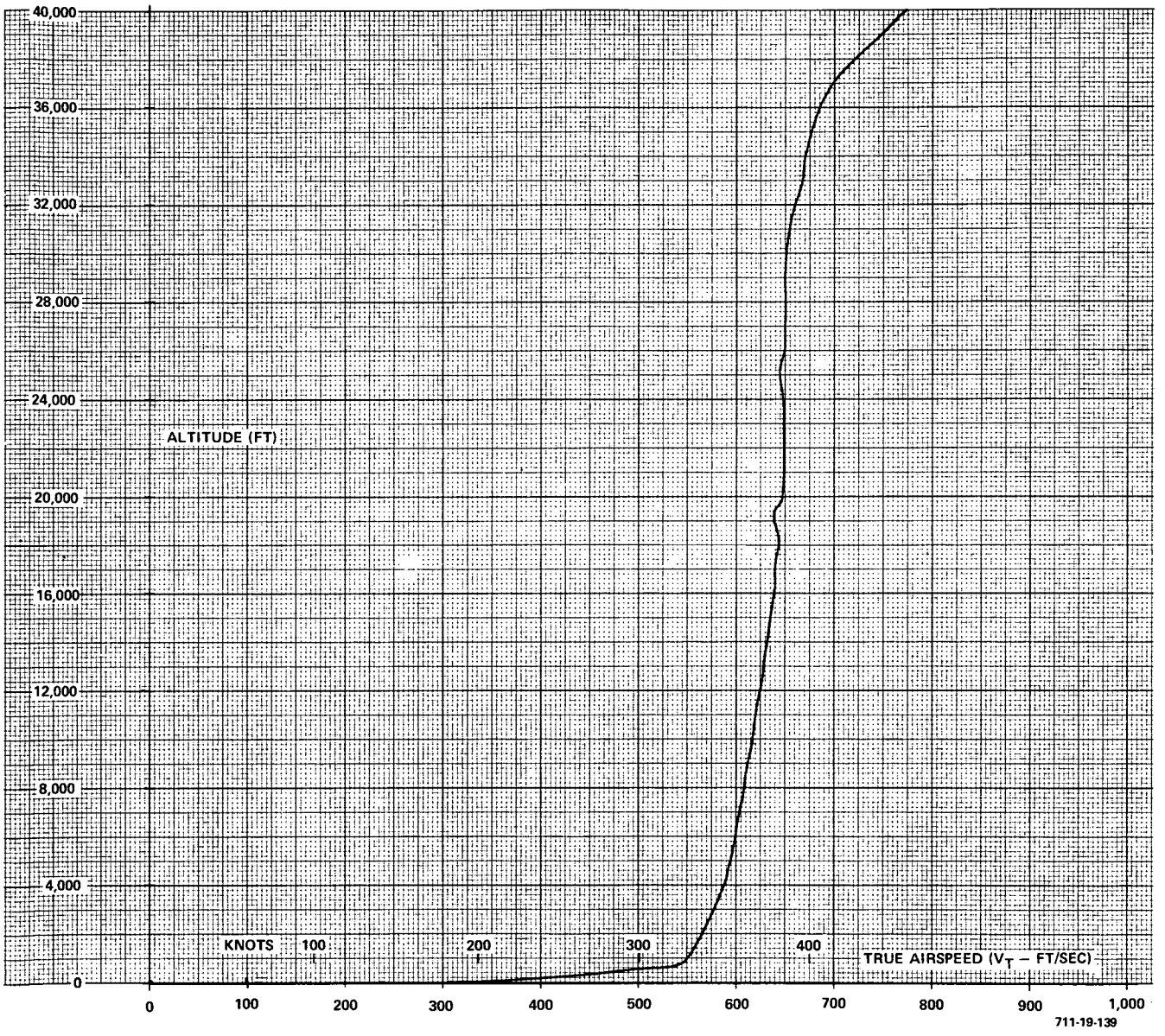

Figure 6-15
Altitude-Velocity History for CV990 SSV from 40,000 feet to Touchdown,
No Speed Brakes or Flaps Deployed, Landing Gear Down at 40,000 feet

terminal glide path for this configuration involves speeds greater than 300 knots. This speed would correspond to the early, twin fin NAR vehicle rather than the more recent MDAC vehicle configuration. This speed is probably an upper bound for the CV-990.

The vertical view of the trajectory shown in Figure 6-14 demonstrates a near perfect prediction of the final turn maneuver onto the glide path. The velocity history demonstrating the relatively high speeds on the final approach path is shown in Figure 6-15.

4. Flight Test Vehicle Recommendations

The CV-990 is recommended as the SSV simulator for flight test evaluation of SSV terminal approach and landing techniques. Reasons for this recommendation are:

- Background of demonstrations of unpowered, high energy approaches with CV-990 at Edwards AFB
- Capable of providing excellent match of more recent SSV aerodynamic characteristics
- *Adequate space for installing the required avionics
- Existing autopilot servo actuator installation can be used ... sufficient control authority is available and system can be operated with required safety constraints. (See Reference 32.)
- Availability of aircraft to NASA

*More detailed descriptions of avionics mechanizations were given in Reference 32.

SECTION VII

CONCLUSIONS AND RECOMMENDATIONS

SECTION VII

CONCLUSIONS AND RECOMMENDATIONS

The conclusions and recommendations derived from the simulations, analyses, and evaluations of terminal approach and landing techniques for five candidate space shuttle vehicles of both the low and high cross-range variety are summarized in the following paragraphs.

1. Consistent automatic instrument landings of unpowered space shuttle vehicles can be made with the same level of performance that is attained today in the landing of conventionally powered transport aircraft. The recommended guidance and control system can achieve nominal touchdown sink rates of 2 feet per second with the 2-sigma performance in the presence of winds and turbulence held below 5 feet per second. The nominal longitudinal position at touchdown can be 800 to 1000 feet beyond the intersection of a -2-1/2-degree glide path and the ground. The 2-sigma longitudinal dispersion in the presence of winds and turbulence is about +1000 and -500 feet from the nominal. Manual and augmented manual landing performance was not sufficiently evaluated to determine a quantitative level of attainable performance. Additional study is needed to fully evaluate the effect of pilot simulator practice on the landing performance.

2. Nominal landing speeds for unpowered space shuttle vehicles range between 165 and 195 knots depending upon the availability of drag brakes for speed management and the range of headwind and tailwind uncertainty which must be accommodated.

3. The segmented or two-phase glide path is the recommended landing technique for both the automatic and augmented manual modes. The use of a fixed shallow glide path following the high energy, steep glide path is most effective with higher approach speeds and high L/D vehicles. For vehicles with lower subsonic L/D's (below about 4.5), and with approach speeds below about 250 knots, a single flareout provides performance approximately equivalent to that which can be obtained with the two-stage flareout technique.

4. As in the case of flareout systems for conventional jet transports, several types of flareout control laws are applicable to the unpowered space

shuttle landing, but the key factor in the flareout system is the predictive or open loop part of the control law. The predictive terms should be updated for off-nominal conditions of velocity, weight, and vertical speed.

5. A flat skid decrab maneuver is recommended. It should be initiated about 8 feet from touchdown to align the vehicle with the runway during cross-wind landings. The maneuver is performed with a combination of closed loop and predictive commands to the rudder with feedforward compensation into the roll axis to help keep wings level. The skid decrab technique is favored over a forward slip alignment technique for space shuttle because it offers greater accuracy and does not complicate speed management.

6. The HCR energy management window at an altitude of 100,000 feet is a 100-nautical mile radius circle with its center at a 20,000-foot low key point which is located about 23 nautical miles forward of the runway. This represents the adjustable range capability from an altitude of 100,000 to 20,000 feet. An additional range capability of about ±7 nautical miles downrange and ±4 nautical miles cross-range exists from 20,000 feet to the first flare altitude.

7. The LCR's energy management capability from an altitude of 100,000 feet until the completion of the high to low angle-of-attack transition maneuver is small and of the same range as the potential navigation errors in that region. The range adjustment window from about 25,000 feet to touchdown is approximately 14 nautical miles downrange and ±4 nautical miles cross-range.

8. The LCR's transition maneuver should be performed at an altitude of about 45,000 feet using a combination of reaction and aerodynamic controls to achieve a nose-over re-orientation in the shortest possible time. The vehicle should then be stabilized at the maximum permissible angle of attack consistent with an adequate margin below wing stall onset. Pull-out of the dive can be achieved by the time an altitude of 25,000 feet is reached if the angle of attack reference is held between 6 and 8 degrees.

9. All of the space shuttle vehicles studied had some degree of inherent lateral-directional instability. Some configurations were severely unstable and unflyable without stability augmentation. A single lateral-directional control

law and a single pitch control law could be used for all vehicles studied with only the gain functions adjusted to accommodate individual vehicle differences. This provided adequate stability and good maneuvering command responses (for both automatic and manual control) throughout each vehicle's terminal area flight envelope.

10. Stabilization of the lateral-directional modes of some space shuttle configurations necessitated high gain augmentation loops that need relatively large surface rate and deflection authorities. Realistic actuator constraints were used in this study, but such high gain loops may pose some potential problems in a practical system.

11. High altitude energy management can be achieved with a guidance scheme that alters the shape of a turning trajectory as a function of departure from a nominal energy program. This system can work with almost any combination of gain parameters that, in turn, give a variety of different trajectories, all of which satisfy the requirement that the vehicle be brought to a specific position at an altitude of 20,000 feet.

12. A simpler high altitude energy management guidance scheme that eliminates much of the requirement for a turning descent can also be used to exploit all of the range adjustment capability of HCR space shuttles. Such a system can be used as the basis of a raw-data manual backup guidance system. In the raw-data mode initial steering to the required heading is provided using a GCA voice communication technique. Required displays are an attitude-director indicator, horizontal situation indicator and air data instruments. Raw deviation data from the steep angle glide path and localizer are presented on a cross-pointer display. After some practice with these techniques in the simulator, pilots can land space shuttle vehicles in IFR conditions without requiring any on-board guidance computers. Good manual handling qualities are required, and they can be provided through a separate control augmentation system.

13. To monitor the performance of the automatic system, the pilot should be provided with a map display that includes a trend vector (predicted trajectory) presentation. He also requires a mode annunciation display which indicates the existing and forthcoming control mode status so that he can follow the progression of automatic mode sequences.

14. Various combinations of navigation devices can provide the information needed for terminal area guidance and control. The recommended navigation system uses microwave scanning beams for lateral and vertical flight path information below about 20,000 feet. A radio altimeter may also be required for final flareout (depending upon the availability and siting of a second vertical scanning beam). At high altitudes conventional NAVAIDS (VOR, DME) and air data are used. INS is used throughout the descent trajectory for either data smoothing or as primary navigation information.

15. The Convair 990 aircraft is recommended as a flight test space shuttle simulator for evaluating terminal area guidance and control techniques. The CV 990 with speed brakes deployed (spoilers) can provide an excellent aerodynamic match of the more recent HCR SSV configurations. An F-104B or a drag plate modified F-106 can also provide the desired aerodynamic characteristics needed to simulate SSV unpowered landings.

REFERENCES

REFERENCES

1. Mueller, George E. "The New Future for Manned Spacecraft Developments", Astronautics and Aeronautics, Volume 7, No. 3, March 1969.

2. Faget, Max, "Space Shuttle: A New Configuration", Astronautics and Aeronautics, Volume 8, No. 1, January 1970.

3. Myers, Dale D. "Space Transportation System Overview and Program Plans", Space Transportation System Technology Symposium, I - Aerothermodynamics and Configurations, NASA TM X-52876, Volume I.

4. Tischler, B. O. "Space Shuttle", Astronautics and Aeronautics, Volume 9, No. 2, February 1971.

5. "Integral Launch and Reentry Vehicle Systems", NASA CR-66862, McDonnell Douglas Astronautics Corporation, November 1969.

6. "Study of Integral Launch and Reentry Vehicle System", NASA CR-102102, North American Rockwell Corporation, December 1969.

7. "Space Shuttle Final Technical Report", NASA CR-102549, General Dynamics/ Convair, October 1969.

8. "Integral Launch and Reentry Vehicle", LMSC-A959837, NASA CR 102627, Lockheed Missiles and Space Corporation, December 1969.

9. "Spacemaster - A Two Stage Fully Reusable Space Transportation System", M-69-36, Martin Marietta Corporation, December 1969.

10. "Aero Design Data Book for Delta Wing Orbiter (SSV-134C)", Pub. No. DB 2.1.5-13000 North American Rockwell (Revisions and enclosures through August 1970).

11. "Orbiter Aerodynamics Data Book, Pub. No. MDC E0407, McDonnell Douglas Astronautics Company - East, June 30, 1971.

12. "Space Shuttle Orbiter Aerodynamics Data Book", LMSC-A966076, Lockheed Missiles and Space Company, Revised 5/1/70.

13. Yoder, J. F., TRW Systems Group (Houston), "Aerodynamics Data for MSC Orbiter 245", TRW Memorandum Report 70.4353-17.

14. Behm, W. F. "Low Crossrange Orbiter Data Package", McDonnell Douglas Astronautics Company Memo No. SSPO-E241-056, August 13, 1970.

15. Dana, W. H. and Gentry, J. R. "Pilot Impressions of Lifting Body Vehicles", NASA TMX-2102, Flight Test Results Pertaining to the Space Shuttlecraft, October 1970.

16. Hoag, P. C. and Schofield, B. L. "IFR Experience with Unpowered, Low Lift-Drag Ratio Landing Approaches", NASA TMX-2102, October 1970.

17. Bray, R. S; Drinkwater III, F. J., and White, M. D. "A Flight Study of a Power-Off Landing Technique Applicable to Reentry Vehicles", NASA TN D-323, July 1960.

18. Matranga, G. J. and Armstrong, N.A. "Approach and Landing Investigation at Lift Drag Ratios of 2 to 4 Utilizing a Straight Wing Fighter Airplane", NASA TMX-31, 1959.

19. Matranga, G. J. "Analysis of X-15 Landing Approach and Flare Characteristics Determined from the First 30 Flights", NASA TN D-1057, July 1961.

20. Matranga, G. J. and Menard, J. A. "Approach and Landing Investigations at Lift-Drag Ratios of 3 to 4 Utilizing a Delta Wing Interceptor Airplane", NASA TMX-125, 1959.

21. Von Doenhoff, A. E. and Jones Jr., G. W. "An Analysis of the Power Off Landing Maneuver in Terms of the Capabilities of the Pilot and the Aerodynamic Characteristics of the Airplane", NACA TN2967, 1953.

22. Schofield, B. L. "Gliding Flight Equations", FTC-TI1M-70-1007, May 1970.

23. Osder, S. S. "Study Report, Terminal Control Energy Management and Landing of Reentry Gliders, Sperry Phoenix Company (presently Sperry Flight Systems Division) Report No. LJ-1262-0214, February 1963.

24. Schofield, B. Lyle, Richardson, D. F. and Hoag, P. C. "Terminal Area Energy Management, Approach and Landing Investigations for Maneuvering Reentry Vehicles Using F-111A and NB-52B Aircraft", Technical Document No. 70-2, USAF Flight Test Center, June 1970.

25. Kock, Berwin M. and Fulton Jr., Fitzhugh L. "Approach and Landing Studies" - Flight Test Results Pertaining to the Space Shuttlecraft, NASA TMX-2101, October 1970.

26. "Space Shuttle System Phase B Study Final Report, Part II-2A, Technical Summary - Orbiter", Report MDC E0308, McDonnell Douglas Astronautics Company, June 30, 1971.

27. Osder, S. S. "Avionics Requirements for All Weather Landing of Advanced SST's, Volume I, Analysis of System Concepts and Operational Problems and Volume II, State-of-the-Art Review of All Weather Landing System Techniques", NASA CR 73092 and CR 73093, April 1967.

28. Dendy, J. B. and Transier, K. G. "Angle of Attack Computation Study", Technical Report No. AFFDL-TR-69-93, October 1969.

29. "Simulation Handbook, Low Cross Range, Straight-Winged Orbiter (MDAC-2)", Report No. 5440-8935-S2, Sperry Flight Systems Division, September 1970.

30. "Simulation Handbook, High Cross Range Delta Wing Orbiter (North American SSV-134C)", Report No. 5440-8935-S3, Sperry Flight Systems Division, October 1970.

31. Wawrzyniak, M. E. "To What Extent Should Space Shuttle Stability and Control Be Provided Through Stability Augmentation", Space Transportation System Technology Symposium, Volume I, Aerodynamics and Configurations, NASA TMX52876, July 1970.

32. "Study Report - Equipment Mechanization and Flight Test Aircraft Selection for Space Shuttle Landing Flight Research", Report No. 70-1323-00-00, Sperry Flight Systems Division, October 1970.

APPENDIX A

EQUATIONS OF MOTION SUMMARY

APPENDIX A

EQUATIONS OF MOTION SUMMARY

This appendix presents the equations utilized in simulating the various vehicles under investigation. Figure A-1 illustrates the versatility of the simulation to accurately model the vehicles aerodynamic characteristics through the use of two and three variable table look-ups. As noted from the figure, all aero coefficients are functions of at least two variables, with many coefficients a function of three variables, i.e., angle of attack, Mach number, and elevator position. Note that velocity information (from which position determinations are made) is defined in terms of a flat earth coordinate frame. This approximation is acceptable for terminal area studies. Figure A-2 provides additional air data information required for the computation of Q, α, β and true airspeed. These supplementary equations also illustrate how the mean and turbulent components of the winds are incorporated into the simulation. Note that the wind components are added into the body axis coordinate system but wind models are specified with respect to an earth-oriented frame. This requires an intermediate coordinate transformation to obtain u_w, v_w and w_w in body coordinates. This transformation and information regarding the wind model is discussed in Appendix B.

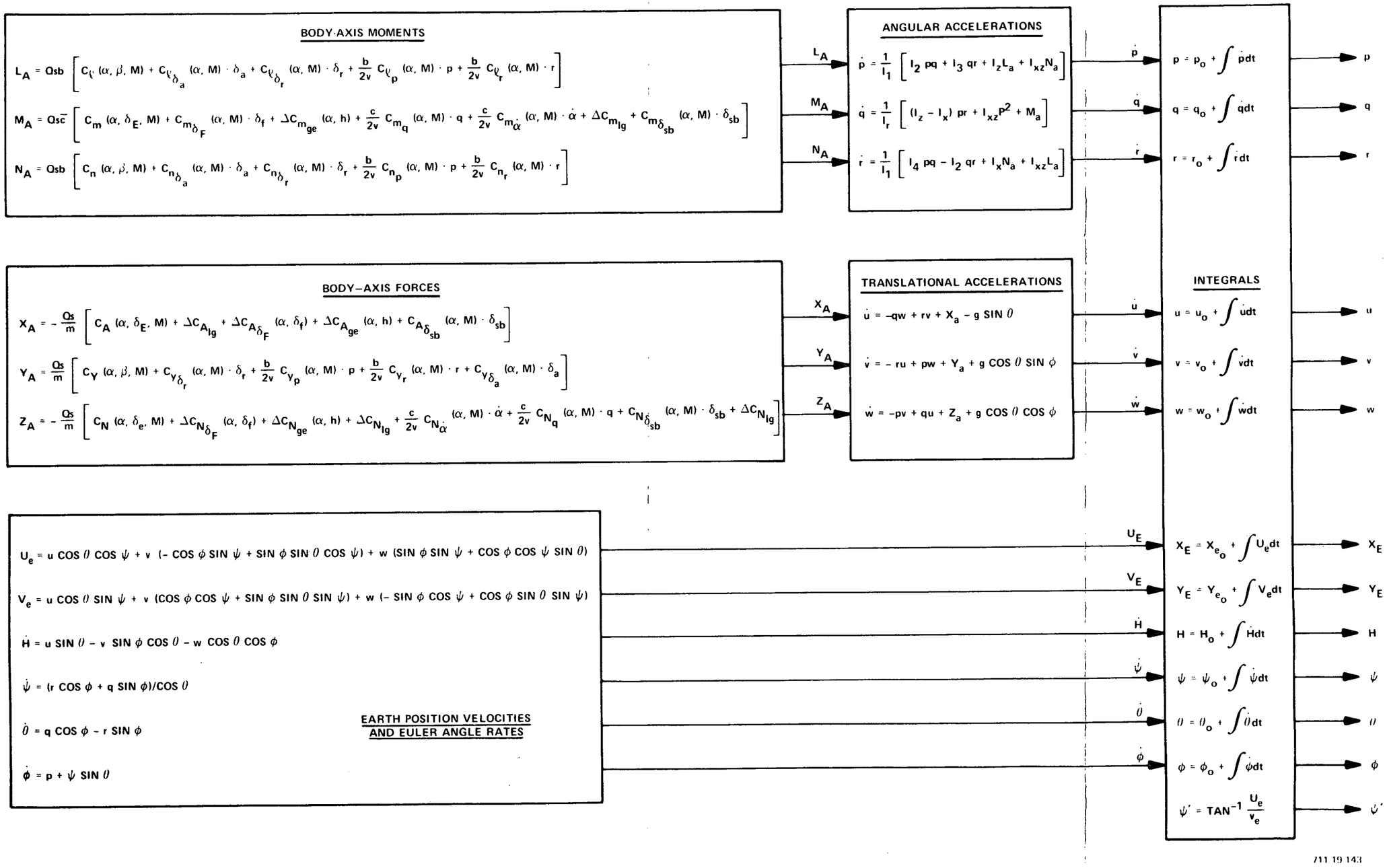

Figure A-1
6-Degree-of-Freedom Equations of Motion

$I_1 = I_X I_Z - {}^1{}_{XZ}{}^2$ M – MASS

$I_2 = I_{XZ}(I_X - I_Y + I_Z)$ S – SURFACE AREA

$I_3 = I_Z(I_Y - I_Z) - I_{XZ}{}^2$

$I_4 = I_X(I_X - I_Y) + I_{XZ}{}^2$

b = WING SPAN (FT)

$\bar{c}$ = MEAN AERO CHORD (FT)

CONSTANTS

$u' = u + u_w$

$v' = v + v_w$

$w' = w + w_w$

u_w, v_w, w_w ARE WIND COMPONENTS EQUAL TO

$u_w = u_{mean} + u_{gust}$

$v_w = v_{mean} + v_{gust}$

$w_w = w_{mean} + w_{gust}$

WIND COMPONENT ADDITIONS*

*WIND COMPONENTS ENTER BODY MOMENT AND FORCE EQUATIONS THROUGH α, β, Q AND MACH.

$V_T = (u'^2 + v'^2 + w'^2)^{1/2}$

$M = V_T/V_A$ (V_A = SPEED OF SOUND AS A FUNCTION OF ALTITUDE)

$Q = 1/2\ \rho V_T{}^2$ (ρ = AIR DENSITY)

$\alpha = \text{TAN}^{-1}\ \frac{w'}{u'}$

$\beta = \text{SIN}^{-1}\ \frac{v'}{V_T}$

$\gamma = \text{TAN}^{-1}\ \frac{\dot{h}}{(u_e{}^2 + v_e{}^2)^{1/2}}$

$V_e = \left(2Q/\rho_o{}^{1/2}\right)$

AIR DATA COMPUTATIONS

711-19-142

Figure A-2
Digital Simulation Aero Data and Wind Model
Additions to Equations of Motion

APPENDIX B

WIND MODEL FOR SPACE SHUTTLE SIMULATIONS

APPENDIX B

WIND MODEL FOR SPACE SHUTTLE SIMULATIONS

1. INTRODUCTION

The wind model defined herein was developed from various references as indicated in the following discussion. The model and its rationalization was prepared by the NASA ARC Guidance and Navigation Branch (Full Scale and Systems Research Division). The wind model for the space shuttle vehicle simulations consists of a mean wind and a turbulent wind. The model for the mean wind satisfies the FAA specifications (Ref B-1) for headwinds, crosswinds and tailwinds. The model also provides an estimate to the mean wind data based on worldwide in-service operation of the United Kingdom Airlines (Ref B-2). A model for this data was presented in Ref B-7. The model for mean wind at high altitudes was obtained from Ref B-3 and B-4. The mean wind is described in a local level coordinate system.

The turbulent wind model was taken from Ref B-3 (Section 3.7, Atmospheric Disturbance). The Dryden model is used to describe u_g, v_g and w_g, the gust components along the X, Y and Z axes of the body, respectively. One variation to the Dryden model was made. The scale lengths (L_u, L_v, L_w) being used are constant for an altitude less than 100 feet, which implies the variances σ_u^2, σ_v^2, σ_w^2 are also constant over that altitude range. The turbulent wind is described in the body axis coordinate system.

2. MEAN WIND

The mean wind is described by

$$V_{mw} = V_o + V_j \left[e^{-\frac{1}{2}\left(\frac{h-h_j}{D_j}\right)^2} - e^{-\frac{1}{2}\left(-\frac{h_j}{D_j}\right)^2} \right] + Sh^2 \qquad \text{(B-1)}$$

where

V_{mw} = mean wind, ft/sec

h = altitude of vehicle cg, ft

V_o = ground wind speed plus wind shear, ft/sec

h_j = altitude of center of jet stream, ft

D_j = thickness of jet stream, ft

S = solar activity constant determining high altitude winds, $ft/sec/ft^2$

V_j = jet stream velocity, ft/sec

The term V_o describes the very low altitude mean wind and shear for approach and landing. For $h \geq 10$ feet,

$$V_o = \frac{(A + B \cos AMW + C \cos^2 AMW)}{(D \log_{10} 10 + E)} V_o \, e^{-\frac{h}{H}} (D \log_{10} h + E) \qquad \text{(B-2)}$$

and for $h < 10$ feet,

$$V_o = \frac{(A + B \cos AMW + C \cos^2 AMW)}{10} V_{os} \, e^{-\frac{10}{H}} h \qquad \text{(B-3)}$$

where

$A = 25.3171$ ft/sec (15 knots)

$B = 12.6585$ ft/sec (7.5 knots)

$C = 4.2195$ ft/sec (2.5 knots)

$D = 0.43$, $E = 0.35$ } numerical data from Ref B-7

AMW = angle describing the direction from which the wind is blowing, radians (indepentent of altitude). Note that AMW is selectable prior to each simulator run if one wishes to evaluate performance with known wind conditions.

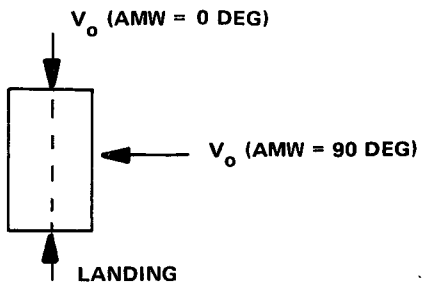

The constants A, B and C are chosen so that at h = 10 feet (approximately touchdown), the term $(A + B \cos AMW + C \cos^2 AMW)$ will be representative of the FAA specification (Ref B-1); i.e., headwinds up to 25 knots, crosswinds up to 15 knots and tailwinds up to 10 knots. The upper limits specified by the FAA document are assumed to represent the 3-sigma value. Consequently, the term $(A + B \cos AMW + C \cos^2 AMW)$ is multiplied by V_{os} which has a normal distribution with m = 1/2 and σ = 1/6. If, for example, AMW = 0, the term

$$(A + B \cos AMW + C \cos^2 AMW)\ V_{os}$$

results in a headwind with a mean of 12.5 knots and 3-sigma values of 0 and 25 knots.

The mean wind, V_{mw}, at low altitudes, is shown in Figure B-1 for the numerical data given in Table B-1. The mean wind has the following shear variation:

h (ft)	Shear	
	ft/sec/100 ft	kt/100 ft
10	39.2	23.2
100	3.92	2.32
300	1.31	0.77

The last two terms of equation (B-1) contribute mainly to the description of the mean wind at higher altitudes. Figure B-2 shows the mean wind specification from Ref B-2. For $h < 32{,}800$ feet, the specification represents the 99-percentile wind shear buildup envelope. For $h > 32{,}800$ feet, the specification represents the 95-percentile design wind speed profile for the eastern test range. Also

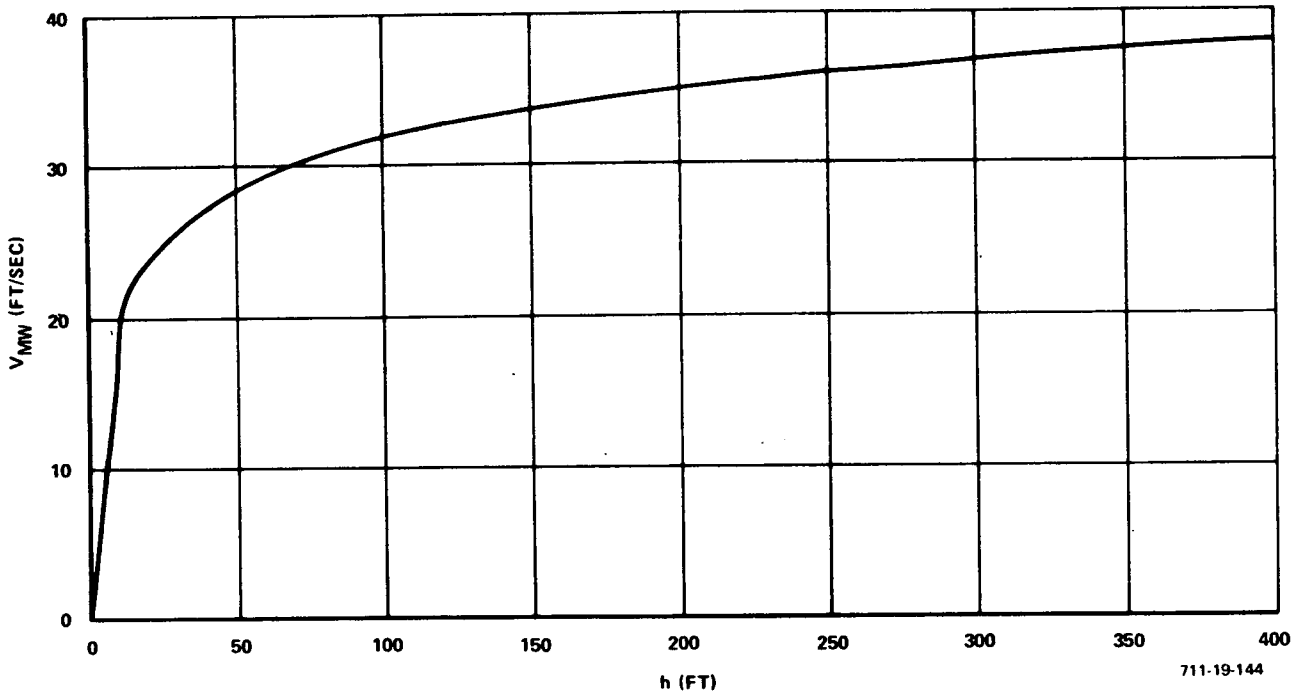

Figure B-1
Mean Wind Profile at Low Altitudes

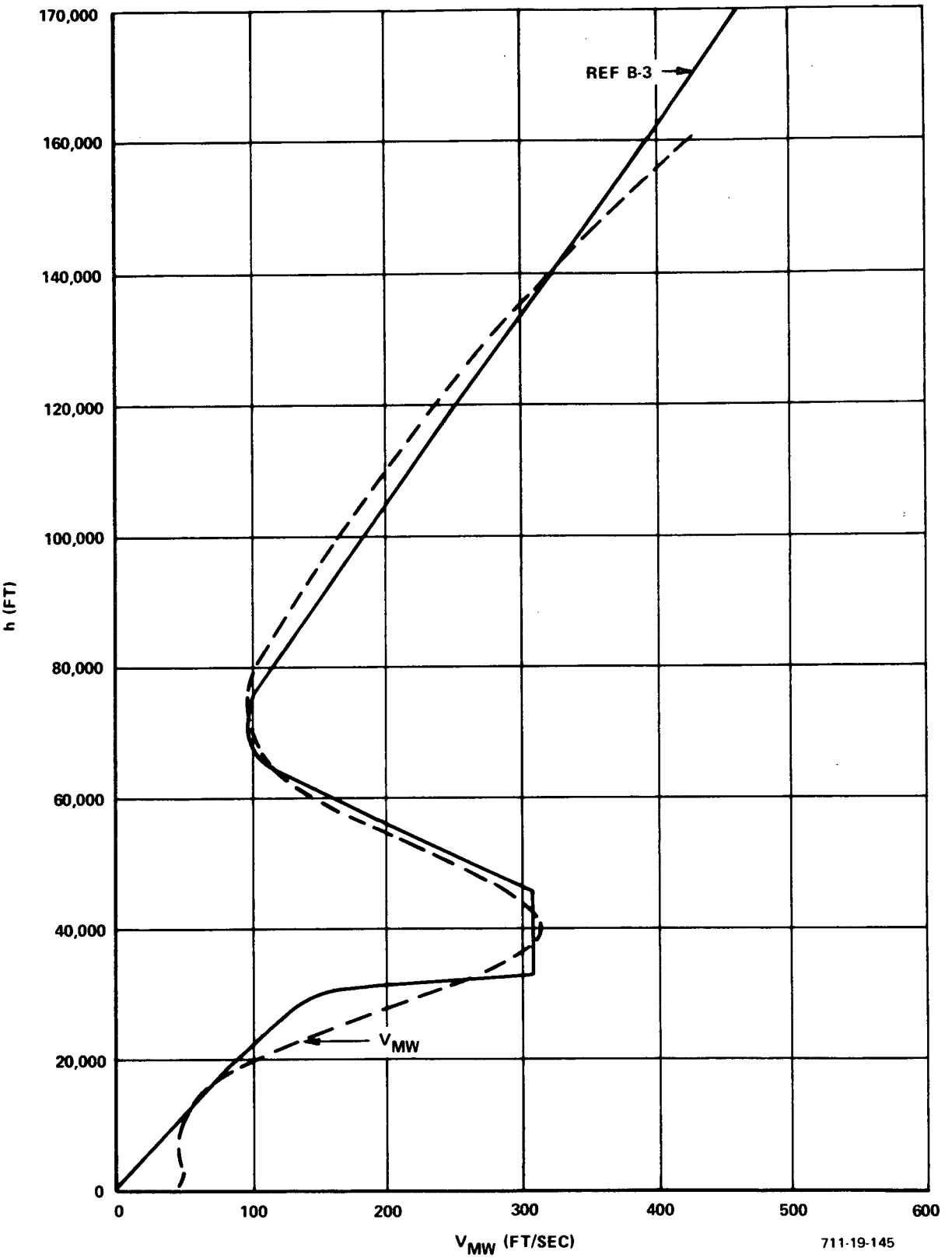

Figure B-2
Mean Wind, Specification and Model Estimate

shown in Figure B-2 is the mean wind described by equation (B-1), using the numerical values given in Table B-1.

TABLE B-1

NUMERICAL CONSTANTS FOR MEAN WIND CALCULATIONS
PRESENTED IN FIGURES B-1 AND B-2

A	25.3171 ft/sec
B	12.6585 ft/sec
C	4.2195 ft/sec
D	0.43
E	0.35
H	10,000 ft
AMW	0°
V_{os}	1/2
h_j	40,000 ft
D_j	13,000 ft
V_j	230 ft/sec
S	1.35×10^{-8} ft/sec/ft^2

3. TURBULENT WIND

The turbulent wind model was taken from Ref B-5. The Dryden model is used with the exception that the scale lengths are held constant for $h < 100$ feet.

a. Scale Lengths

The scale lengths are defined as follows:

$$L_u = L_v = L_w = 1750 \quad , \quad h \geq 1750 \text{ ft}$$

$$L_u = L_v = 145\, h^{1/3} \quad , \quad 100 \leq h < 1750 \text{ ft} \qquad \text{(B-4)}$$

$$L_u = L_v = 145\ (100)^{1/3} \quad , \quad h < 100 \text{ ft}$$

$$L_w = h \quad , \quad h < 1750 \text{ ft} \tag{B-5}$$

b. Variance

The standard deviation, σ_u, was obtained by approximating the data given in Figure 8, page 435, of Ref B-5. The approximations are

$$0 < h \leqslant 100 \text{ ft}$$

$$3\sigma_u = 6.8 \text{ ft/sec} \tag{B-6}$$

$$100 < h \leqslant 60{,}000$$

$$3\sigma_u = -0.720 \log_{10} h + 8.240 \tag{B-7}$$

$$600{,}000 < h \leqslant 90{,}000$$

$$3\sigma_u = -27.259 \log_{10} h + 135.046 \tag{B-8}$$

$$h > 90{,}000$$

$$\sigma_u = 0 \tag{B-9}$$

The variances, σ_v^2 and σ_w^2, can be obtained from

$$\frac{\sigma_u^2}{L_u} = \frac{\sigma_v^2}{L_v} = \frac{\sigma_w^2}{L_w}$$

Since $L_u = L_v$, then $\sigma_u = \sigma_v$ and

$$\sigma_w = \sqrt{\frac{L_w}{L_u}}\ \sigma_u \quad , \quad h \geqslant 100 \text{ ft}$$

$$\sigma_w = \sqrt{\frac{100}{145\ (100)^{1/3}}}\ \sigma_u \quad , \quad h < 100 \text{ ft}$$

c. Simulation

The power spectra densities, ϕ (Ω), for the three turbulent components (u_g, v_g, w_g) are given in Table B-2. Also, the linear filters, G(s), necessary to mechanize the gust components are given in the table. For an analoge computer simulation, u_g would be derived as follows:

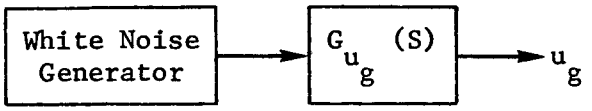

For a digital computer simulation, u_g would be obtained from

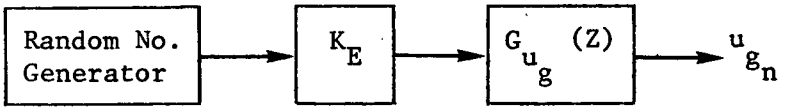

where the gain K_E is required because the output of the random number generator is a discrete signal (Ref B-6). The gain K_E is defined as

$$K_E = \sqrt{\frac{\pi}{T\,\sigma_z^2}}$$

where

T = sampling time

σ_z^2 = variance of random number generator

TABLE B-2

SPECTRA AND FILTERS FOR TURBULENT WINDS

Spectra	Filters
$\phi_{u_g}(\Omega) = \sigma_u^2 \frac{2L_u}{\pi} \frac{1}{1 + (L_u \Omega)^2}$	$G_{u_g}(S) = \frac{\frac{\sigma_u}{\sigma_z} \sqrt{\left(\frac{2L_u}{\pi V}\right)\left(\frac{\pi}{T}\right)}}{1 + \frac{L_u}{V} S}$
$\phi_{v_g}(\Omega) = \sigma_v \frac{L_v}{\pi} \frac{1 + 3 (L_v \Omega)^2}{\left[1 + (L_v \Omega)^2\right]^2}$	$G_{v_g}(S) = \sigma_v \frac{L_v}{\pi T} \frac{1 + \sqrt{3} \frac{L_v}{V} S}{\left(1 + \frac{L_v}{V} S\right)^2}$
$\phi_{w_g}(\Omega) = \sigma_w \frac{L_w}{\pi} \frac{1 + 3 (L_w \Omega)^2}{\left[1 + (L_w \Omega)^2\right]^2}$	$G_{w_g}(S) = \sigma_w \frac{L_w}{\pi V} \frac{1 + \sqrt{3} \frac{L_w}{V} S}{\left(1 + \frac{L_w}{V} S\right)^2}$

4. CONVERSION OF WIND COMPONENTS TO BODY AXIS

Since the gust components are generated in a local level coordinate system and the mean wind components are generated in an earth axis system, an intermediate step is required to convert the gust components into earth axis. Denoting the earth axis components as u_{g_N}, v_{g_E}, and w_{g_D}; and the local level components as u_{g_L}, v_{g_L}, w_{g_L}, the transformation is

$$\begin{bmatrix} u_{g_N} \\ v_{g_E} \\ w_{g_D} \end{bmatrix} = \begin{bmatrix} \cos\psi & -\sin\psi & 0 \\ \sin\psi & \cos\psi & 0 \\ 0 & 0 & 1 \end{bmatrix} \begin{bmatrix} u_{g_L} \\ v_{g_L} \\ w_{g_L} \end{bmatrix} \tag{B-10}$$

With both gust and mean wind components in earth axis, a total earth axis wind component is generated through a direct addition

$$\begin{bmatrix} u_{w_N} \\ v_{w_E} \\ w_{w_D} \end{bmatrix} = \begin{bmatrix} u_{m_N} + u_{g_N} \\ v_{m_E} + v_{g_E} \\ w_{m_D} + w_{g_D} \end{bmatrix} \tag{B-11}$$

where u_{w_N}, v_{w_E}, and w_{w_D} are the total north, east, and down components of wind, respectively. Since the wind components are summed into the equations of motion in body axis, the final transformation required is summarized below, where u_{w_B}, v_{w_B}, and w_{w_B} are body axis components.

$$\begin{bmatrix} u_{w_B} \\ v_{w_B} \\ w_{w_B} \end{bmatrix} = \begin{bmatrix} C\theta C\phi & C\theta S\psi & -S\theta \\ (-C\phi S\psi + C\psi S\theta S\psi) & (C\psi C\psi + S\psi S\theta S\psi) & C\theta S\phi \\ (S\psi S\phi + C\phi C\psi S\theta) & (-C\psi S\phi + C\phi S\psi S\theta) & C\phi C\theta \end{bmatrix} \begin{bmatrix} u_{w_N} \\ v_{w_E} \\ w_{w_D} \end{bmatrix} \tag{B-12}$$

where $C\theta = \cos\theta$, $S\psi = \sin\psi$, etc.

REFERENCES

B-1. "Automatic Landing Systems", FAA Advisory Circular AC No. 20-57, effective January 29, 1968.

B-2. "Circulation of Proposed Wind Model Appendix for Project Paper 417" based on United Kingdom Aeronautical Research Board Regulatory Document (AEEC - Airlines Electronic Engineering Committee), AEEC Letter No. 70-2-40.

B-3. Daniels, Glenn E. "Terrestial Environment (Climatic) Criteria for Use on Space Vehicle Development, 1969 Revision", NASA TM X 53872, Aero-Astrodynamics Laboratory, Marshall Space Flight Center, September 8, 1969.

B-4. Scoggins, James R., Susko, Michael. "FPS-16 Radar/JIMSphere Wind Data Measured at the Eastern Test Range", NASA TM X 53290, Aero-Astrodynamics Laboratory, Marshall Space Flight Center, July 9, 1965.

B-5. Chalk, C. R., Neal, T. P. Harris, T. M. Prichard, F. E. "Military Specifications - Flying Qualities of Piloted Airplanes", Background Information and User Guide for MIL-F-8785B(ASG), AFFDL TR-69-72, August 1969.

B-6. Neuman, Frank, Foster, John D. "Investigation of Digital Automatic Aircraft Landing System in Turbulence", NASA TN D 6066, October 1970.

B-7. "Second Monthly Progress Report on Contract No. NAS2-6077", Bell Aerospace Company.